CHARACTERIZATION AND SYSTEMS INTEGRATION OF MICROREACTORS

By

David J. Quiram

B.S. Chemical Engineering
University of Virginia, 1995

M.S. in Chemical Engineering Practice
Massachusetts Institute of Technology, 1997

Submitted to the Department of Chemical Engineering in Partial Fulfillment of the Requirements for the Degree of

Doctor of Philosophy

at the

Massachusetts Institute of Technology

February 2002

Signature of Author .....
Department of Chemical Engineering
December 20, 2001

Certified by .....
Klavs F. Jensen
Lammot du Pont Professor of Chemical Engineering
Thesis Supervisor

Certified by .....
Martin A. Schmidt
Professor of Electrical Engineering
Thesis Supervisor

Accepted by .....
E. Daniel Blankschtein
Professor of Chemical Engineering
Graduate Officer

Abstract of Dissertation Presented to the Department of Chemical Engineering of the Massachusetts Institute of Technology in Partial Fulfillment of the Requirements for the Degree of Doctor of Philosophy

CHARACTERIZATION AND SYSTEMS INTEGRATION OF MICROREACTORS

By

David J. Quiram

February 2002

Thesis Supervisors: Klavs F. Jensen and Martin A. Schmidt

Microfabrication technology presents the opportunity to create highly instrumented, micro-scale chemical reactors that bring with them the potential for new analytical capabilities, point-of-use synthesis, and highly parallel screening methods. However, the use of integrated circuit-like reaction devices, such as the MIT thin-film microreactor, also gives rise to a spectrum of new engineering challenges with respect to reactor system integration and scale-up schemes. This work demonstrates the integration of multiple microreactors operating in parallel within a system that includes gas flow control components and the associated electronic circuitry. The system built is equivalent to a conventional laboratory reactor system but in 1/10th of the space.

Fluidic and electronic interfaces, thermal management, and operational safety are all considerations in microreactor packaging. A standard microchip socket from Texas Instruments was selected as the first level packaging. The sockets have mechanical attributes that lend them to, with minor reworking, simultaneous fluidic and electronic connection.

This selection makes PC board mounting of the reactor devices straightforward. Shut-off microvalves and proportional microvalves from Redwood Microsystems, with their control electronics, have also been mounted on PC boards to control the gas flow in the system. This allows the entire system: reactors, device electronics, and gas distribution manifold to be mounted on standard CompactPCI cards and housed in a commercially available chassis.

A Kaparel CompactPCI chassis is used to house the microreactor system. Electrical connections between the boards are achieved through a standard backplane and custom-built rear I/O PC boards. The system is comprised of a temperature controller card that regulates temperature for auxiliary heaters in the system; a gas mixing board that mixes the feed gas for the microreactors; two microreactor boards that each contain two microreactors with their feed flow controllers; and two heater circuit boards that provide power to the microreactor heaters. A National Instruments embedded real time processor is used to provide closed-loop control and monitor system alarms. A host PC, running LabVIEW 6, is used as the human machine interface for operator interaction and historical data logging.

Dedicated to my parents and brother. Without their support for all of these years, I would have never made it this far. Thank you.

ACKNOWLEDGMENTS

I am indebted to many people for completing this project. Nearly all of the work reported in this document took place from the fall of 1998 to the fall of 2001 at the Experimental Station Laboratory of DuPont in Wilmington, Delaware. A large group of people contributed to this project, and I apologize to anyone I may have forgotten. In particular, I would like to thank Jim Ryley, Pat Mills, and Mark Wetzel for advising, leading, and supporting me during my time at DuPont. The team that was assembled to create the microreactor system was in many ways remarkable, and I cannot think of success being achievable without everyone's participation. The core team members were Jim Ashmead, Dick Bryson, Emil Hergenroeder, Dan Kraus, Russ Mitchell, Jim Ryley, Alan Stamford, and Mark Wetzel. All of these people contributed significantly to the final product in their area. Although the background of the participants varied widely, the team was able to succeed in putting together a complex system that depended on each sub-component.

I would especially like to thank Dan Krauss for helping in the final days of the project and in meeting and exceeding expectations in the task of putting together the control system and software. He spent much more time then he or I ever anticipated in debugging and optimizing the software to get it running. I would also like to apologize for taking so much of his time during the last few months I worked at DuPont.

The contributions of the other team members is no less significant and probably will never be visible to anyone reading this document. The real complexity of such a

system can only be understood by those involved in building and debugging it. The following three hundred pages of text are my attempt to impress upon the reader the thought and effort that went into its construction, but upon reflection I do not think I succeeded. I could have easily written two thousand pages describing in agonizing detail all of the engineering that went into this project. In fact, I have a three-ring binder much thicker than this thesis, full of technical specifications for components and system construction. This binder does not even address the software components.

Finally, I would like to thank the other DuPont personnel who helped me throughout my time there on the various tasks I had to face. In particular, Scott McCracken and Tom Delaney oriented me into the Experimental Station environment, and gave me the skills I needed to succeed there. Also, many of the DuPont craft workers helped me throughout my stay. These included Mike Briscoe, Frank Colubrial, Jeff Fleischutt, Joe Pio, Steve Raker, and Donna Work. It was really a pleasure working and learning from these people.

TABLE OF CONTENTS

Page

LIST OF TABLES

LIST OF FIGURES

CHAPTER 1
MICROREACTORS AND STARBUCKS®

New concepts in chemical engineering are becoming increasingly rare. One study points out that although the number of major new innovations in the chemical industry was 40 in the period between 1930 and 1949, it declined dramatically to only 3 between 1970 and 1985[1]. From a business perspective, the chemicals industry is considered mature. Rapid advances or step changes in technology do not occur often. Currently, innovation in business strategy can be just as important as innovations in technology[2]. This is shown in the adoption of new management styles in the Chemicals Processing Industry (CPI), such as total quality management and, more recently, six sigma[3,4]. Nonetheless, conditions seem favorable for the pursuit of radical technology to meet increasingly demanding environmental regulations and global competitive pressures[5]. These factors indicate that the change in the chemical industry in the next 100 years could be just as dramatic as the changes in the last 100 years[6,7].

One promising emerging technology is the development of microreactors, or miniaturized chemical reactors, for on-site and on-demand chemical production[8-13]. The idea behind MicroReaction Technology (MRT), the term used to described this field, originated in the late 1980's when an ordinary appliance generated an extraordinary idea[14]. The basic observation was that hundreds of thousands of gallons of coffee are produced every day with a relatively small piece of equipment that is operated both where the consumer wants it and when he needs it. This leads even further to consider how much coffee could be produced by a single coffee maker running virtually continuously. If

chemical reactors could be made on the same scale, even a small device would be capable of generating a significant amount of product over a long period of time. This microreactor would also have the advantage of reducing the need for transportation and storage of hazardous or unstable chemicals. For example, the 10 channel packed-bed microreactor developed at MIT with an operating flow rate of 80 std. cm^3/min could produce approximately 100 kg/yr of phosgene[15].

What is a Microreactor?

A natural series of questions then arises on how best to take advantage of this idea. The most important of which are

- How big should these reactors actually be?
- How should these reactors be made?
- What advantages do these reactors have?
- Where will these reactors be used?

Microreactor Size

In the field today, microreactors generally have a characteristic channel dimension of less than 0.5 mm[16]. Larger dimensions increase the throughput rate, but may decrease the advantages that small dimensions can provide. To overcome throughput limitations with such small channels, many reactor designs use a large number of channels operating in parallel. This is not distinctly different from the monolithic catalysts that have been commercially available for decades.

From a theoretical perspective, any advantage in size is not achieved until the channel dimensions are reduced to the characteristic length scales for heat and mass transfer. The characteristic length of mass transfer is given by

$$\delta_D = \sqrt{D_{AB}\tau_m} \tag{2.1}$$

where δ_D is the characteristic diffusion length of component A in B, D_{AB} is the diffusion coefficient of component A in B, and τ_m is the time allowed for mass transfer. D_{AB} is typically on the order of 0.1 cm^2/s for mixtures of gases. Assuming that the residence time for a microreactor is on the order of 1 second, this gives a characteristic diffusion length on the order of 1 mm. For liquids, the diffusion coefficient is much smaller and this results in the need to design specialized mixing structures–a task that has received considerable attention over the past decade.

Similarly, the characteristic length of heat transfer is given by

$$\delta_H = \sqrt{\alpha\tau_h} \tag{2.2}$$

where δ_H is the characteristic length of heat transfer, α is the thermal diffusivity of the fluid, and τ_h is the time allowed for heat transfer. α is generally on the order of 0.1 cm^2/s for gases, and this gives a characteristic length of heat transfer on the order of 1 mm assuming again that there is a 1 second residence time in the microreactor.

Small channel dimensions also lead to a laminar flow velocity profile under most conditions. This can be an advantage or disadvantage, depending on the application. For example, a laminar flow field makes modeling of the microreactor much easier[17]. This behavior has also been used as an advantage in the design of micro-extractors[16,18]. On the other hand, turbulent flow is preferred in a channel if intimate mixing is desired between two

streams. Turbulence would also reduce temperature and concentration gradients present in laminar systems.

For these reasons, the channel dimension perpendicular to flow has been kept to less than 0.5 mm in most microreactor designs. Mixing structures for liquids use considerably smaller dimensions (usually around 50 μm) because of the slower diffusion process. The length of the reaction channels is more variable but is on the order of 1 cm. However, this length depends on the desired throughput rate and the needed reactor residence time. Ultimately, the designer must consider trade-offs between pressure drop, throughput, reaction requirements, and cost in selecting the appropriate microreactor dimensions.

Microreactor Fabrication

A large variety of materials and fabrication methods are available for producing microreactors. In general, the need for a specific material will partially dictate the fabrication method. However, in many cases, a variety of materials may be equally applicable in terms of chemical and thermal compatibility. In these instances, the cheapest material with the most cost effective fabrication method is chosen. This gives a significant advantage to plastics and certain readily machined metals. Microfluidic plastic devices can be mass-produced using hot embossing, injection molding, and casting[19-21]. In addition, prototypes can be made cost effectively using conventional machining equipment. The biggest disadvantage to plastic devices is the low temperature range of the material (less than 200°C for most plastics)[20-22]. Punching of metal parts for microreactors has also been used to create devices in a cost effective manner[16]. In addition, metals can be machined using conventional technology or micro-ElectroDischarge Machining (μEDM). This technique has the capability of producing structures with minimum feature sizes of 10

μm[21]. Thus, the extensive experience with metals in chemical processing can be directly used in developing microreactors. The ability of a well-equipped machine shop to produce microreaction devices significantly expands the number of potential players beyond those with access to silicon microfabrication facilities.

Silicon has also played a prominent role in microreactors due to the micromachining experience of the Integrated Circuit (IC) and MicroElectroMechanical Systems (MEMS) industries. Silicon is an excellent material because of its chemical inertness, which can be improved by oxidizing the surface[23], and its large operating temperature range. Single crystal silicon also has a high thermal conductivity, 157 W/(m·K) compared to 236 W/(m·K) of aluminum[24]. In addition, it is possible to integrate silicon microreactors with sensors, such as for temperature and pressure. This gives the advantage of more precise control and performance information. Unfortunately, this information comes at a price since the machining requires specialized silicon processing equipment. Mass production is possible, but high volumes are needed to drive down cost. Even then, some processes, such as Deep Reactive Ion Etching (DRIE), are not economically favorable at this time.

Other materials and fabrication methods, such as ceramics and LIGA, an electroplating technique of microstructures created using a synchotron radiation source, are available for building devices as well. Ultimately, cost and reaction requirements will dictate the material and fabrication method. However, the designer must keep in mind the enabling characteristics of miniaturization. If the selected material and fabrication technology cannot produce a microreactor that has advantages over a larger conventional reactor, the extra expense of miniaturization is not justified. For that reason, the Jensen research group at MIT has focused on silicon microreactors because silicon allows the integration of sensors,

actuators, and microstructures. These features produce reactors with characteristics that are not possible on the macro scale, such as thermal time constants on the order of milliseconds and submillimeter control of temperature. Likewise, the Institut für Mikrotechnik Mainz (IMM) has focused on metal, multi-channel microreactors that can be produced using punching. The small channel dimensions and the high thermal conductivity of metal give extraordinary heat transfer characteristics. Metal punching makes the devices cost competitive with conventional technology.

Advantages to Miniaturization

Currently, the motivating force behind reactor miniaturization has been a technology push instead of a pull. Researchers have identified potential advantages for these devices, but the CPI remains skeptical at their applicability. Since there is no killer application for microreactors at this time, there has been little pull toward microreactor research by industry. Thus, the advantages of microreactor technology have been classified in broad terms and have not necessarily been demonstrated in a viable commercial setting. The original motivation behind microreactor research was driven by five key factors[13,25,26]:

- Safety
- Technical advantages
- Distributed production
- Easier scale-up
- High throughput screening techniques

These advantages of MicroReaction Technology are summarized below.

Safety

An important advantage of microreactors for chemical production is the inherent safety in having reactor volumes so small that the system could be designed to contain even the worst-case accident scenarios. Microreactors, with their narrow channel size, hold such a

minor quantity of chemicals that a total failure would merely require temporary shut-down and reactor replacement. The small quantity of chemicals released by a failure would not pose an environmental threat. For example, a failure of the MIT membrane microreactor for one minute before shutdown would release ~30 mg of chemicals. Furthermore, a worst-case explosion in the scale-up microreactor system discussed in this dissertation would release the equivalent energy of 0.00023 lbs of TNT. The design of a containment system to handle a hazardous chemical or energy release on this level would be straightforward.

Operating reactions in a microreactor is also safer because of the high surface-to-volume ratio that increases the heat transfer rate away from the reaction zone. For example, microchannel heat exchangers/reactors can easily have overall heat transfer coefficients that exceed 20 $kW/(m^2 \cdot K)$, where conventional heat exchangers have overall heat transfer coefficients of less than 2 $kW/(m^2 \cdot K)$[16]. Furthermore, the high surface-to-volume ratio also acts to lessen the contribution of homogeneous free-radical chain mechanisms that induce a runaway reaction[27]. As part of its exploratory work in the field, DuPont researchers performed several reactions that required or produced toxic intermediates in a silicon wafer stack microreactor[13]. Researchers have also reported operating reactions in microreactors that would be considered unsafe or impossible to run on a larger scale because of the explosion potential[27-31].

Recently, health and the environment have become critical factors in the CPI. Not only must processes be designed to be safe, but it now makes economic sense to decrease the impact of processes on the health of workers and the surrounding community[32-34]. This means reducing chemical releases and minimizing the amount of waste being disposed. In the past, batch processes were favorable for producing small quantities of chemicals in

campaign-oriented manufacturing. The disadvantage is that large amounts of waste can be generated in the startup, shutdown, and cleaning of batch processes. Switching production to a continuous process can significantly reduce the amount of waste associated with the process and ultimately improve its economics[35]. In the future, small quantity continuous production using microreactors may be more favorable then using batch production processes for these reasons.

Technical advantages

Microreactors have technical advantages for some reactions because of their physical characteristics. They can either improve the performance of a reaction by increasing selectivity and yield or decreasing energy consumption. The high surface-to-volume ratio increases heat transfer to and away from the reaction zone. It also plays a role in quenching gas-phase free radicals that may compete with the desired heterogeneous reactions. Other phenomena, such as surface tension, also change in importance due to size. Even under similar operating conditions, microreactors have been shown to increase selectivity and/or yield for a number of industrial gas and liquid phase reactions[16,26,36-42]. In addition, microreactors are capable of running reactions that are impossible on a larger scale due to safety reasons. For example, the direct fluorination of aromatic compounds has already been demonstrated by two groups[29,31,43]. Normally, this reaction would not be attempted in a conventional reactor because of the highly exothermic nature and poor selectivity.

In addition, certain reactor configurations may favor microfabrication, such as membrane reactors. The Jensen group has produced a palladium membrane microreactor that is capable of performing a hydrogenation reaction while keeping the hydrogen stream from having direct contact with the rest of the feed[44]. This microreactor is capable of high

hydrogen diffusion rates through a palladium membrane because of the fabrication techniques used.

Distributed Production

Benson and Ponton[5] originally recognized distributed chemical production as being a key factor in the future of the CPI. They identified the key advantages to this as being the reduction of the footprint of chemical facilities, avoidance of transportation of hazardous chemicals, and the elimination of storage of hazardous or unstable chemicals. Their concept was to have miniaturized chemical plants used in place where the product was needed. This point-of-use mini-chemical plant has advantages over a larger-scale manufacturing facility since it eliminates the need for hazardous chemical storage and transportation. For example, methyl isocyanate production has already been demonstrated in a microfabricated reactor[13]. Using minichemical plants would avoid chemical storage by designing them to have flexible production schedules and for quick startup and shutdown. Parallel arrays of microreactors offer extraordinary flexibility for production levels since the reactors can be individually turned on or shutdown to increase or decrease production as necessary. This allows an individual microreactor to be designed for one particular set of conditions instead of compromising the design to operate over a variety of flow rates and feed compositions[45].

Easier Scale-up

Scaling-up microreactors for chemical production is often thought to be easier since the scale-up involves creating arrays of microreactors operating in parallel. The advantage being that the reactor studied in the laboratory would ultimately be the reactor used for commercial production. This avoids the transition from laboratory scale to pilot plant scale to commercial plant, which can be accompanied by severe difficulties. In support of the

improved safety aspects, this also avoids working with poorly understood reactions on the pilot scale. A recent explosion in a DuPont pilot plant in Mexico, where one worker was seriously injured, emphasizes this point. The work shown in this dissertation suggests that numbering-up microreactors is not necessarily easier—it simply changes the nature of the engineering problems that must be solved. The eventual goal would be to create well-designed scale-up schemes that could be used for a wide-variety of cases. At this time, no such standard methods exist, and commercial use of microreactors has focused on only one or two devices operating in parallel.

High-Throughput Screening Techniques

The field of combinatorial chemistry was still young when the first microreactors were being built, but it was apparent even then that massively parallel testing of catalysts favors smaller reactor sizes. Although there are many screening techniques that do not use microreactors per se, it is believed that ultimately a microreactor would be needed for catalyst evaluation. Currently, the initial fast screens are used to identify potential hits, but further work must still be done in more standard laboratory reactors. This is due to the inability of the fast screening techniques to mimic the conditions of typical catalyst use and to provide the high accuracy data that is required for evaluation. Microreactors could play an intermediate role where they are used after a fast screening method, but before more in-depth laboratory studies. Because of the speed of the techniques being developed, even a small percentage of hits in one screening test could take weeks in a conventional catalyst test station to evaluate. Another approach would be to use the microreactors as a primary screen, but use rational catalyst design to produce likely hits that are worthy of study[46].

Where would microreactors be used?

In the end, economics determines where microreactors should lie in the CPI. Although distributed production may be a compelling reason to adopt the technology, it needs to be cost competitive when compared to the current centralized large-scale chemical plant. This requires analyzing reactions to find ones that favor being run in a microreactor or cannot be run in a conventional reactor. In addition, production requirements cannot be so high that microreactor production is not feasible. For favorable economics, the product should be of high-value or have excessive transportation cost. A risk analysis method could be used to estimate the economic advantages of microreactors due to increased safety.[1]

Currently, microreactors are put in place of conventional reactors for commercial production. In this case, reactions have been identified that are low volume and favor the small size. CPC[2] and the IMM[3] are both marketing microreactors that can be used on chemical sites for production. The technology has not developed to the point where distributing microreactor systems to the product end-user is appropriate. Ultimately, these mini-chemical plants should be highly automated and require little oversight and maintenance by plant operators.

Looking forward, consumer applications offer the largest potential commercial market for the technology. In this case, the use of microreactors in distributed energy systems is the most likely application. An enormous effort is being placed on the development of highly efficient fuel cells for providing mobile power, and potentially even

---

[1]Unfortunately, this is difficult since commercial experience with the technology is limited. Little information is available on failure rates and scenarios.
[2]Cellular Process Chemistry GmbH, Hanauer Landstr. 526/G58 III, D-60343 Frankfurt am Main, Germany, +49(0)-69-4109-2320, info@cpc-net.com.
[3] Institut für Mikrotechnik Mainz GmbH, Carl-Zeiss-Straße 18-20, 55129 Mainz, Germany, +49/(0)6131/990-0, imminfo@imm-mainz.de.

supplementing electric utilities. Fuel cells need a source of hydrogen or methanol, which could be provided by a microreactor system. Work is currently underway by PNNL and MIT in this field[47].

Project Motivation

Past work in microreaction technology has focused on building devices that take advantage of miniaturization and demonstrate its benefits. Unfortunately, this effort has left the larger task of integrating microreactors into functioning systems relatively unexplored. Only recently have microreactors been used in commercial processes, and this use has been for niche applications that could immediately benefit from the technology. The IMM has made initial efforts into microreactor integration schemes, but their devices do not address the control and monitoring issues[48]. CPC has also produced SELECTO™, a commercial microreactor system by integrating pumps and a mixing type of microreactor. However, no previous effort has demonstrated multiple reactors running in parallel with an integrated fluid handling and control system for each reactor.

As a first step toward developing more complex microreactor systems, DuPont and MIT have collaborated on developing a stand-alone gas-phase microreactor system that integrates valves, mass flow controllers, pressure sensors, microreactors, and control electronics. This device is capable of having four independent reaction channels running simultaneously on two microreactor dies. Each channel has independent flow and temperature control. In addition, the feed gas for the microreactors is mixed in the system using microvalves and mass flow controllers. A real-time Programmable Logic Controller (PLC) controls the microreactor system with a host PC allowing operator interaction. Product analysis is performed using conventional methods, but could be integrated into the

system. The focus was not to build and test a new microreactor design, but to build a MEMS-based system that had the same functionality as a conventional component system. This effort addresses the key challenges in microreactor integration as well as demonstrating prototype packaging schemes.

Literature Review

The state-of-the-art in MicroReaction Technology has been summarized recently in a number of sources, which both describe current and past devices along with potential applications of the technology[16,49,50]. The best source for recent advances in the field is the proceedings from the latest annual International Conference on Microreaction Technology (IMRET). There is no journal devoted to the subject at this time, and papers are published in a variety of respected journals.

Despite the explosive growth in the field, very limited resources have been placed on developing integrated microreactor systems for chemical production. Most integrated devices are in the area of micro-Total Analysis Systems (μTAS) where analysis is the focus instead of production. Other integrated microfluidic MEMS devices have been developed for High Throughput Screening (HTS). Integrated microreaction devices for chemical production have received some focus recently, but no sophisticated systems have previously been demonstrated.

Microfluidic Integration in μTAS

Although a μTAS device does not necessarily contain a microreactor, recent work has produced some high-level designs that integrate components that would typically be used in a microreaction system. Work that demonstrates this kind of integration will be highlighted here whether it is for biochemical or chemical analysis. There are numerous research efforts

aimed at integrating microfluidic components that do not have any direct correlation with microreaction systems for the CPI. For example, the proceedings from the last μTAS meeting in the Netherlands describes many systems focused on DNA replication and separation[51]. Although integrated in the sense that they contain a microreactor for the DNA Polymerase Chain Reaction (PCR), the fluid control techniques used, such as electrokinetic forces or micropumps, are not readily adaptable for the use of chemical production except on the smallest of scales (nanoliter to microliter ranges).

The device most directly suitable for the CPI being developed is Sandia's μChemLab, which consists of a sample collector/concentrator, a gas chromatograph, a chemically selective Surface Acoustic Wave (SAW) detector, and a gas flow control module[52,53]. A rendering of the final system is shown in Figure 1-1. The sample collector consists of a membrane with a microheater covered by a chemically absorbent gel. The gel absorbs the desired analytes and releases them upon heating into the micro-GC column. The detector for the column is a SAW sensor that not only gives a signal when analyte passes through it, but is chemically selective as well. These three devices are coupled on a novel Printed Circuit Board (PCB) that provides both electrical and fluidic interconnections. In addition to the previous devices, the PCB also contains a miniature 3-way valve for bypassing the GC column and a gas inlet/outlet manifold. A separate board that contains a microprocessor and memory along with the power control and user interface electronics controls the components. In many ways, this is similar to the scale-up microreactor system developed at DuPont. Unfortunately, there are no detailed publications describing the finer points of the integration, such as the gas pumping mechanism or even the method of fluidic interconnection between components.

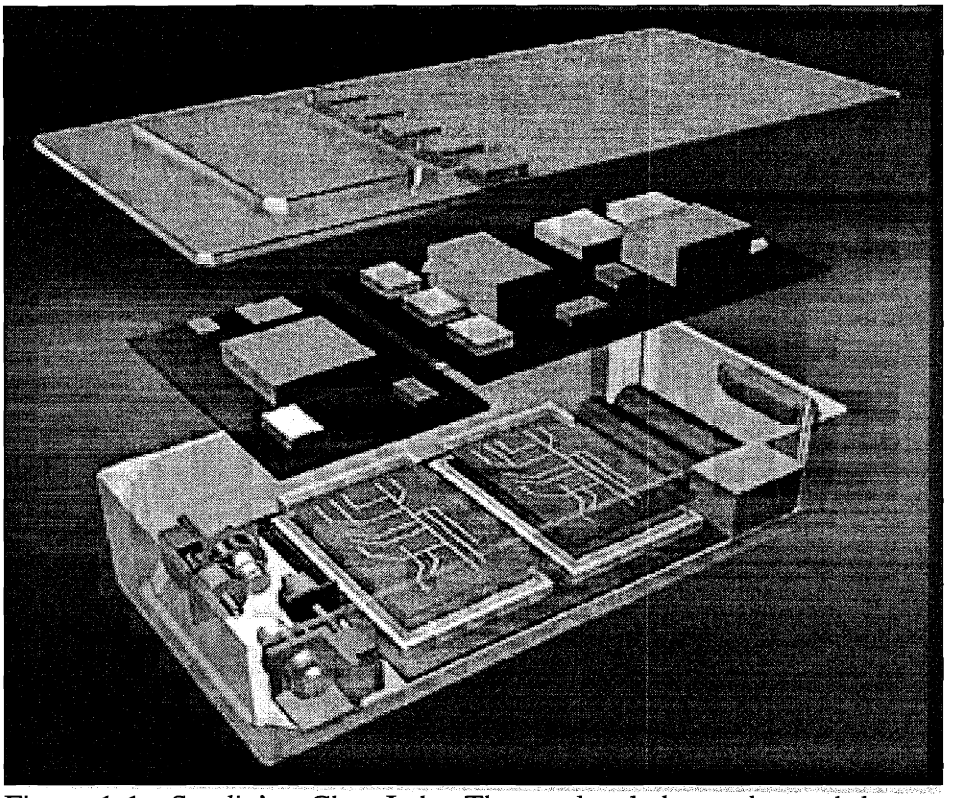

Figure 1-1. Sandia's μChemLab. The top level shows the push-button controls and viewing screen; the middle level shows the electronics hardware; and the bottom level contains the microfluidic components[54].

A less sophisticated, but currently functioning, μTAS for the analysis of low concentrations of toxic metals has been developed by PNNL[55-57]. Two fluidic integration methods were developed for this system. In one version, a stacked architecture is used, where each layer serves a particular function such as mixing[55-57]. In the other version, the components are placed horizontally on a microfluidic platform[55]. An electrochemical cell is used as the detection device. The cell is integrated with reservoirs for the buffer and sample solution along with micro-pumps for each reservoir. The micro-pumps used are electrokinetically actuated and were obtained from the IMM. A picture of the partially packaged stacked-architecture system is shown in Figure 1-2. Unfortunately, no information

is given on how the electronics are integrated with the microfluidic structures. However, due to the low number of connections required for this system, this was not a challenge in the design.

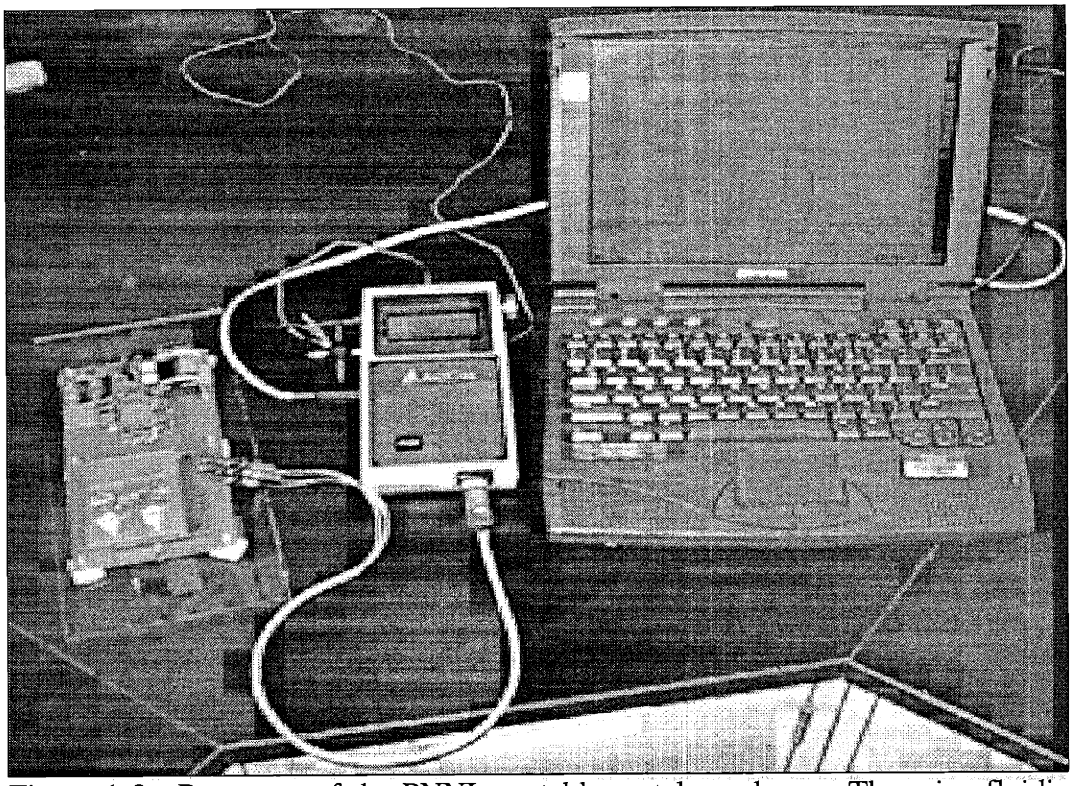

Figure 1-2. Prototype of the PNNL portable metals analyzer. The microfluidic system is mounted on the printed circuit board at left[55].

The alternative fluidic integration method is based on a planer architecture that allows for easy plug-in of the micro-pumps and electrochemical cell. Again no information is given on how electronics were connected to the microfluidic system. The functionality of this version was tested by analyzing a solution for Pb^{2+}. The μTAS was found to be capable of detecting Pb^{2+} on the parts per billion level, and it had similar performance to a macro-scale electrochemical cell.

At Transducers 97, Richter and coworkers presented a microanalysis system as a demonstration of a microfluidic system[58]. Their device was meant to demonstrate how

microfluidic components from a variety of sources could be integrated into a functioning system. It was composed of three micro-pumps, three flow sensors, two conductivity sensors, and two passive check valves. This demonstration unit was designed to perform a sample injection, clean the system between injections, and perform a sensor calibration.

Although one of the main goals of the work was to develop a standardized design methodology for microfluidic components, their results in this effort are discussed only briefly. In the paper's conclusions, the authors acknowledge that standardization is a very complex task, and that it is not achievable in a short time period. Their call for standardization is well justified since researchers building a μTAS device usually also fabricate the individual components for it. This leads to a large amount of repetitive work in the design of pumps, valves, detectors, and even fluidic couplers. Unfortunately, this kind of standardization does not usually come in the early development stages of an emerging technology. Either an industry organization has to make a concerted effort to develop a standard (for example, the Blue Tooth standard for short range wireless communication), or the industry leader creates a de-facto standard (for example, the Windows™ operating system by Microsoft). Since the commercial industry for μTAS has not developed at this point, neither of these two methods is feasible.

The MESA research institute made another attempt at standardization, where they fabricated several standard microfluidic modules such as flow sensors and pumps[59]. These were incorporated into a demonstration device designed for the optical detection of pH change using a pH indicator. This system consisted of two micro-flow sensors, two micro-pumps, and a microfabricated optical absorption detector. The microfluidic devices were mounted on a Mixed Circuit Board (MCB) that consisted of an epoxy Printed Circuit Board

(PCB) on the top and a polycarbonate substrate. Fluidic channels and vias were machined in both layers to connect the individual components. The PCB provided a means of electrical connection between the components and the control circuitry. However, it is not clear how the electrical connections between the microfluidic devices and the PCB were made. Presumably soldering or wire bonding was used. Beneath the MCB there were two more PCB layers that contained the control and communication circuitry needed for the system. The system was packaged very cleanly, but the complexity was not very high due to its purpose as a demonstration of their concept. Unfortunately, they have not published results on continued work in their effort to standardize components.

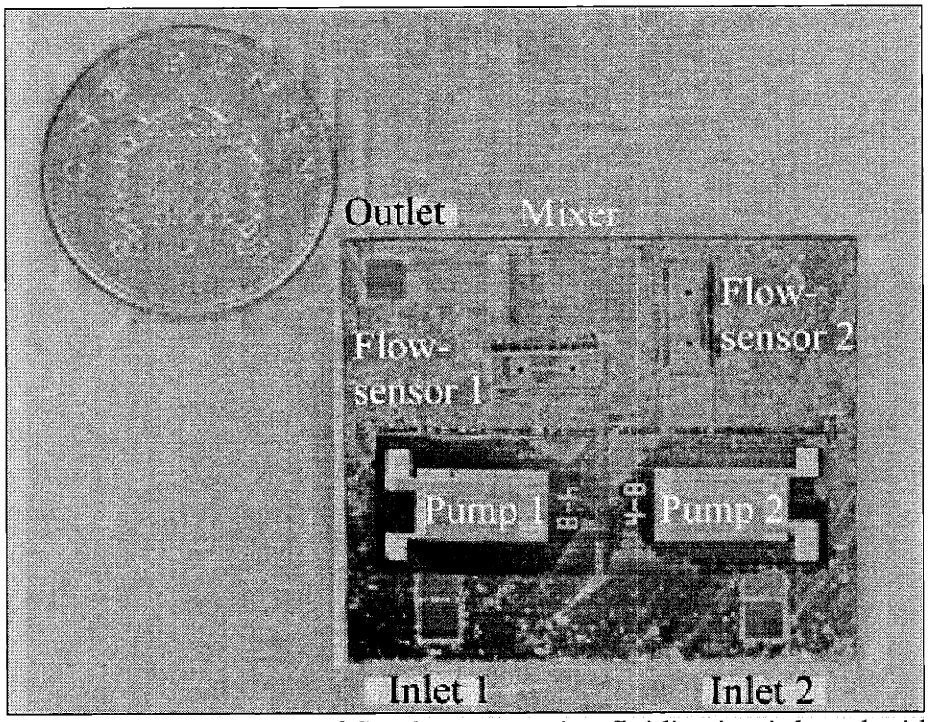

Figure 1-3. University of Southampton microfluidic circuit board with pumps, flow sensors, and a mixer[61].

Researchers at the University of Southampton have also designed and fabricated a demonstration mixed circuit board system[60,61]. This device, which is shown in Figure 1-3, has two pumps and flow sensors operating in parallel with a mixing/reaction chamber

bringing the fluids together. Their MCB consists of a Pyrex top layer anodically bonded to a silicon bottom layer. However, all of the micromachining is done in the Pyrex layer and the silicon is used only to seal the channels. The microfluidic components are then mounted on the Pyrex layer by another anodic bonding step. The authors do not describe any special techniques used for the electrical interconnections in their paper. Follow-up work describing the development of more complex systems has not been published.

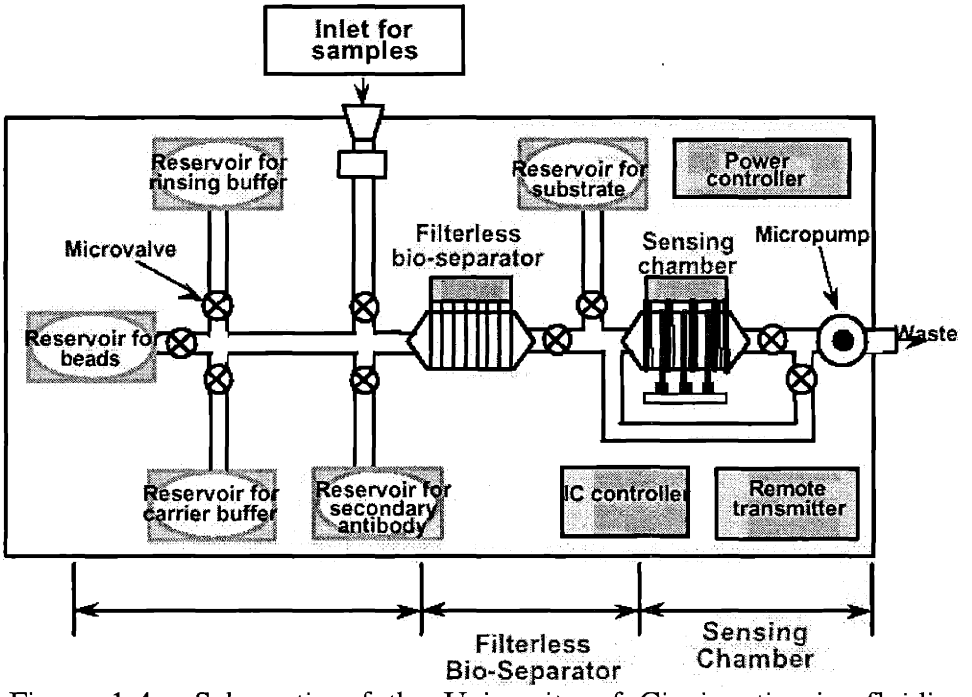

Figure 1-4. Schematic of the University of Cincinnati microfluidic system for biochemical sensing[62].

The Ahn research group at the University of Cincinnati have developed a considerably more complex integrated microfluidic device using the mixed circuit board concept[42,62]. Figure 1-4 shows a schematic of this system, which performs biochemical detection using magnetic beads. Its components include microvalves, micropumps, biofilters, flow sensors, and an imunnosensor. Their fourth generation system, shown in Figure 1-5, contains an impressive amount of integration with two MCB's stacked vertically

(one containing reagent reservoirs and the other performing biochemical detection). The MCB's are connected to four PCB layers that contain the electronic circuitry needed for the microfluidics as well as a microcontroller to direct the performance of assays.

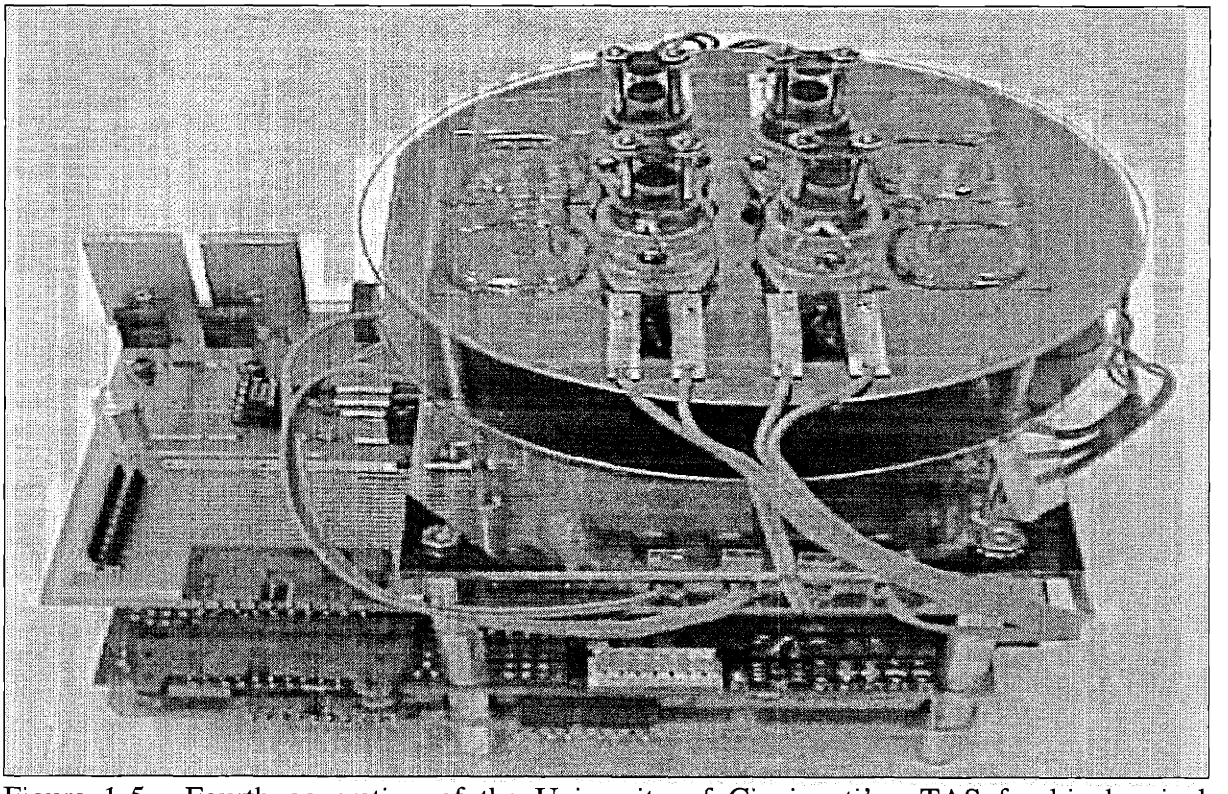

Figure 1-5. Fourth generation of the University of Cincinnati's μTAS for biochemical sensing. The top two circular layers contain the microfluidic components[62].

The substrate of the mixed circuit board is a glass top layer bonded to a silicon bottom layer. The microfluidic components all consist of a glass bottom layer that is high temperature bonded to the MCB. The MCB is patterned with a gold layer to provide electrical interconnections between the devices. Soldering is used for the electrical interconnections from the microfluidic components to the MCB. This group has also developed a novel technique for fluidic interconnections between the MCB layers. Figure 1-6 shows a close up of the two MCB layers for a better view of these connections.

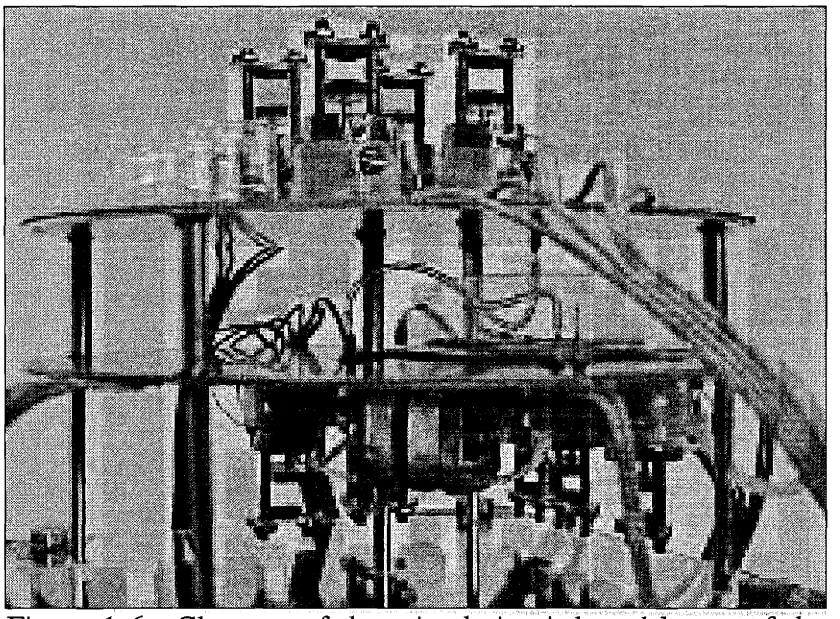

Figure 1-6. Close-up of the mixed circuit board layers of the University of Cincinnati's μTAS[62].

Fluidic connections are made using PEEK™ tubing and a micromachined glass structure. Figure 1-7 shows the structure in a stack of glass wafers where a smaller diameter hole forms a shelf over the larger diameter hole. To join the structure to the tubing, a piece of tubing is inserted and then force and heat are applied to flow the plastic tubing into the larger diameter hole. This creates a flange that seals the tubing to the glass wafer[63].

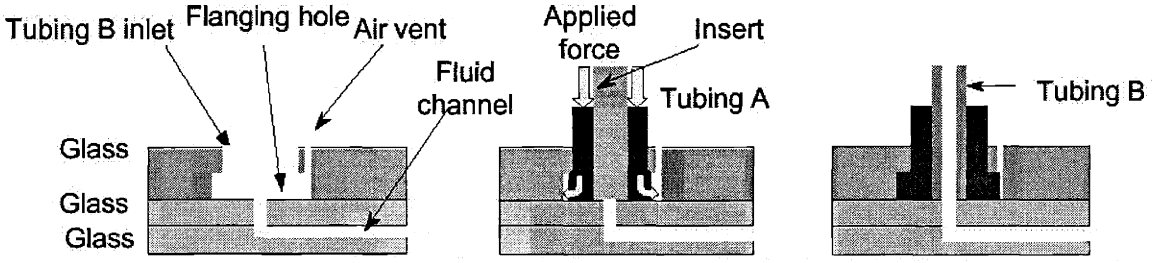

Figure 1-7. Schematic diagram of the University of Cincinnati's interconnect method: (a) bonded glass wafer assembly; (b) flanging operation; and (c) assembled view[63].

Microfluidic Integration in HTS

The development of complex microfluidic systems for High Throughput Screening (HTS) applications has not been described in the literature. However, it is quite likely that the major companies participating in the development of combinatorial methods for materials screening have developed or are developing such systems. In particular Symyx[4], has indicated in conference presentations that they are building systems that incorporate microreactors for screening purposes[64]. Their ongoing collaboration with the IMM is also well known[65]. Their focus is on developing a secondary level of catalyst testing technology to be used after the primary mass screening is performed[64]. It is quite likely that HTE[5] and Avantium[6] are also working on developing complex microreactor systems for catalyst screening, but no information is available on their efforts.

The pharmaceutical industry has already benefited greatly from HTS techniques. Vast compound libraries are being searched for possible pharmaceutical applications; however, much of the testing being performed does not use microfluidics. Instead, robotics is used to handle small quantities of compounds using parallel arrays of pipettes. It is likely that the pharmaceutical industry will begin to use microfluidic systems in the near future. Examples of companies performing research in this area include Abott Laboratories[66], AstraZeneca[67], SmithKline Beecham Pharmaceuticals[68], Caliper[69], and ACLARA[70]. However, the devices being developed handle only very small quantities of chemicals and their methods for both fluid manipulation and detection are often not directly

[4] Symyx Technologies, Inc., 3100 Central Expressway, Santa Clara, CA 95051, (408) 764-2094.
[5]HTE Aktiengesellschaft, Kurpfalzring 104, 69123 Heidelberg, Germany, +49 (0) 62 21.74 97 – 0.
[6]Avantium Technologies, Zekeringstraat 29, 1014 BV Amsterdam, The Netherlands, +31 (0)20 586 8080, info@avantium.nl.

applicable to microreactor systems for use in the CPI. Orchid BioSciences appears to be developing more complex, integrated microfluidic systems for HTS, but little information is available on their research[71-74]. Figure 1-8 shows a conceptual drawing of an Orchid multilayer microfluidic device that contains valves and reaction chambers.

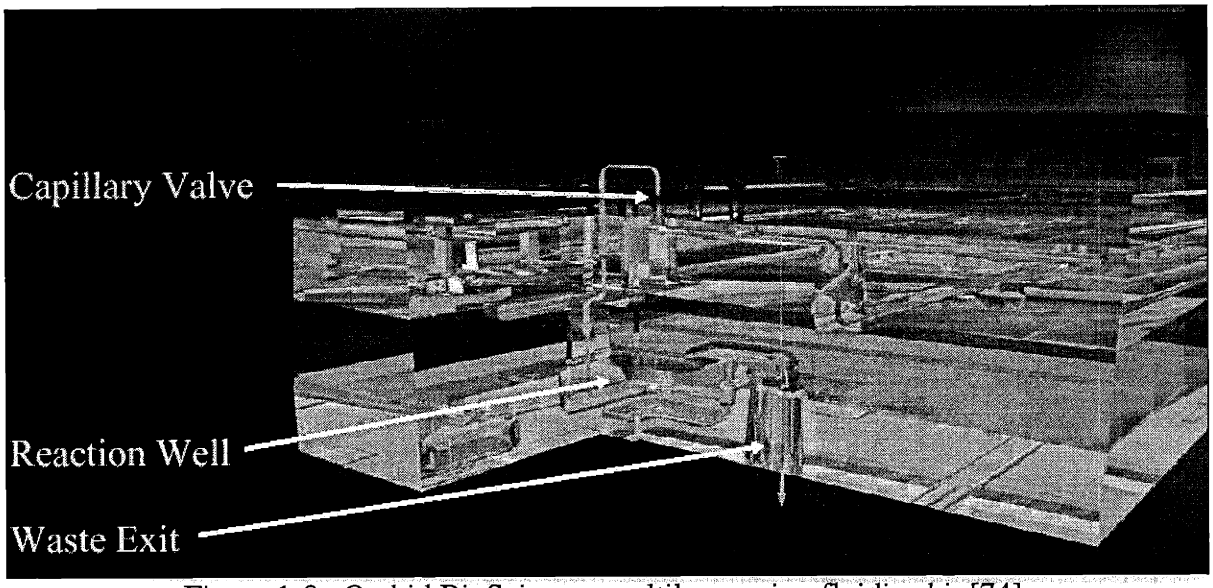

Figure 1-8. Orchid BioSciences multilayer microfluidic chip[74].

Microfluidic Integration in Chemical Production

Research in microreactors for chemical production began in the late 1980's at DuPont[14,75]. This work culminated in an extensive experimental effort that built various microreactor designs with different materials, heating methods, and catalysts[13,75]. An example of an early DuPont microreactor design for producing methyl isocyanate, which is an intermediate in the production of agricultural chemicals, is shown in Figure 1-9. This layered design integrates heat exchange and reaction to yield a system the successfully manages the large amount of heat generated by the reaction. DuPont also tested a number of other reactions that involved hazardous reactants and/or products as a proof-of-concept. This early work focused on integration of microreactor components through the stacking of layers.

However, it did not address the problem of connecting arrays of reactors to increase overall throughput.

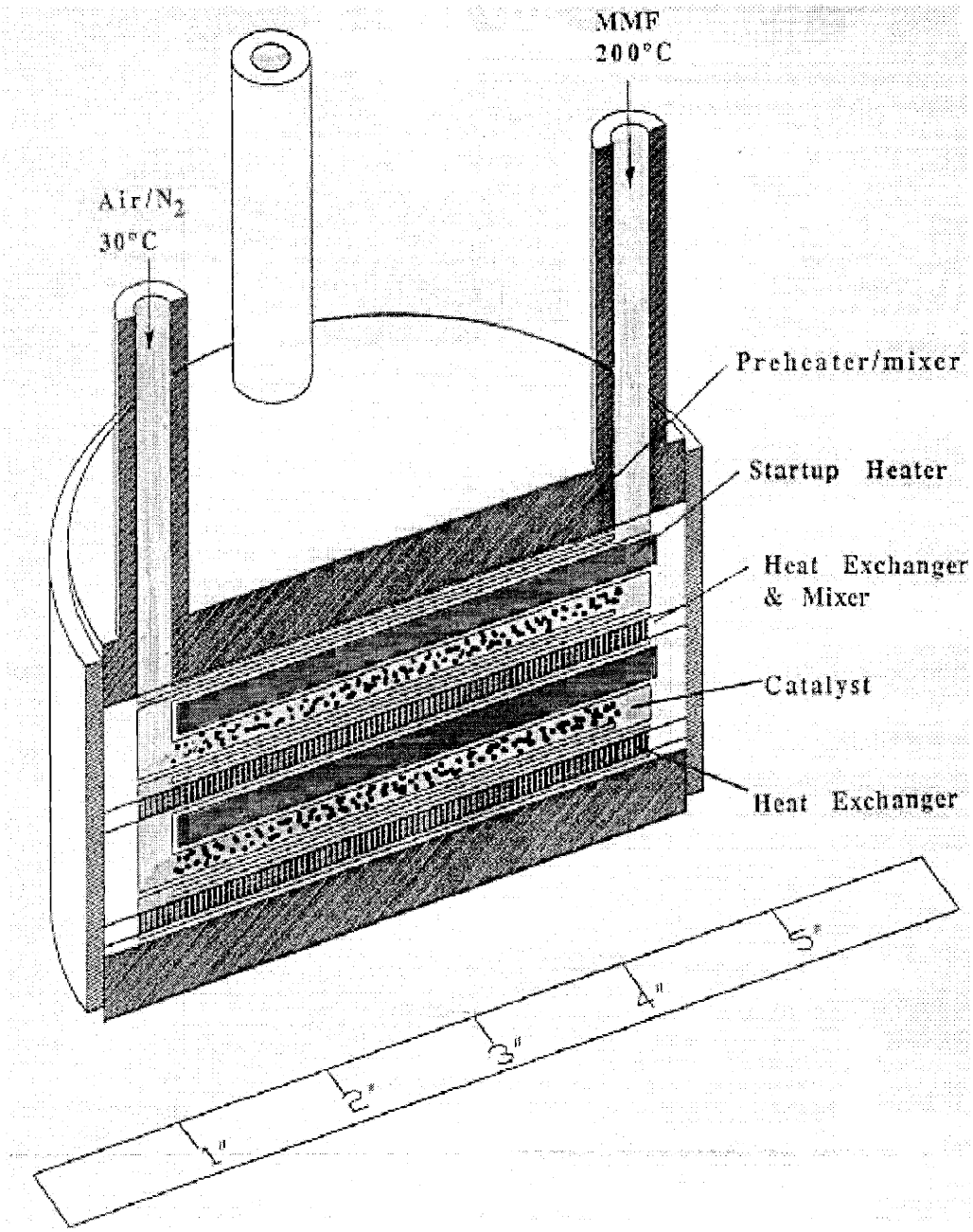

Figure 1-9. Methyl isocyanate microreactor concept from DuPont[75].

CRL and AstraZeneca have developed massively parallel microfluidic systems for extraction using micro-contactors[76]. As a first step they developed a device that connected

ten of the CRL 120 channel micro-contactor devices in parallel. This system operated at a flow rate of approximately 10 ml/hour of both aqueous and organic phases. Subsequently, they developed a high throughput unit that incorporates 50 of the CRL 120 channel micro-contactors. The design of this system placed a greater emphasis on maintainability and flexibility. Standard fittings were used to connect the individual micro-contactor arrays into a sub-assembly of five arrays. The sub-assemblies were based on a polypropylene frame that incorporated the liquid distribution manifold for the system. Liquids to the system were gravity fed, and it was capable of handling aqueous and organic phase inputs at approximately 250 ml/hour each. Their system was tested using 3-hydroxy-nitrobenzoic acid transfer from ethyl acetate to aqueous sodium carbonate. Although the fluid manifold developed in this work was impressive, the system control and automation still needs development, and this is the subject of present work.

Pacific Northwest National Laboratories is also developing microreaction/microfluidic systems for chemical production[77]. A primary focus for their effort is the portable production of hydrogen for use in fuel cells[47]. In this area, they are working on systems for both man portable and automotive applications. Although they have built and tested many of the system components, no work has been published on component integration and system control.

Even more impressive is their effort in collaboration with NASA to develop a miniature chemical plant for in-situ resource utilization on future Mars missions[78]. The goal of this program is to produce liquid fuels using the resources available on Mars and small amounts of materials transported for the mission. Their design, shown in Figure 1-10, will produce methane from hydrogen, which is transported to Mars, and carbon dioxide

available in the Martian atmosphere. In this case, microreaction technology may allow a substantial reduction in the weight of equipment and a corresponding savings in launch costs (it costs approximately $10,000/lb to place material in orbit). When completed, this would be the most complex microreaction system built to-date and fulfill Benson and Ponton's vision of a completely autonomous mini-chemical plant[5]. The problems associated with its construction are sizeable considering the forces the system must sustain during launch and landing. Even more challenging is that it must run completely unattended for its designed operating time of 330 days.

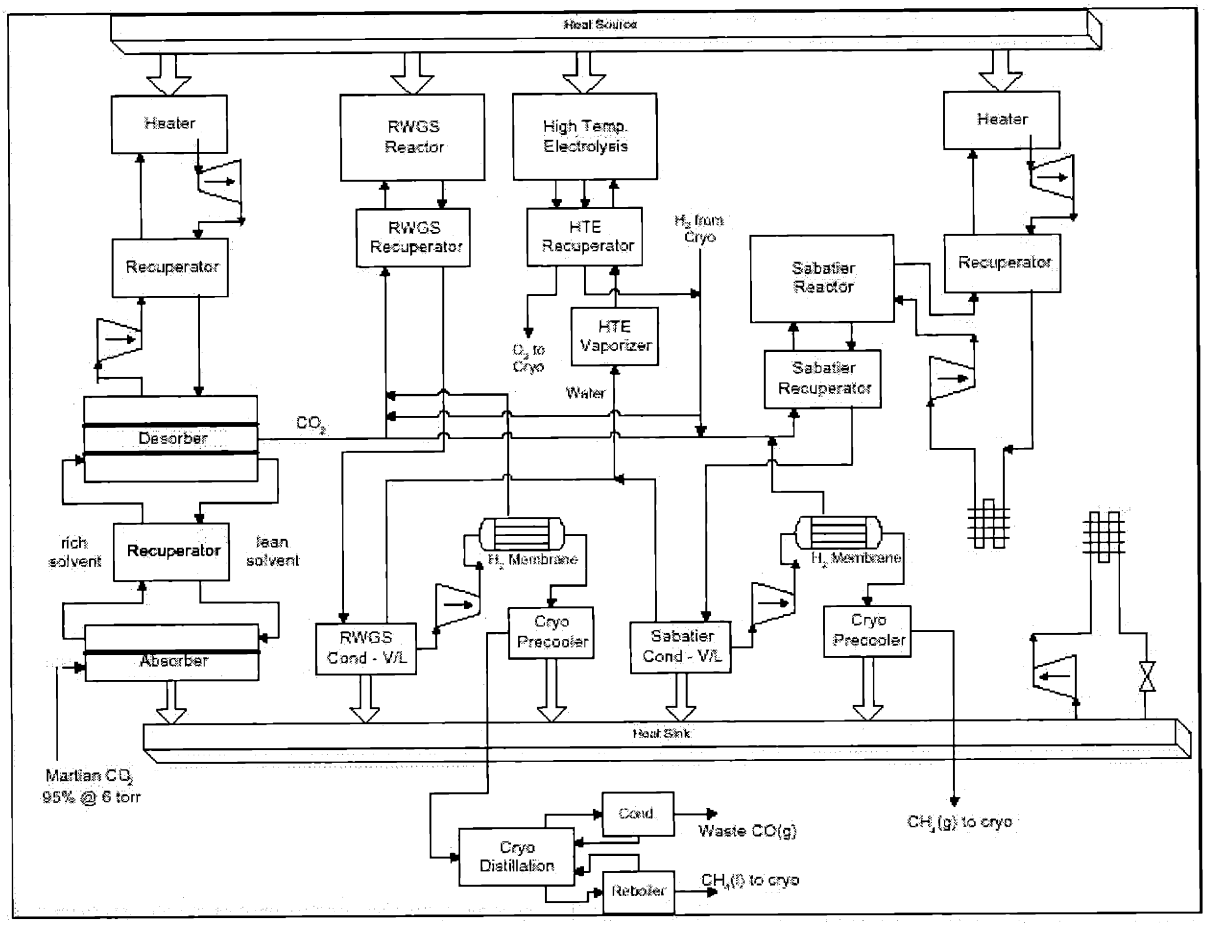

Figure 1-10. Block diagram of a miniature chemical plant designed by PNNL for in-situ resource utilization in future Mars missions[78].

The IMM has begun to address the problem of integrating microreactors with other components for commercial systems. Already, a large number of their microfluidic devices are available for sale[79]. Commercial use of these devices has mainly been limited to replacement of conventional components due to improved performance through the use of micro-scale devices[36,37]. However, recent work has developed components for systems that can be assembled in either stacked or planar configurations.

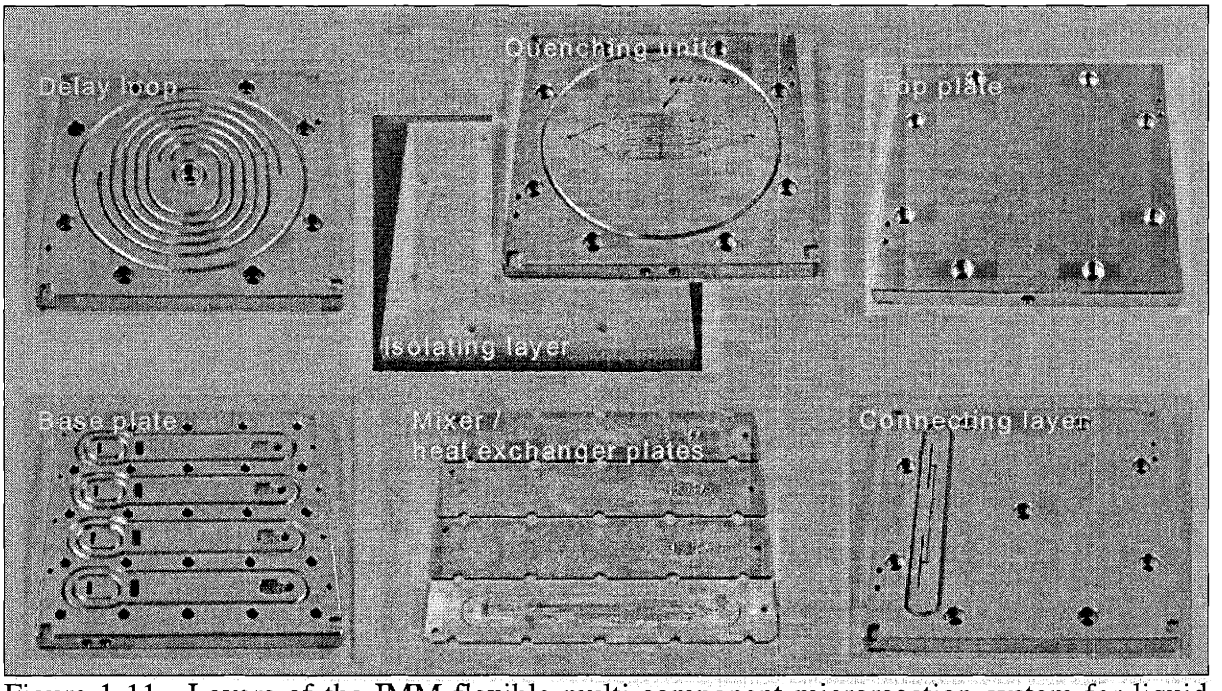

Figure 1-11. Layers of the IMM flexible multi-component microreaction system for liquid phase reactions[81].

The stacked microreactor systems, designed for liquid-liquid phase reactions, consist of fluid supply layers, reactor layers, delay layers, and quenching layers[80,81]. Figure 1-11 shows examples of different layers used in the system. The reactor layer has an integrated heat exchanger to remove or provide heat for the reaction. There are also thermocouple wells in this layer to monitor the reaction temperature in eight different locations. The system architecture allows for easy exchange, addition, or removal of components as desired. This

design addresses the problem of fluidic interconnection through vias machined in the individual layers. The throughput of the system can be adjusted by selecting reactor layers with differing number of reaction channels operating in parallel (8, 16 or 24). The method of sealing between layers has not been discussed in the literature, but it probably uses pressure in combination with a gasket or o-ring. They also have not discussed methods for parallel scale-up through the connection of multiple units and control systems.

The IMM has also developed a modular microreactor system that connects components in a planar configuration. Figure 1-12 shows a schematic of the concept of this system in which modules are readily connected to each other to form a system. This idea is realized by placing each module in a standard housing that has hook-type of connectors on the inlet and outlet, as shown in Figure 1-13. This provides a flexible and quick method to connect various modules. The hooks on the housing mate the two adjacent modules and an o-ring seal between the modules assures integrity of the connection. The advantage of this method is that microfluidic devices only need to be designed once so that they can be inserted into a standard housing. An entirely new system can be configured using the various modules very easily. An adapter plate with a hook fitting on one end, and conventional tube fittings on the other end provide connection with conventional fluidic equipment. These components could be easily connected to a manifold for parallel scale-up that was equipped with these hook connectors. The problem of analyzing individual reactor performance of such a system still remains if many devices are used simultaneously. Also it is not clear how individual components in such a system could be controlled to obtain maximum performance for the entire system.

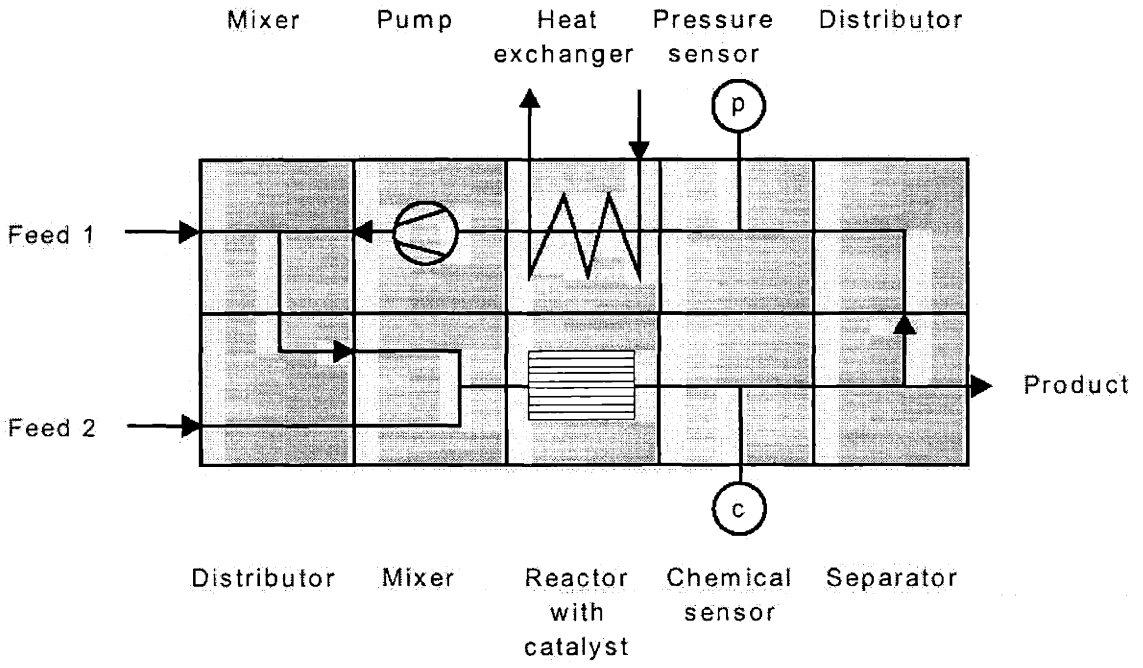

Figure 1-12. IMM concept of a modular microreactor system[81].

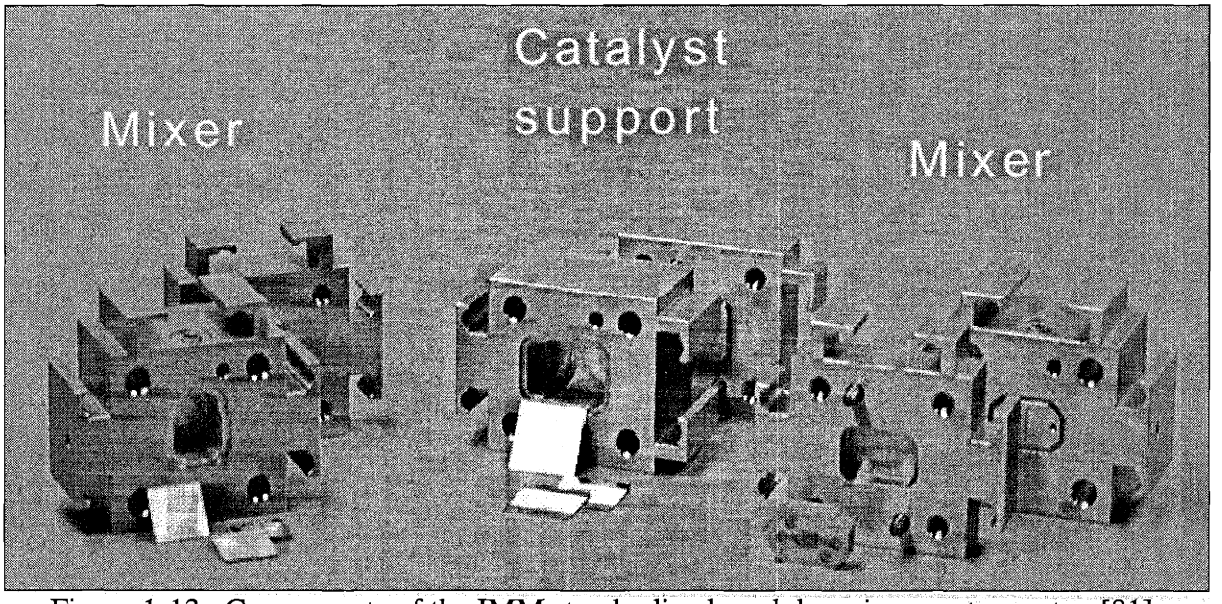

Figure 1-13. Components of the IMM standardized modular microreactor system[81].

Cellular Process Chemistry (CPC) is the first company to actively market integrated microreaction devices that can operate as a standalone system[82]. Their SELECTO™ unit, shown in Figure 1-14, is comprised of three modules: a pumping module, a reaction module,

and a residence time module. It is designed for liquid-liquid reactions and is capable of handling a temperature range from –70°C to 230°C. Flow rates can be varied from 0.1 ml/min to 20.0 ml/min. SELECTO™ has been tested with a number of different liquid-liquid phase chemistries to verify its performance[41].

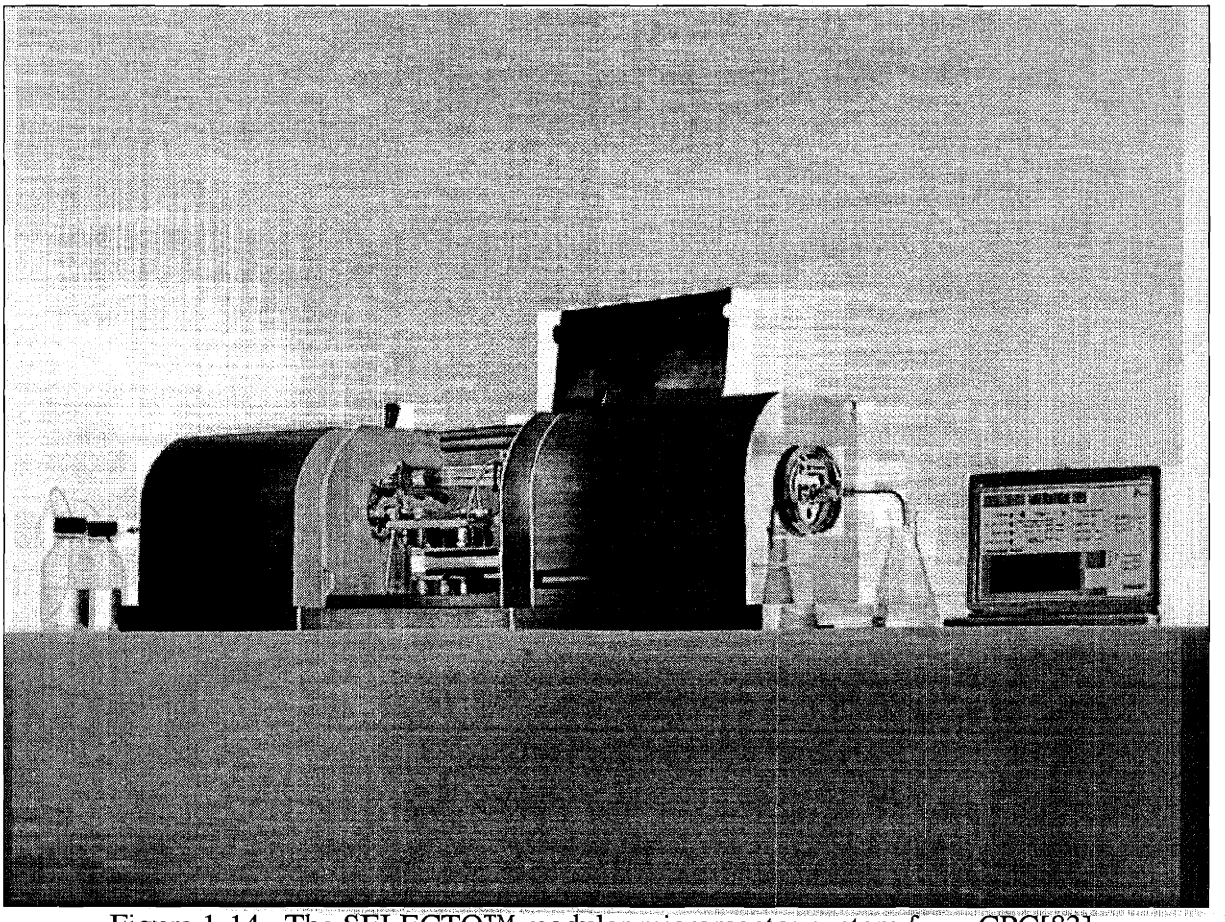

Figure 1-14. The SELECTO™ modular microreactor system from CPC[83].

The pumping module, shown in Figure 1-15, is used to transport reactants that are stored external to the system to the reaction module. It allows for the metering of reagents to the system and contains pressure sensors to monitor the process. The components used in this module are conventional in design, and plastic tubing with standard fittings are used to

connect the components. The pumping control and pressure sensing electronics are contained within the module.

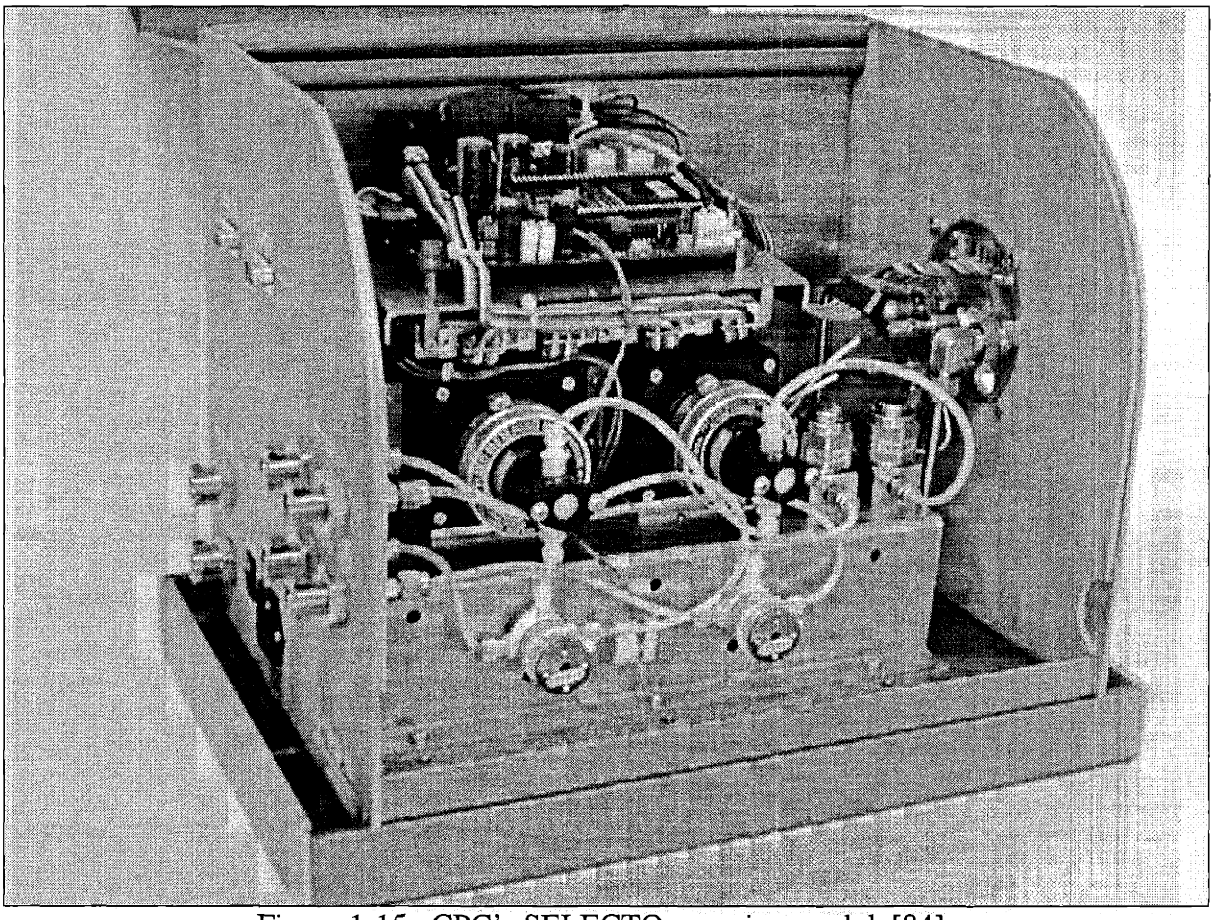

Figure 1-15. CPC's SELECTO pumping module[84].

The SELECTO™ reaction module, shown in Figure 1-16, contains a CYTOS™ reactor that can be easily interchanged with another CYTOS™ unit. The reactor is a microstructured stainless steel stacked plate reactor that has an integrated heat exchanger. The total reactor volume is 1 ml, and the heat exchanger volume is 12 ml. The reaction temperature is controlled with the heat exchanger fluid. The CYTOS™ module is inserted and removed with a clamping mechanism. The method of fluidic interconnection to the

CYTOS™ module is not clear. Standard tubing and tube fittings are used elsewhere in the module for conveying fluids.

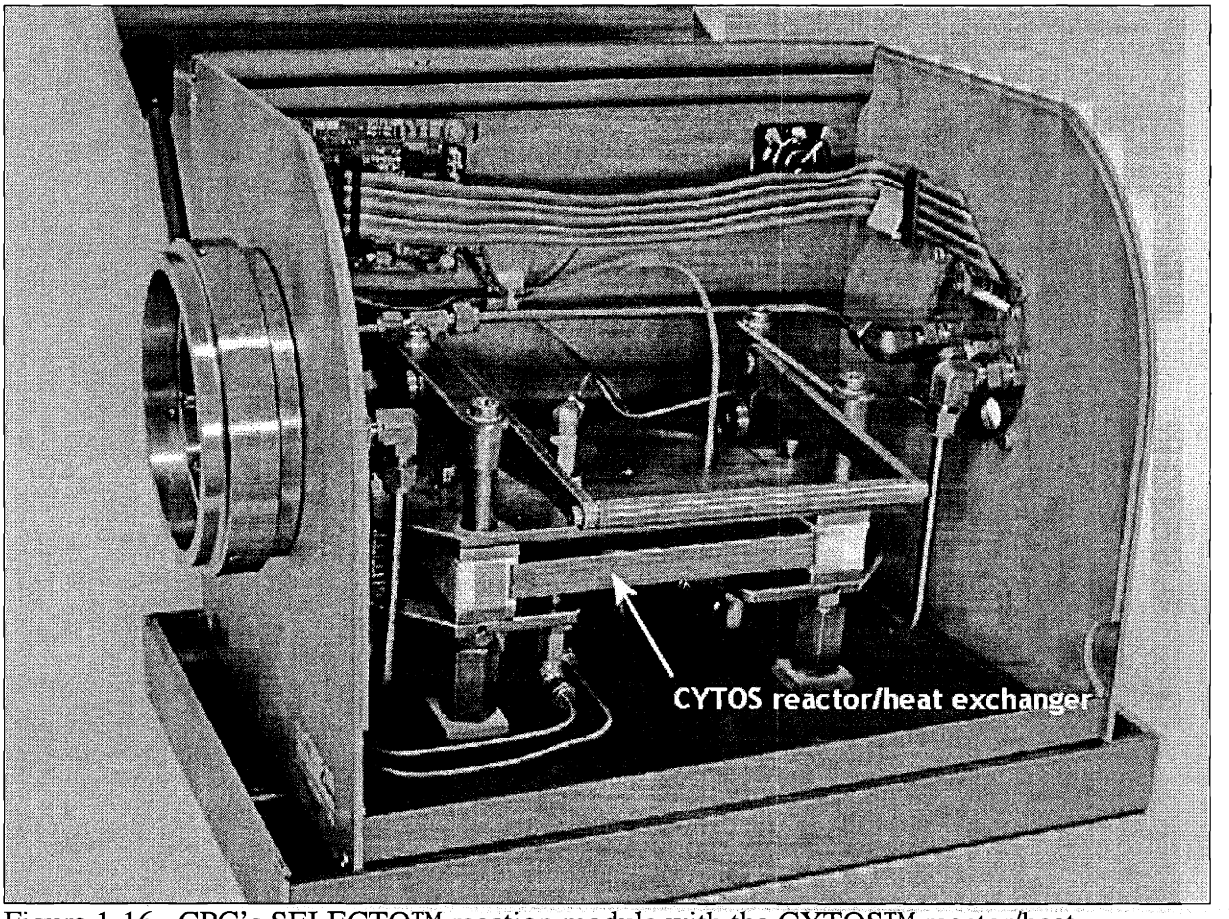

Figure 1-16. CPC's SELECTO™ reaction module with the CYTOS™ reactor/heat exchanger[84].

The mixed reactants are sent to the delay module, which is shown in Figure 1-17, where they are kept at controlled conditions for the reaction to continue to completion. The delay module is temperature controlled with the heat exchanger fluid, but the internal construction is not specified. The SELECTO™ unit is controlled using a computer interface. External fluidic connections are needed to supply reagents and handle products. Other connections are needed with a heat exchanger fluid that is at the proper temperature for reaction. Overall, the device is fairly simplistic with a low level of monitoring and control,

but this suffices for its purpose, which is to replace test tube synthesis for small quantities of chemicals.

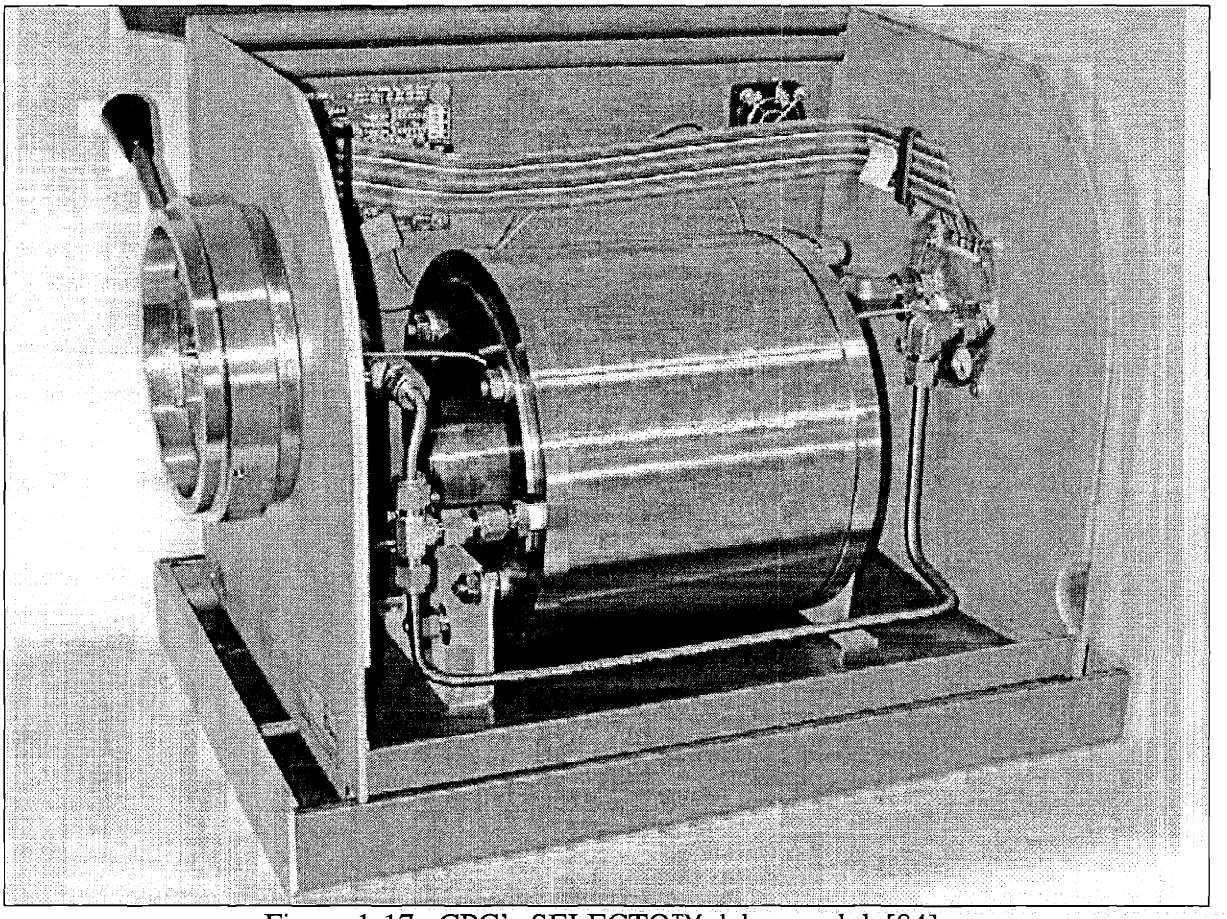

Figure 1-17. CPC's SELECTO™ delay module[84].

Thesis Objectives

A wide variation of microreactor designs have already been developed. However, the area of integrated microreactors into complex systems is relatively unexplored. Ease of scale-up has often been cited as a major advantage of microreaction technology, but no scale-up systems have been demonstrated to date. The idea that connecting reactors to operate in parallel is straightforward, but the challenge is in the details of such a design. A

multidisciplinary approach must be used combining the specialties of chemical, electrical, mechanical engineering, and computer science for such a system.

This thesis first addresses the problem of microreactor design through finite element modeling of microreactors. Particular attention is paid to the heat transfer characteristics of these systems. New microstructures are developed along with the evolution of older components. The simulations are ultimately used to develop a microreactor the can be incorporated into a parallel scale-up system. Finally, these models are then used again for understanding the operating behavior of these devices.

The main objective of this work was to build and demonstrate a scale-up microreaction system with integrated flow control, temperature control, and safety monitoring features. The purpose of building this system, also known as the Automated, Integrated Microreactor System (AIMS), was to identify challenges that face designers attempting microreactor scale-up and to then develop solutions. These challenges include the packaging of microreactors to handle numerous electrical and fluidic connections; methodology for making electrical and fluidic connections between devices in a scaleable fashion; and the development of a real-time control system for automated operation and safety monitoring.

Thesis Outline

The presentation of work is organized around the progression of development of the AIMS. Chapter 2 discusses the modeling techniques used to analyze microreactors and how they aided in new reactor designs. After this, the design of the scale-up microreactor is described along with its fabrication techniques. The chapter concludes with the testing procedures used after device fabrication. Chapter 3 focuses on the packaging method

developed for incorporating the microreactors into an integrated fluidic and electronic system. The various packaging alternatives considered are discussed along with the method finally selected. Testing of the implemented packaging method is then described in the closing.

The integration of the microreactors into a complete testing system is the subject of Chapter 4. Comparisons are made with conventional laboratory catalyst test stations used at DuPont. A detailed description of all of the mechanical and electrical components above the packaging level of the AIMS is given. The initial testing and debugging of the completed system is discussed in closing. Chapter 5 continues the theme of Chapter 4 but is dedicated to describing the control hardware and software assembled for the AIMS. The chapter concludes with a description of the debugging and validation methods used for the control system.

Chapter 6 gives a brief description of the Process Safety Management (PSM) techniques used to ensure safe operation of the AIMS. More detailed safety information on the AIMS along with its Standard Operating Procedures (SOP's) can be found in the Appendix. Chapter 7 describes the laboratory protocols used in testing the AIMS under reaction conditions. It also discusses the gas analysis methods implemented and how the reaction data was analyzed. Chapter 8 then documents the results of testing the AIMS with the methane oxidation and ammonia oxidation reactions. It also describes the problems encountered during testing, and closes with a discussion of how the operation of the AIMS compared with conventional laboratory catalyst test systems. Chapter 9 summarizes the work accomplished in this project and outlines areas that need focus for further development of integrated microreactor systems.

References

1. Bozdogan, K. (1989) "The transformation of the US chemicals industry", In *Working Papers of the MIT Commission on Industrial Productivity*, MIT Press, Cambridge, MA.

2. Slywotzky, A.J. (1995) *Value Migration: How to Think Several Moves Ahead of the Competition*, Havard Business School Press, Boston, MA.

3. Deshpande, P.B., Makker, S.L. and Goldstein, M. (1999) "Boost competitiveness via six sigma", *Chemical Engineering Progress,* Sept. 1999, pp. 65-70.

4. Deshpande, P.B. (1999) "Science, spirituality, and six sigma", *Reflections,* May 1999, pp. 1-4.

5. Benson, R.S. and Ponton, J.W. (1993) "Process miniaturization—a route to total environmental acceptability?", *Chemical Engineering Research and Design: Transactions of the Institution of Chemical Engineers,* **71, Part A**, pp. 160-168.

6. Keller, II.G.E. and Bryan, P.F. (1999) "Process engineering: moving in new directions", *Chemical Engineering Progress,* Jan. 2000, pp. 41-49.

7. Katzer, J.R., Ramage, M.P. and Sapre, A.V. (2000) "Petroleum refining: poised for profound changes", *Chemical Engineering Progress,* July 2000, pp. 41-51.

8. Hendershot, D.C. (1999) "Process minimization: making plants safer", *Chemical Engineering Progress,* Jan. 2000, pp. 35-40.

9. Stankiewicz, A.I. and Moulijn, J.A. (1999) "Process intensification: transforming chemical engineering", *Chemical Engineering Progress,* Jan. 2000, pp. 22-34.

10. Baltzer Science Publishers (1999) "Microreaction technology", *Industrial Catalysis News,* **99**(6), pp. 2-8.

11. Green, A., Johnson, B. and John, A. (1999) "Process magnifies profits", *Chemical Engineering,* Dec. 1999, pp. 66-76.

12. Shanley, A. (1997) "Microreactors find new niches", *Chemical Engineering,* Mar. 1997, p. 30.

13. Lerou, J.J., Harold, M.P., Ryley, J.F., Ashmead, J.W., O'Brien, T.C., Johnson, M., Perrotto, J., Blaisdell, C.T., Rensi, T.A., and Nyquist, J. (1996) "Microfabricated minichemical systems: technical feasibility", In *Microsystem Technology for Chemical and Biological Microreactors*, Presented at Workshop on Microsystem Technology, Feb. 20-21, 1995, Mainz, Germany, pp. 51-92.

14. Lerou, Jan J. (2000) Personal communication, Mountain View, CA, Aug. 30, 2000.

15. Ajmera, S.K., Losey, M.W., Jensen, K.F., and Schmidt, M.A. (2001) "Microfabricated packed-bed reactor for phosgene synthesis", *AIChE Journal,* **47**(7), pp. 1639-1647.

16. Ehrfeld, W., Hessel, V. and Löwe, H. (2000) *Microreactors: New Technology for Modern Chemistry*, Wiley-VCH, New York.

17. Hsing, I.M., Srinivasan, R., Harold, M.P., Jensen, K.F., and Schmidt, M.A. (2000) "Simulation of micromachined chemical reactors for heterogeneous partial oxidation reactions", *Chemical Engineering Science,* **55**, pp. 3-13.

18. Burns, J.R. and Ramshaw, C. (1999) "Development of a microreactor for chemical production", *Chemical Engineering Research and Design: Transactions of the Institution of Chemical Engineers,* **77, Part A**(3), pp. 206-211.

19. Becker, H., Heim, U., and Rötting, O. (2000) "Technologies for the microfabrication of microfluidic devices: the polymer foundry concept", Presented at IMRET 4: 4th International Conference on Microreaction Technology, Mar. 5-9, 2000, Atlanta, GA, pp. 425-431.

20. Becker, H. and Gärtner, C. (2000) "Polymer microfabrication methods for microfluidic analytical applications", *Electrophoresis,* **21**, pp. 12-26.

21. Niggemann, M., Ehrfeld, W., and Weber, L. (2000) "Micro molding of fluidic devices for biochemical applications", In Ehrfeld, W., (Ed.) *Microreaction Technology: Industrial Prospects*, Presented at IMRET 3: Third International Conference on Microreaction Technology, Apr. 18-21, 1999, Frankfurt, pp. 113-121.

22. Maluf, N. (2000) *An Introduction to Microelectromechanical Systems Engineering*, Artech House, Boston.

23. Losey, M.W., Isogai, S., Schmidt, M.A., and Jensen, K.F. (2000) "Microfabricated devices for multiphase catalytic processes", Presented at IMRET 4: 4th International Conference on Microreaction Technology, Mar. 5-9, 2000, Atlanta, GA, pp. 416-422.

24. Petersen, K.E. (1982) "Silicon as a mechanical material", *Proceedings of the IEEE,* **70**(5), pp. 420-457.

25. Ehrfeld, W., Hessel, V., Möbius, H., Richter, Th., and Russow, K. (1996) "Potentials and realization of microreactors", In *Microsystem Technology for Chemical and Biological Microreactors*, Presented at Workshop on Microsystem Technology, Feb. 20-21, 1995, Mainz, Germany, pp. 1-28.

26. Jäckel, K.P. (1996) "Microtechnology: application opportunities in the chemical industry", In *Microsystem Technology for Chemical and Biological Microreactors*, Presented at Workshop on Microsystem Technology, Feb. 20-21, 1995, Mainz, Germany, pp. 29-50.

27. Srinivasan, R., Hsing, I.-M., Berger, P.E., Jensen, K.F., Firebaugh, S.L., Schmidt, M.A., Harold, M.P., Lerou, J.J., and Ryley, J.F. (1997) "Micromachined reactors for catalytic partial oxidation reactions", *AIChE Journal,* **43**(11), pp. 3059-3069.

28. Hagendorf, U., Janicke, M., Schüth, F., Schubert, K., and Fichtner, M. (1998) "A Pt/Al_2O_3 coated microstructured reactor/heat exchanger for the controlled H_2/O_2-reaction in the explosion regime", Presented at Process Miniaturization: 2nd International Conference on Microreaction Technology, Mar. 9-12, 1998, New Orleans, pp. 81-87.

29. Jähnisch, K., Baerns, M., Hessel, V., Ehrfeld, W., Haverkamp, V., Löwe, H., and Wille, Ch.G.A. (2000) "Direct fluorination of toluene using elemental fluorine in gas/liquid microreactors", *Journal of Fluorine Chemistry,* **105**, pp. 117-128.

30. Janicke, M.T., Kestenbaum, H., Hagendorf, U., Schüth, F., Fichtner, M., and Schubert, K. (2000) "The controlled oxidation of hydrogen from an explosive mixture of gases using a microstructured reactor/heat exchanger and Pt/Al_2O_3 catalyst", *Journal of Catalysis,* **191**, pp. 282-293.

31. Hessel, V., Ehrfeld, W., Golbig, K., Haverkamp, V., Löwe, H., Storz, M., Wille, Ch., Guber, A.E., Jähnisch, K., and Baerns, M. (2000) "Gas/liquid microreactors for direct fluorination of aromatic compounds using elemental fluorine", In Ehrfeld, W., (Ed.) *Microreaction Technology: Industrial Prospects*, Presented at IMRET 3: Third International Conference on Microreaction Technology, April 18-21, 1999, Frankfurt, pp. 526-540.

32. Dyer, J.A. and Mulholland, K.L. (1998) "Follow this path to pollution prevention", *Chemical Engineering Progress,* Jan. 1998, pp. 34-42.

33. Dyer, J.A. and Mulholland, K.L. (1999) *Pollution Prevention: Methodology, Technologies, and Practices*, AIChE, New York.

34. Lovins, A.B., Lovins, L.H. and Hawken, P. (1999) "A road map for natural capitalism", *Harvard Business Review,* May 1999-June 30 1999, pp. 145-158.

35. Dyer, J.A., Mulholland, K.L. and Keller, R.A. (1999) "Prevent pollution in batch processes", *Chemical Engineering Progress,* May 1999, pp. 24-29.

36. Stoldt, J., Wurziger, H., Krummradt, H., Kopp, U., Hohmann, M., and Schwesinger, N. (2000) "Experiences with the use of microreactors in organic synthesis", In Ehrfeld, W., (Ed.) *Microreaction Technology: Industrial Prospects*, Presented at IMRET 3: Third International Conference on Microreaction Technology, April 18-21, 1999, Frankfurt, pp. 181-186.

37. Bayer, T., Pysall, D., and Wachsen, O. (2000) "Micro mixing effects in continuous radical polymerization", In Ehrfeld, W., (Ed.) *Microreaction Technology: Industrial Prospects*, Presented at IMRET 3: Third International Conference on Microreaction Technology, April 18-21, 1999, Frankfurt, pp. 165-170.

38. Kursawe, A. and Hönicke, D. (2000) "Epoxidation of ethene with pure oxygen as a model reaction for evaluating the performance of microchannel reactors", Presented at IMRET 4: 4th International Conference on Microreaction Technology, Mar. 5-9, 2000, Atlanta, GA, pp. 153-166.

39. Antes, J., Tuercke, T., Marioth, E., Schmid, K., Krause, H., and Loebbecke, S. (2000) "Use of microreactors for nitration processes", Presented at IMRET 4: 4th International Conference on Microreaction Technology, Mar. 5-9, 2000, Atlanta, GA, pp. 194-200.

40. Löwe, H. and Ehrfeld, W. (1999) "State-of-the-art in microreaction technology: concepts, manufacturing and applications", *Electrochimica Acta,* **44**, pp. 3679-3689.

41. Cellular Process Chemistry, Inc. "Sample reactions", http://www.cpc-net.com/reactions.shtml, (Mar. 29, 2001).

42. Ahn, C.H., Henderson, H.T., Halsall, H.B., Heineman, W.R., Helmicki, A.J., Nevin, J.H., Bhansali, S., and Schlueter, K.T. "A generic microfluidic system for remote bio/chemical sensors", http://www.mems.uc.edu/~cahn/research/ahn_a01.html, (Apr. 4, 2001).

43. Chambers, R.D. and Spink, R.C.H. (1999) "Microreactors for elemental fluorine", *Chemical Communications,* pp. 883-884.

44. Franz, A., Jensen, K.F., and Schmidt, M.A. (2000) "Palladium based micromembranes for hydrogen separation and hydrogenation/dehydrogenation reactions", In Ehrfeld, W., (Ed.) *Microreaction Technology: Industrial Prospects*, Presented at IMRET 3: Third International Conference on Microreaction Technology, Apr. 18-21, 1999, Frankfurt, pp. 171-180.

45. Quiram, D.J., Jensen, K.F., Schmidt, M.A., Mills, P.L., Ryley, J.F. and Wetzel, M.D. "Integrated microchemical systems: opportunities for process design", In *FOCAPD '99 Computer-Aided Design for the 21st Century*, Presented at 5th International Conference on Foundations of Computer-Aided Process Design, July 18-23, 1999, Breckenridge, CO.

46. Lerou, J.J. and Ng, K.M. (1996) "Chemical reaction engineering: a multiscale approach to a multiobjective task", *Chemical Engineering Science,* **51**(10), pp. 1595-1614.

47. Daymo, E.A., VanderWiel, D.P., Fitzgerald, S.P., Wang, Y., Rozmiarek, R.T., LaMont, M.J., and Tonkovich, A.Y. (2000) "Microchannel fuel processing for man portable power", Presented at IMRET 4: 4th International Conference on Microreaction Technology, Atlanta, GA, pp. 364-369.

48. Lohf, A., Ehrfeld, W., Hessel, V., and Löwe, H. (2000) "A standardized modular microreactor system", Presented at IMRET 4: 4th International Conference on Microreaction Technology, Atlanta, GA, pp. 441-451.

49. Jensen, K.F. (2001) "Microreaction engineering -- is smaller better?", *Chemical Engineering Science,* **56**, pp. 293-303.

50. Haswell, S.J. and Skelton, V. (2000) "Chemical and biochemical microreactors", *Trends in Analytical Chemistry,* **19**(6), pp. 389-395.

51. (2000) In van den Berg, A., Olthuis, W. and Bergveld, P., (Eds.) *Micro Total Analysis Systems 2000*, Presented at μTAS 2000 Symposium, May 14-18, 2000, Enschede, The Netherlands.

52. Frye-Mason, G., Kottenstette, R., Lewis, P., Heller, E., Manginell, R., Adkins, D., Dulleck, G., Martinez, D., Sasaki, D., Mowry, C., Matzke, C., and Anderson, L. "Hand-held miniature chemical analysis system (μChemLab) for detection of trace concentrations of gas phase analytes", In van den Berg, A., Olthuis, W. and Bergveld, P., (Eds.) *Micro Total Analysis Systems 2000*, Presented at μTAS 2000 Symposium, May 14-18, 2000, Enschede, The Netherlands, pp. 229-232.

53. Singer, N. (1998) "'Lab-on-a-chip' efforts show progress", *Sandia LabNews,* Jan. 16 1998,

54. Nighswonger, G. (1999) "Micromachines: a big future for small devices", *Medical Device & Diagnostic Industry,* Nov. 1999,

55. Lin, Y., Matson, D.W., Bennett, W.D., Thrall, K.D., and Timchalk, C. "Integrated microfluidics/electrochemical sensor system for field-monitoring of toxic metals", In Ehrfeld, W., (Ed.) *Microreaction Technology: Industrial Propects*, Presented at IMRET 3: Third International Conference on Microreaction Technology, April 18-21, 1999, Frankfurt, Germany, pp. 588-596.

56. Matson, D.W., Martin, P.M., Bennett, W.D., Johnston, J.W., Stewart, D.C., and Bonham, C.C. (2000) "Sputtered coatings for microfluidic applications", *Journal of Vacuum Science & Technology, A,* **18**(4), pp. 1998-2002.

57. Martin, P.M., Matson, D.W., Bennett, W.D., Lin, Y., and Hammerstrom, D.J. (1999) "Laminated plastic microfluidic components for biological and chemical systems", *Journal of Vacuum Science & Technology, A,* **17**(4), p. 2264--2269

58. Richter, M., Prak, A., Naundorf, J., Eberl, M., Leeuwis, H., Woias, P., and Steckenborn, A. (1997) "A chemical microanalysis system as a microfluid system demonstrator", In *Proceedings of Transducers 97, 9th International Conference on Solid-State Sensors and Actuators*, Presented at Chicago, pp. 303-306.

59. van den Berg, A. and Lammerink, T.S.J. (1998) "Micro total analysis systems: microfluidic aspects, integration concept and applications", In Manz, A. and Becker, H., (Eds.), *Microsystem Technology in Chemistry and Life Sciences*, Springer, New York, pp. 21-49.

60. Schabmueller, C.G.J., Koch, M., Evans, A.G.R., and Brunnschweiler, A. (1999) "Design and fabrication of a microfluidic circuitboard", *Journal of Micromechanics and Microengineering,* **9**(2), pp. 176-179.

61. Koch, M., Schabmueller, C.G.J., Evans, A.G.R., and Brunnschweiler, A. (1999) "Micromachined chemical reaction system", *Sensors and Actuators A,* **74**, pp. 207-210.

62. Choi, J.-W., Wijayawardhana, A., Okulan, N., Oh, K.W., Han, A., Bhansali, S., Govind, V., Schlueter, K.T., Heineman, W.R., Halsall, H.B., Nevin, J.H., Helmicki, A.J., Henderson, H.T., and Ahn, C.H. "Development and characterization of a generic microfluidic subsystem toward portable biochemical detection", In van den Berg, A., Olthuis, W. and Bergveld, P., (Eds.) *Micro Total Analysis Systems 2000*, Presented at μTAS 2000 Symposium, May 14-18, 2000, Enschede, The Netherlands, pp. 327-330.

63. Puntambekar, A. and Ahn, C.H. "Self-aligning microfluidic interconnects with low dead volume", In van den Berg, A., Olthuis, W. and Bergveld, P., (Eds.) *Micro Total Analysis Systems 2000*, Presented at μTAS 2000 Symposium, May 14-18, 2000, Enschede, The Netherlands, pp. 323-326.

64. Bergh, H.S., Cong, P., Engstrom, J.R., Guan, S., Hagemeyer, A., Liu, Y., Lugmair, C., Markov, V., Self, K., Turner, H., Van Erden, L., and Weinberg, W.H. "High-throughput screening of combinatorial heterogeneous catalyst libraries", Presented at IMRET 4: 4th International Conference on Microreaction Technology, Mar. 5-9, 2000, Atlanta, GA.

65. Lukas, S. (2000) "Development of MEMS", *R&D Magazine,* June 2000, p. 11.

66. González, C., Maslana, G., Olson, J., and Pan, J. "Miniature tools for combinatorial chemistry", In van den Berg, A., Olthuis, W. and Bergveld, P., (Eds.) *Micro Total Analysis Systems 2000*, Presented at μTAS 2000 Symposium, May 14-18, 2000, Enschede, The Netherlands, pp. 63-66.

67. Monaghan, P.B., Manz, A., and Nichols, W.W. "Microbiology on-a-chip", In van den Berg, A., Olthuis, W. and Bergveld, P., (Eds.) *Micro Total Analysis Systems 2000*, Presented at μTAS 2000 Symposium, Enschede, The Netherlands, pp. 111-114.

68. Skelton, V., Greenway, G., Haswell, S., Styring, P., Morgan, D., Warrington, B., and Wong, S. "The design of a continuous flow combinatorial screening micro reactor system with on-chip detection", In van den Berg, A., Olthuis, W. and Bergveld, P., (Eds.) *Micro Total Analysis Systems 2000*, Presented at μTAS 2000 Symposium, May 14-18, 2000, Enschede, The Netherlands, pp. 59-62.

69. Kopf-Sih, A.R. "Commercializing lab-on-a-chip technology", In van den Berg, A., Olthuis, W. and Bergveld, P., (Eds.) *Micro Total Analysis Systems 2000*, Presented at μTAS 2000 Symposium, May 14-18, 2000, Enschede, The Netherlands, pp. 233-238.

70. Boone, T.D., Ricco, A.J., Gooding, P., Björnson, T.O., Singh, S., Xiao, V., Gibbons, I., Williams, S.J., and Tan, H. "Sub-microliter assays and DNA analysis on plastic microfluidics", In van den Berg, A., Olthuis, W. and Bergveld, P., (Eds.) *Micro Total Analysis Systems 2000*, Presented at μTAS 2000 Symposium, May 14-18, 2000, Enschede, The Netherlands, pp. 541-544.

71. Levine, A.W., Cherukuri, S.C., and Matey, J.R. of Sarnoff Corporation, (1999) "System for liquid distribution", USA, Patent #5,958,344.

72. Ramsey, J.M. of Lockheed Martin Energy Research Corporation, (1999) "Apparatus and method for performing microfluidic manipulations for chemical analysis and synthesis", USA, Patent #5,858,195.

73. Orchid BioSciences, Inc. "Orchid's Technologies", www.orchid.com, (Apr. 5, 2001).

74. Swenson, R.E. (1999) "Recent results of chemical synthesis on a microfluidic chip", Presented at Microchemical Systems and Their Applications, June 16-18, 1999, Reston, VA.

75. Ryley, J.F. (1999) "Microchemical system applications - DuPont experience", Presented at Microchemical Systems and Their Applications, June 16-18, 1999, Reston, VA.

76. Shaw, J., Nudd, R., Naik, B., Turner, C., Rudge, D., Benson, M., and Garman, A. "Liquid/liquid extraction systems using microcontactor arrays", In van den Berg, A., Olthuis, W. and Bergveld, P., (Eds.) *Micro Total Analysis Systems 2000*, Presented at μTAS 2000 Symposium, May 14-18, 2000, Enschede, The Netherlands, pp. 371-374.

77. Brenchley, D.L., Wegeng, R.S., and Drost, M.K. (2000) "Development of micro-chemical and thermal systems", Presented at IMRET 4: 4th International Conference on Microreaction Technology, Mar. 5-9, 2000, Atlanta, GA, pp. 322-326.

78. TeGrotenhuis, W.E., Wegeng, R.S., Vanderwiel, D.P., Whyatt, G.A., Viswanathan, V.V., Schielke, K.P., Sanders, G.B., and Peters, T.A. (2000) "Microreactor system design for NASA in situ propellant production plant on MARS", Presented at IMRET 4: 4th International Conference on Microreaction Technology, Mar. 5-9, 2000, Atlanta, GA, pp. 343-348.

79. Institut für Mikrotechnik Mainz "Institut für Mikrotechnik Mainz Homepage", http://www.imm-mainz.de/, (Apr. 8, 2001).

80. Richter, Th., Ehrfeld, W., Hessel, V., Löwe, H., Storz, M., and Wolf, A. (2000) "A flexible multi-component microreaction system for liquid phase reactions", In Ehrfeld, W., (Ed.) *Microreaction Technology: Industrial Prospects*, Presented at IMRET 3: Third International Conference on Microreaction Technology, Apr. 18-21, 1999, Frankfurt, pp. 636-644.

81. Ehrfeld, W. (1999) "Microreactor components and systems - basic properties, fabrication methods, and commercial applications", Presented at Microchemical Systems and Their Applications, June 16-18, 1999, Reston, VA.

82. Cellular Process Chemistry, Inc. "Homepage", http://www.cpc-net.com/, (Mar. 29, 2001).

83. Cellular Process Chemistry, Inc. "SELECTO™", http://www.cpc-net.com/selecto.shtml, (Mar. 29, 2001).

84. Cellular Process Chemistry, Inc. "Modules of SELECTO™", http://www.cpc-net.com/modules.shtml, (Mar. 29, 2001).

CHAPTER 2
SCALE-UP MICROREACTOR DEVELOPMENT

The major difficulties in designing microfabricated devices are the lack of both experience and modeling tools for system development. A microfabricated device is typically constructed using information derived from past experience, engineering analysis, and literature searches. In some cases, detailed simulation tools can be used, but they are not universally applicable. CoventorWare™[1] is an example of one popular software package for the design of MEMS. It includes the capability to model moving structures, electromagnetic fields, heat transfer, and fluid flow in one package. However, no effort is currently being placed on solving single or multi-phase reacting flows since Coventor's target microfluidic consumers are biotechnology companies. On the other hand, other software more commonly used for chemical reactor design, such as CFD-ACE+[2] and Fluent[3], can be used for simulating reactive flows on the micro-scale. This remains a difficult problem to solve though on even the most current simulators if there is a high degree of coupling between the governing equations of momentum, heat, and mass transfer.

For these reasons, it was decided to make only small modifications to the previous T microreactor designs rather than to begin with an entirely new concept. These modifications were such that detailed analysis could be performed on their effect using simulation tools

---

[1] CoventorWare™ is the new name for the software that replaces MEMCAD and FlumeCAD. CoventorWare™ is a product of Coventor, Inc., 4001 Weston Parkway, Cary, NC 27513, (919) 854-7500.

[2] CFD-ACE+ is a product of CFD Research Corporation, 215 Wynn Dr., Huntsville, AL 35805, (256) 726-4800.

before the microreactor was even built. This avoided going through several design iterations to develop a microreactor that could be incorporated into a scale-up system. A fast development time for the microreactor was important for the project since the electrical and fluidic packaging depended on the microreactor design and the packaging would also dictate some key features of the microreactor.

T Microreactor Description

At the beginning of this project, the Jensen research group had previously demonstrated a prototype microreactor, which was referred to as the T reactor. It consisted of two inlet flow channels with flow sensors and a reaction channel with local heating and temperature sensing devices[1,2]. Figure 2-1 shows the top and cross-sectional views of this microreactor. The branches of the T structure are the feed channels, which have integrated flow sensors. The gas feeds contact each other at the center of the T, and the reaction takes place down the length of the main channel in the catalyst region. The channels are nominally 0.5 mm wide and 0.5 mm deep, and they are sealed on top by a 1 μm thick silicon nitride membrane (this membrane is impermeable to gas flow). The channels are sealed from the bottom by an aluminum plate, which is epoxied to the reactor die. Gas enters and exits the microreactor from holes that are drilled into the aluminum sealing plate. The microreactor is fabricated starting with a single-crystal silicon wafer using photolithography and etching techniques to define the channel structures and metal layers. Srinivasan[1] has previously given a more in-depth description of the design procedure, physical characteristics, and the fabrication method of the T reactor[2].

---

[3] Fluent is a product of Fluent, Inc., 10 Cavendish Ct., Centerra Park Lebanon, NH 03766, (603) 643-2600.

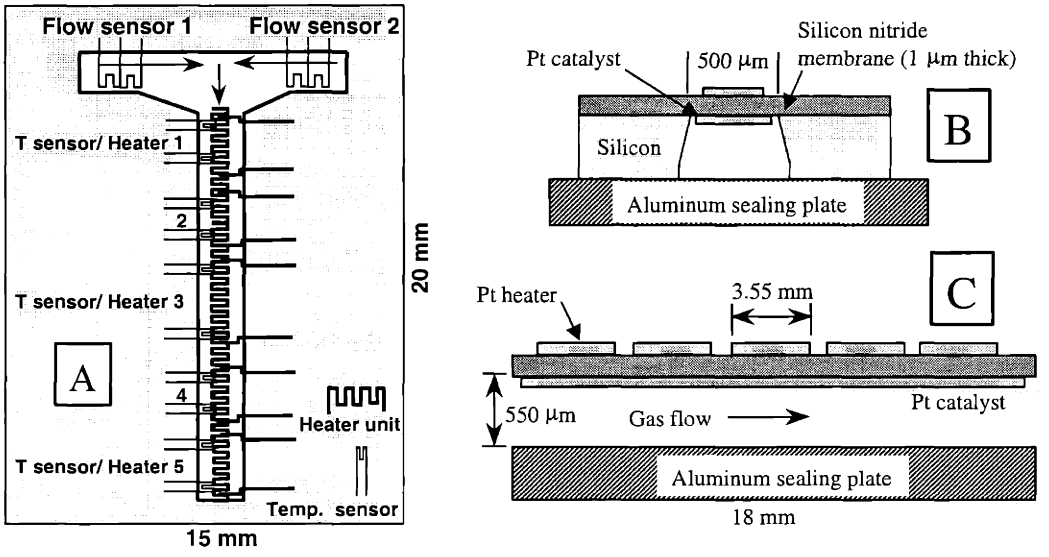

Figure 2-1. Schematic of the T microreactor: (A) Top view; (B) Cross-section perpendicular to flow; (C) Cross-section parallel to flow.

The reaction channel has platinum heaters and temperature sensors on the outer side of the membrane and a platinum catalyst on the channel side. There are five heater segments over the reaction channel and two flow sensors over the inlet channels. The heater segments are 3.55 mm in length and 0.3 mm wide, and they are centered in the channel. Each segment has one temperature sensor located on the upstream end and one located on the downstream end. These structures are made using photolithography techniques to define the shape and Physical Vapor Deposition (PVD) to form the platinum layer.

Microreactor Modeling

The analysis of modifications for the scale-up microreactor was simplified since a simulation methodology had already been developed to understand the original T microreactor[3,4]. Fortunately, the gas phase microreactor's small dimensions create laminar flow fields making modeling easier. Typically, reactions are operated with a flow rate of 10-20 cm^3/min at standard conditions (sccm), and this results in Reynolds numbers between 10

and 50, depending on the gas and the reactor temperature. Since the flow is typically in the laminar regime, models for approximating turbulence are not needed. Moreover, for the flow rates on the lower end, diffusive processes dominate convective processes, which causes the governing equations to be strongly elliptic rather than hyperbolic. The modeling is also simplified by the use of a thin-film catalyst in the T microreactor, which avoids the approximations for heat and mass transfer that are necessary in modeling packed bed reactors. In these cases, the inclusion of simplified lumped parameter approximations make it difficult to predict the performance of a new design when reactor data on a similar design is not available.

Unfortunately, the characteristics of microreactors highlight new problems that are infrequently encountered in traditional reactor modeling. For example, in modeling the T microreactor the length scales of important features vary widely from ~ 0.5 mm (channel width/depth) to 0.0001 mm (platinum layer thickness). Another problem found in modeling reacting flows for the T reactor is the extremely broad temperature range inside the reaction channel (from 125°C to 500°C for ammonia oxidation). This requires a robust kinetic model of the system of interest, which is difficult to find since most kinetic data is taken over a relatively small range of temperatures. The traditional problems present in modeling full size reactors are also encountered in these systems. Specifically, the species, momentum, and energy balances are strongly coupled for systems with highly exothermic or endothermic reactions. For example, past work in modeling and experiments have shown ignition/extinction behavior in the T microreactor for ammonia oxidation[1-5]. Further aspects of microreactor modeling are provided below.

Model Description

The simulation models developed are based on the conservation equations present in all chemical reactor analysis: mass, momentum, energy, and species. A detailed description of these equations and the boundary conditions used in the problem formulation can be found in the works by Hsing[3,4]. The general issues in developing numerical solvers for reacting flow models are the choice of numerical scheme used for discretization; the solution technique used for the resulting sets of nonlinear algebraic equations obtained; and the techniques used to detect and solve complicating aspects, such as multiple steady states.

The Galerkin Finite Element Method (GFEM) approach was chosen for the discretization of the conservation equations due to its broad generality and its excellent convergence properties in handling elliptic problems. As part of the discretization process, the physical domain of the system must be transformed into a computational domain via a mesh. A commercial mesh generator, ICEM CFD[4], is used to convert a CAD drawing of the microreactor into a discretized mesh. The boundary conditions for the mesh are then added using a preprocessor. This makes the simulation tools completely general in their applicability to microreactors with differing geometries.

Newton's method is used to solve the large set of nonlinear algebraic equations generated by the discretization procedure. Each Newton iteration, in turn, produces a sparse set of linear equations that are solved using a frontal algorithm[6]. Although Newton's method has a quadratic convergence property, the initial guess must be sufficiently close to the real solution for convergence. This becomes difficult for the highly nonlinear behavior exhibited by reaction systems that display ignition/extinction behavior. To address this

[4] ICEM CFD/CAE is a product of PTC, 140 Kendrick St., Needham, MA 02494, (781) 370-5000.

problem, Keller's pseudo-arc length continuation scheme was used to trace the solution branches around the limit points of the ignition/extinction S curve[7,8]. Other numerical problems also arise when the element mass transfer Peclet numbers become greater than one so that the problem is convection dominated, which causes the governing equations to become hyperbolic. To retain the convergence properties of the GFEM approach, the Brooks-Hughes Streamline Upwind Petrov-Galerkin (SUPG) scheme was implemented[9]. More details concerning the numerical issues involved in microreactor simulation have been given previously[3,4].

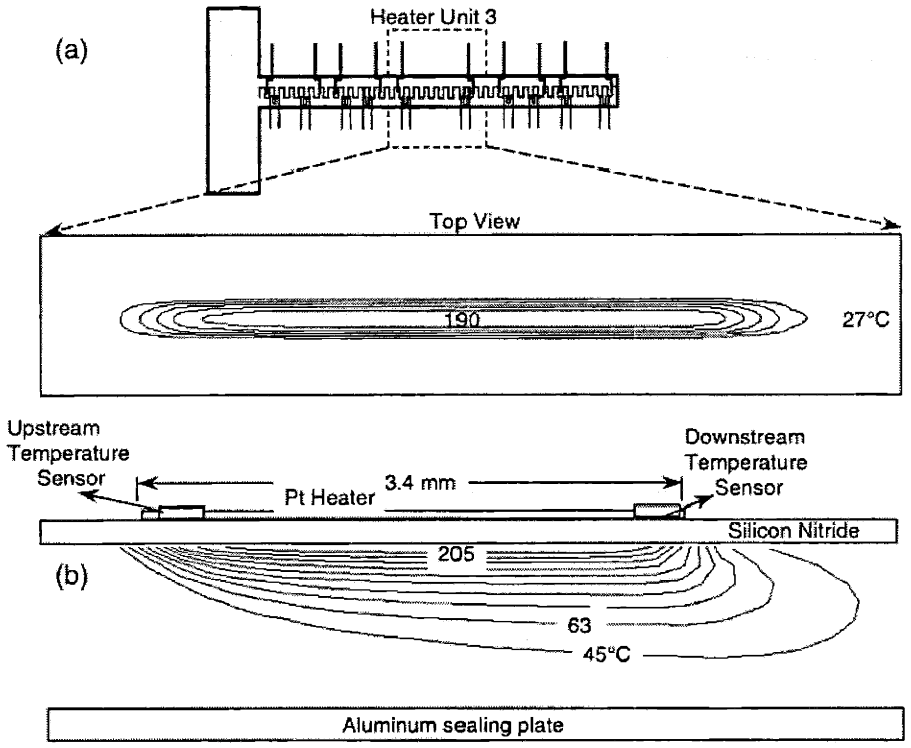

Figure 2-2. Temperature isotherms around the third heater segment on the silicon nitride membrane with a flow rate of 25 sccm of oxygen. (a) Top view (b) Cross section through the flow channel[3].

Thermal Modeling

The first use of this model was to understand the temperature profiles in the T microreactor. It demonstrated the extremely localized heating produced by the microfabricated resistive heating devices, as shown in Figure 2-2[3]. To validate the model, temperature measurements were taken in the heated region for a range of gas flow rates (Re < 150) and heater powers. These measurements were successfully reproduced in the simulation results[1,3,4].

Prediction of Bifurcation Behavior

Although predicting the reactor temperature profile is important, the simulations are more valuable if they successfully model reactor operation. Thus, an attempt was made to reproduce the experimentally observed ignition/extinction behavior, which occurs for fast, highly exothermic reactions, such as ammonia oxidation[1,2]. Bifurcation behavior is exhibited because of the limited rate of heat removal to the surrounding atmosphere and through the silicon nitride membrane. Although a simple 1-D heat transfer analysis can be used to qualitatively predict bifurcation behavior in the T microreactor, the experimentally observed behavior was too complex for this analysis. During a partial oxidation reaction, ignition occurred near the end of the heater segment and the ignition front then moved to the beginning of the heater segment. This was visually observable since high temperatures cause the membrane to buckle creating dark spots on the microreactor membrane[1,2].

This phenomenon was modeled by first starting with a low heater power in the simulation; continuing with this parameter until ignition was first observed; and then increasing the heater power to track the movement of the reaction front. The model showed that ignition first occurred at the downstream end of the heater segment and moved to the

upstream end as more power was added[3,4]. This also suggested that increasing the rate of heat removal from the reaction zone could eliminate the presence of multiple steady states.

Simulations as a Design Tool

The success of the model in reproducing experimental results led to its use as a tool for studying the effect of reactor design changes. This was first applied to studying the effect that changing the membrane material and thickness would have on the rate of heat removal from the reaction zone. The goal was to increase the heat transfer rate away from the microheaters to prevent ignition/extinction behavior. However, if the rate was too high, the heaters would not provide a sufficient temperature rise for reaction to occur because they would fail by electromigration. Simulations were used to predict the temperature versus heater power curve for the new microreactor design, which used a 2.6 μm silicon membrane instead of a 1 μm silicon nitride membrane. This predicted curve was extremely close to the experimental results that were obtained after the device was fabricated[4,5].

Design of a Micro Flow Sensor

For the next version of the T microreactor, a flow anemometer was added to measure gas flow rate in the microreactor channels. An anemometer functions by detecting changes in the temperature field around a heater element caused by changes in gas flow rate as depicted in Figure 2-3. This problem was constrained with the use of a 1 μm thick silicon nitride film as the membrane material, a channel width of 0.5 mm, and a channel depth of 0.5 mm. The adjustable parameters were the length of the heater segment, the power input into the heater, and the placement of the temperature sensor(s) around the heater segment. In addition to optimizing the sensor design, knowledge of the effect of the gas properties and membrane material/thickness on flow sensor performance was also desired.

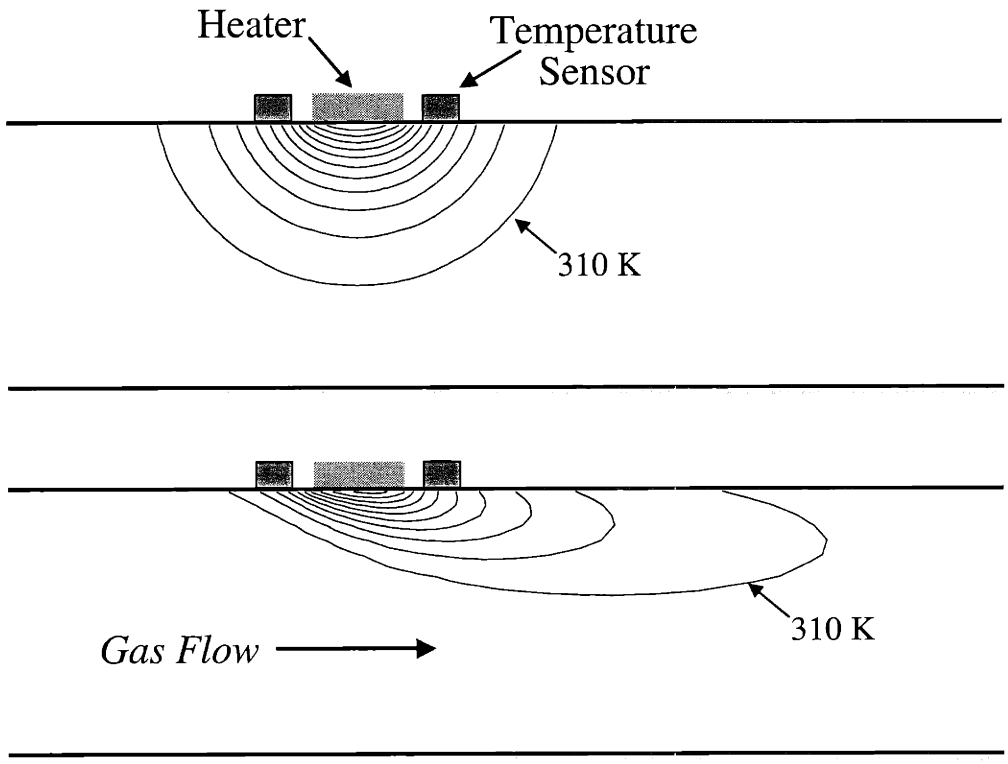

Figure 2-3. Contour plot of the gas temperature at the channel center around the heater: (top) 0 sccm oxygen flow rate; (bottom) 30 sccm oxygen flow rate (Contours range from 310 to 460 K with 15 K intervals).

Figure 2-4a shows the temperature profile down the centerline of the channel at various gas flow rates. To better show how the temperature profile changes with flow rate, Figure 2-4b gives the differential temperature profile, which is the difference between the temperature profile of interest and the temperature profile obtained in the absence of flow. This figure indicates that the most sensitive configuration for this type of anemometer is to place the temperature sensor slightly upstream of the heater. The explanation for this result is given in Figure 2-3, which shows that increasing the flow rate has the effect of flattening/broadening the contour lines after the heater segment. For the region before the heater segment, the spacing between contour lines narrows indicating that the temperature

gradient becomes steeper in front of the heater segment. Thus, changing the flow rate has a large effect on the temperature profile immediately in front of the heater segment.

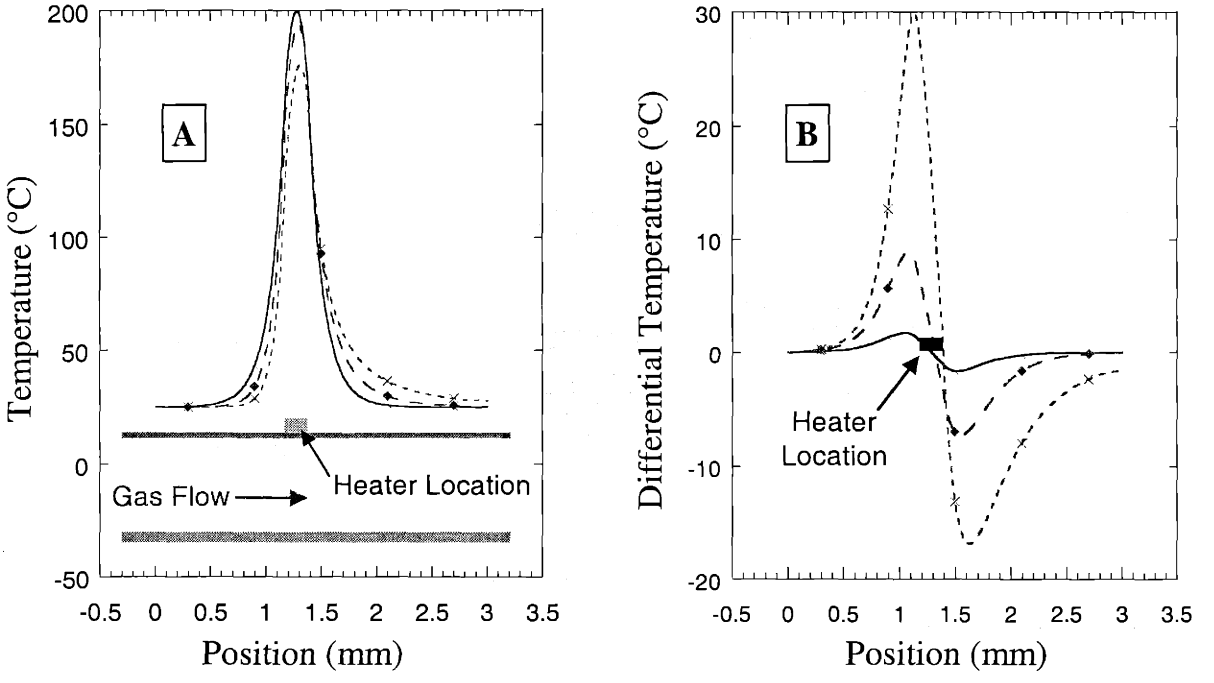

Figure 2-4. (A) Temperature profile along the center of the membrane around the flow sensor heater for various gas flow rates: (—) no flow; (---◆---) 10 sccm; (···×···) 30 sccm; (B) Differential temperature profile (—) 1 sccm; (---◆---) 5 sccm; (···×···) 20 sccm.

Next, the effect of the heater segment length was explored, and this result is illustrated in Figure 2-5a. The simulations gave the expected result that increasing the heater segment length resulted in the temperature difference peaks being taller and broader. It also had the effect of moving the peak locations slightly farther (~6 μm) from the heater. The effect of increasing the heater length was not large considering there is a factor of four difference between the shortest and longest segment. Nonetheless, a 200 μm heater was used for both the design and the remaining sensitivity studies shown here because the temperature sensor length of 90 μm requires broad peaks. These could also be obtained by increasing the

heater power, as shown in Figure 2-5b. However, there were concerns for the membrane stability (the membrane buckles at high temperatures, which can lead to breakage) and the electromigration limits of the platinum heater lines. Thus, for these simulations, the maximum temperature in the heater segment under no flow conditions was kept constant at 200°C by adjusting the total power in the heater segment. For each design variation, the power was first adjusted so that the maximum temperature under the no flow condition was 200°C.

The effect of the thermal conductivity and thickness of the membrane on the flow sensor performance was also explored because of the possibility of future changes in the fabrication process. Moreover, the thermal conductivity of the silicon nitride membrane is uncertain since its value depends strongly on the deposition process. To address this problem, a series of simulations were performed exploring the range of reasonable thermal conductivity values of thin film silicon nitride. Figure 2-5c shows these results, which demonstrate that changing the thermal conductivity of the membrane has no effect on the differential temperature peak location. This is extremely important, since it means that the optimum temperature sensor location is insensitive to changes in the membrane thermal conductivity. Of course, changing the thermal conductivity does affect the differential temperature peak heights and breadths because decreasing the resistance to heat transfer in the solid phase decreases the flow sensor's performance. In this case, changing the thermal conductivity from 1.2 W/(m·K) to 10.0 W/(m·K) results in a 35% loss in sensitivity. This result also applies to changes in membrane thickness since it has the same effect on the heat transfer behavior. That is, doubling the membrane thermal conductivity is equivalent to

doubling the membrane thickness. This relationship will hold as long as there is not a significant temperature variation inside the membrane along its depth direction.

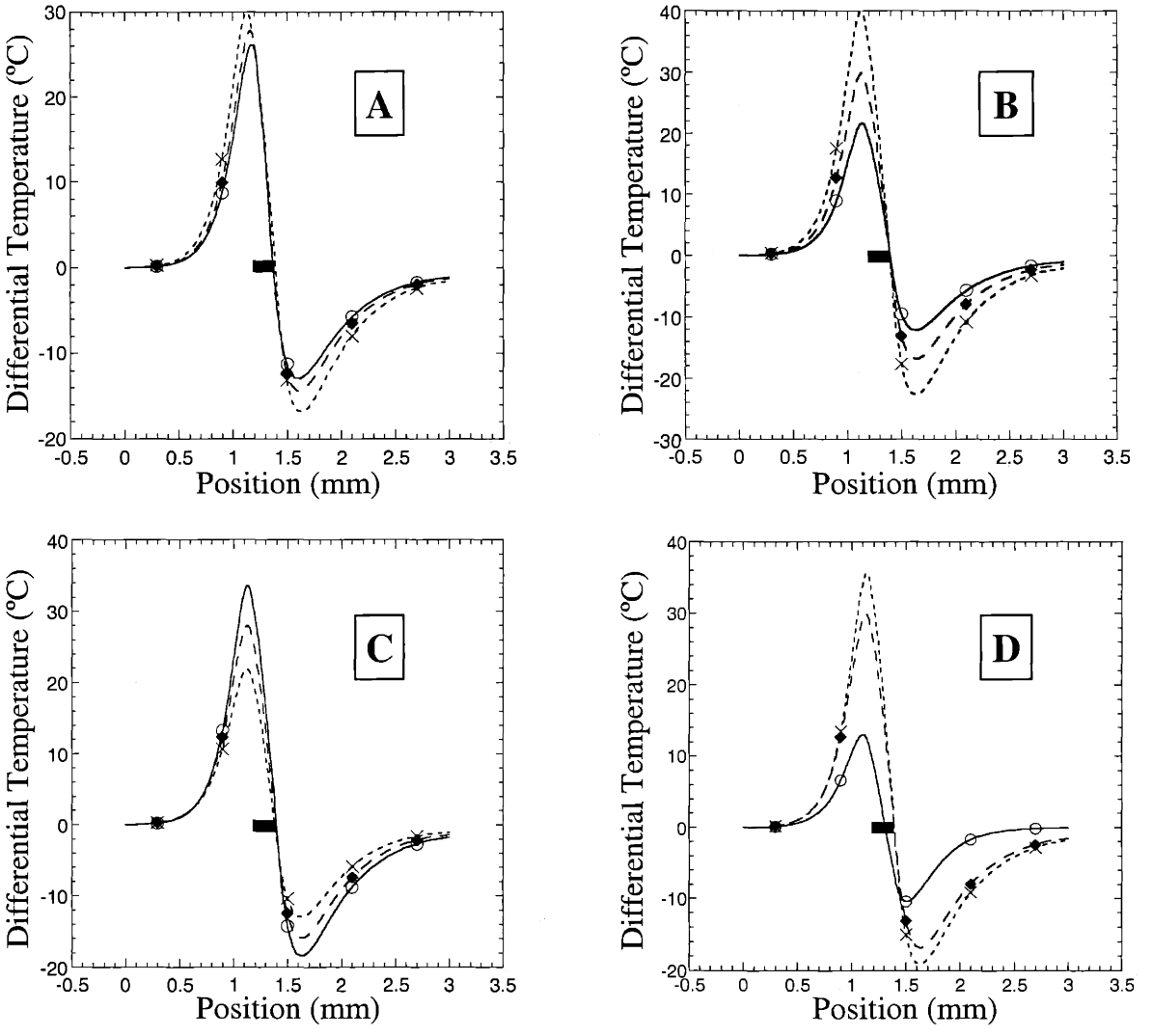

Figure 2-5. Effect of design parameters on the differential temperature profile for a 20 sccm oxygen flow rate. (A) Heater length (—O—) 50 μm; (---◆---) 100 μm; (···×···) 200 μm; (B) Heater power (—O—) 12.0 mW; (---◆---) 17.2 mW; (···×···) 24.0 mW; (C) Membrane thermal conductivity (—O—) 1.2 W/(m·K); (---◆---) 4.5 W/(m·K); (···×···) 10 W/(m·K); (D) Gas properties (—O—) Hydrogen; (---◆---) Oxygen; (···×···) Ammonia.

The previous results shown were all generated using oxygen as the flowing gas. However, the flow sensor will be used for a variety of gases in future testing, so the effect of the gas properties on the flow sensor performance is of considerable importance. Figure 2-5d shows a comparison of the differential temperature profiles for hydrogen, oxygen, and ammonia. The thermal diffusivity, α, for these gases ranges from 1.4×10^{-5} m^2/s for ammonia to 1.3×10^{-4} m^2/s for hydrogen. This range encompasses most common gases, so Figure 10 serves as an indicator of the robustness of the design. Because of the high thermal diffusivity of hydrogen, it has a relatively short and narrow peak that is slightly farther from the heater (~24 μm) compared to ammonia and oxygen. Therefore, the flow sensor loses two-thirds of its sensitivity switching from ammonia to hydrogen. In practice, the power to the heater can be increased to accommodate the loss in sensitivity, but physical limitations may not always allow this. On the positive side, this indicates that the device could also be used to measure the thermal diffusivity of a gas. The value for the diffusivity could provide a rough estimate of the product gas composition of the reactor. However, this requires knowledge of the flow rate since the effect of flow rate and gas thermal diffusivity have very similar effects on the membrane temperature profile as shown in Figure 2-4b and Figure 2-5d.

Microreactors with the flow sensor design detailed above were fabricated and tested to determine its performance. As shown in Figure 2-6, the flow sensor is extremely responsive to changes in flow rate between 0 and 10 sccm. Sensitivity decreases as the flow rate increases further due to the development of a thermal boundary layer. Fortunately, flow rates typically used in this microreactor design are less than 20 sccm. As predicted by the simulation results, the experimental data clearly indicates that the upstream temperature

sensor outperforms the downstream temperature sensor. Figure 2-6 also shows an excellent agreement between the experimental flow sensor performance and the performance predicted by the simulation. For these results, the experimental data was first used to determine the appropriate value of thermal conductivity for the silicon nitride membrane since this value is highly dependent on the deposition procedure. Once this was obtained, the simulation tools were used to model flow sensor performance. The value of thermal conductivity found for the silicon nitride membrane was 13.1 W/(m·K). This is in the range of thermal conductivity for bulk silicon nitride, which is reported from 7 W/(m·K) to 43 W/(m·K) depending on the preparation method and measurement temperature[10,11]. However, silicon nitride thin films have lower thermal conductivities that are highly dependent on the deposition process and film thickness. The literature values for these vary from 1.2 to 13 W/(m·K)[12-15].

From this analysis, it is clear that both the gas and membrane properties play substantial roles in determining the heat transfer characteristics of the T microreactor. Since the gas properties and flow rates are fixed by the reaction system of study, the designer must alter the membrane material/thickness to achieve the appropriate heat transfer characteristics. In addition to altering the membrane, the heater layout can also be modified to increase heat removal (by decreasing the distance between the heater and the side walls) or to increase the thermal uniformity of the reaction zone.

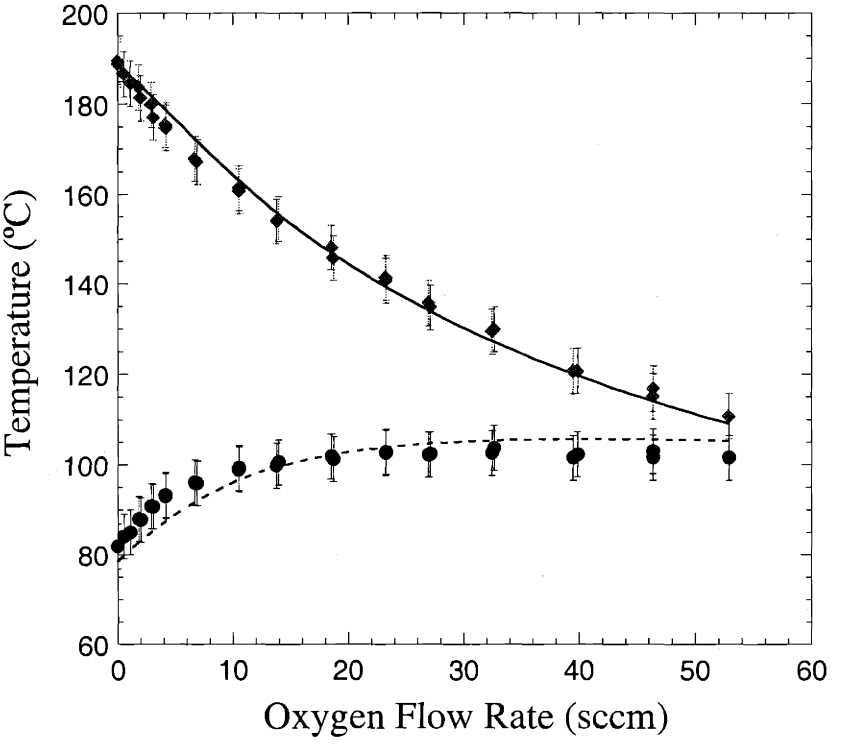

Figure 2-6. Upstream and downstream temperature sensor measurements for varying flow rates of oxygen; (◆) Upstream temperature sensor measurement (experimental); (—) (simulation); (●) Downstream temperature sensor measurement (experimental); (---) (simulation).

Redesign of the Heater Segment

The original T microreactor heater design consisted of a 50 μm platinum line that meandered across the 300 μm heater width down the length of the channel. This design is effective in providing uniform power for the heated zone, but it results in a non-uniform temperature across the heater. To reduce this effect, the heater was split into two symmetrically placed segments along the length of the channel as illustrated in Figure 2-7. The simulation tools were then used to evaluate the effectiveness of this design. Figure 2-8 shows the results for both the silicon nitride and the silicon membrane reactors. Because silicon has a much higher thermal conductivity than silicon nitride (157 W/(m·K) to 13.1

W/(m·K) respectively), its thermal uniformity for the new design is excellent. The simulations also indicated that there is no significant difference in the thermal uniformity between the two membrane materials for the old heater design.

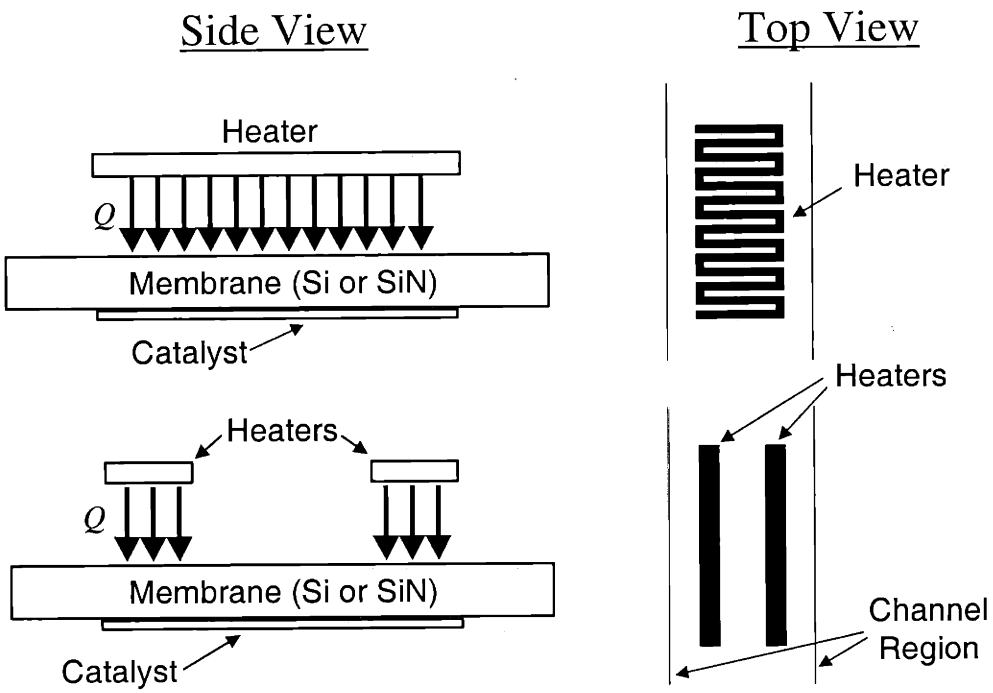

Figure 2-7. Top and side view schematics of the two heater designs: old heater design (top), new heater design (bottom).

This initial study was performed with no gas flow and no reaction was occurring. By increasing the gas flow rate, the heat flux to the gas phase is increased, and this decreases the temperature across the heater as shown in Figure 2-9. Fortunately, the thermal non-uniformity—the difference between the maximum temperature of the heater and the temperature in the center of the channel—increases by only 5.4°C for a 100 sccm change in flow rate.

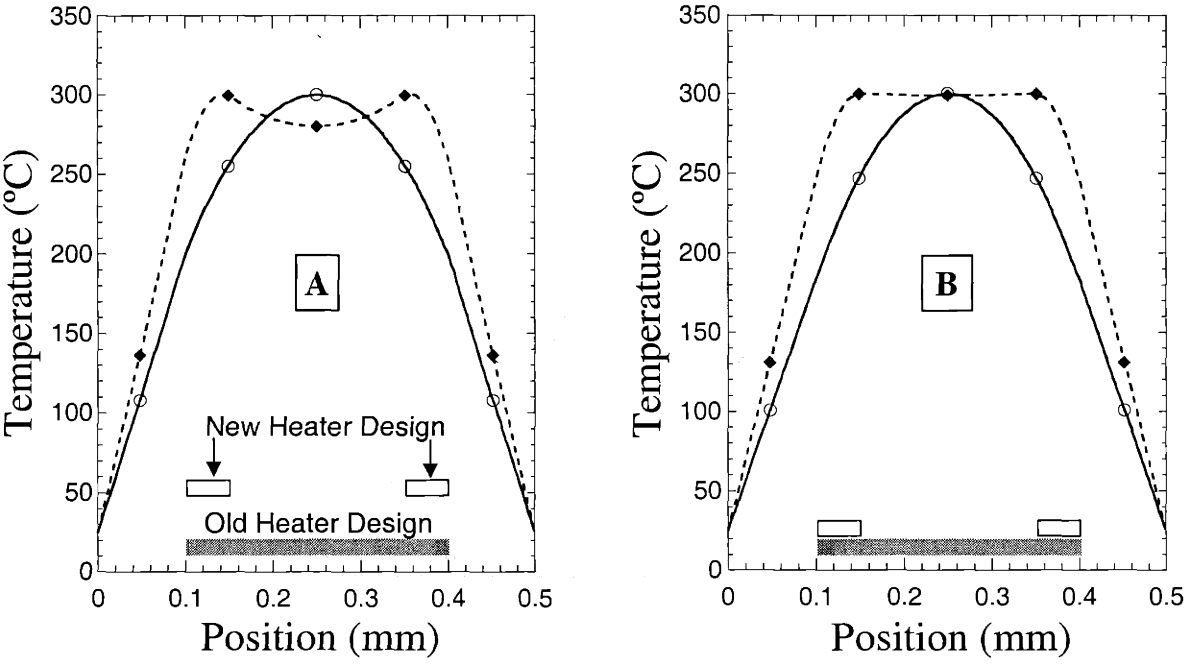

Figure 2-8. Temperature profile across the membrane for the heater designs. (A) Silicon nitride membrane reactor; (B) Silicon membrane reactor. (—O—) Old heater design; (---◆---) New heater design.

The effect of adding a highly exothermic reaction on the thermal uniformity was then studied using the ammonia oxidation system. Figure 2-10 shows the temperature profile across the channel for various NH_3 concentrations that vary from the ignition to the extinction regime. For the cases shown, only the 5% NH_3 feed is operating at the lower steady-state of the S curve. This is indicated by the 19% conversion found for this case, which is considerably less than the 58% to 68% conversions found for the upper steady-state cases. Because the reaction provides an additional heat source in the center of the channel, a reactor operating in the ignition regime has a much higher level of thermal uniformity. For extremely exothermic reactions at high conversions, the temperature profile observed will resemble the profile for the meandering heater design with a hot spot in the center of the channel (see Figure 2-8). Clearly, it is possible to design reactors that have very uniform

temperatures, but detailed knowledge of the reaction kinetics must be known. Regardless, the thermal profiles provided by the models under non-reacting conditions were invaluable in shortening the design time of the scale-up microreactors.

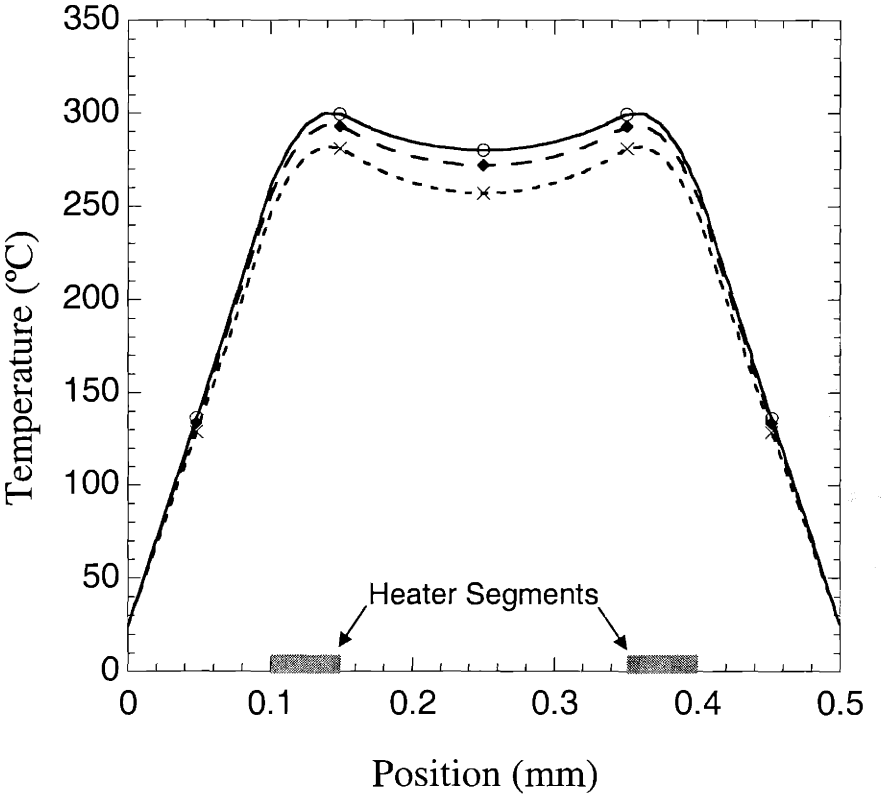

Figure 2-9. Effect of gas flow rate on the thermal uniformity of the new heater design (silicon nitride membrane reactor). (—○—) 0 sccm; (- -◆- -) 50 sccm; (---×---) 100 sccm.

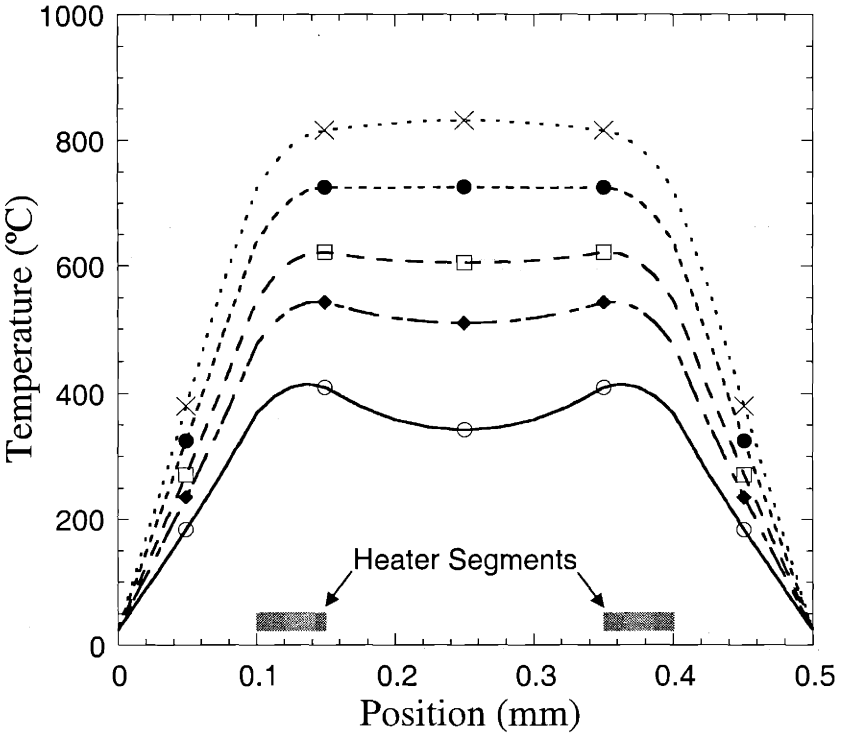

Figure 2-10. Effect of reaction heat generation on the thermal uniformity of the new heater design for ammonia oxidation (—○—) 5% NH_3 in air (19% conversion); (— -◆— -) 7.5 % NH_3 in air (58% conversion); (- -□- -) 10% NH_3 in air (66% conversion); (···×···) 15% NH_3 in air (68% conversion).

First Generation Scale-up Microreactor

The flow sensor and heater designs discussed in the preceding sections were first incorporated into a Y shaped microreactor for scale-up as shown in Figure 2-11. This microreactor consists of two inlet flow channels and a reaction channel. The inlet flow channels form the branches of the Y and one of the new gas flow sensors is placed on each. The reaction channel contains two heater segments that utilize the split heater design as shown in Figure 2-12. Two temperature sensors, one upstream and one downstream, are present on each heater segment. For this design, the heaters have two independently

operating sides, but the intent was to place these heaters in series and power them with a single circuit.

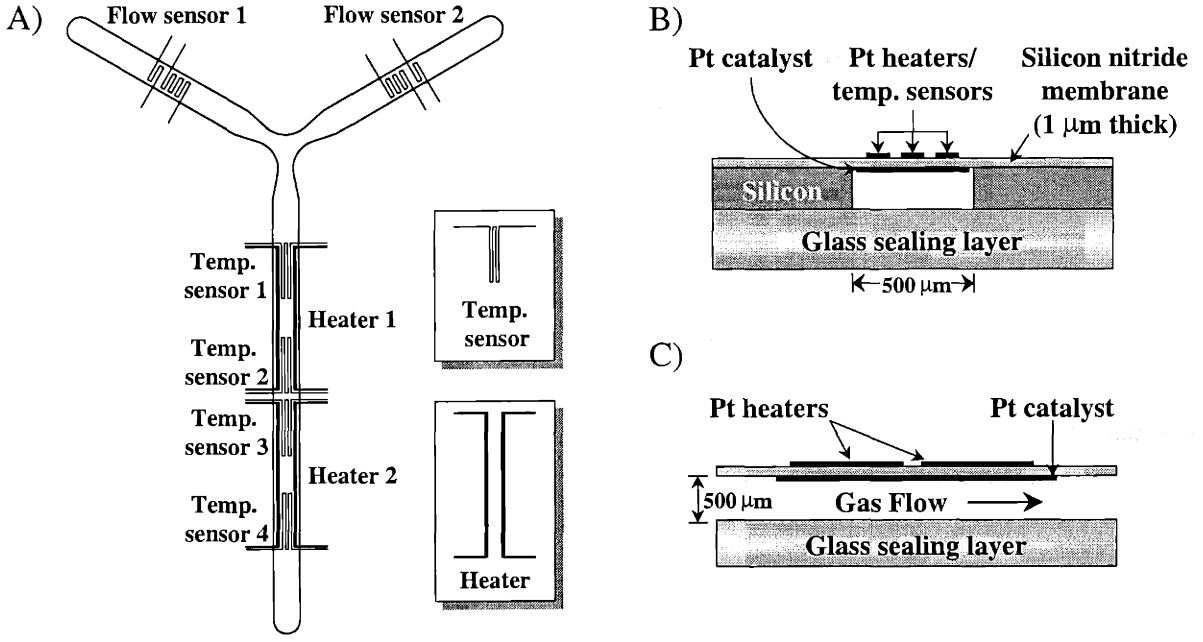

Figure 2-11. Schematic of the Y scale-up microreactor. A) Top view B) Cross-section perpendicular to flow C) Cross-section parallel to flow.

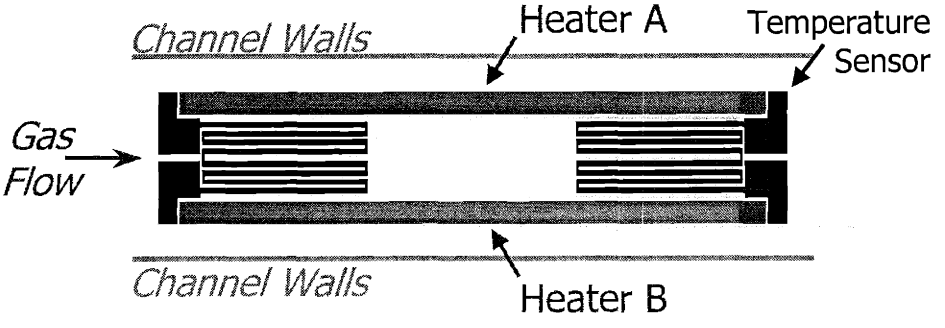

Figure 2-12. Layout of the Y reactor heater segment with temperature sensors (electrical leads from sensors and heaters are not shown). The temperature sensor at the left is the upstream sensor.

The motivation behind the Y shape and the use of rounded corners was to reduce the stress concentrations in the silicon nitride membrane at the intersection of the feed channels. It was believed that this design would provide a membrane that was much more robust and

thus able to withstand higher reaction temperatures for longer periods of time. Because of the shape of the reactor, a KOH etch could not be used to form the channels in the silicon wafer. Instead, a Deep Reactive Ion Etch (DRIE) process was used.

The simulation tools were again used to examine the power requirements of the platinum heater lines in the device. The main concern was that the heater segments may require more power than could be provided by the platinum lines because of electromigration. After performing this study, the length of the heater segment was determined to be 2.8 mm with a 50 μm line width. The temperature sensors inside the segment were made to be 0.8 mm long with a 10 μm line width. The heater and temperature sensor cover 0.3 mm of the 0.5 mm channel width. Figure 2-13 shows a picture of one of the fabricated Y microreactors.

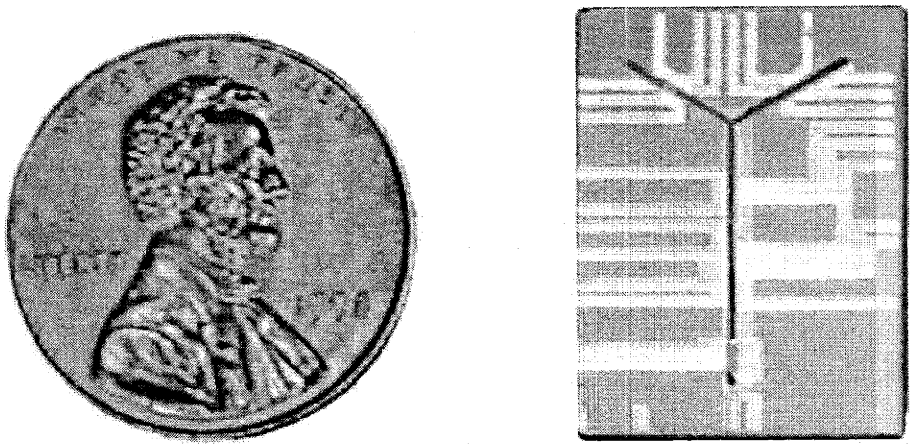

Figure 2-13. Y microreactor designed for the scale-up system.

Although this microreactor was successfully fabricated, the DRIE processing step caused considerable difficulty since the boundary between the bulk silicon and the silicon nitride film was often undercut by the etch. This phenomenon is known as footing or notching and is caused by a differential charging of sidewalls and bottom features that occurs

when over etching a silicon layer over top of a dielectric film[16]. The difficulties of DRIE and methods for improving etch performance have since been described in more detail in work done at the Microsystems Technology Laboratory (MTL) at MIT[17-20].

This problem of footing prevented the realization of a robust silicon nitride membrane for the microreactor. The number of functioning reactors per processed wafer was not particularly good. Furthermore, the DRIE processing step was slow in that only one wafer could be processed at a time and etching took over four hours. The tool was also in high demand for other projects, so this created a large bottleneck in microreactor wafer processing.

Second Generation Scale-Up Microreactor

With this information in mind, it was decided to revise the scale-up microreactor and remove the feed gas-mixing region from the die; instead, pre-mixed feed gas would be sent to the microreactor. First, by premixing the feed gas it was no longer necessary to have two intersecting channels and a single channel would form the microreactor. This would eliminate the stress concentrations created at the center of the Y structure in the membrane and the channel etch could again be done with KOH. The second reason was to improve reaction data analysis by directly analyzing the feed gas to the microreactors. This would allow comparison of the feed gas analysis to the product gas analysis to determine conversion and selectivity.

Scale-Up Microreactor Description

Figure 2-14 shows a schematic of the microreactor design that was used for this project. The reaction channel is 0.5 mm wide, 0.5 mm deep, and 11 mm long. It has seven distinct zones for heating and temperature sensing that cover a total length of 7 mm. The gas

flow sensors present on the feed inlet channels of the Y microreactor were removed, and only micro-heaters and micro-temperature sensors were incorporated in this design. The heater and temperature sensor design was modified, as shown in Figure 2-14d, to provide higher spatial resolution for controlling the reaction zone temperature profile. More heater zones were not added due to space limitations for electrical leads on the die. Each heater is 0.94 mm in length and the temperature sensors are 0.77 mm long. The width of the heater/temperature sensor segments were 0.3 mm, which left 0.1 mm of space between the heater and silicon channel walls.

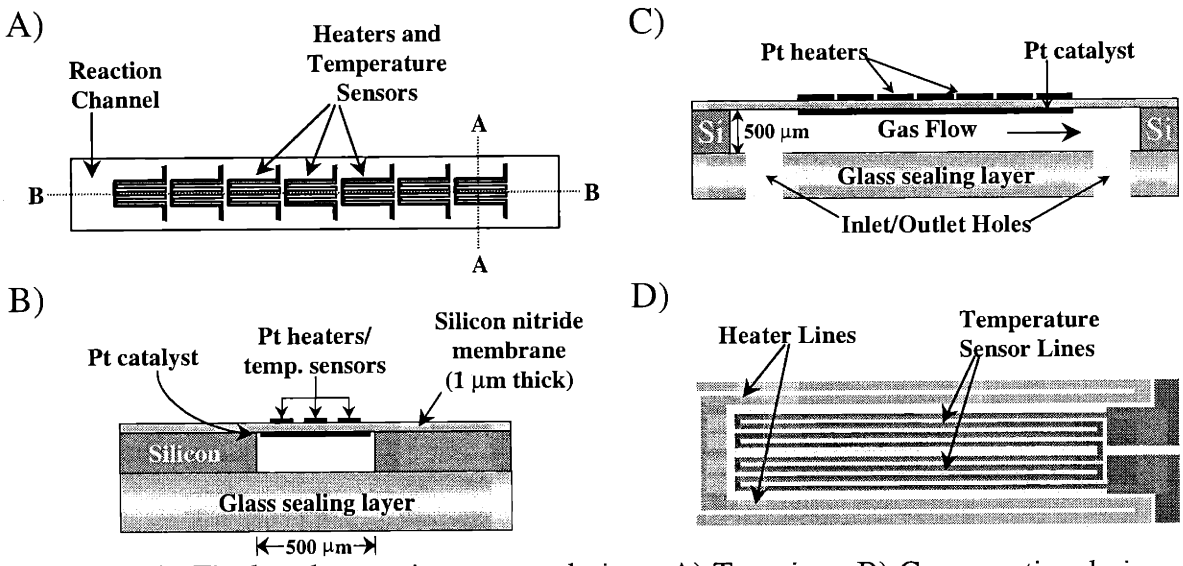

Figure 2-14. Final scale-up microreactor design. A) Top view B) Cross-sectional view AA C) Cross-sectional view BB D) Enlargement of heater and temperature sensor configuration.

Two reaction channels were incorporated on each microreactor die due to a restriction on the die size placed by the packaging method chosen, which will be discussed in the following chapter. The required die size, 20.3 mm by 28.2 mm, was large enough that it did not make sense to incorporate only a single reaction channel. Figure 2-15 shows the scale-up microreactor die layout with dimensions. This microreactor has 56 electrical

interconnections (not shown in Figure 2-15) that need to be made to operate the 14 heaters and 14 temperature sensors.

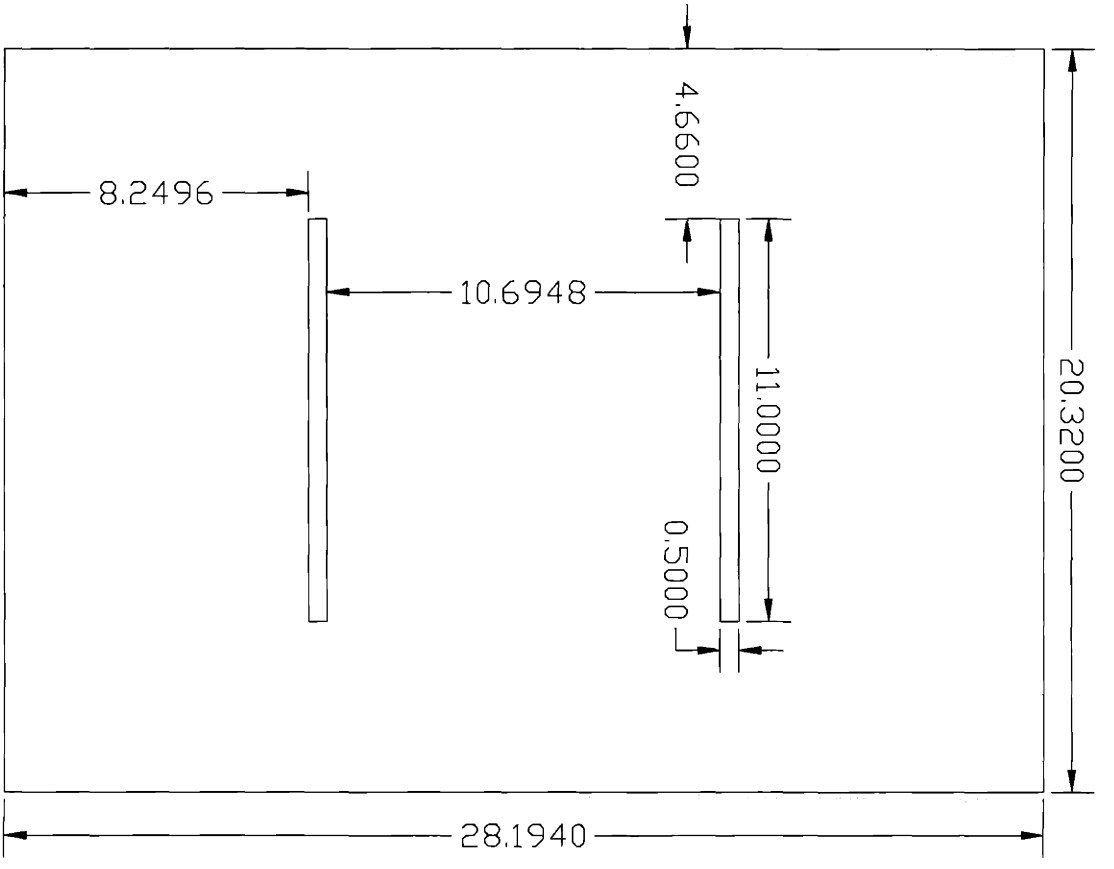

Figure 2-15. Scale-up microreactor drawing showing channel locations. Drawing units are in millimeters.

Microfabrication Process for the Scale-Up Reactor

The fabrication process for this microreactor was similar to the process developed for the T microreactor, but some modifications were made. Figure 2-16 illustrates the main fabrication steps by showing a cross-section of the wafer after each step. The majority of wafer processing took place at the DuPont microfabrication facility in building E357 at the Experimental Station Laboratory (ESL)[5]. Low stress silicon nitride depositions were done

[5] DuPont Experimental Station, Wilmington, DE 19880.

either at MIT's MTL or by ACT MicroDevices[6]. However, all the processing for the Y microreactor discussed earlier was done at MTL.

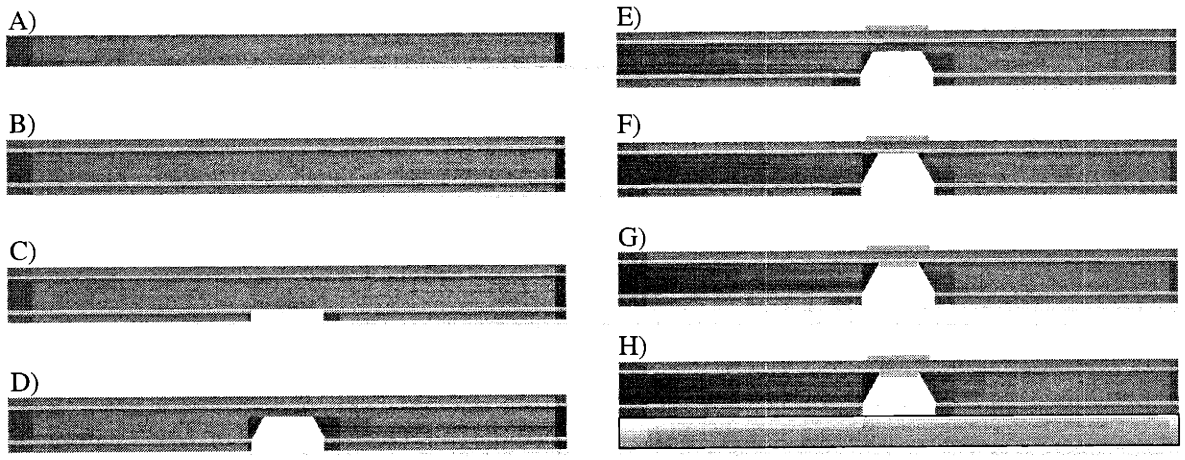

Figure 2-16. Fabrication sequence for the scale-up microreactor. A) Start with DSP silicon wafer 101.6 mm in diameter and 508 μm thick. B) Deposit 1 μm of low-stress silicon nitride on top of 0.1 μm of dry thermal oxide. C) Using a photoresist mask, plasma etch through silicon nitride on backside of wafer to define channel geometry. D) Using the silicon nitride as a mask, perform a timed KOH etch of the silicon to leave about 25 μm of silicon below the silicon nitride membrane. E) Perform PVD of 0.1 μm platinum metal layer on the front side of wafer using a lift-off process to define the heater and temperature sensor microstructures. F) Complete the KOH etch of the silicon to the silicon nitride membrane. G) Using a shadow mask, deposit 0.1 μm platinum metal layer on the backside of the silicon nitride membrane to act as a catalyst. Platinum layer annealed at 400°C for 1 hour. H) Anodically bond the backside of the wafer to a Pyrex® 7740 wafer.

The starting point for the microfabrication process was Double-Side Polished (DSP) single crystal {100}-oriented silicon wafers obtained from Riotech[7]. The wafers were 4 inches in diameter and 0.020 inches in thickness. A dry silicon oxide film was first grown on the wafers to aid in the anodic bonding step done later in the process. The MIT batch of wafers had 0.1 μm of dry thermal oxide grown. The ACT batch of wafers had the same thickness of silicon dioxide, but it was deposited using LPCVD. A low-stress LPCVD

[6] ACT MicroDevices, Inc., 7586 Peppers Ferry Loop, Radford, VA 24141, (540) 639-1986.

silicon-rich silicon nitride film was then deposited on the silicon oxide layer. The MIT silicon nitride film was 1 μm thick. The ACT silicon nitride film was 0.75 μm thick. Figure 2-16b shows a cross-section of the wafer after this step.

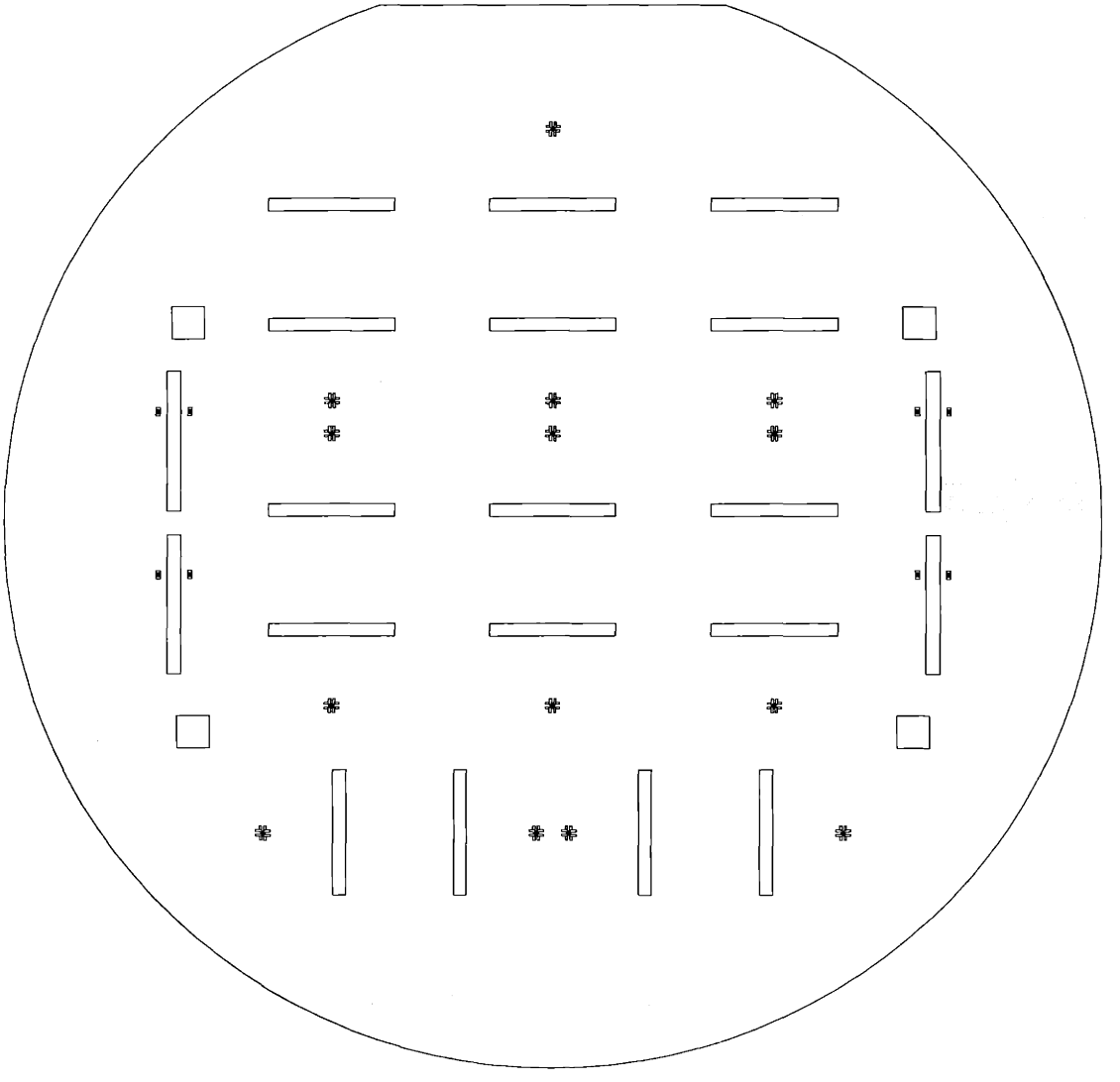

Figure 2-17. Dark field mask layout used to define reactor channels in the silicon nitride film. Eight scale-up microreactor dies are produced on a silicon wafer. Four single channel microreactor dies are also produced for other testing.

[7] Riotech, Inc., 3369-T White Mountain Blvd., Lakeside, AZ 85929, (520) 368-5013.

A photolithography step was then performed to define the channels in the silicon wafer. Hexamethyldisilazane (HMDS) from Arch Chemicals[8] was first applied to the wafer surface to aid in photoresist adhesion. A spin-coater was used to deposit HiPR 6517 positive photoresist on the wafers. The photoresist was also manufactured by Arch Chemicals. The photoresist was then exposed with a dark field mask, which is shown in Figure 2-17, to define the reaction channel geometry. The dark field mask was manufactured by Photronics[9]. After photoresist development and post-baking, the silicon nitride film on the backside of the wafer was plasma etched with the photoresist as the etch mask. Figure 2-16c shows a cross-section of the wafer after this step.

The reactor channels were then partially etched using a 30% KOH solution at 70°C. This anisotropic etch was timed to leave about 25 μm of silicon at the bottom of the channel. Figure 2-16d shows a cross-section of the wafer after this step. The silicon nitride layer was the masking material in this etch since it is not attacked by KOH. It should be noted that KOH etches preferentially the <100> direction of silicon and very slowly in the <111> direction at a ratio of as much as 400 to 1. This leaves a V-shaped groove in the silicon wafer instead of a channel with sidewalls perpendicular to the wafer surface as illustrated in Figure 2-18.

[8] Arch Chemicals, Inc., 501 Merritt 7, P.O. Box 5204, Norwalk, CT 06856, (800) 797-1629.
[9] Photronics, 15 Secor Rd., Brookfield, CT 06804, (203) 775-9000.

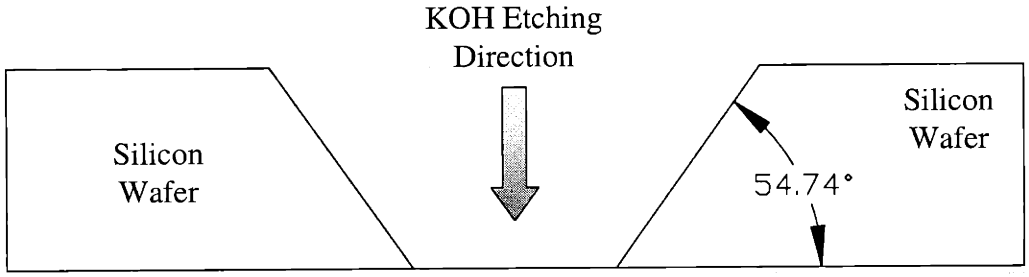

Figure 2-18. Detail of the cross-section of the reaction channel etched in the silicon wafer.

The second photolithography step was then performed to define the platinum metal structures on the microreactor dies. A lift-off process using AZ 5214-E IR negative photoresist from Clariant[10] was used to define the platinum metal geometries. A light-field mask, shown in Figure 2-19, was used to pattern the photoresist. This mask was also manufactured by Photronics. After development of the photoresist, a 0.1 μm layer of platinum was deposited onto the wafer surface using an electron beam PVD process. Thicker layers are difficult to deposit and remove successfully using a lift-off process. Microstrip from RBP Chemical Corporation[11] was used to remove the remaining photoresist along with the platinum layer on top of it to complete this step. Figure 2-16e shows a cross-section of the wafer after this step.

[10] Clariant Corporation, Business Unit Electronic Materials, 70 Meister Ave., Somerville, NJ 08876, (908) 429-3500.
[11] RBP Chemical Corporation, 150 S. 118th St., Milwaukee, WI 53214, (800) 558-0747.

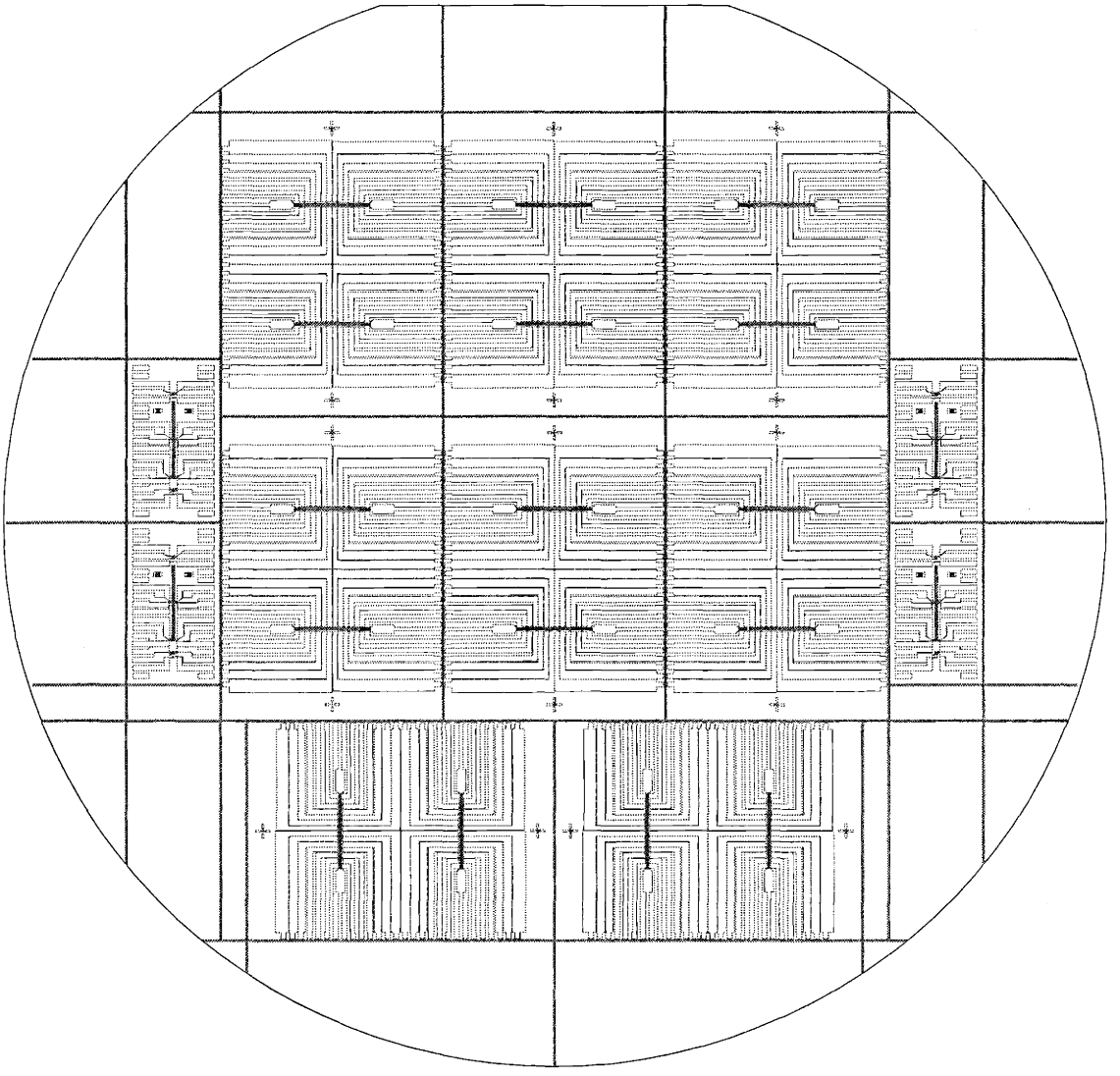

Figure 2-19. Light field mask used to define the platinum metal layer on the microreactor wafers. The metal lines between microreactor dies are used as guides for dicing the reactor chips.

Originally, it was hoped that the silicon nitride layer on the bottom of the wafer could be removed using an unmasked plasma etch. The reason for this was to provide a better bonding surface for the anodic bonding step at the end of the process. Silicon nitride does not bond well with Pyrex® whereas silicon oxide gives a strong bond[21,22]. Unfortunately, it was found that the plasma etch to remove the silicon nitride layer resulted in a poor bonding surface because the silicon nitride layer did not etch uniformly. After several

attempts were made at bonding the wafers with the silicon nitride layer removed, it was decided that it would be better to bond directly to the silicon nitride.

The 25 μm of remaining silicon supporting the silicon nitride membrane was then removed using a 10% KOH solution at 80°C. Figure 2-16f shows a cross-section of the wafer after this step. A different KOH solution formula was used as this offered higher selectivity between etching silicon and silicon oxide. The previous formula has a faster etch rate of silicon. The metalization on the front side of the wafer was protected using a Teflon® wafer holder shown in Figure 2-20. The holder formed a seal against the front side of the wafer preventing the aqueous KOH from contacting the platinum metal deposited in the previous step. This holder was previously made in-house at DuPont.

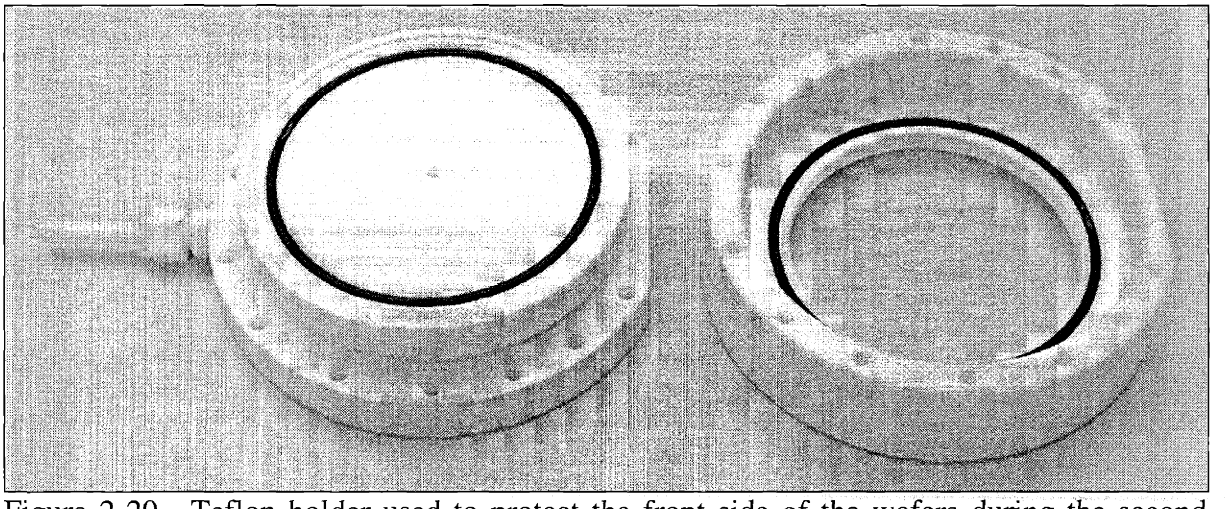

Figure 2-20. Teflon holder used to protect the front side of the wafers during the second KOH etch. A Viton® o-ring was used for sealing to the wafer.

The platinum catalyst was then deposited on the channel-side of the silicon nitride membrane using electron-beam PVD. A shadow mask limited the deposition of platinum to only the channel the area of the reactors. This mask, shown in Figure 2-21, was laser machined from stainless steel and was attached to the wafers prior to placement in the e-

beam equipment using Scotch® tape. A shadow mask was used instead of photolithography because the presence of the freed membranes made the microreactors too fragile for photolithography. The platinum metalization on both sides of the wafer was annealed at 400°C for one hour under nitrogen. Figure 2-16g shows a cross-section of the wafer after this step.

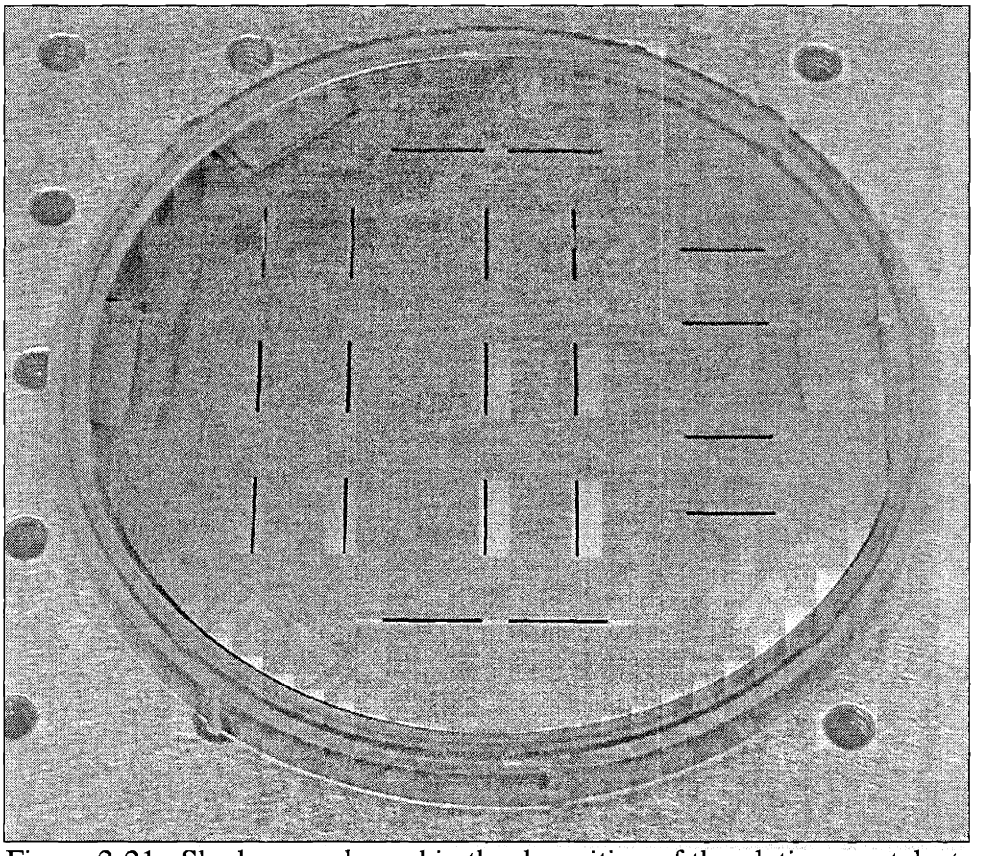

Figure 2-21. Shadow mask used in the deposition of the platinum catalyst.

A Pyrex® 7740 wafer was then anodically bonded to the backside of the microreactor wafer as illustrated in Figure 2-16h. This bonding step was done at 460°C for 5 hours with the applied voltage being stepped up to 900 Vdc. Typically anodic bonding of Pyrex® is done between 180 and 500°C with the applied voltage ranging from 200 to 1000 V[23]. The aggressive bonding conditions were necessary because the Pyrex wafer was being bonded to

a silicon nitride surface instead of silicon or silicon oxide, which is preferred. The Pyrex wafer had fluidic inlet and outlet holes drilled in it before the bonding step. A coarse alignment between the silicon wafer and Pyrex wafer was acceptable since the fluidic ports were relatively large features.

The final step was dicing the wafer using a diesaw. The sawblade used was 0.008[12] inches thick, 400 grit, with a 37 μm particle size. Figure 2-22 shows a picture of a completed microreactor.

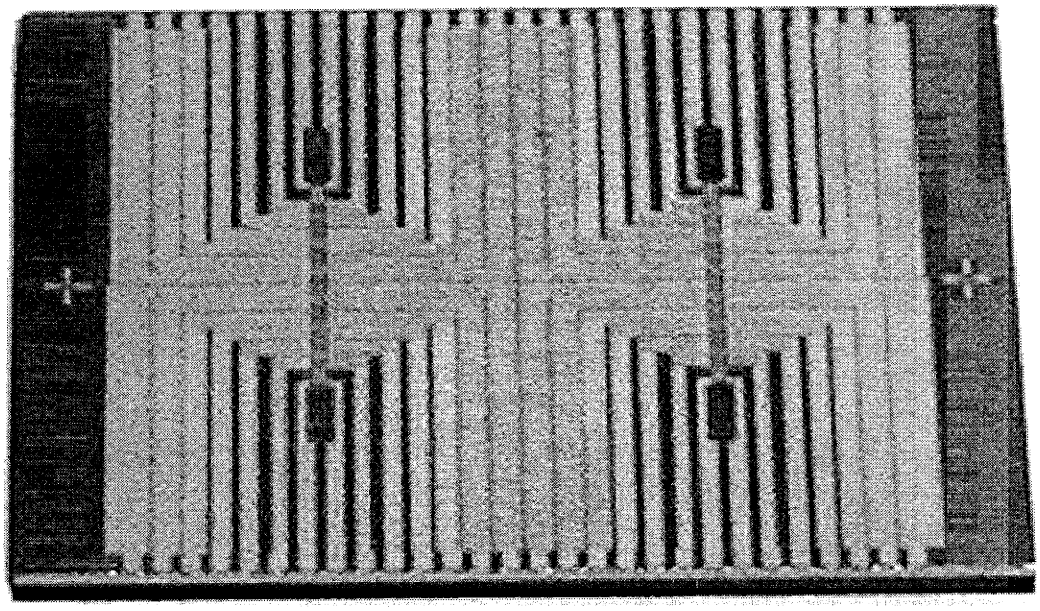

Figure 2-22. Microreactor used in the scale-up microreactor system.

Testing Procedures

The testing procedures described here refer to the determination of platinum resistivity on temperature. Additional testing for microreactor functionality is described in Chapter 3 after the microreactor packaging methods have been introduced. Microreactor

[12] Initially the diesaw blade was 0.006 inches thick, but this was found to be too thin.

testing under reaction conditions is described in Chapters 7 and 8, which describe the methods and results for the scale-up system testing.

Determination of the Temperature Coefficient of Resistivity for Platinum

The dependence of platinum resistivity on temperature (the temperature coefficient of resistivity or α) is used as the basis for the Resistive Temperature Devices (RTD's) in the microreactor. Unfortunately, this relationship is highly dependent on the deposition process of the platinum layer. Even platinum deposited under the same conditions in the same machine, but in different runs may exhibit different values of α. The equation used for determining temperature as a function of the platinum structure resistance is given below.

$$\frac{R}{R_o} = 1 + \alpha(T - T_o) \tag{2.1}$$

Where R is the measured resistance, R_o is the resistance at a reference temperature, T is the temperature of the RTD, and T_o is the reference temperature. The reference temperature used in this project was the triple point of water, 0.01°C. Unfortunately, many researchers employing (2.1) do not report the reference temperature that was used to calculate alpha. Under further examination of (2.1), it is clear that any value of α will depend on the reference temperature used. Thus, it is difficult to compare α values reported in literature and misguided to use these values in temperature calculations unless the reference temperature is known. Note that (2.1) is a simplification of the more accurate equations used for Standard Platinum Resistance Thermometers (SPRT's) as specified in the ITS-90 standard[24]. However, the accuracy given by (2.1) is sufficient for the microreactor RTD's and fits the experimental data quite well.

Determination of the temperature coefficient of resistivity was done by raising the temperature of the entire microreactor die and recording the measured resistance. This was

done for temperatures ranging from 22°C (room temperature) to approximately 275°C. Higher temperatures were not used because of limitations of the testing apparatus. Although it would have been ideal to use higher temperatures, the value of α should not change until the structure of the platinum begins to change. This temperature depends on the annealing conditions of the platinum. The resistance data from these experiments were used to determine the α value through a least squares fit of the data for each group of wafers (where a group is specified as wafers that underwent the platinum deposition at the same time).

The equipment used in this experiment was taken from the anodic bonding apparatus used at DuPont in their microfabrication facility. Figure 2-23 shows a schematic of the test setup. Testing was done on whole wafers before they had been cut into chips on the diesaw. This made handling the devices substantially easier. The wafer was placed on a heated cylindrical aluminum block 4" in diameter. The block temperature was monitored using a 1/16" thermocouple and a 0.020" thermocouple that were also inserted in holes in the block. A 1/16" type K thermocouple was used for temperature control with a series CN-2010 Omega Temperature Controller[13]. The temperature was also monitored with a 0.020" type K thermocouple with an Omega model HH21 Microprocessor Thermometer. This thermocouple and temperature monitor were checked and calibrated against a NIST calibrated SPRT, model 5626 from Hart Scientific[14], to ensure its accuracy. The aluminum cylindrical block was heated from below by another cylindrical aluminum block that had four ¼" heating cartridges inserted inside it (not shown in Figure 2-23). This block was also 4" in

[13] Omega Engineering, Inc., One Omega Drive, Stamford, CT 06907-0047, (800) 848-4286.
[14] Hart Scientific Inc., 799 E. Utah Valley Drive, American Fork, UT 84003-9775, (800) 438-4278.

diameter. The heated blocks and wafer were surrounded by insulating ceramic material to help ensure temperature uniformity.

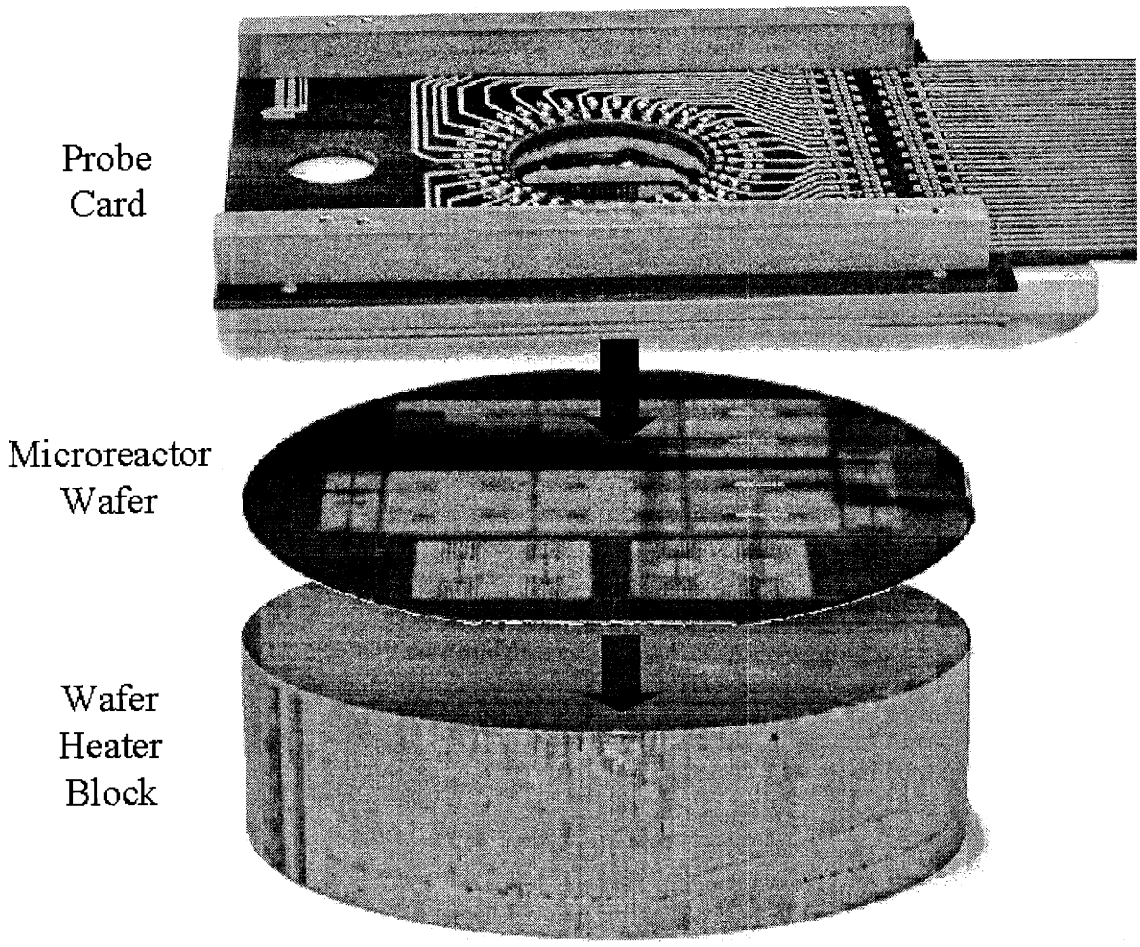

Figure 2-23. Schematic of the test setup for the platinum resistance characterization experiment.

The resistance of the microreactor heater and temperature sensor structures was measured using a custom-manufactured probe card, which is shown in Figure 2-23. A Tektronix[15] DMM916 multimeter was connected to the probe card leads to measure the resistance of three structures on the microreactor at each temperature. Temperatures higher than 275°C were not used because the probe card began to get too hot at this point and

[15] Tektronix, Inc., 14200 SW Karl Braun Dr., Beaverton, OR 97077, (800) 835-9433.

discoloration of the resin holding the probe card pins was observed. Structure resistances were recorded starting at room temperature (approximately 22°C) up to around 275°C in 25°C increments. Resistances of these structures were again recorded as the wafer was cooled back to room temperature in 50°C increments.

Fabrication and Testing Results

Fabrication of the first-generation scale-up microreactor met with considerable difficulty due to the DRIE step. The processing for this reactor was performed at MIT. Most of the fabrication attempts were done with an etch-to-membrane process, which was a much simpler procedure than the alternative bonding based process. Unfortunately, this resulted in low reactor yield. The difficulties with the DRIE step and the lack of available processing time on this machine caused a change of the microreactor design.

This second-generation reactor used only slots as the reaction channel and feed gas mixing was done off-chip. This allowed most of the wafer processing to be performed at DuPont. Two main batches of wafers were fabricated, one with an MIT deposited silicon nitride film and one with an ACT deposited film. The MIT batch was processed first, but poor membrane stability resulted in a very low yield of intact channels per wafer. The survival rate was only around 30%. The reason for the poor survival rate was not known, but the membranes that did survive processing appeared to be very tensile. Because of this, a batch of wafers was sent to ACT for silicon nitride deposition. Originally, the silicon nitride film on the backside of the wafers was removed with a plasma etch, but the non-uniformity in the thickness of the wafer left a very poor surface for bonding. This again resulted in poor reactor yield. Bonding directly to the silicon nitride on the backside circumvented this problem. Although anodic bonding to silicon nitride does not result in the strongest bond,

the process was good enough for this application. With this change the fabrication yield went up to around 70% microreactor survival per wafer.

A summary of the results of the testing to determine the temperature coefficient of resistivity for the microreactor platinum thin films is given below. Only the testing results of the ACT wafers are described because these reactors were ultimately the ones used in the AIMS testing.

Temperature Coefficient of Resistivity for Platinum

The values of the temperature coefficient of resistivity for the platinum used as the microreactor temperature sensors ranged from 0.00205 to 0.00226, where the reference temperature used was the triple point of water, 0.01°C. Table 2-1 lists the values for α for each of the ACT microreactor groups along with their error value. The value listed is the α value calculated using a least squares fit of the resistance data and the corrected temperature from the Omega Microprocessor Thermometer used in the experiment. This value is corrected since this monitor was calibrated against a NIST SPRT, and this calibration was used to determine the actual measured temperature. Although the temperature monitor was close in calibration to the NIST second source standard, this did make a slight difference in the calculated alpha value.

Table 2-1. Temperature coefficient of resistivity for the platinum on the ACT wafers.

ACT Wafer Group	α	Error
1	0.00216	0.00004
2	0.00205	0.00008
3	0.00226	0.00006

The error values for α were determined by also calculating its value using the temperatures measured by the Omega Temperature Controller. It was believed that wafer

temperature measurement had the largest associated error and that the two temperature values recorded reflected this error. Note that the α values determined are relatively close with respect to the measurement error. This is expected since all of the wafers involved had very similar processing conditions.

Conclusions

The first generation Y microreactor design was not acceptable for the scale-up project because too much emphasis was placed on microfabrication techniques. The focus of this project instead required more time and effort placed on designing the system that was to use the microreactors. However, a new microreactor design was necessary to accommodate the packaging methodology, which is discussed in Chapter 3. The slot scale-up microreactor design allowed easier fabrication and eventually provided a good yield with the ACT silicon nitride wafers.

The temperature coefficient of resistivity of the platinum thin films deposited on the microreactors was found to be slightly different for the three platinum deposition groups (0.00216, 0.00205, and 0.00226). This variation is expected and is partly attributed to the error in the determined α values. The reference temperature used for the RTD equation, (2.1), was 0.01°C, the triple point of water.

Characterization of the microreactor heaters and temperature sensors will be discussed in Chapter 3 with the testing of the microreactor packaging. Testing under non-reacting flow conditions will also be discussed in that chapter. The results of reaction testing will be discussed with the results of the scale-up system testing in Chapter 8.

References

1. Srinivasan, R., Hsing, I.-M., Berger, P.E., Jensen, K.F., Firebaugh, S.L., Schmidt, M.A., Harold, M.P., Lerou, J.J., and Ryley, J.F. (1997) "Micromachined reactors for catalytic partial oxidation reactions", *AIChE Journal,* **43**(11), pp. 3059-3069.

2. Srinivasan, R. (1998) *Microfabricated Reactors for Partial Oxidation Reactions*, Ph.D. Dissertation at the Massachusetts Institute of Technology, Cambridge, MA.

3. Hsing, I.M., Srinivasan, R., Harold, M.P., Jensen, K.F., and Schmidt, M.A. (2000) "Simulation of micromachined chemical reactors for heterogeneous partial oxidation reactions", *Chemical Engineering Science,* **55**, pp. 3-13.

4. Hsing, I.-M. (1998) *Simulation Strategies for Microfabricated Chemical Systems*, Ph.D. Dissertation at the Massachusetts Institute of Technology, Cambridge, MA.

5. Quiram, D.J., Hsing, I.-M., Franz, A.J., Jensen, K.F., and Schmidt, M.A. (2000) "Design issues for membrane-based, gas phase microchemical systems", *Chemical Engineering Science,* **55**, pp. 3065-3075.

6. Hood, P. (1976) "Frontal solution program for unsymmetric matrices", *International Journal for Numerical methods in Engineering,* **10**, pp. 379-399.

7. Keller, H.B. (1997) "Numerical solution of bifuraction and nonlinear Eigenvalue problems", In Rabinowitz, P.H., (Ed.), *Applications of Bifurcation Theory*, Academic Press, New York, pp. 359-384.

8. Keller, H.B. (1982) "Practical procedures in path following near limit points", In Glowinski, R. and Lions, J., (Eds.), *Computing Methods in Applied Sciences and Engineering*, North-Holland, New York, pp. 177-183.

9. Brooks, A.N. and Hughes, T.J.R. (1982) "Streamline upwind/Petrov-Galerkin formulations for convection dominated flow with particular emphasis on the incompressible Navier-Stokes equations", *Computer Methods in Applied Mechanics Engineering,* **32**, pp. 199-259.

10. Shackelford, J.F. and Alexander, W. (2000) *CRC Materials Science and Engineering Handbook*, 3rd ed, CRC Press, New York.

11. Bauccio, M. (1994) *ASM Engineering Materials Reference Book*, 2nd ed, ASM International, Materials Park, OH.

12. Zhang, X. and Grigoropoulos, P.C. (1995) "Thermal conductivity and diffusivity of free-standing silicon nitride thin films", *Review of Scientific Instruments,* **66**(2), pp. 1115-1120.

13. Mastrangelo, C.H., Yu-Chong, T., and Muller, R.S. (1990) "Thermophysical properties of low-residual stress, silicon-rich, LPCVD silicon nitride films", *Sensors and Actuators A,* **A21-A23**, pp. 856-880.

14. Govorkov, S., Ruderman, W., Horn, M.W., Goodman, R.B., and Rothschild, M. (1997) "A new method for measuring thermal conductivity of thin films", *Review of Scientific Instruments,* **68**(10), pp. 3828-3834.

15. Eriksson, P., Andersson, J.Y., and Stemme, G. (1997) "Thermal characterization of surface-micromachined silicon nitride membranes for thermal infrared detectors", *Journal of Microelectromechanical Systems,* **6**(1), pp. 55-61.

16. Arnold, J.C. and Sawin, H.H. (1991) "Charging of pattern features during plasma etching", *Journal of Applied Physics,* **70**(10), pp. 5314-5317.

17. Ayón, A.A., Zhang, X., and Khanna, R. (2000) "Ultra deep anisotropic silicon trenches using deep reactive ion etching (DRIE)", Presented at Solid-State Sensor and Actuator Workshop, June 4-8, 2000, Hilton Head, SC, pp. 339-342.

18. Ayón, A.A., Ishihara, K., Braff, R.A., Sawin, H.H., and Schmidt, M.A. (1999) "Microfabrication and testing of suspended structures compatible with silicon-on-insulator technology", *Journal of Vacuum Science and Technology B,* **17**(4), pp. 1589-1593.

19. Ayón, A.A., Braff, R.A., Bayt, R., Sawin, H.H., and Schmidt, M.A. (1999) "Influence of coil power on the etching characteristics in a high density plasma etcher", *Journal of the Electrochemical Society,* **146**(7), pp. 2730-2736.

20. Ayón, A.A., Braff, R.A., Lin, C.C., Sawin, H.H., and Schmidt, M.A. (1999) "Characterization of a time multiplexed inductively coupled plasma etcher", *Journal of the Electrochemical Society,* **146**(1), pp. 339-349.

21. Weichel, S., de Reus, R., Bouaidat, S., Rasmussen, P.A., Hansen, O., Birkelund, K., and Dirac, H. (2000) "Low-temperature anodic bonding to silicon nitride", *Sensors and Actuators A,* **82A**, pp. 249-253.

22. Plaza, J.A., Esteve, J., and Lora-Tamayo, E. (1998) "Effect of silicon oxide, silicon nitride and polysilicon layers on the electrostatic pressure during anodic bonding", *Sensors and Actuators A,* **67A**, pp. 181-184.

23. Madou, M. (1997) *Fundamentals of Microfabrication*, CRC Press, New York.

24. Preston-Thomas, H. (1990) "The International Temperature Scale of 1990 (ITS-90)", *Metrologia,* **27**(1), pp. 3-10.

CHAPTER 3
MICROREACTOR PACKAGING

The scale-up microreactor design was constrained by the need for an easy to use packaging method that provided both electrical and fluidic connections between the microreactor and other scale-up system components. The factors in selecting the packaging method included 1) compact size, 2) thermal and chemical compatibility with reactor operating conditions, 3) ability for fast reactor replacement; and 4) robust connections. Size was a critical issue since the system being designed was to have multiple microreactors running in parallel. Although the micro-heaters on the reactors were not a significant heat load, the entire reactor had to be heated in excess of the boiling points of the feed and product stream components. In addition, the materials that come into contact with these gas streams had to be chemically compatible. Because these microreactors fail often, replacing a microreactor should be a quick and easy task. Similarly, little work should be required to insure that the electrical and fluidic connections have been properly made.

Choosing the Microreactor Packaging Scheme

Previous experience with microreactor testing at MIT and DuPont was of little value since the MIT testing apparatus was unsuitable and the microreactors developed at DuPont were quite different in form and functionality. For example, initial testing of the T microreactor was done using a probe card, similar to the one shown in Figure 3-1. However, this required precision aligning equipment and resulted in a test setup with a large footprint due to the probe card size and the micro-positioners used. Wire bonding was a sub-optimal

choice because of the time required to replace chips without the use of an automated wire bonder. Furthermore, the presence of fragile wires extending from the top plane of the microreactor would make it difficult to apply the sealing force needed for a gasket or o-ring based fluidic connection.

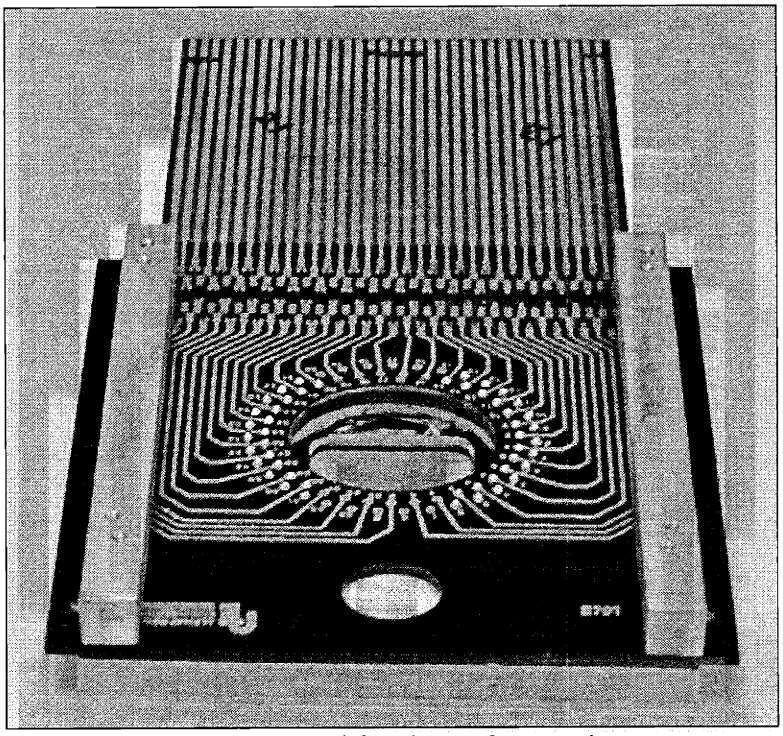

Figure 3-1. Probe card for the scale-up microreactor.

To solve the microreactor packaging problem, a number of options were considered: a spring contact probe based fixture, a Known Good Die (KGD) socket, Tape Automated Bonding (TAB) based fixture, and a parallel plate PC board fixture. Table 3-1 gives a comparison of these options.

Table 3-1. Comparison of microreactor packing options.

	Spring Contact Probe Fixture	Known Good Die Socket	TAB Fixture	Parallel PC Board Fixture
Fabrication	Simple	Prefabricated	Complicated if prefabricated TAB tape fixture is not available	PCB fabrication is simple, but designing aligning fixture could be difficult
Cost	~ $700 per fixture	~ $100 per socket	~ $3000 per fixture due to expense of TAB tape masks	~$300 per fixture
Development Time	Potentially long due to inexperience in their use	N/A	Long if TAB tape fixture must be designed	Potentially long due possible difficulty in making electrical contacts with dies
Electrical Connections	Simple to the microreactor, but individual wire connections from the probes to the PC board	Potentially difficult to design microreactor to align with socket's pins. Sockets are designed for PC board mounting.	Alignment between the TAB tape and microreactor bond pads could be difficult.	Difficult to align top PCB with microreactor die. May need solder bumps on the PCB or microreactor for electrical contact.
Fluidic Connections	Simple since pins do not interfere in accessing microreactor fluidic ports	Potentially difficult to modify sockets for fluidic connections	TAB tape fixture must be designed with fluidic connections or a prefabricated fixture altered	Must add metal piping to bottom PCB for transfer lines
Microreactor Fabrication	Flexible microreactor design	Microreactor must be designed for socket	Flexible since TAB tape will be designed for microreactor	Flexible, but very large bond pads needed
Materials Compatibility	Good since fixture can be made from various materials	Socket will not come into contact with fluids	Good as long as fixture material is chosen appropriately	Good, but metal transfer lines are required in fixture
Thermal Compatibility	Good since fixture can be made from various materials	Good since socket is rated at 1508C max. temp.	High temperature tapes available	Not all PCB materials will be thermally compatible

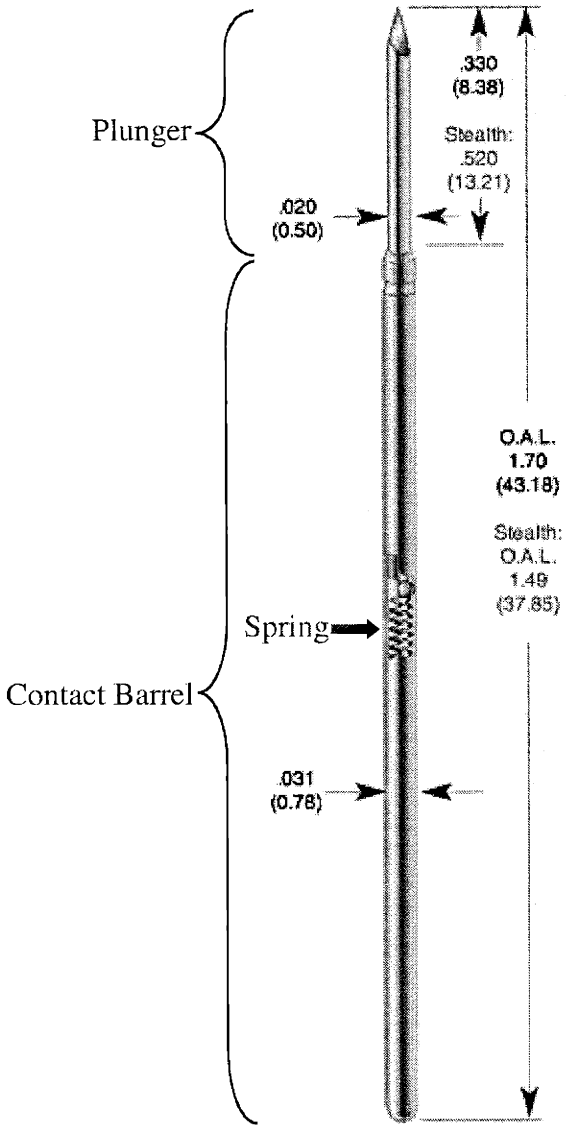

Figure 3-2. POGO®-72 spring contact probe from ECT[1]. Illustration adapted from ECT website[1].

A spring contact probe test fixture was strongly considered since it would be relatively simple to machine and is flexible to the microreactor design. Spring contact probes, example shown in Figure 3-2, make electrical connections through spring-loaded pins that are aligned with the bond pads of the die to be tested. Because of the spring, the

[1] Everett Charles Technologies, 700 E. Harrison Ave., Pomona, CA 91767, (909) 625-5551.

pins do not have to be perfectly planar in their fixture, which simplifies design. In the case of a microreactor fixture, this is also an advantage since the probes will apply a force to the top of the microreactor. This force can be used to seal the fluidic connections on the bottom of the microreactor.

The disadvantages foreseen in using spring contact probes were the expense of the fixture, the need to wire the pins individually to the PC board, and the possibility of design difficulties. The fixtures would be expensive to fabricate since the pins cost between $15 and $30 each, and approximately 16 pins would be needed for each microreactor (assuming four heaters and four temperature sensors per reactor). In any fixture design the pins would have to be individually wired to the PC board with microreactor sense and drive circuitry. This would result in clutter around the fixture and would require more space in the system. The main drawback to this option was the possibility of problems with designing the fixture. The main concern being that all the pins might not align with the microreactor bond pads and that the force applied to the top of the microreactor might not be well distributed—this could cause the membranes to fracture.

Known Good Die sockets were also strongly considered for microreactor packaging. These sockets, which were originally intended for use in die testing on production lines, are available in a variety of sizes and pin counts. The advantage of this technology is that the sockets are prefabricated, which eliminates the front-end design work. In addition, since the sockets are manufactured on a large-scale they are cheaper than the other packaging options. There was some concern about adding fluidic connections to the packaging and the need to heat the microreactors to prevent product condensation. Also there was the problem that the microreactors would have to be designed to fit into the KGD sockets and the bond pads

would have to be carefully placed to align with the socket's pins. It was believed that these obstacles could be avoided by choosing an appropriate KGD package.

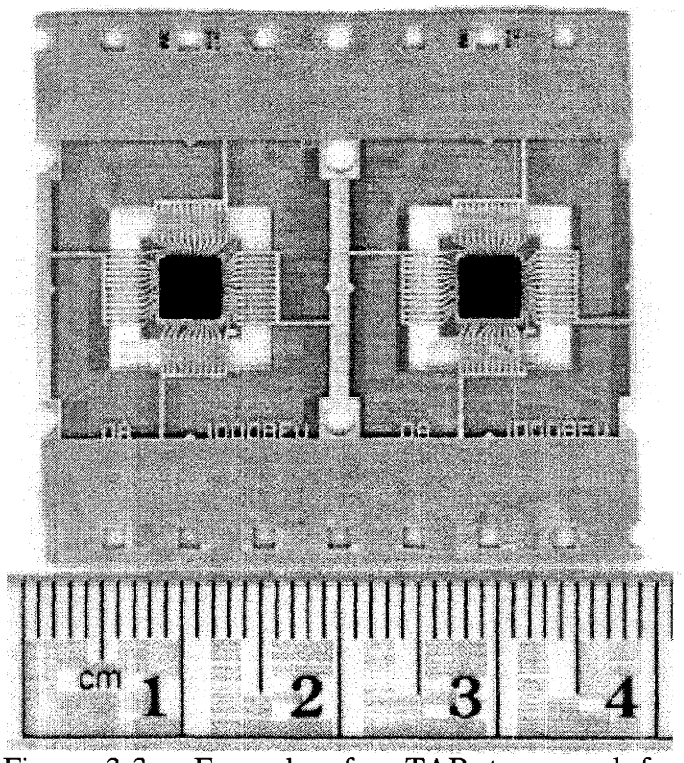

Figure 3-3. Example of a TAB tape used for electrical connections to an IC[2].

A fixture using TAB tape was considered since they are commonly used for IC packaging. TAB tape is a flexible interconnection device that has wire leads defined on it using photolithography, as shown in Figure 3-3. The wire leads on the tape are used to transition from the very small bond pads on an IC to the large bond pads on a PC board. Although using a TAB tape would allow a flexible microreactor design, there would have been substantial initial costs in manufacturing the masks used for the tape. This would result in each fixture costing on the order of thousands of dollars. A further concern was the difficulty in designing a fixture that would align the TAB tape with the microreactor bond pads. There was no previous experience in DuPont in using this technique. Thus, the best

solution would be to use prefabricated TAB based test fixture and adapt it to microreactor testing.

Finally, an overlay PC board fixture was also considered for microreactor packaging. In this case, a PC board would be designed with electrical contacts aligned to the microreactor bond pads. Although, this kind of alignment is achievable using standard PC board manufacturers, it was not clear that electrical contact could be made by simply laying a PC board on top of the microreactor die. It was believed that solder bumps would probably be necessary on the die or the PCB, but this would also be difficult since all of the bumps would have to be exactly the same height. In addition, most PC board materials did not have a high enough temperature rating for use.

Ultimately, the microreactor packaging problem was solved using the DieMate™ Known Good Die socket manufactured by Texas Instruments[2]. The packaging fixtures using spring contact probes or TAB tape were not used because of the possibility of long times needed for fabrication if the first design was not successful. In addition, the TAB tape fixture would have been considerably more expensive than the other options. The PC board overlay system was not used because of the uncertainty in making electrical connections. The KGD socket identified had the best combination of characteristics since it was cheap compared to other methods, and the DieMate™ socket could be easily modified to allow fluidic connections.

TI designed the DieMate™ socket to be used with a chip mounting assembly for die testing, as shown in Figure 3-4. However, the die assembly that fits in the socket was not

[2] Texas Instruments Incorporated, 34 Forest Street, P.O. Box 2964, Attleboro, MA 02703-0964, (508) 236-3800.

needed since the microreactor dies were considerably larger than conventional IC dies. Thus, it was decided to design the microreactor to fit directly in the socket as shown in Figure 3-5.

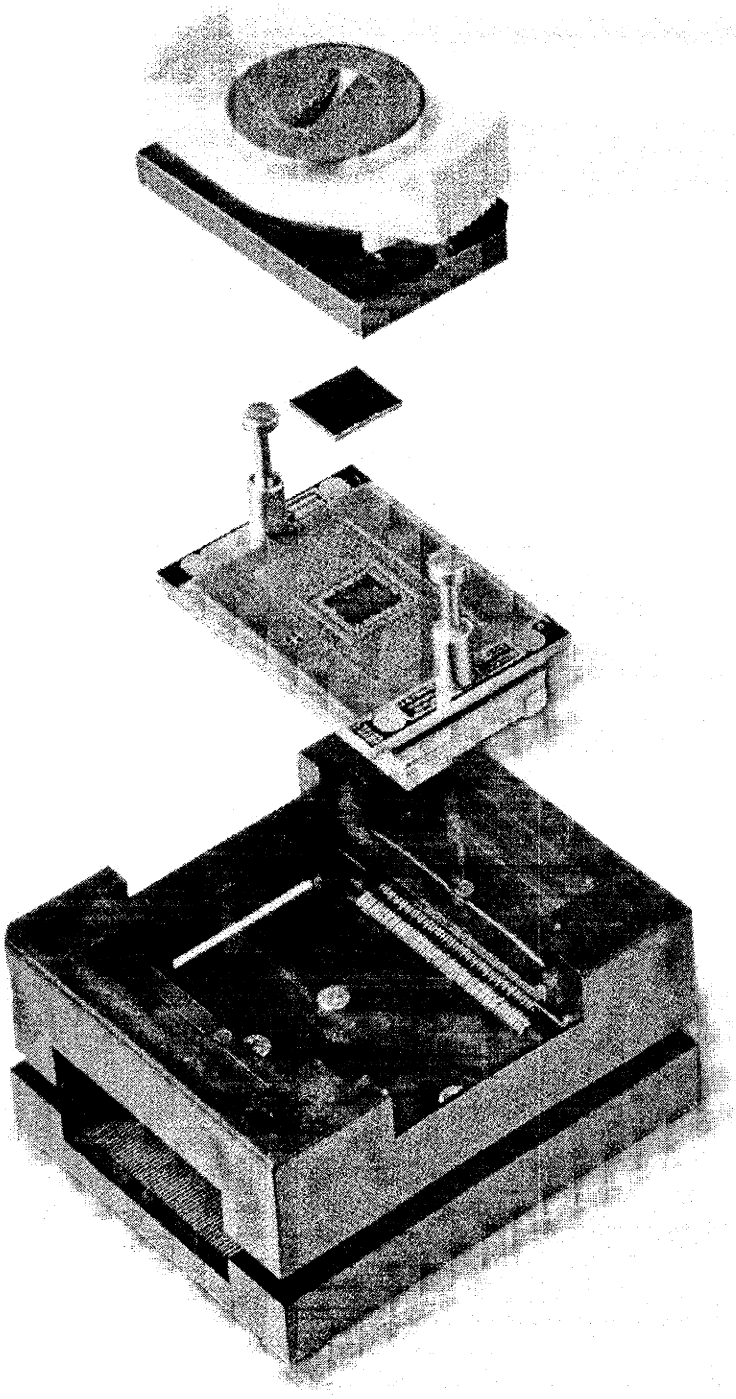

Figure 3-4. Exploded view of the DieMate™ KGD socket showing, from top to bottom, the lid, a die, the substrate, and the burn-in test socket[3]. The scale-up system uses only the burn-in test socket.

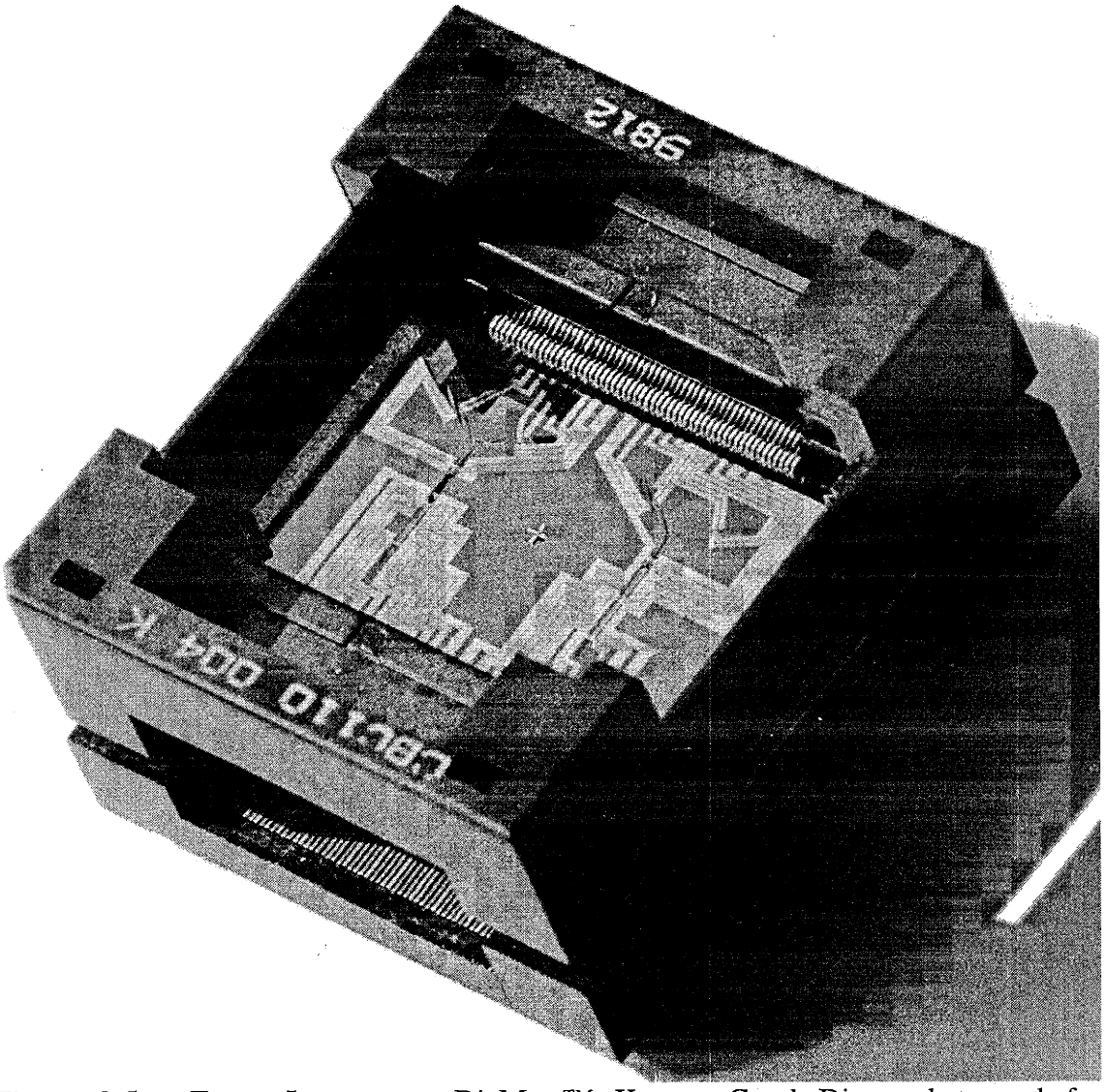

Figure 3-5. Texas Instruments DieMate™ Known Good Die socket used for microreactor packaging in the scale-up system.

The DieMate™ socket chosen for the microreactor scale-up system was the 110 pin version, part number CBC110 004 K. TI also manufactures 56 and 280 pin sockets. The 280 pin socket would have required a microreactor die size of 1.25" by 1.25". This was too large because it limited the number of dies to four per processed silicon wafer. This is illustrated in Figure 3-6, which shows a mock-up mask layout for the Y reactor design that was to be used in the 280 pin socket. Because of the low number of dies per wafer and the low

probability that any of the dies would have all four reactor membranes intact after processing, it was decided to use the smaller 110 pin socket. The 56 pin socket was not used since it uses the same die size as the 110 pin socket, and it was not available at the time the order for the sockets was placed.

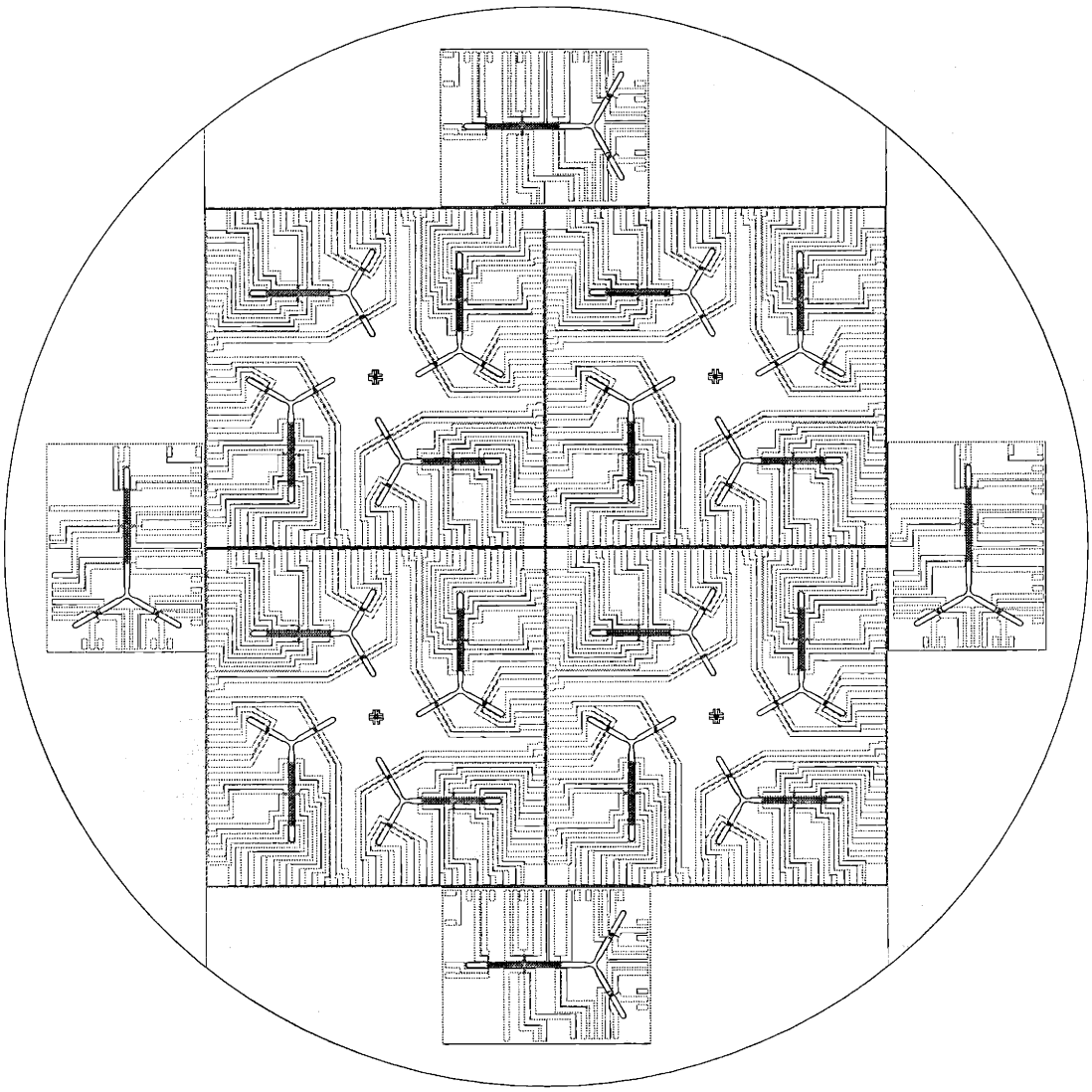

Figure 3-6. Microreactor die layout on a 4" wafer. The dies in this figure were designed for use in the 280 pin DieMate™ socket.

DieMate™ Electrical Interconnect Details

The DieMate™ socket holds the die in place and makes electrical contact with it using a row of pins on each side of the socket, as shown in Figure 3-5. The pins are forced into contact with the die by four springs that are placed on each corner of the socket. These springs are visible in Figure 3-7, which shows a side view of the DieMate™ socket. The springs force the upper piece of the socket away from the bottom piece. This force is redirected by the pins to press on the die in the socket. The latching force of the pins on the die is adjustable from 0.5 to 12 pounds, more than sufficient to form a gas-seal using o-rings. By pressing on the top piece of the socket, the springs are compressed and the pins of the socket are lifted off and away from the microreactor die. This allows for easy replacement of the microreactor.

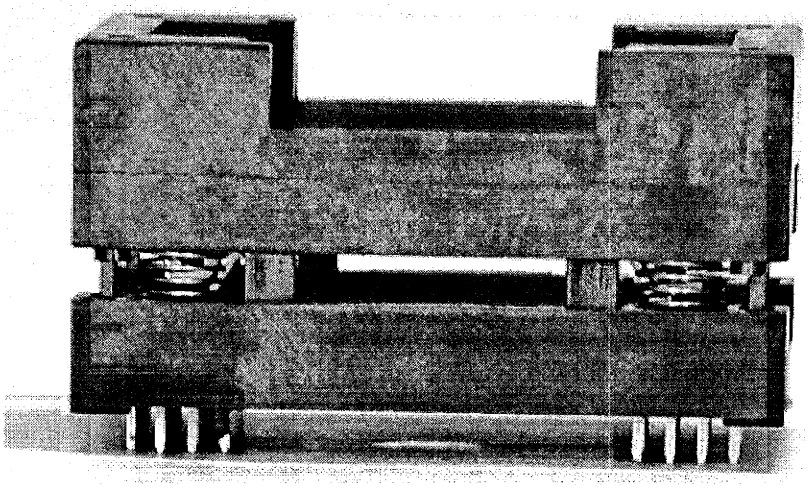

Figure 3-7. Sideview of DieMate™ socket.

The bond pads of the microreactor die and the pins of the DieMate™ socket are self-aligning in this system. The socket has ledges 1.1 mm underneath the pins that the microreactor die rests on, as shown in Figure 3-8. The die is carefully cut from the silicon wafers to fit inside the socket so that it is flush with the walls of the ledges, see Figure 2-15

for die dimensions. When a die is placed in the socket, the tight tolerance of the chip design to the socket insures proper alignment of the DieMate™ pins with the microreactor bond pads. The thickness of the microreactor die, 1.3 mm, results in a moderate force from the pins to the die.

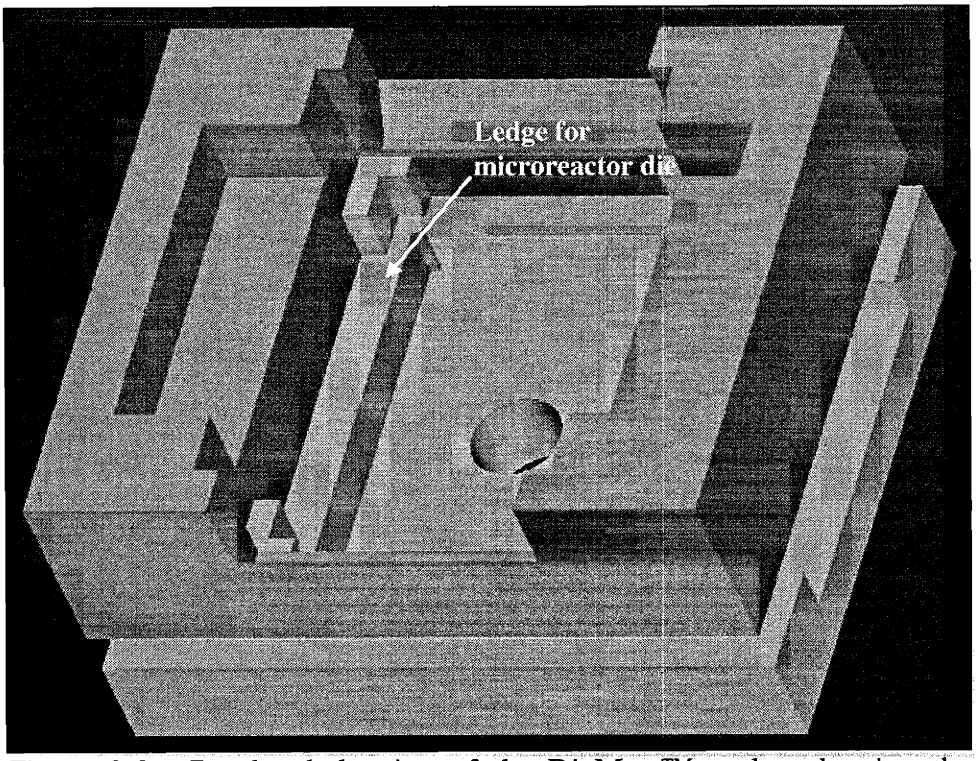

Figure 3-8. Rendered drawing of the DieMate™ socket showing the resting location of the microreactor die.

The layout of the bond pads did take advantage of the excess number of pins of the socket—only 56 electrical connections were needed for the scale-up microreactor die. Only every other pin in the socket was used by the microreactor. This gave a better tolerance on bond pad to pin alignment, with a bond pad pitch of 0.8 mm. More importantly, it allows a larger lead width, which reduces the electrical resistance in the leads to the micro-heaters and micro-temperature sensors. In the case of the micro-heaters, high resistance in the leads causes unnecessary power dissipation over the bulk silicon of the microreactor die. For the

micro-temperature sensors, the larger the resistance is outside of the RTD structure the greater the inaccuracy of the temperature measurement.

Figure 3-9 is a rendered version of the scale-up microreactor die that shows the metalization on the die. Note that a large amount of the silicon area is covered by the lead lines. However, some of the leads on the die are still narrow; this was done to make the resistances in all the leads to be approximately the same. This simplified the design of the electrical circuits controlling the micro-heaters and micro-temperature sensors.

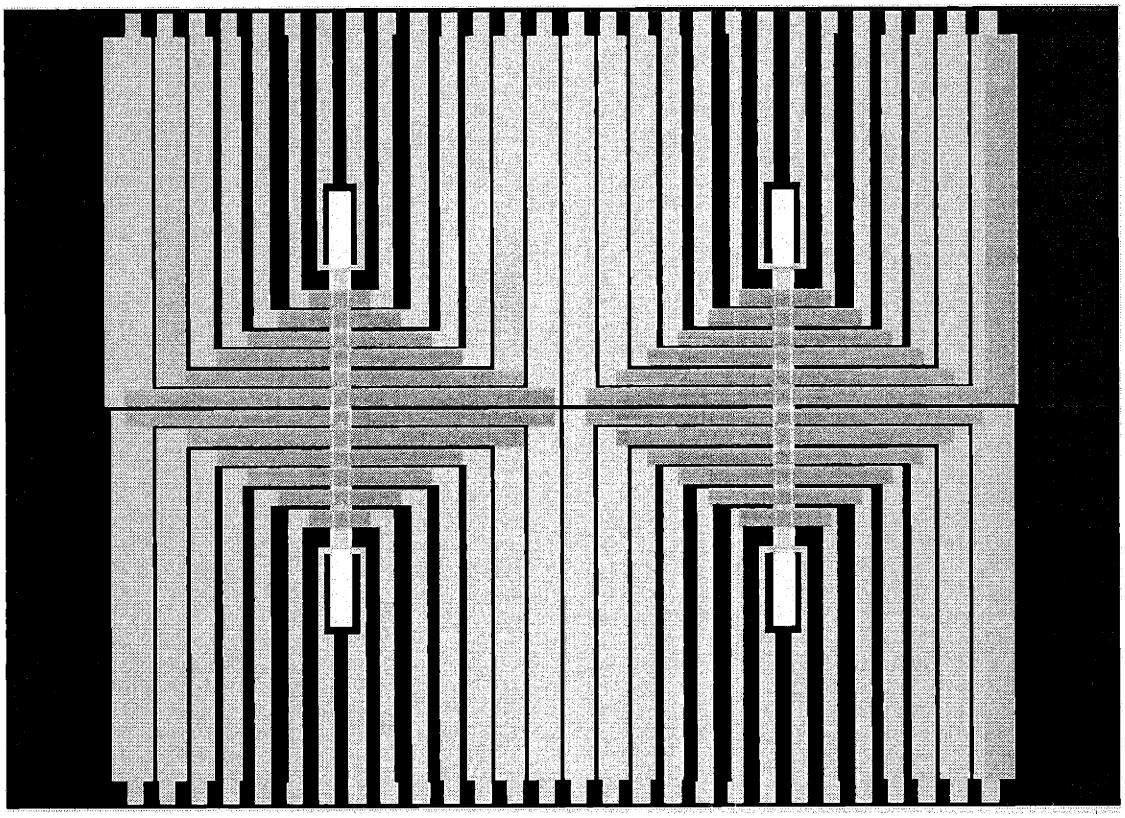

Figure 3-9. Rendered top view of the scale-up microreactor die. Metalization is shown in gray, silicon substrate is blue, and exposed membrane is in yellow.

The 56 electrical leads from the DieMate™ socket are carried to the external sensing and driving circuitry for the micro-heaters and micro-temperature sensors by mounting the socket on a custom-designed PC board. This connection is straightforward using the

DieMate's pins, which are visible in Figure 3-7. This mounting concept was first tested on a prototype multilayer PC board built for this project shown in Figure 3-10. The pins on the DieMate™ socket are altered by removing every other row of pins according to drawing D1489014[3][4]. This was done to make the artwork simpler on the PC board.

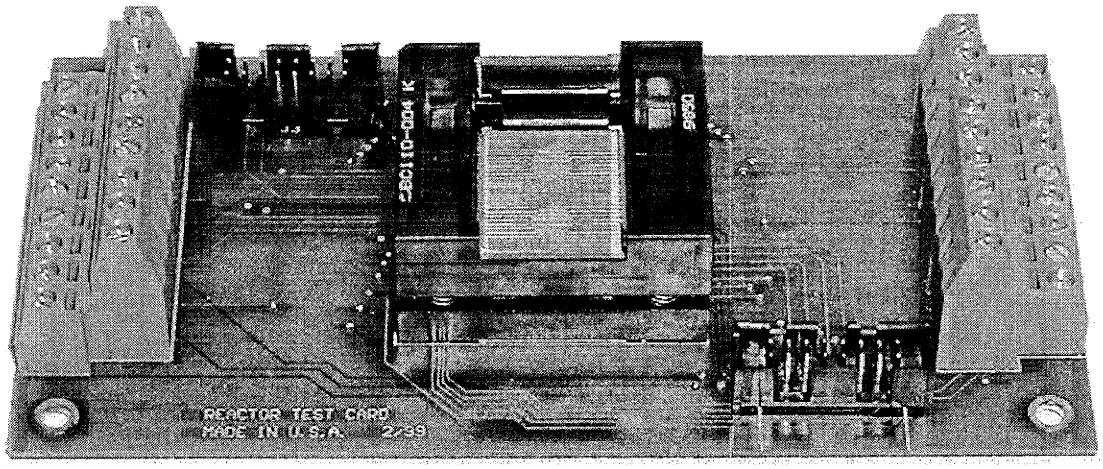

Figure 3-10. Prototype PC board used to test the scale-up microreactor.

DieMate™ Fluidic Interconnect Details

Since the DieMate™ socket was designed for use with integrated circuits, the fluidic interconnections had to be made by modifying the socket even further. The solid bottom of the socket, visible in Figure 3-4, was removed using conventional machining techniques to allow the placement of a manifold[4] underneath the microreactor die. A picture of the DieMate™ manifold is shown in Figure 3-11, and Figure 3-12 illustrates the complete microreactor packaging scheme. The DieMate™ manifold extends up into the socket where

[3] Where appropriate, references are given to the mechanical drawings used in designing the microreactor system. Access to drawings can be obtained by contacting the Beech Street Information Center of DuPont, 101 Beech St., Building 18, Wilmington, DE, (302) 695-0550.

[4] This manifold is subsequently referred to as the DieMate™ manifold.

it forms a seal with the Pyrex® bottom of the microreactor die using Kalrez® o-rings. The o-rings were 9/64" O.D. and 3/64" I.D., part number AS-568A K# 002, and were manufactured by DuPont Dow Elastomers[5]. The sealing force is provided by the pins pressing on the top of the microreactor and the socket head cap screws pushing the DieMate™ manifold upward, into the socket.

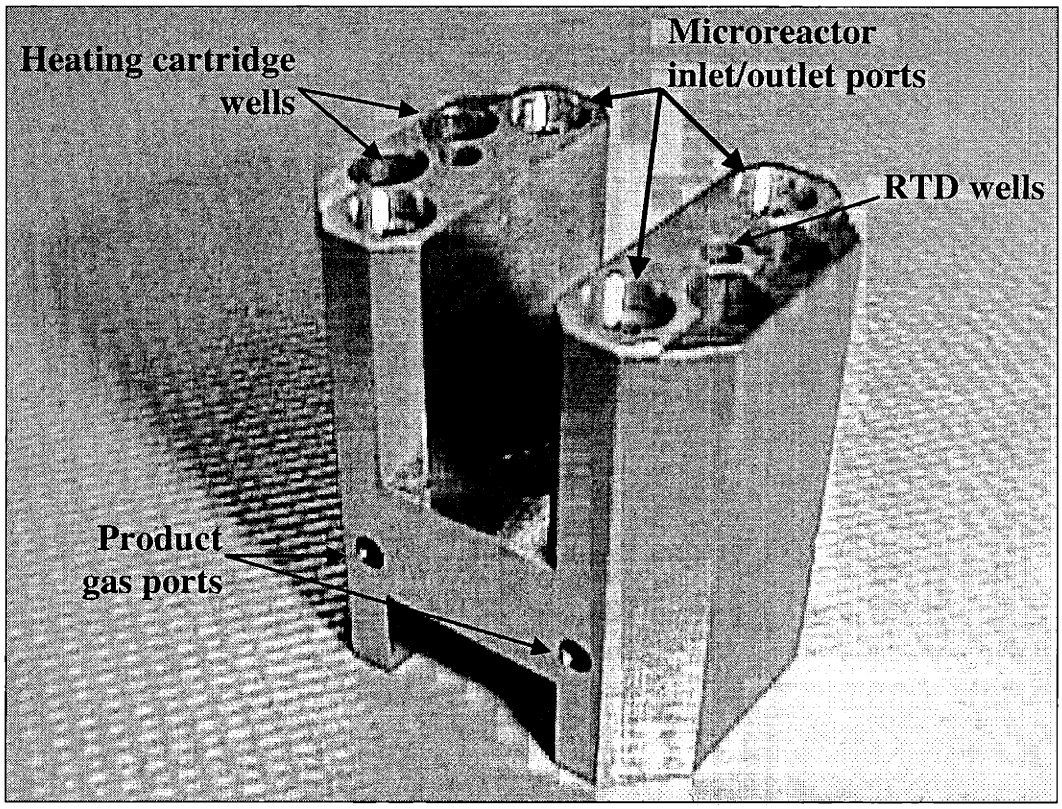

Figure 3-11. DieMate™ manifold used for fluidic connections and microreactor heating.

From Figure 3-12 it is not clear how the DieMate™ manifold is held in position inside the socket. The bottom of the DieMate™ socket is altered according to drawing D1489014[4], as shown in Figure 3-13. The bottom layer is almost completely removed except for two areas that contain socket head cap screws, which hold the DieMate™ socket

[5] DuPont Dow Elastomers L.L.C., Newark, DE, 19711.

together. The DieMate™ manifold piece mates with a T shaped metal piece[6] around these two remaining areas of the socket bottom layer as illustrated in Figure 3-14. Socket head cap screws that extend through the DieMate™ manifold and into the DieMate™ manifold nut plate are used to bring these pieces closer together. This effectively raises the DieMate™ manifold into the socket and forces the top of the manifold to come into contact with the bottom of the microreactor. The design of the DieMate™ manifold is specified in drawing D1489015[5]. The design of the DieMate™ manifold nut plate is specified in drawing D1489017[6].

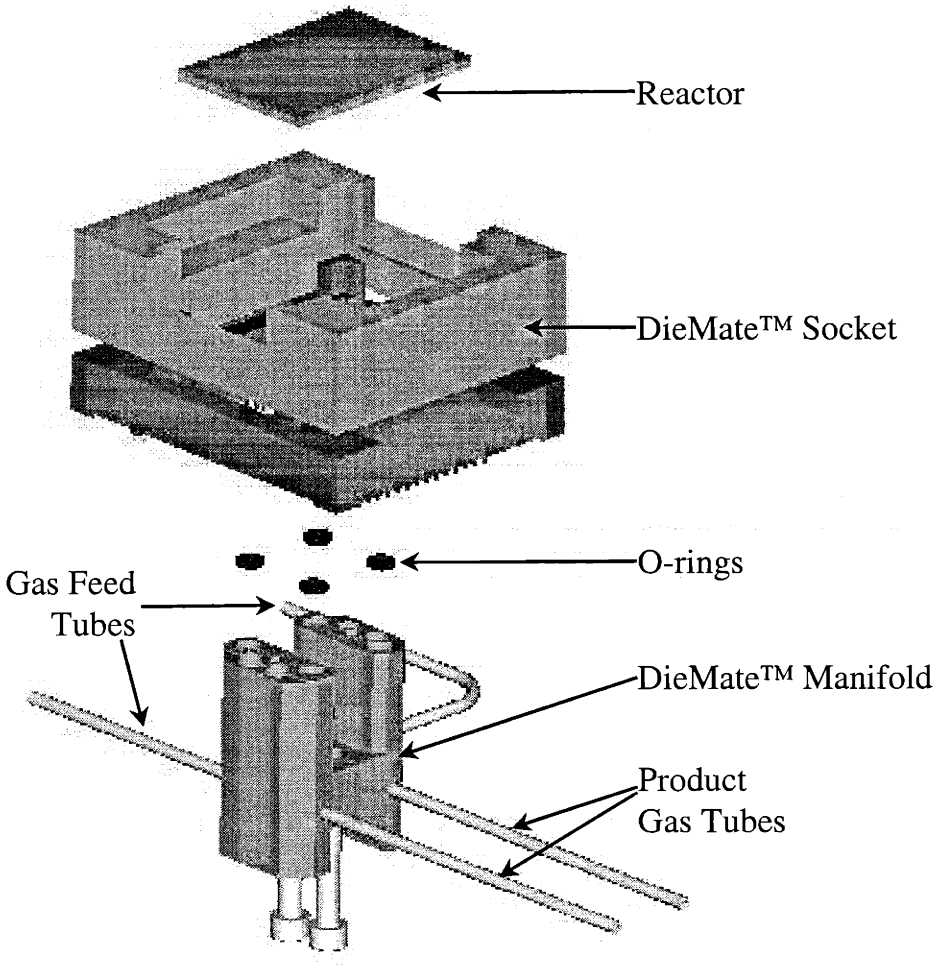

Figure 3-12. Exploded view of the DieMate™ packaging assembly.

[6] This piece is subsequently referred to as the DieMate™ manifold nut plate.

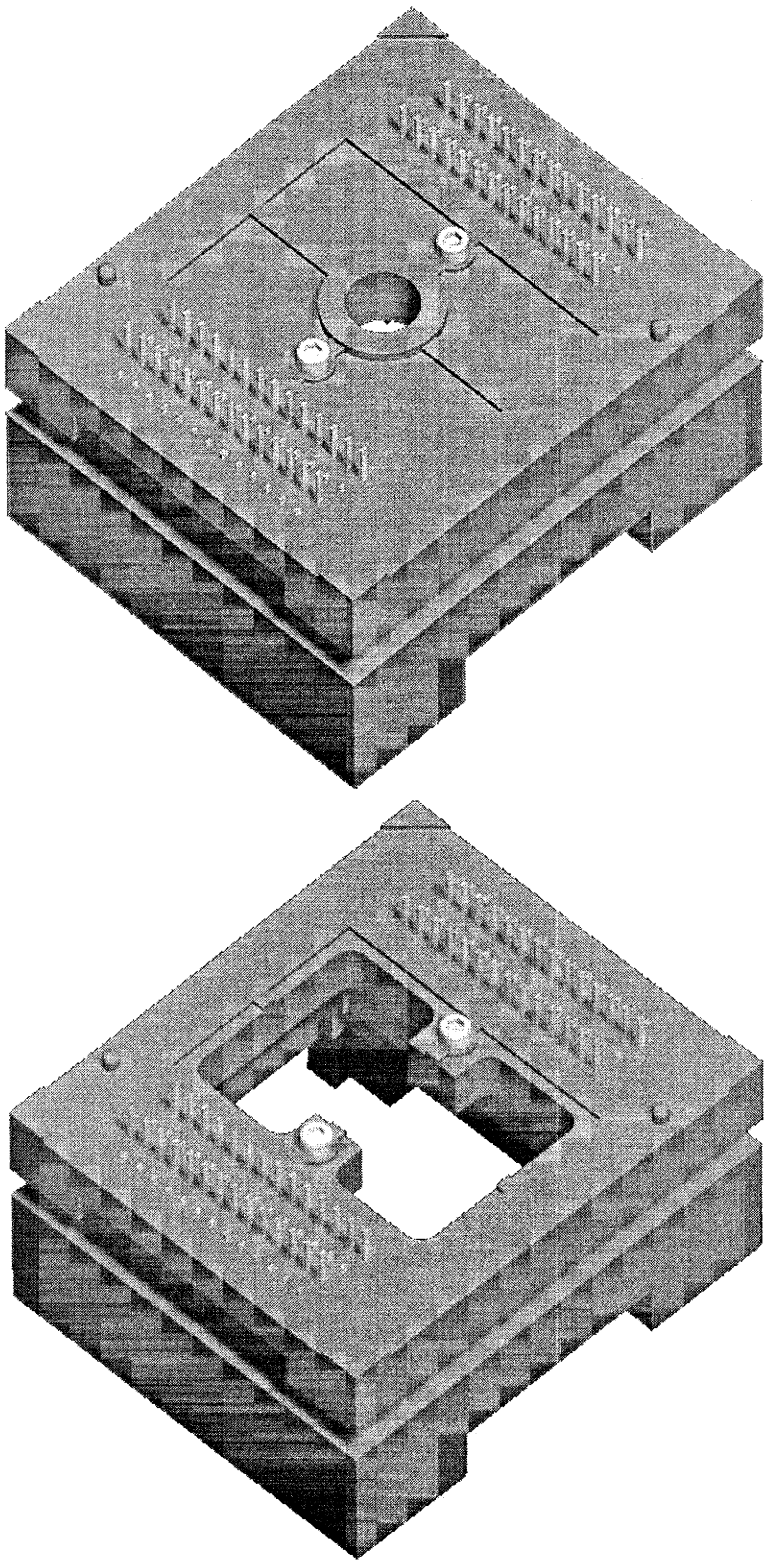

Figure 3-13. Rendered views of the DieMate™ socket showing the unaltered socket (top) and the altered socket (bottom). Note that the unnecessary pins have been removed in both views.

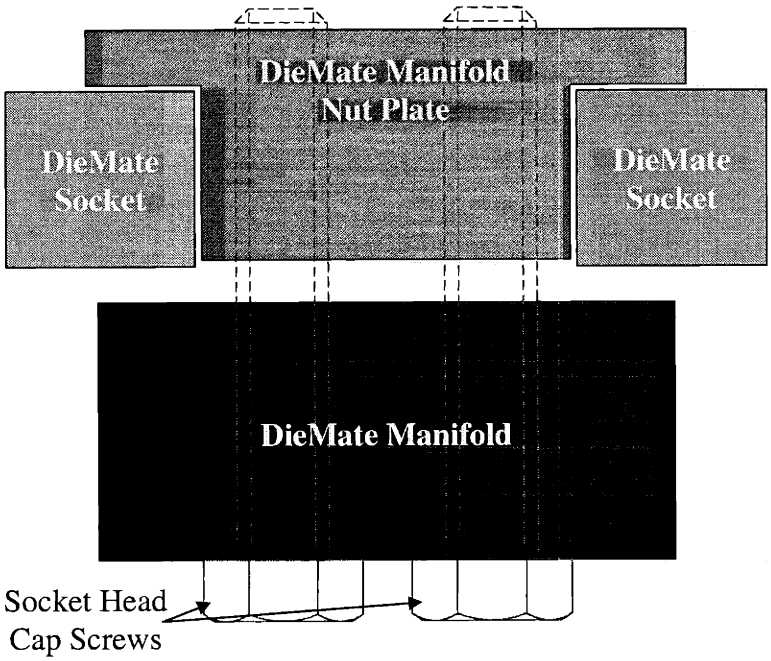

Figure 3-14. Cross-section showing how the DieMate™ manifold is held in the DieMate™ socket. Note that the DieMate™ manifold nut plate is tapped for the socket head cap screws, but the DieMate™ manifold is not.

The DieMate™ manifold also functioned as the microreactor die heater since it had four holes drilled in it for 1/8" O.D. heating cartridges. The heating cartridges each provided 15 W of power using a 48 Vdc power supply. The heating cartridges were custom manufactured by Technical Industrial Products[7], part number ITPHEA001, and were 1" in length. The temperature of the DieMate™ manifold was monitored using two 100 Ω platinum Resistive Temperature Devices (RTD) manufactured by Technical Industrial Products. One of the RTDs in the manifold had a two-wire configuration, part number RTD15-100L-SS116-1-PVC24-12-2, and the other had a four-wire configuration, part

[7] Technical Industrial Products, 703 Kenilworth Ave., Cherry Hill, NJ 08002, (877) 847-8367.

number RTD15-100L-SS116-1-PVC28-12-4[8]. Both types were 1/16" O.D. and 1" in length. Figure 3-11 shows where the heating cartridges and RTDs were placed in the manifold.

Fabrication of the DieMate™ manifold was done using conventional machining techniques with 316L stainless steel as the substrate. Although the thermal conductivity of stainless steel is not that high compared to other metals, it is chemically compatible with the gases used for the experiments. It could also easily handle the 200°C temperature required for microreactor heating. The DieMate™ manifold nut plate was also machined from 316L stainless steel. Gases do not come into contact with this piece, so its material of construction is not as critical. To prevent galling and seizing of the socket head cap screws in the DieMate™ manifold nut plate, the screws are coated with Swak®, a thread lubricant manufactured by CAJON[9], part number MS-PTS-6.

The feed and product gas transfer lines were connected to the DieMate™ manifold using silver solder. These lines were 0.062" O.D., 0.030" I.D. 316L stainless steel tubing obtained from Valco Instruments[10]. Figure 3-15 shows the DieMate™ manifold with the 1/16" transfer lines attached. Silver solder was used instead of welding for joining because it is very difficult to weld 1/16" stainless steel tubing. The small amount of silver that might contact the feed and product gases was not expected to cause problems during reaction experiments. Corrosion of the silver solder joints or the solder acting catalytically was not observed during the experiments. The DieMate™ manifold piping assembly is detailed in drawing D1489016[7].

---

[8] The CAL temperature controllers could only be configured for two-wire RTD's, but the NI analog input cards were configured for four-wire RTD's to improve the measurement accuracy.

[9] CAJON Company, 9760 Shepard Road, Macedonia, OH 44056.

[10] Valco Instruments Co., Inc., 7806 Bobbitt, Houston, TX 77255, (800) 367-8424.

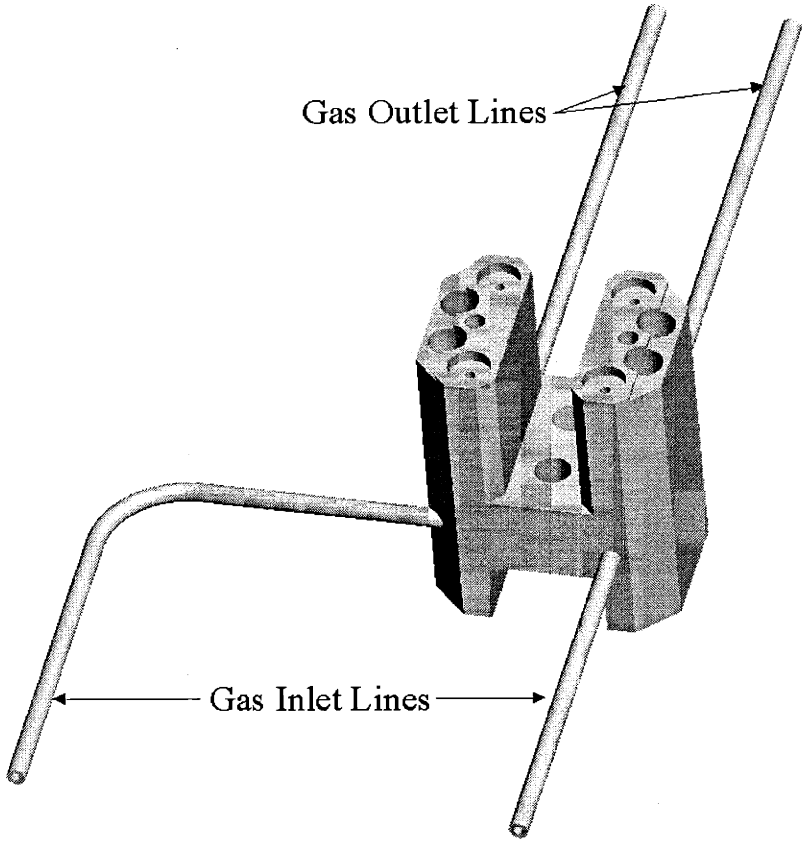

Figure 3-15. DieMate™ manifold piping assembly.

The DieMate™ manifold is insulated to improve thermal uniformity and to prevent exposure of the DieMate socket to excess temperature[11]. Figure 3-16 shows the insulated DieMate™ manifold before attachment of the 1/16" transfer lines. The insulation is ceramic fiber strip, which was obtained from McMaster-Carr[12]. The fiber strip is 1" in width, 1/8" in thickness, catalog number 87575K87. Its specified thermal conductivity is 0.38 (BTU.in)/(hr.ft^2.8F), and its maximum operating temperature is 2300°F.

[11] The DieMate™ socket maximum temperature specification is 150°C.
[12] McMaster-Carr, P.O. Box 440, New Brunswick, NJ 08903-0440, (732) 329-3200.

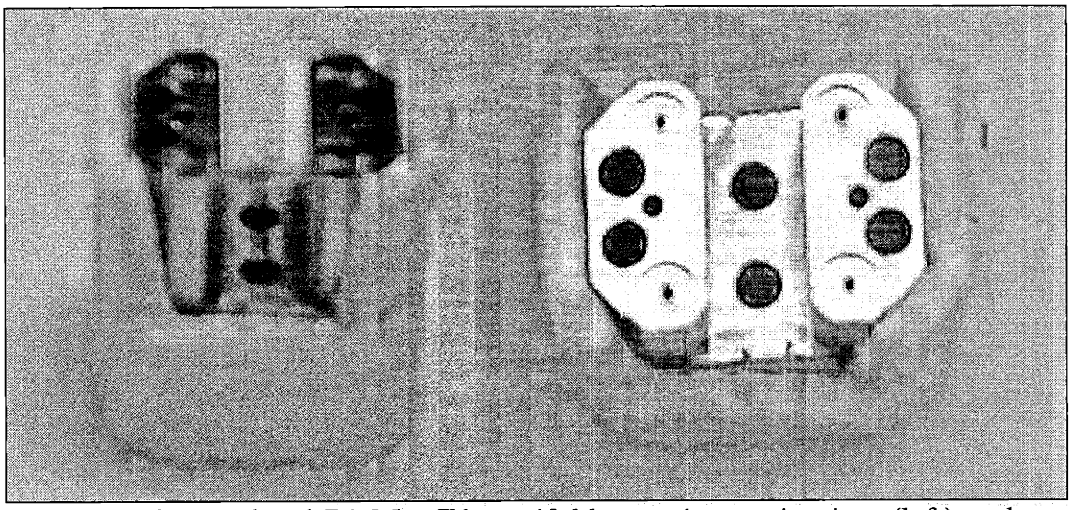

Figure 3-16. Insulated DieMate™ manifold: top isometric view (left) and top view (right).

Testing Procedures

The microreactor packaging along with the microreactor itself was tested for functionality. The experiments discussed here are 1) the electrical testing of the microreactor and modified DieMate™ socket; 2) the determination of the operating temperature range of the DieMate™ manifold mounted in a DieMate™ socket; and 3) the determination of the integrity of the gas seals of the DieMate™ manifold with the microreactor chip. Microreactor testing under reaction conditions is discussed in Chapters 7 and 8.

Electrical Testing of the Microreactor and DieMate™ Socket

Electrical testing of the connection of the DieMate™ socket with the microreactor die was necessary to ensure its ability to perform in the scale-up system. A prototype PC board with a mounted DieMate™ socket was custom-built for this testing by Phillipsburg Electronics[13]. It was shown earlier in this chapter in Figure 3-10. The microreactor PC board was used to connect the microreactor heater and temperature sensor structures with

[13] Phillipsburg Electronics, Inc., 500 Williams St., Easton, PA 18042, (610) 250-0142.

their appropriate driver circuitry. This circuitry was also custom-built for this project. Testing of the microreactor structures thus served a dual purpose of verifying their functionality along with the functionality of the driver and sensor circuit boards. These boards were prototypes of the circuits to be used in the scale-up system.

Electrical testing was done on both the first and final generation scale-up microreactors. Each had its own microreactor PC board used for testing since the bond pad pattern was different in the two microreactor designs. The testing setup used for this experiment is shown in Figure 3-17. A computer running LabVIEW v5.1 from National Instruments[14] (NI) was used to monitor and control the testing through a NI SCXI-1001 chassis with two NI SCXI-1141 analog input modules and a NI PCI-6713 analog output board. Figure 3-18 shows the SCXI chassis along with the microreactor circuit boards used in this experiment.

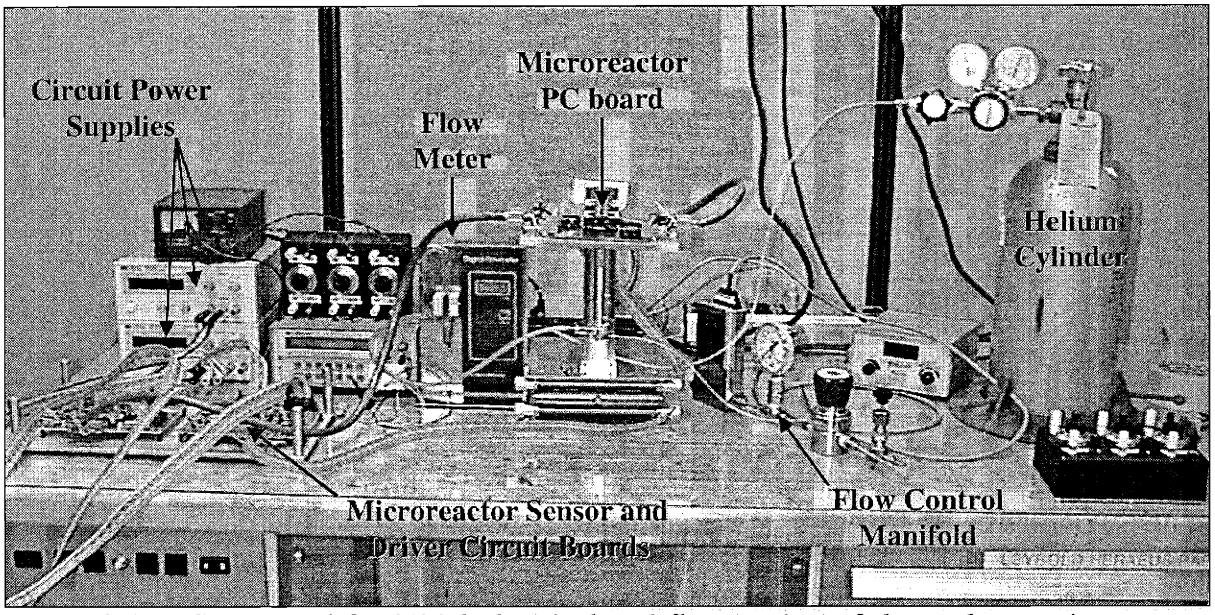

Figure 3-17. Setup used for initial electrical and flow testing of the scale-up microreactor and DieMate™ socket.

[14] National Instruments Corporation, 11500 N Mopac Expwy., Austin, TX 78759-3504, (512) 795-8248.

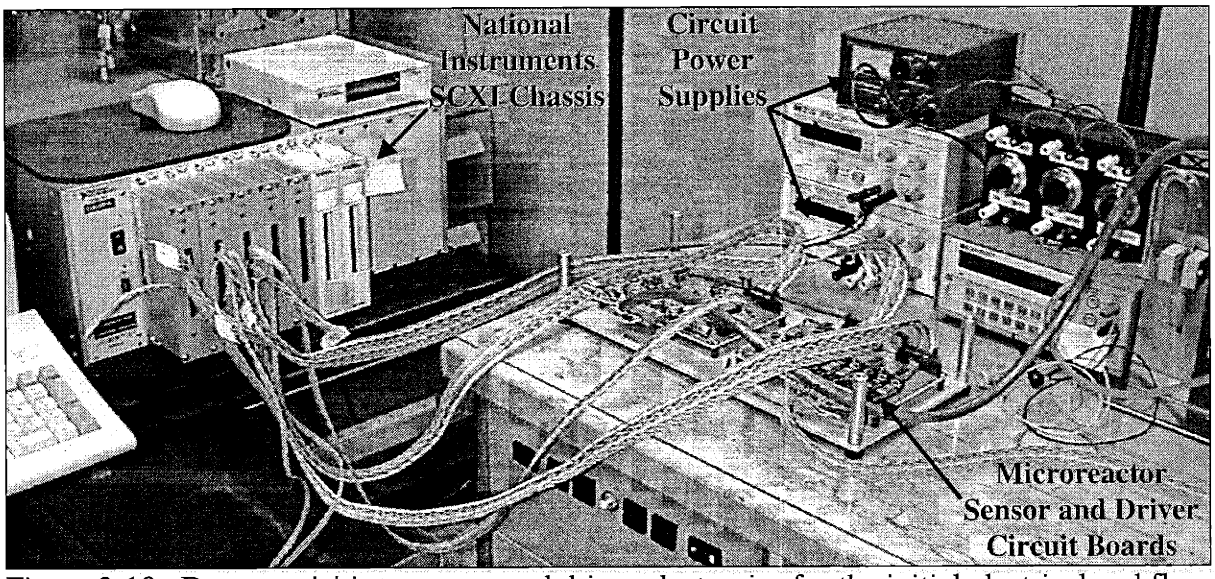

Figure 3-18. Data acquisition, sensor, and driver electronics for the initial electrical and flow testing of the scale-up microreactor and DieMate™ socket.

The testing procedure consisted of measuring the resistances of the microreactor heaters and temperature sensors at room temperature; verifying the ability of the microreactor heaters to obtain temperatures in excess of 200°C; and determining the dynamic temperature response of the microreactor heaters. The resistances of the microreactor device structures were measured to ensure they had relatively uniform resistances. This would allow the electrical circuitry to be adjusted to operate better for the scale-up system. The final scale-up microreactor was designed to have approximately the same measured resistance for all of the temperature sensors on a die and for all of the heaters on a die. The measured resistance refers to the resistance measurement of the structure taken at the microreactor bond pads. The scale-up microreactor design did not incorporate features for four point resistance measurements, so the lead resistance to the structure is added to its resistance. This uniform measured resistance feature was not incorporated into the first generation, Y, microreactor.

The microreactor heaters also had to be able to produce temperatures in excess of 200°C without breaking the reactor membrane or failing from electromigration. This

temperature was used as a minimum since the ammonia oxidation reaction requires a membrane temperature of approximately 200°C to produce measurable conversions. The design of both generations of scale-up microreactors had used simulations to predict the microreactor heater temperature at which electromigration would occur. This temperature was chosen to be around 600°C, but only data from previous microreactor experiments was available to predict when electromigration would occur. Furthermore, high temperature testing was clearly needed to determine the membrane stability since this was the most likely failure mode.

Dynamic testing of the microreactor heater was done to determine its response time, so the data acquisition and control electronics could be chosen accordingly. This data was later used to develop temperature control algorithms for the microreactor. In addition, this testing was useful in demonstrating another safety feature of these microreactors—high membrane temperatures can be quickly reduced. The dynamic step response of the microreactor heaters was fit to a first order plus time delay model as described by the following equation:

$$y(t) = KM(1 - e^{-(t-\theta)/\tau}) \tag{3.1}$$

where $y(t)$ is the process response; t is time; K is the process gain; M is the magnitude of the process input step change; θ is the process time delay; and τ is the process time constant.

The resistance measurements were taken with a Tektronix DMM916 multimeter and the NI data acquisition system described previously. The microreactor temperature sensors operate through a resistance measurement performed by the sensor circuitry. The NI equipment allowed for the rapid collection of this data. The multimeter was needed to measure the resistances of the heater structures since the sensor circuits do not measure this

directly. In addition, the multimeter was used to tune[15] and verify the accuracy of the temperature sensor circuits and the data acquisition equipment.

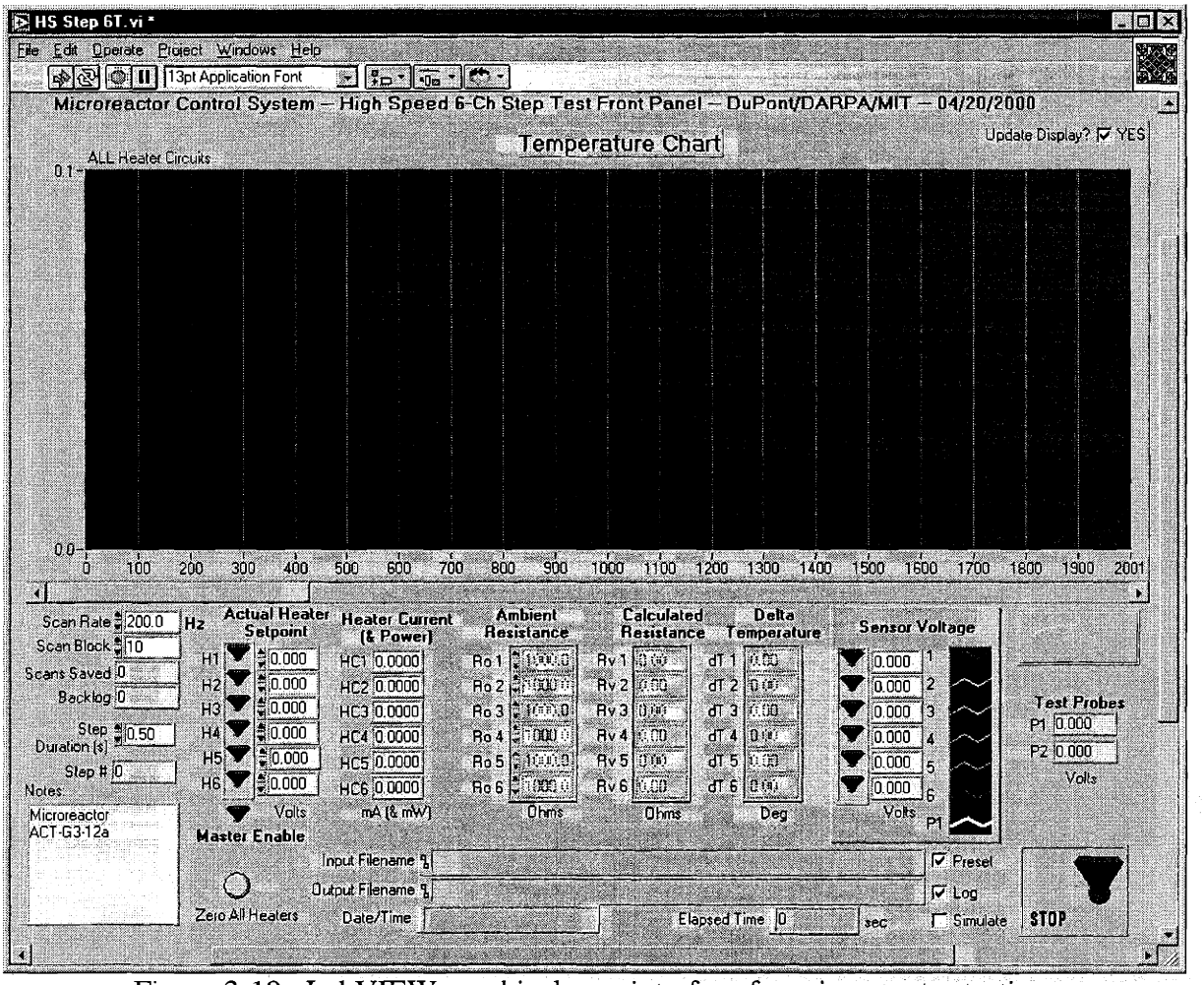

Figure 3-19. LabVIEW graphical user interface for microreactor testing.

The NI data acquisition system was used to verify the ability of the microreactors to reach a 200°C membrane temperature. A LabVIEW Virtual Instrument (VI) was created to allow the operator to adjust the power voltage to the microreactor heaters and monitor the temperature sensor resistances. Figure 3-19 shows the panel for this VI. This VI was also used for the dynamic heater testing. Besides the ability to manually change heater set points

[15] The temperature sensor circuits contain an adjustable potentiometer that is tuned to

through the user interface, it is also capable of automatically performing step changes in the heater voltage set points and recording the temperature sensor response. Because of the fast thermal response of the microreactors, data was recorded at a rate of 4000 Hz for these dynamic tests. The equipment was capable of reading data at faster rates, but 4000 Hz was sufficient to capture the dynamic behavior of the heaters. The LabVIEW VI automated this testing by reading in a data file containing the desired step changes and then performing these step changes at a user-defined time interval.

Determination of the Operating Temperature Range of the DieMate™ Manifold

The purpose of this test was to verify the operation of the DieMate™ socket at the desired operating temperature of the DieMate™ manifold, which was 200°C. Because the maximum specified operating temperature of the DieMate™ socket is given as 150°C, it was necessary to determine the maximum temperature setting of the DieMate™ manifold before the temperature adversely affected the DieMate™ socket. There was some flexibility in the operating temperature of the manifold since the goal was to prevent water condensation in the lines. However, the desired temperature set point of the DieMate™ manifold was well above 100°C since the entire microreactor die had to be heated through thermal contact with the manifold.

One of the prototype PC boards manufactured by Phillipsburg Electronics was used for this test to represent the actual PC boards in the scale-up system. The DieMate™ socket on the PC board was modified as described earlier to accommodate the DieMate™ manifold. Figure 3-20 shows top and bottom views of this board. A microreactor die with broken membranes was placed in the socket during testing to measure the temperature on the top surface of the die with a thermocouple. The DieMate™ manifold was placed into the

---

improve their accuracy.

DieMate™ socket with the reactor die mounted on top. Four heating cartridges, which were wired in parallel, were used to heat the manifold. Specifications for these cartridges were given previously. Two type J 1/16" thermocouples were used to measure the temperature of the DieMate™ manifold (one thermocouple for control and one for over-temperature sensing). A CAL[16] 3200 temperature controller was used to adjust the power to the four heating cartridges in the DieMate™ manifold. A second CAL 3200 temperature controller was used for interlocking in the event of an over-temperature excursion. An additional type J 20 mil thermocouple was used to measure the surface temperature of the microreactor die. It was not attached to the die in anyway, and temperature measurements were taken by manually holding the tip of the thermocouple against the bottom of the reaction channels. The DieMate manifold was wrapped in insulation, as shown in Figure 3-16, to mimic how the manifold would be used in the scale-up system.

The testing procedure was to gradually raise the temperature of the DieMate™ manifold starting at 45°C in 5°C to 15°C increments and let the manifold stabilize for about ½ hour at the new temperature. At 25°C increments starting at 150°C longer term stability testing was done with the manifold remaining at temperature for a period of two hours. The manifold was cooled and removed from the socket after the longer term tests to examine the socket for thermal damage.

[16] CAL Control Inc., 1580 S.Milwaukee Ave., Libertyville, IL 60048, (847) 680-7080.

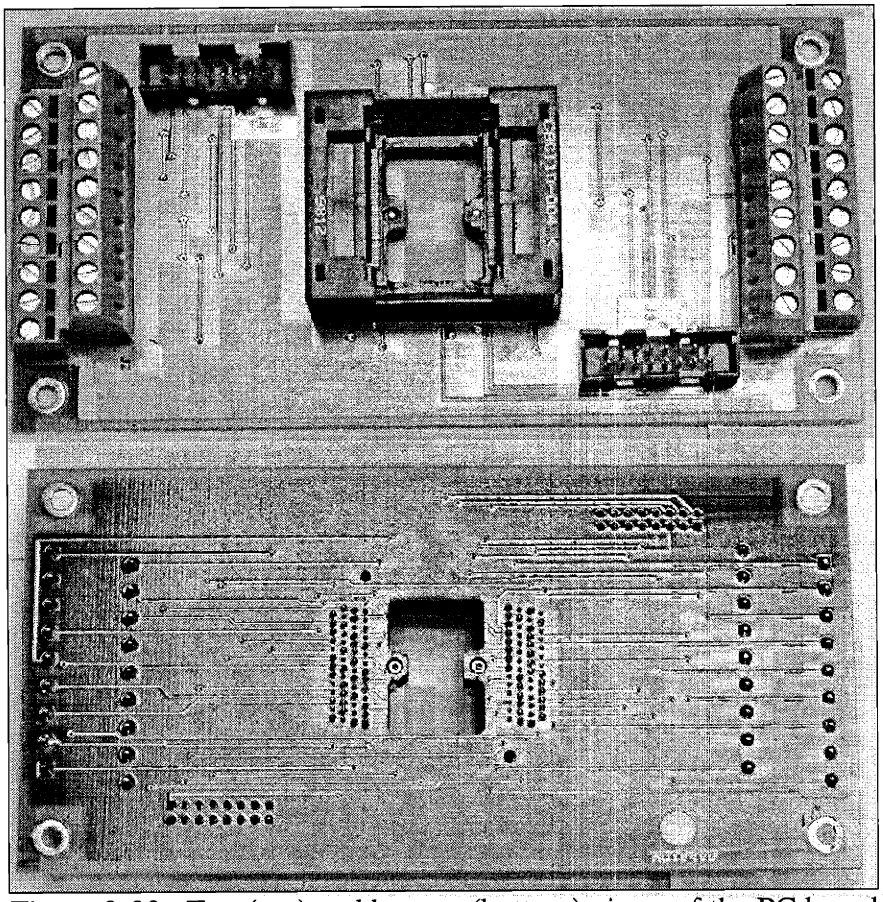

Figure 3-20. Top (top) and bottom (bottom) views of the PC board used for temperature testing of the DieMate™ manifold and socket.

Fluidic Testing of the Microreactor Packaging

The O-ring seals of the DieMate™ manifold to the microreactor die were tested for fluidic integrity at room temperature and at 200°C. The flow testing setup is shown in Figure 3-17. The gas used for this testing was helium. Flow to the microreactor channels was controlled using a gas flow manifold consisting of a Tylan[17] Mass Flow Controller (MFC), a 0-25 psig GO[18] Back Pressure Regulator (BPR), and a pressure gauge to monitor the pressure

[17] Millipore Corp., Microelectronics Division, 915 Enterprise Blvd., Allen, TX 75013-8003, (617) 275-9200.
[18] GO Regulator, Inc., P.O. Box 3300, Corona, CA 92878, (909) 270-6304.

after the MFC. In addition, there was a two-stage pressure regulator with gauges connected to the valve of the helium cylinder.

Testing was done by establishing a flow rate of 50 ml/min of helium through one of the microreactor channels. This flow rate was chosen since it was the maximum anticipated flow rate that the microreactors would be operated at. An Alltech Associates[19] digital bubble flow meter was used to measure the gas flow rate. After the flow rate was established, and the DieMate™ manifold had stabilized at the set point temperature for ½ hour a Gow-Mac[20] model 21-250 gas leak detector was used to check for helium leaking from the microreactor gas seals to the DieMate™ manifold. This leak detector operates by using a thermal conductivity sensor to locate leaks. Helium was used as the gas in the flow testing since it has a large difference in thermal conductivity from air. This instrument can detect helium leak rates down to 1.0×10^{-5} ml/s.

Results

A summary of the results for the testing procedures described in this chapter is given below. Because of the amount of data obtained in some of the tests, only the data relevant to the testing of the Automated, Integrated Microreactors System is given. In general, test results concerning microreactor performance are only given for the microreactors with the ACT silicon nitride film since these reactors were the only ones used for scale-up system testing. These reactors are divided into three groups, where the microreactors in each group had their platinum deposition done at the same time.

---

[19] Alltech Associates Inc., Applied Science Labs, 2051 Waukegan Rd., Deerfield, IL 60015, (312) 948-8600.

[20] Gow-Mac Instrument Co., 277 Brodhead Rd., Bethlehem, PA 18017, (610) 954-9000.

Resistances of Microreactor Structures

Room temperature resistances of the microreactor heaters and temperature sensors revealed that the device resistances were quite uniform on a single die. The variability of the structure resistances, using the sample standard deviation as its measure, revealed that the heaters had an average variability of less than 1% on a die and the temperature sensors had an average variability of 2.6% on a die. However, the structure resistances vary more from die to die as well as from group to group. Table 3-2 summarizes the results of this testing by reactor group and the devices as a whole. Eleven reactor dies from six different wafers were used to determine these statistics.

Table 3-2. Microreactor Structure Resistances.

Device	Average Resistance (Ohms)	Resistance Variability (Ohms)[21]
Group 1, Heaters	512	10
Group 2, Heaters	482	11
Group 3, Heaters	477	18
Group 1, Temperature Sensors	1700	100
Group 2, Temperature Sensors	1590	130
Group 3, Temperature Sensors	1650	170

The large variation in resistances between different reactors in the same group results mainly from slight deviations in the photolithography of the platinum thin film layer. Because of variations in the exposure of different areas of the wafer, the platinum line-widths can vary by a micron across a wafer. In addition, across individual wafers the development process differed slightly by the amount of time spent in the developer. This also affects the line-width of the platinum structures. Because the temperature sensors only have a line-width of 10 μm, even a difference of 1 μm will cause a 10% variation in the device

resistance. The variation of the structure resistances on a single die are mainly caused by the layout of the metalization since it was impossible to make all of the lead resistances exactly the same.

Microreactor Heater Dynamic Response Results

Through the use of the LabVIEW VI created for electrical testing a large volume of data was collected on the dynamic response of the microreactor heaters. Numerous step tests were performed with the magnitudes, starting temperatures, and ending temperatures being varied. Tests were also performed on microreactor heaters operating alone and in groups (for example, three heaters being stepped simultaneously).

A program was written to automate the data analysis since the amount of data was large (more than 100 step changes in a data file), and the calculations were straightforward to apply. MATLAB[22] v. 5.3 was used for this purpose due to its capabilities of performing matrix calculations and programming simplicity. In addition, the Signal Processing Toolbox was used to fit the data to a first order response model.

Figure 3-21 shows an example of a heater step response with a fitted first-order plus time delay model. It was found that the first order model was quite good in describing the dynamic response of the heaters. The transient cooling response of the microreactor heaters was also described quite well by a first order plus time delay model. For these tests, the heater voltage underwent a step change that corresponded to a change in the heater power. However, the heater power was not strictly a step change due to the change in resistance of the platinum heaters with temperature. This effect can be seen in Figure 3-21. The

[21] The standard deviation of the sample is used to determine the variability in the structure resistance.
[22] MATLAB, The MathWorks, Inc., 3 Apple Hill Dr., Natick, MA 01760, (508) 647-7000.

MATLAB analysis fitted the temperature response to the power instead of voltage since power is a more direct measure of the energy being dissipated by the microreactor heaters.

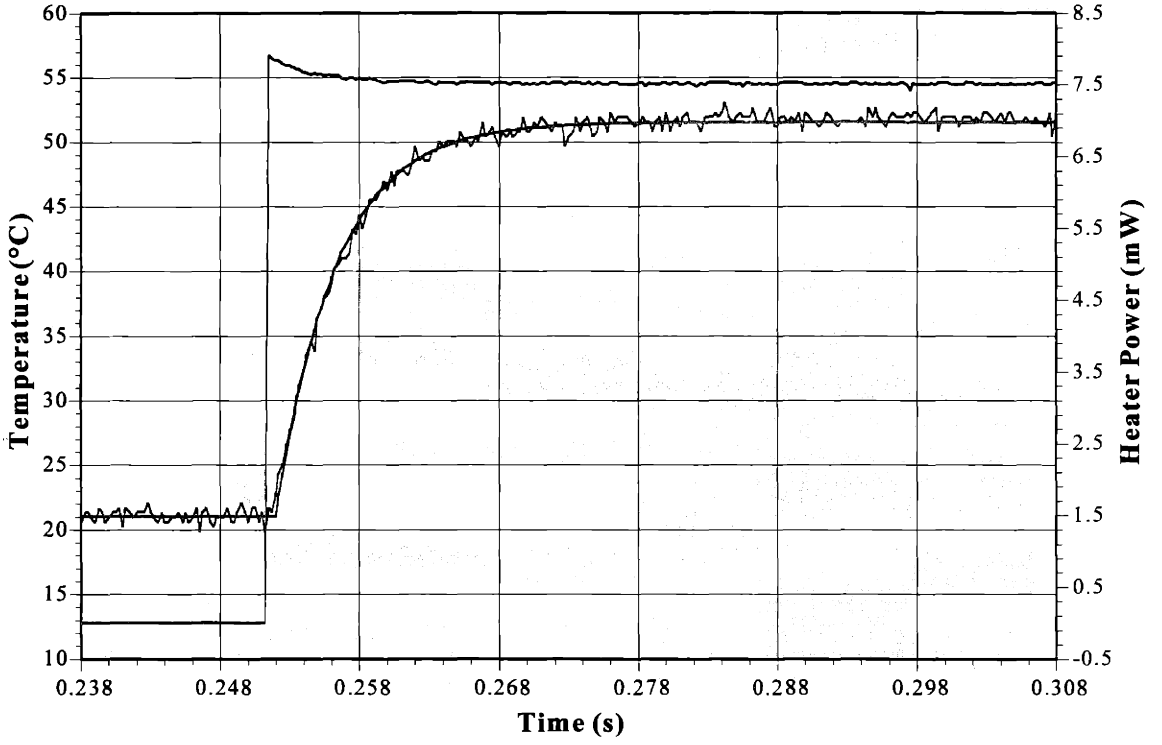

Figure 3-21. Microreactor heater dynamic response for a heater voltage step change from 0 to 2 V. — Measured heater segment temperature. — Predicted first order plus time delay model temperature. — Power applied to the heater segment. Model gain is 4.1°C/V. Model time constant is 4.5 ms. Model time delay is 0.5 ms. The test was done on the first heater segment with air in the reactor channel under no flow conditions with microreactor #ACT-G1-13a.

A complete step response analysis for a single scale-up microreactor channel is shown in Figure 3-22 and Figure 3-23, which show a plot of the first order gains and time constants, respectively. The testing results illustrated in these figures are very similar to the other microreactors tested. These data indicate that the first order model parameters of the microreactor heaters depend on the magnitude of the step change and the initial and ending conditions of the step change. This can be seen in the order apparent in the data groupings in Figure 3-22 (On close inspection, one can seen that the groupings have a linear relationship

between the temperature change and the gain). For this microreactor, the first order model gain varies from 2 to 5. The first-order time constant graph did not display the type of order shown in the gain graph when the data is grouped according to beginning and ending temperature. However, in this graph there is definitely an asymmetry since cooling is a slower process than heating for the microreactor heaters. The time constant increases as the magnitude of the cooling temperature change increases. No such relationship is apparent for the heating process except from going to the smallest to largest step changes. For this microreactor, the first-order time constant varies from 1 to 6 milliseconds, but most of the data points are in the range of 3 to 6 milliseconds. The time delay calculated does not show such a wide variation and is relatively constant at 0.25 milliseconds (the time resolution of the data measurement). The variation in the parameter values increase as the magnitude of the step change becomes small (less than 100°C). This type of behavior is expected since the smaller temperature changes are studied over a wider variation of conditions.

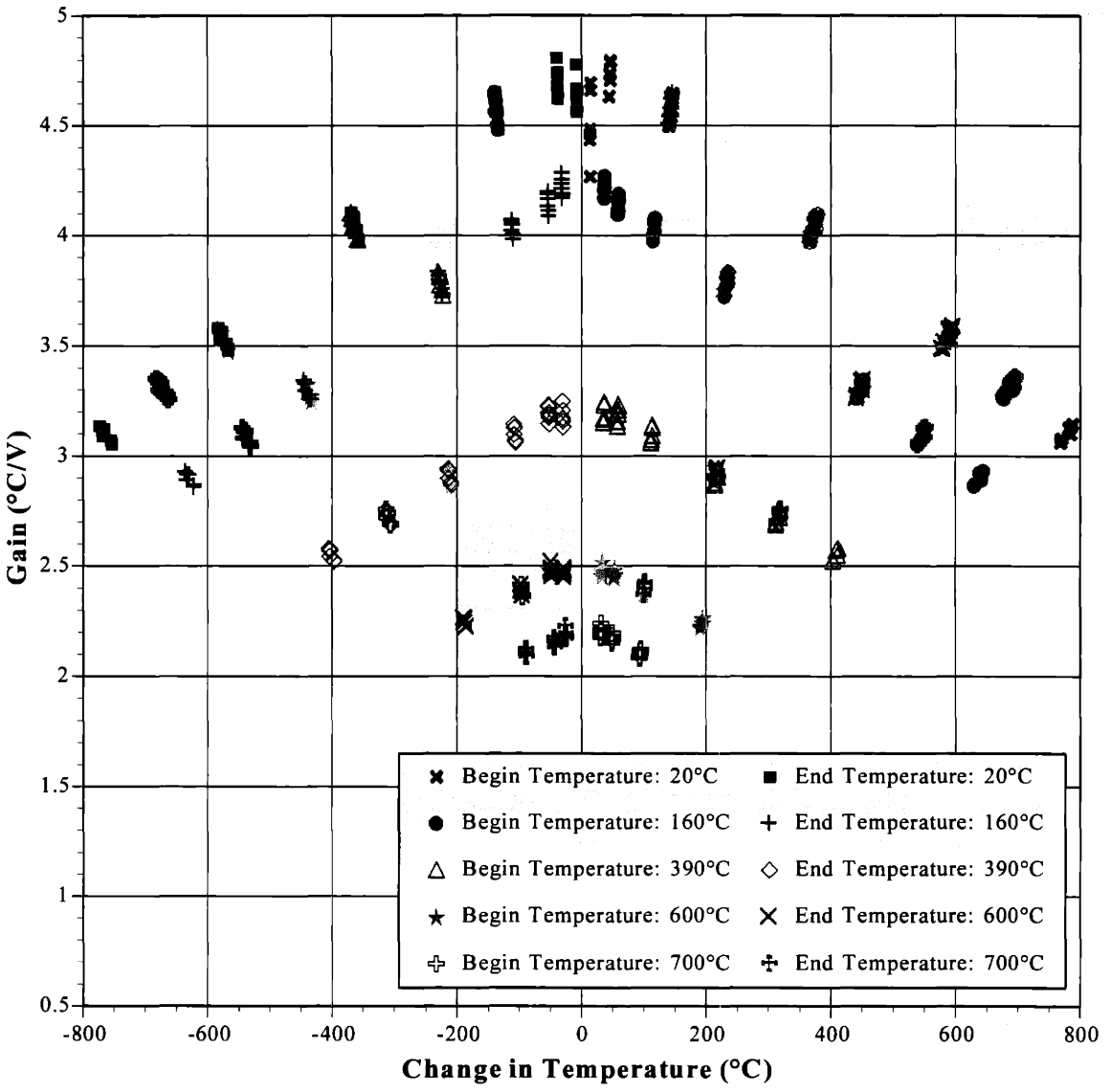

Figure 3-22. Microreactor heater first-order gain plotted as a function of the change in temperature in the step response test (end temperature – begin temperature). Data is shown for the first six heaters in the microreactor channel with the tests being performed on individual heaters. Data is grouped according to the beginning or ending temperature of the test. The test was done with air in the reactor channel under no flow conditions with microreactor #ACT-G1-11b.

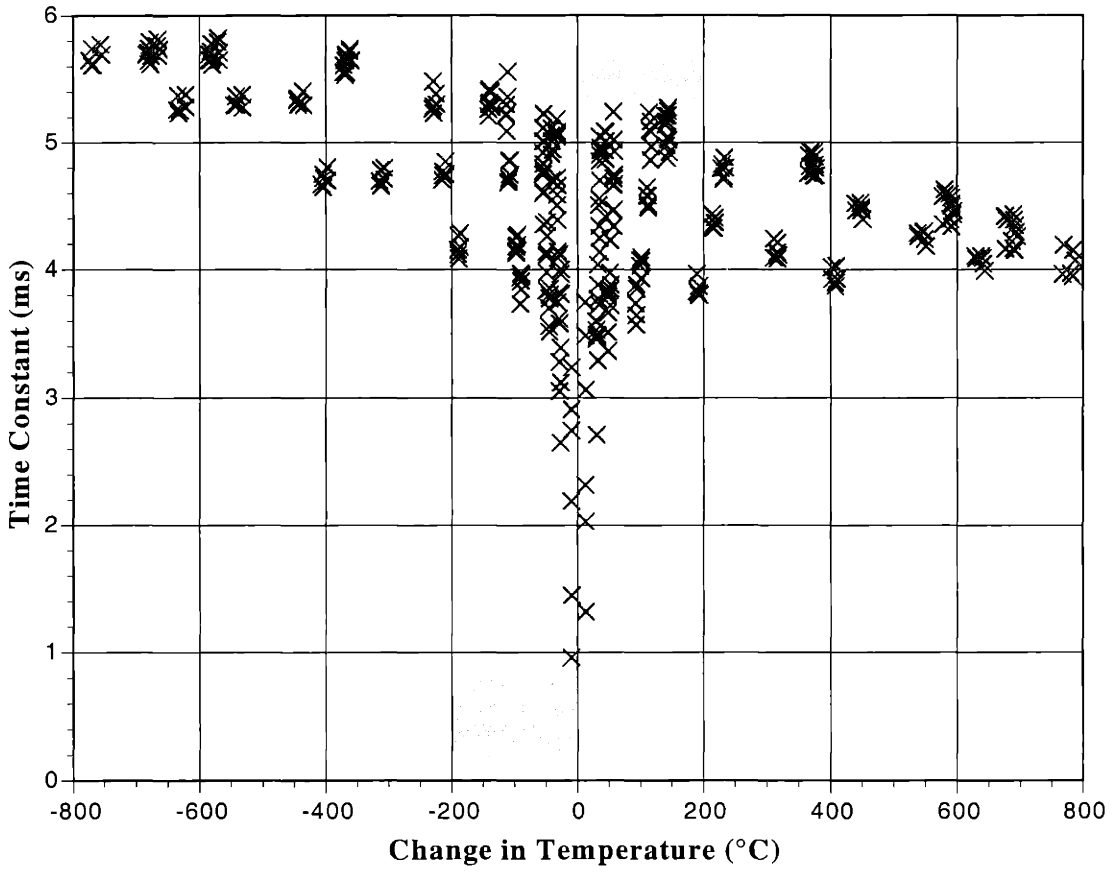

Figure 3-23. Microreactor heater first-order time constant plotted as a function of the change in temperature in the step response step (end temperature – begin temperature). Data is shown for the first six heaters in the microreactor channel with the tests being performed on individual heaters. Data is not grouped as in Figure 3-22. The test was done with air in the reactor channel under no flow conditions with microreactor #ACT-G1-11b.

Operating Temperature Range of the DieMate™ Manifold

This testing revealed that the DieMate™ socket was not damaged by any temperatures in the desired operating range of the DieMate™ manifold, which was up to 200°C. The maximum temperature that the manifold was raised to was 250°C (the over temperature thermocouple measured 238°C) in this experiment. It remained at this temperature for 3 ½ hours. After this test the DieMate™ socket was closely examined and no damage could be find. The PC board the socket was mounted on was discolored where it

came into direct contact with the manifold. This damage can be seen in Figure 3-24 around the socket head cap screws used to hold the socket together. However, the PC board used in this testing was incorrectly machined, and there should not have been any of the board present in this area. More importantly, the regions of the DieMate™ socket that did come into direct contact with the manifold were not damaged. Higher temperatures were not used in this test since it was not foreseeable that the DieMate™ manifold would ever be heated passed 250°C, even in the event of an over-temperature excursion.

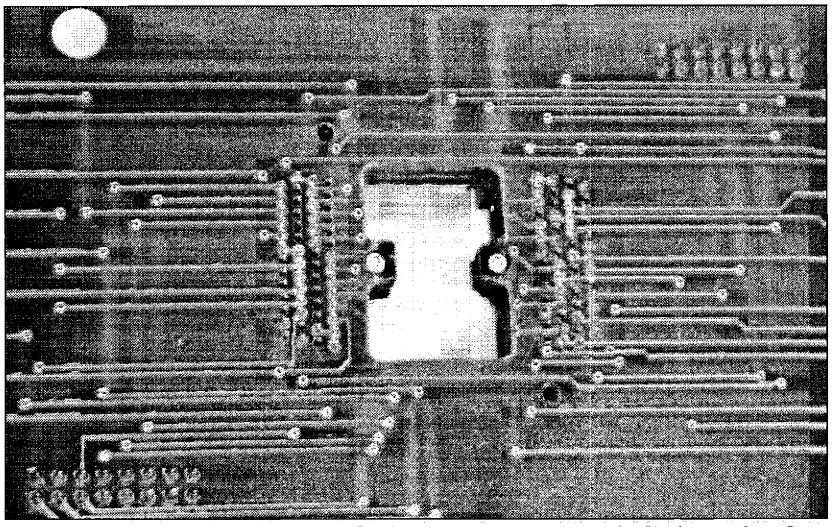

Figure 3-24. Damage of the microreactor PC board after temperature testing of the DieMate™ manifold at 250°C.

Gas Seal Test Results

Using the gas leak detector, it was not possible to detect any helium leaking from the microreactor or DieMate™ manifold at room temperature or 200°C at a helium flow rate of 50 sccm through the microreactor channels[23]. This test was repeated several times with the socket head cap screws, which were used to provide the sealing force of the manifold against

[23] Other experiments indicated that the maximum pressure for these connections was 60 psig, but this did not influence microreactor operation since they could not be operated above 7 psig.

the microreactor bottom, being loosened after each successive test. Only after the screws had been loosened to the point that there was no or little contact force were leaks detected at high or low temperature. Thus, as long as the microreactor was properly inserted into the DieMate™ socket, the fluidic seals should not leak. This was important since it is difficult to test the reactors for fluidic leaks inside the scale-up system.

Conclusions

The final scale-up microreactor design successfully completed preliminary testing under non-reacting conditions without the need for further modifications. There was no difficulty in establishing electrical contact between the pins of the DieMate™ socket and the bond ponds of the microreactor dies. The measured resistances of the temperature sensors and heaters were quite uniform with variations of less than 3% for both structures. The microreactor heaters were able to achieve membrane temperatures above 600°C[24]. Dynamic testing of the heaters revealed a dependence of the first order model gain on the size of the step change and the starting temperature. The heater first order time constant depended only on the size of the step change. There was essentially no time delay in the heaters as most estimates placed it at 0.25 ms, which was the data collection rate and thus, the error in the measurement.

The DieMate™ manifold's temperature could be raised up to 250°C with no visible damage occurring to the DieMate™ socket even after an extended time period. This is well above the desired operating temperature of the DieMate™ manifold, 200°C. The integrity of the fluidic seals between the DieMate™ manifold and the microreactor dies were also

[24] The actual temperature of the heater becomes difficult to measure above 600°C because of structural changes that begin to occur at these high temperatures in the platinum metalization.

examined at room temperature and 200°C. If the microreactor was placed into the socket properly, no gas leaks could be detected from these seals. With these successful tests, the project proceeded to developing an integrated microreactor system.

References

1. Everett Charles Technologies "POGO-72 high-performance bias ball POGO", *Everett Charles Technologies Homepage,* http://www.ectinfo.com/files/product/frame_pogo.html, (July 5, 2001).

2. Electronic Packaging Program at Cornell University (1998) "Tape Automated Bonding (TAB)", *Electronic Packaging Program at Cornell University Homepage,* http://www.afep.cornell.edu/facility/resources/gallery/tab.html, (July 5, 2001).

3. Carter, T. and Craig, E. (1997) "Known Good Die comes of age," *Semiconductor International,* Oct., 1997, pp. 175-180.

4. ENSER Corporation (2000) "DieMate Modification", E.I. du Pont de Nemours & Co., Inc., Wilmington, DE, Mar. 3, 2000, Drawing number D1489014.

5. ENSER Corporation (2000) "DieMate Manifold", E.I. du Pont de Nemours & Co., Inc., Wilmington, DE, Mar. 13, 2000, Drawing number D1489015.

6. ENSER Corporation (2000) "Nut Plate", E.I. du Pont de Nemours & Co., Inc., Wilmington, DE, Mar. 13, 2000, Drawing number D1489017.

7. ENSER Corporation (2000) "DieMate Manifold Weldment", E.I. du Pont de Nemours & Co., Inc., Wilmington, DE, Mar. 13, 2000, Drawing number D1489016.

CHAPTER 4
MICROREACTOR SYSTEM DESIGN

The Automated, Integrated Microreactor System (AIMS) is designed to be functionally equivalent to a conventional heterogeneous gas phase catalyst testing system, such as those in use at DuPont. These systems are comprised of 1) a bank of Mass Flow Controllers (MFCs) to mix the feed gas for the reactors; 2) a bank of reactors and MFCs for individual reactor control; and 3) a feed and product gas analysis system. A block diagram of this structure is shown in Figure 4-1. The difference in the AIMS is the use of MicroElectricalMechanical System (MEMS) components such as microvalves and micro-MFC's to replace conventional components. For this system the gas analysis equipment, including the GC and the necessary sampling valves, is kept in conventional form.

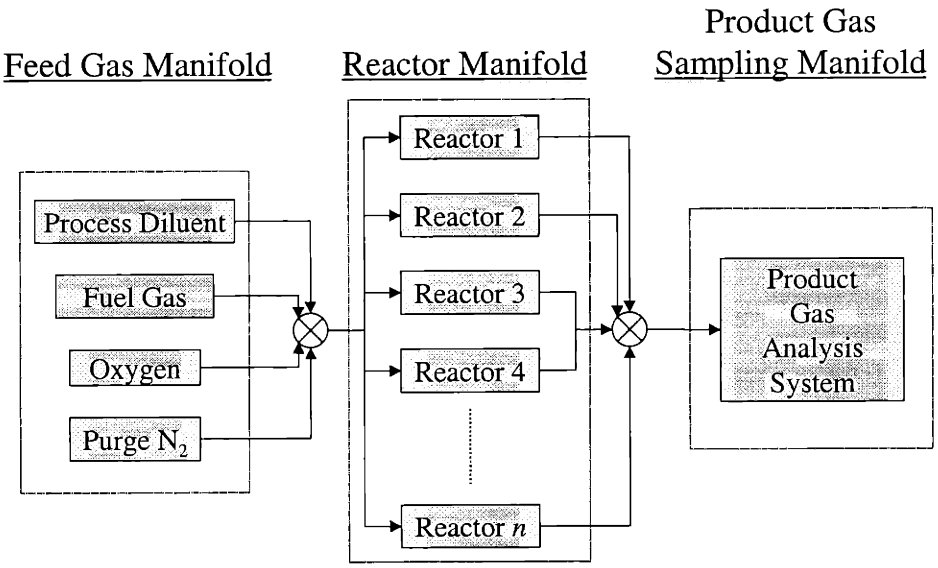

Figure 4-1. Block diagram of a typical laboratory reactor system.

Process Description

Figure 4-2 shows the piping diagram of the system[1]. The flow is from left to right in the diagram. The process gas cylinders for the system are shown at the left. Three gases are used during a run: a fuel, an oxidizer, and a diluent. The fuel gas in the AIMS is a light hydrocarbon or ammonia. The fuel is generally diluted with helium and nitrogen. Helium is added to dilute the mixture to safer level. In the case of ammonia, this also raises the condensation pressure of the mixture, which simplifies handling. Nitrogen is used as a calibration gas, but krypton is used for the ammonia oxidation reaction since nitrogen is also a product in this case. The oxidizer used is pure oxygen. The diluent used is helium or nitrogen.

Single stage forward pressure regulators located next to the AIMS, as shown in Figure 4-3, control the upstream feed gas pressure. These regulators are in turn fed from two-stage pressure regulators on each of the gas supply cylinders (not shown in Figure 4-2). There is a pressure relief valve after the two-stage regulator on each of the process gases to prevent over pressurization of the system (not shown in Figure 4-2). These relief valves are set at 80 psig. In addition, any flammable gas cylinders are also equipped with flame arrestors (not shown in Figure 4-2). All the process gases flow through 0.5 μm filters before entering the system as required by the microvalves used in the AIMS.

[1] Some detail concerning gas delivery to the system has been excluded for simplification.

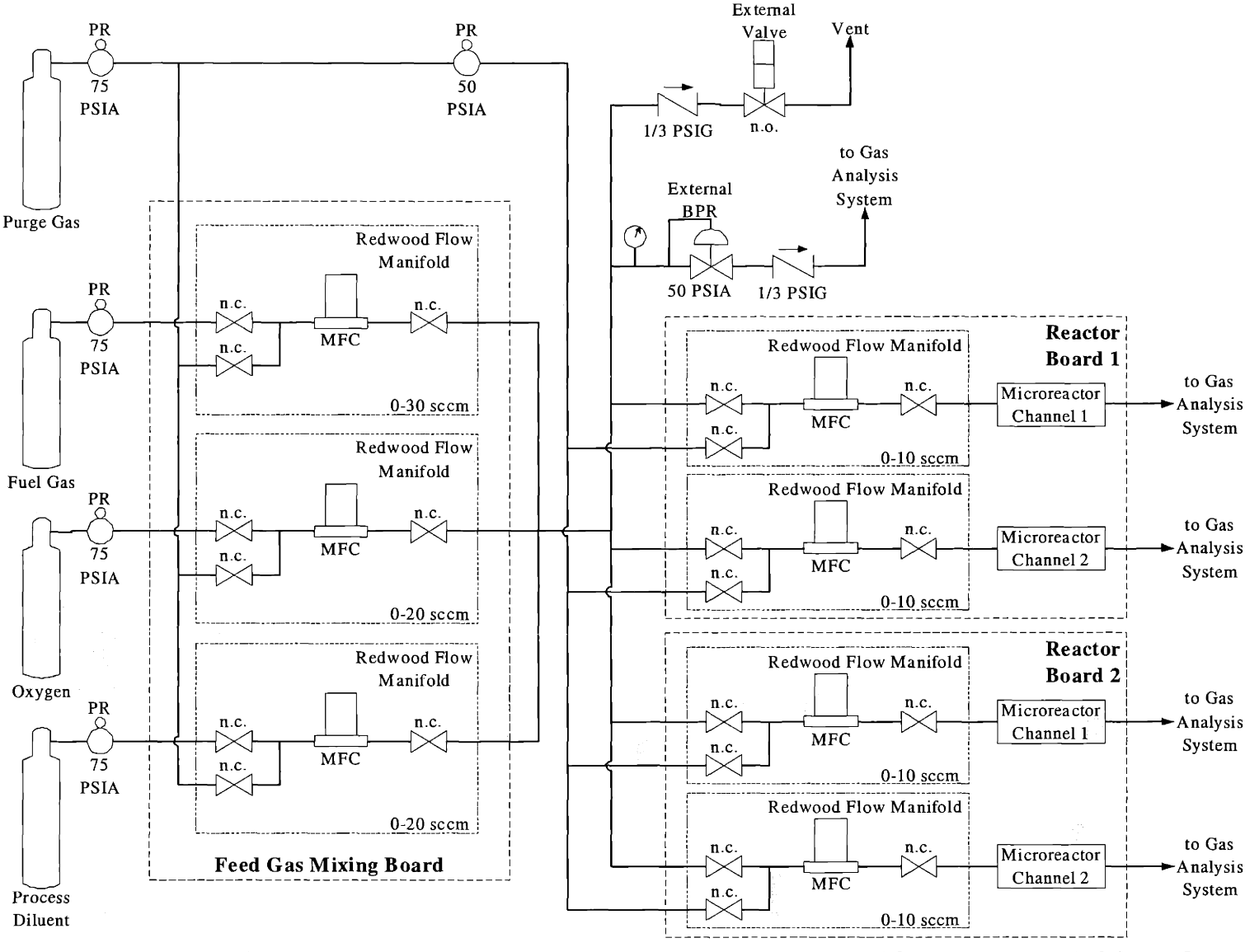

Figure 4-2. Piping diagram of the scale-up microreactor system. Figure adapted from drawing W1495427[1].

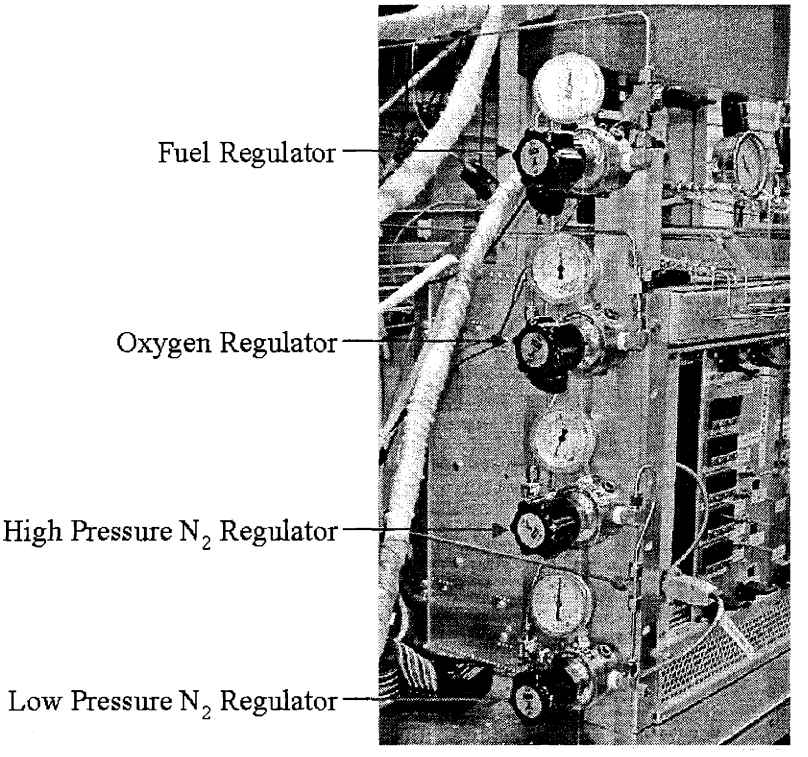

Figure 4-3. Process gas manifold for the microreactor system.

The reactor feed gas mixture is controlled by a bank of MFCs that adjust the flow rate of each of the process gases. These are shown in the diagram directly after the cylinders and the feed gas pressure regulators. The reactor feed mixing takes place on the feed gas mixing board in the AIMS chassis. This board consists of three manifolds that control the process gas flow rates using a Redwood Microsystems[1] MEMS-Flow® MFC and three Redwood Microsystems normally closed Shut-Off Valves (SOV's)[2].

The Redwood flow manifold has two normally closed SOV's that are teed into the feed of a Redwood MicroSystems MEMS-Flow® MFC. One normally closed SOV is for the process gas and the other is for the purge gas. During startup and shutdown, the process gas

[1] Redwood MicroSystems, Inc., 959 Hamilton Ave., Menlo Park, CA, 94025, (650) 617-1200.
[2] This assembly is referred to as the Redwood flow manifold.

valve is closed and the purge gas valve is opened to remove any reactive gases from the system. There is another normally closed SOV after the MFC that can be used to isolate the line from the rest of the system. Note that this arrangement is also used for the process diluent stream. This was done to allow for the use of a second fuel stream if desired.

The AIMS differs from conventional reactor systems in that all the valves are normally closed. Ideally, the system should purge itself with nitrogen if there is a power failure. Unfortunately, the Redwood MicroSystems SOV's are not available in a normally open configuration. This results in trapped process gas in the Redwood flow manifold in the event of power failure or emergency stop (e-stop) condition. However, the pressure downstream of the feed gas mixing board is vented through an external normally open valve. Although some process gas remains in the system the small volume of the lines helps to minimize the hazard of this situation.

Another difference in the configuration of the MFC line is the absence of forward and back pressure regulators around the MFC's to control the pressure drop across the MFC. This arrangement does not work with the Redwood MicroSystems MFC's because they control flow by adjusting the pressure drop across a flow restrictor. Thus, their operation is sensitive to the inlet and exit pressures of the mass flow controller. In the Microreactor System the Redwood MFC's operate with fixed upstream and downstream pressures, but these are set by their design specifications and are not normally adjusted during operation.

After the feed gas mixing board, the feed gas stream is connected with the reactor boards, an external Back Pressure Regulator (BPR), and an external normally open valve. The external BPR and valve are isolated from the system by 1/3 psig check valves. One check valve is placed before the vent valve, and the other check valve is located after the

back pressure regulator. This prevents back flow of gases to the feed stream altering its composition, and reduces the possibility of oxygen from the atmosphere entering the feed and possibly forming an explosive mixture. The BPR regulates the feed gas pressure to the reactor boards and is set at 35 psig according to the specifications of the Redwood MFC's. The external normally open valve is used to vent gas pressure in the external lines in the event of a power failure or emergency-stop condition. Figure 4-4 shows the external piping of the AIMS.

The reactor feed gas is split to two lines going to the two reactor boards. Each reactor board has two Redwood flow manifolds to control the flow going to each channel of the microreactor die (each die has two independently controlled reaction channels). These Redwood flow manifolds are identical to the ones in the feed gas mixing board except for their designed operating inlet and exit pressures. After the Redwood flow manifold, the feed gas flows to the DieMate™ manifold and microreactor, which are heated to 200°C to prevent product condensation. The product transfer line after the DieMate™ manifold is heat traced to the exit of the system chassis. From there, the product gas enters the gas analysis system.

Again a power failure or e-stop condition results in process gas being trapped in the system. The pressure downstream of the Redwood flow manifolds in the reactor boards is essentially atmospheric since these lines ultimately flow to vent. There is a small amount of pressurized mixed feed gas trapped in the Redwood flow manifold, but its volume is only 0.270 cm^3. Furthermore, the microreactor heaters have a very small time constant, approximately 3 ms, so they return almost immediately to the temperature of the microreactor die. See the Process Hazards Analysis in the Appendix for a detailed safety analysis of the system.

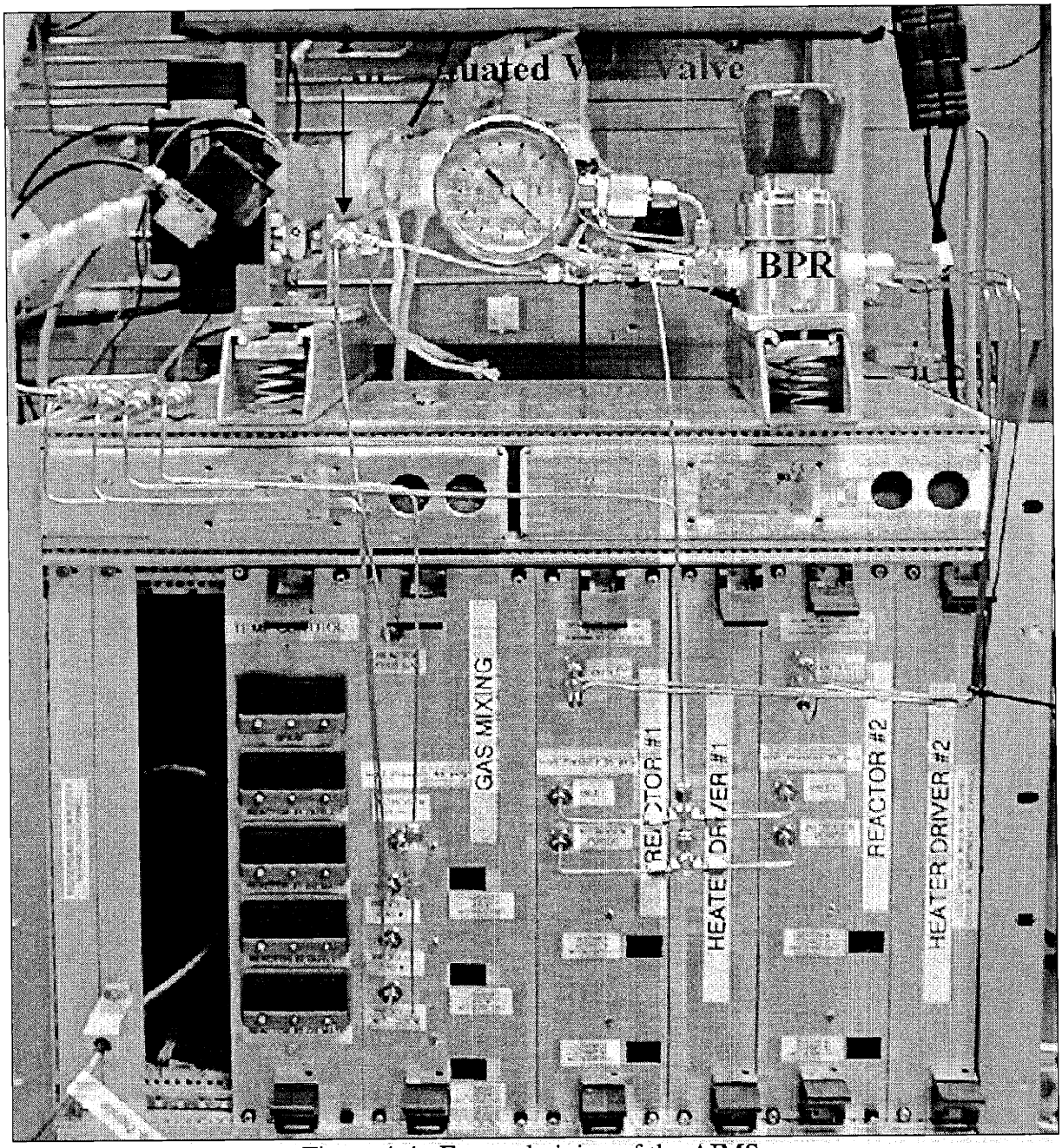

Figure 4-4. External piping of the AIMS.

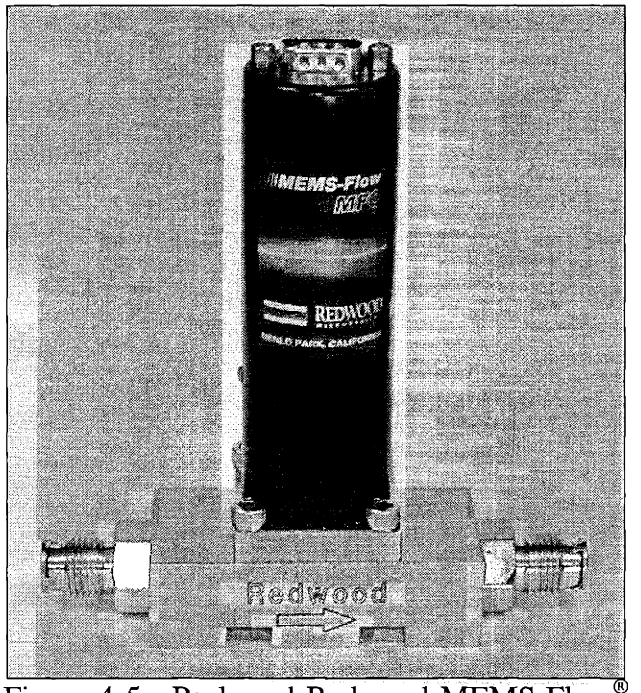

Figure 4-5. Packaged Redwood MEMS-Flow® mass flow controller.

Component Descriptions

Redwood Flow Manifolds

The MEMS components in the system besides the reactors are the microvalves and micro-MFCs. They are manufactured by Redwood MicroSystems. In order to reduce their size, the components used in the system are not placed in their standard packages. Instead, the MFC is combined with three SOVs on a 316 L stainless steel flow manifold[3] designed for this project. This part is detailed in drawing D1488666[2]. A MEMS-Flow® MFC in its original packaging is shown in Figure 4-5, and Figure 4-6 shows the Redwood flow manifold.

[3] This manifold is subsqsequently referred to as the Redwood valve manifold.

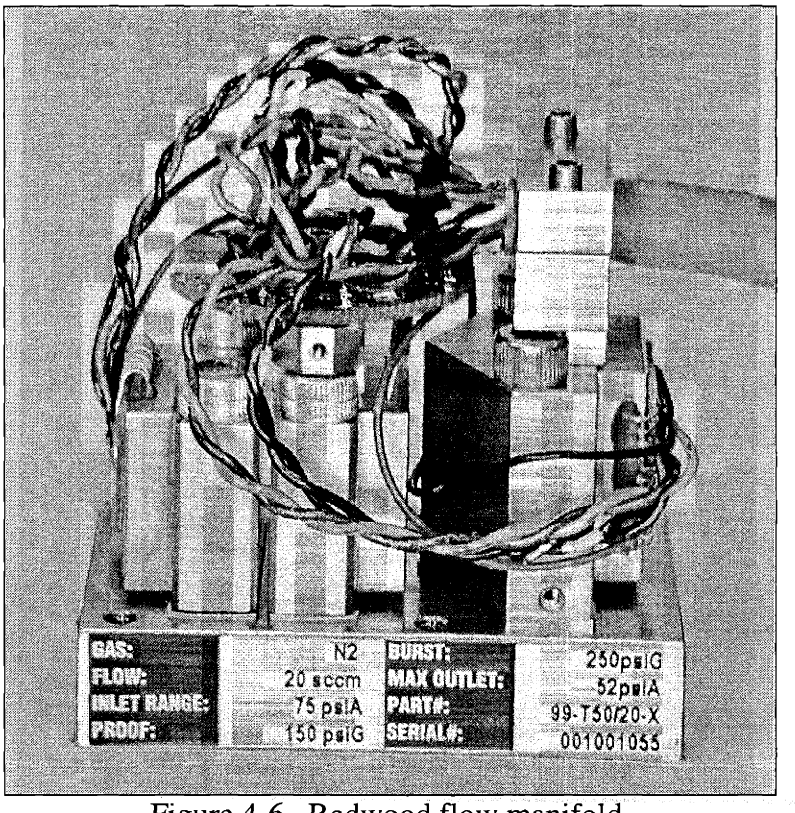

Figure 4-6. Redwood flow manifold.

The electronics for the Redwood flow manifold are also repackaged by mounting them on a custom designed PC board. Figure 4-7 shows the original electronics packaging from Redwood MicroSystems and Figure 4-8 shows the repackaged electronics. The custom designed PC boards are made from FR-4 laminate. The design and assembly of this electronics packaging is detailed in drawings D1492264[3], W1492265[4], and W1492266[5].

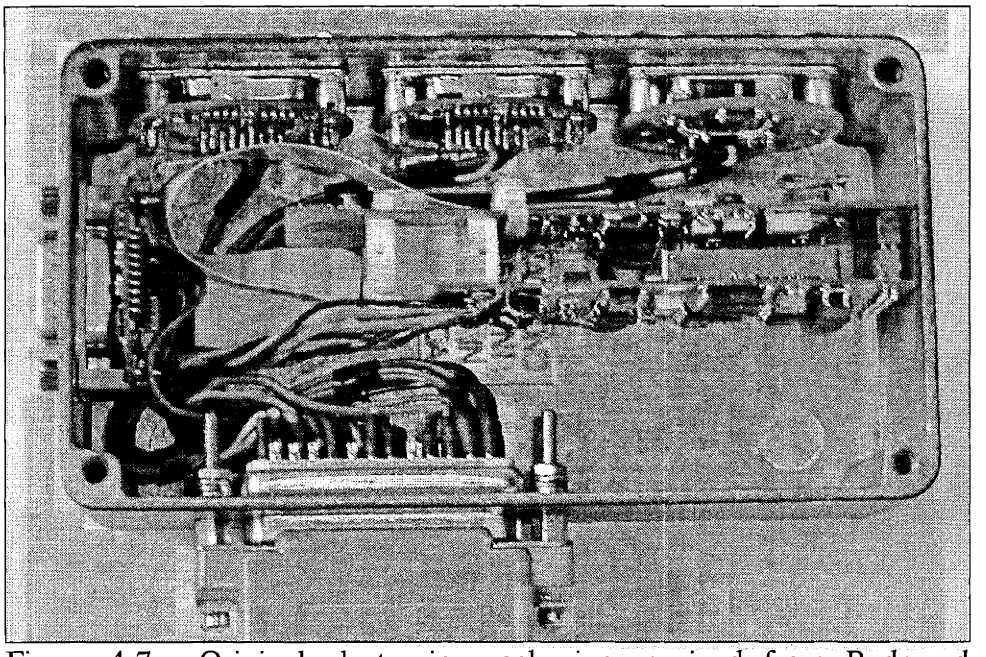

Figure 4-7. Original electronics packaging received from Redwood MicroSystems.

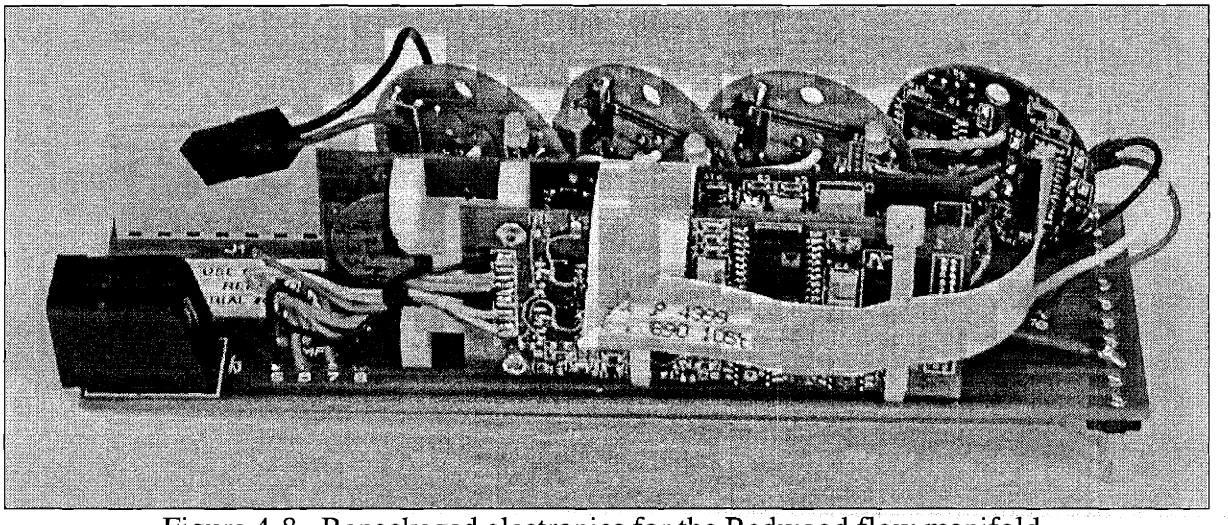

Figure 4-8. Repackaged electronics for the Redwood flow manifold.

The SOV's are normally closed valves, and they have a specified leak rate of 0.1 ml/min. The MFC proportional valve is normally open. The design inlet and outlet pressures of the feed gas mixing MFC's are 75 psia and 50 psia, respectively. The design inlet and outlet pressures of the reactor MFC's are 50 psia and 14.7 psia, respectively. Both

the MEMS-Flow® MFC's and the microvalves have a proof pressure of 150 psig and a burst pressure of 250 psig. Other than the microreactors, these devices are the most likely to fail due to over pressurization. The operating temperature range of these components is between 0°C and 55°C.

System Boards

Packaging of the Redwood flow manifolds and microreactors is achieved by mounting the devices on standard 6U CompactPCI boards[4]. The boards are then inserted in a chassis and the electrical connections between the boards are then made through the backplane, ribbon cables, and rear I/O boards. Further details on the chassis design are given later in this chapter. All the boards in the microreactor chassis are made out of FR-4 laminate, which is constructed of multiple plies of epoxy-resin-impregnated woven glass cloth. Its upper operating temperature limit is 130°C, and its UL flammability classification is 94V-0, which means samples self-extinguish within 10 seconds after flame application[6].

Temperature Controller Board

The temperature controller board, shown in Figure 4-9, consists of five CAL[5] 3300 temperature controllers. These controllers are used to maintain the temperature of the DieMate™ manifolds and the product transfer lines by controlling power to their respective heaters. Two controllers are used for the DieMate™ manifolds (one for each reactor board). Two controllers are used for the transfer lines from the DieMate manifold to the front panel (one for each reactor board). The fifth controller is a spare. The design of the temperature controller board is specified in drawings W1489754[7], W1489755[8], D1489756[9], and D1489757[10].

---

[4] 6U designates the height of the board since the Compact PCI standard supports many different board heights.

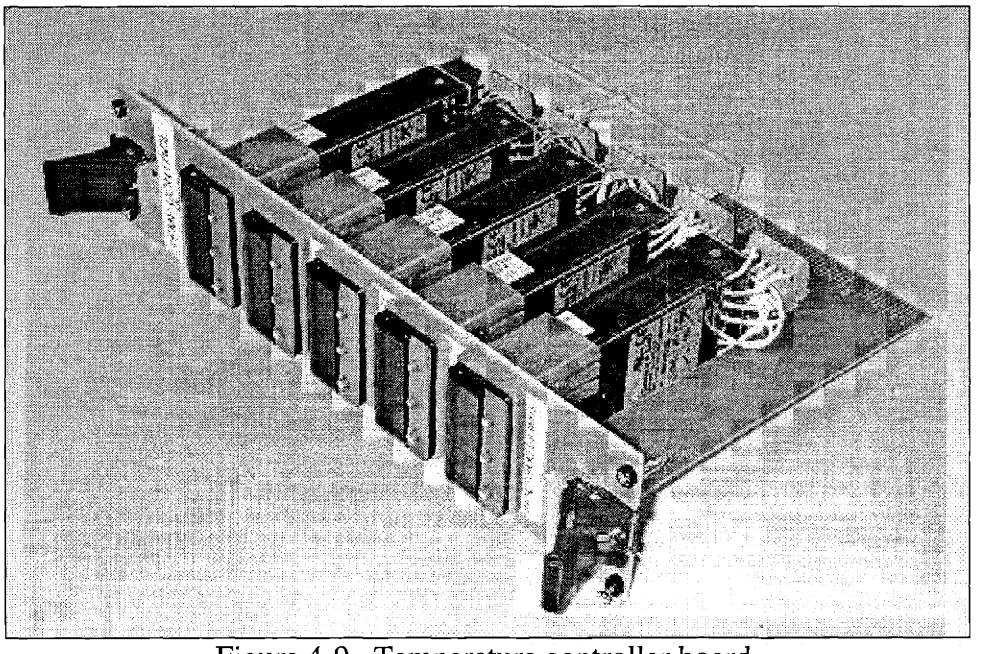

Figure 4-9. Temperature controller board.

Feed Gas Mixing Board

The feed gas mixing board, shown in Figure 4-10 and Figure 4-11, controls the composition of the feed gas to the reactors. It has three Redwood flow manifolds to meter each of the three feed gases: fuel, oxygen, and diluent. The front of the card contains the system feed gas inlets for fuel, oxygen, diluent, and purge gas. All of these gases enter the system at 75 psia. Serial communication to the Redwood flow manifolds for diagnostic purposes is available through three, four conductor RJ-11 jacks on the front of the card. The tubing assembly, shown in Figure 4-11, was constructed from 1/16" 316 L stainless steel tubing and fittings provided by Valco. The T-junctions were custom-built for this project and are described in drawing D1489022[11]. Silver solder was used to attach the 1/16" tubing to the T-junctions. The tubing assembly is described in drawings D1489021[12], D1489023[13], D1489024[14], and D1489025[15]. The serial numbers for the Redwood

[5] CAL Control Inc., 1580 S.Milwaukee Ave., Libertyville, IL 60048, (847) 680-7080.

flow manifolds used for the fuel gas line, the oxygen line, and the purge gas line are 001001054, 001001053, and 001001052, respectively. Construction of the feed gas mixing board is described in drawings D1489750[16], D1489751[17], W1489752[18], and W1489753[19].

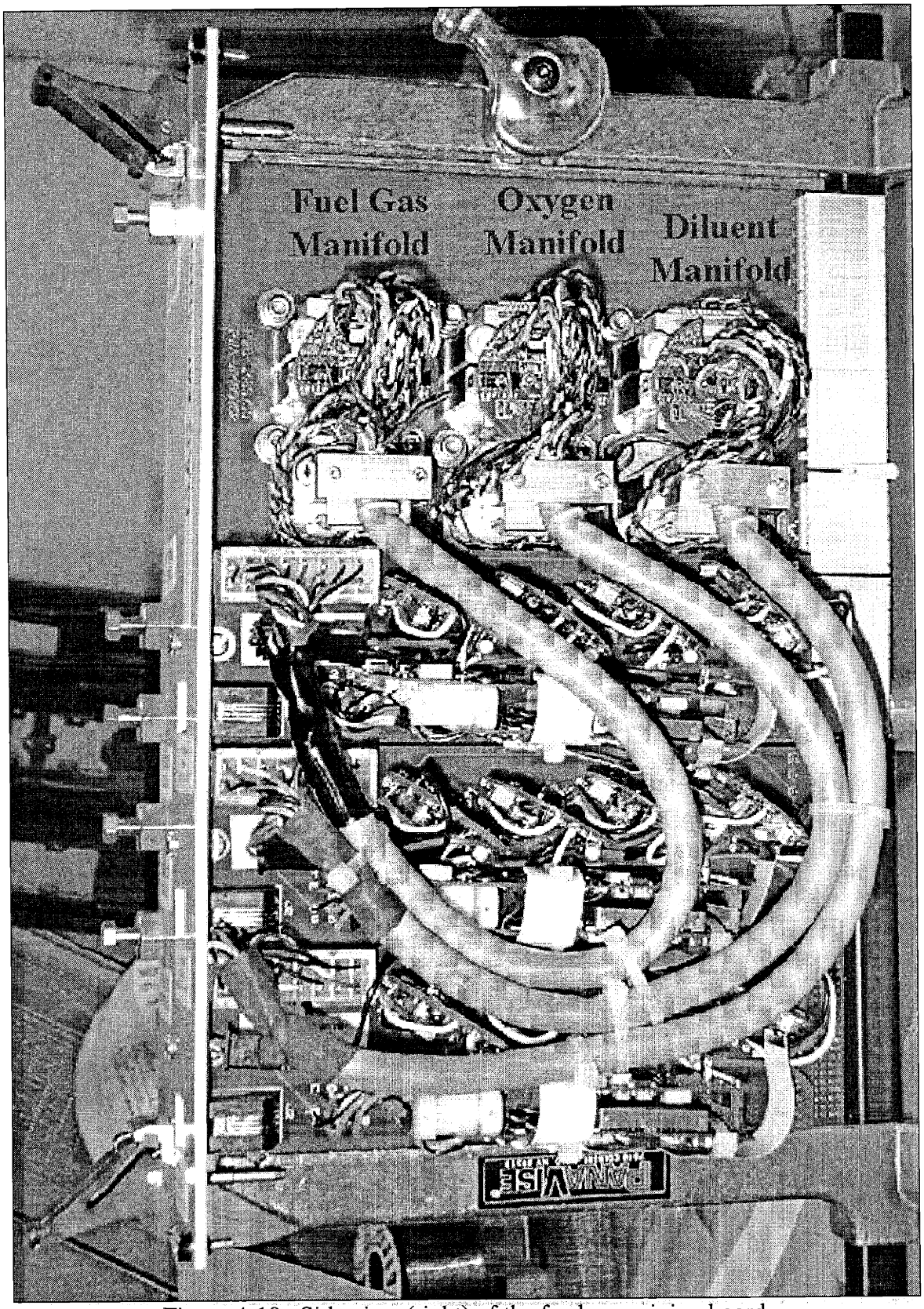

Figure 4-10. Side view (right) of the feed gas mixing board.

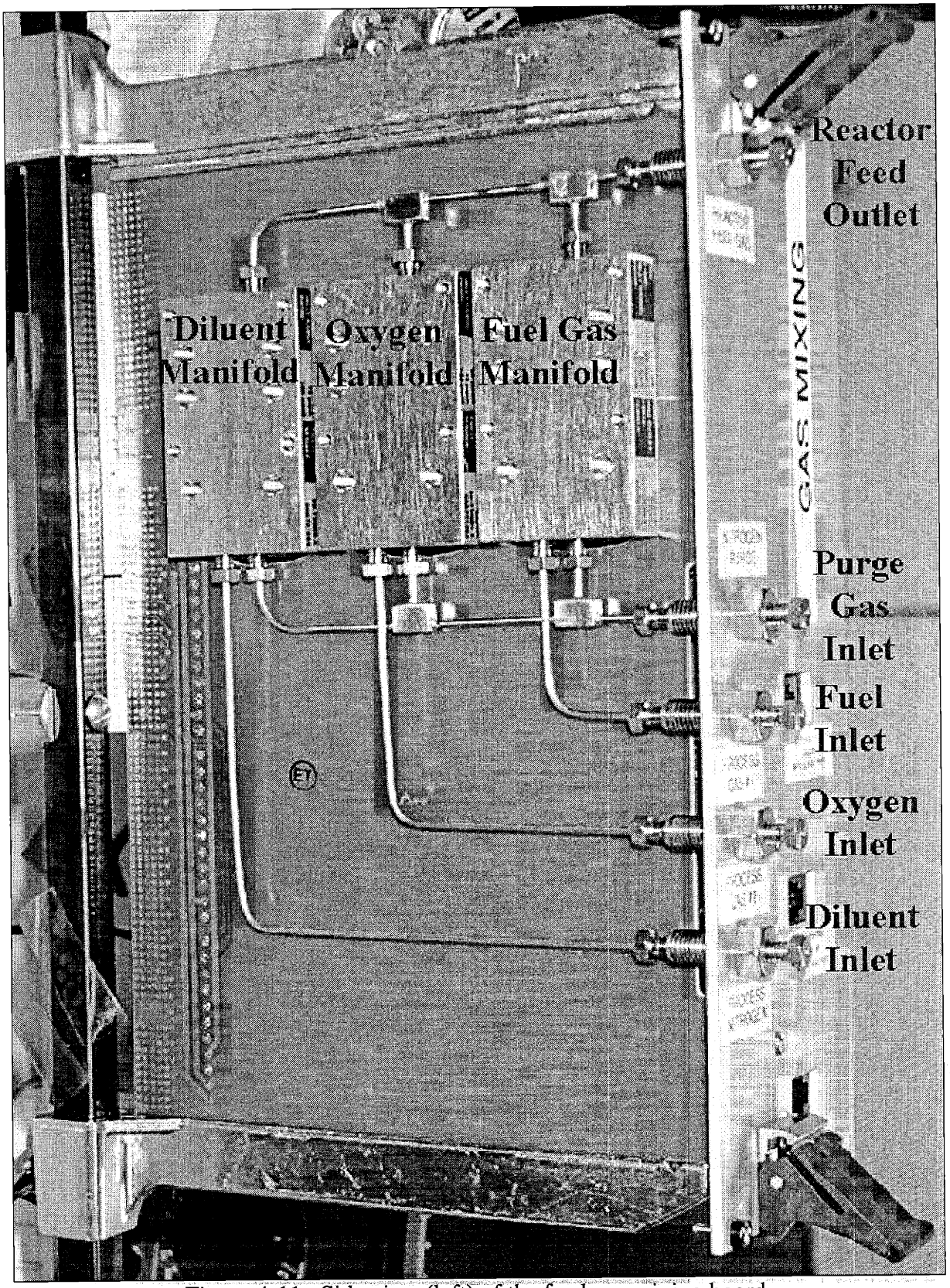

Figure 4-11. Side view (left) of the feed gas mixing board.

Reactor Boards

Two reactor boards are used in the DARPA Microreactor System. Each board contains a microreactor die with two independent reaction channels along with two Redwood flow manifolds to control the feed gas flow rate to each channel. Figures 4-11 through 4-13 show different views of a reactor board. The front of the board has gas inlets for the reactor feed and the purge gas. In addition, there are two gas outlets, one for each reaction channel. The inlet and outlet fittings are 1/16" 316 L stainless steel obtained from Valco. There are two, four conductor RJ-11 jacks on the front for serial communications with the Redwood flow manifolds.

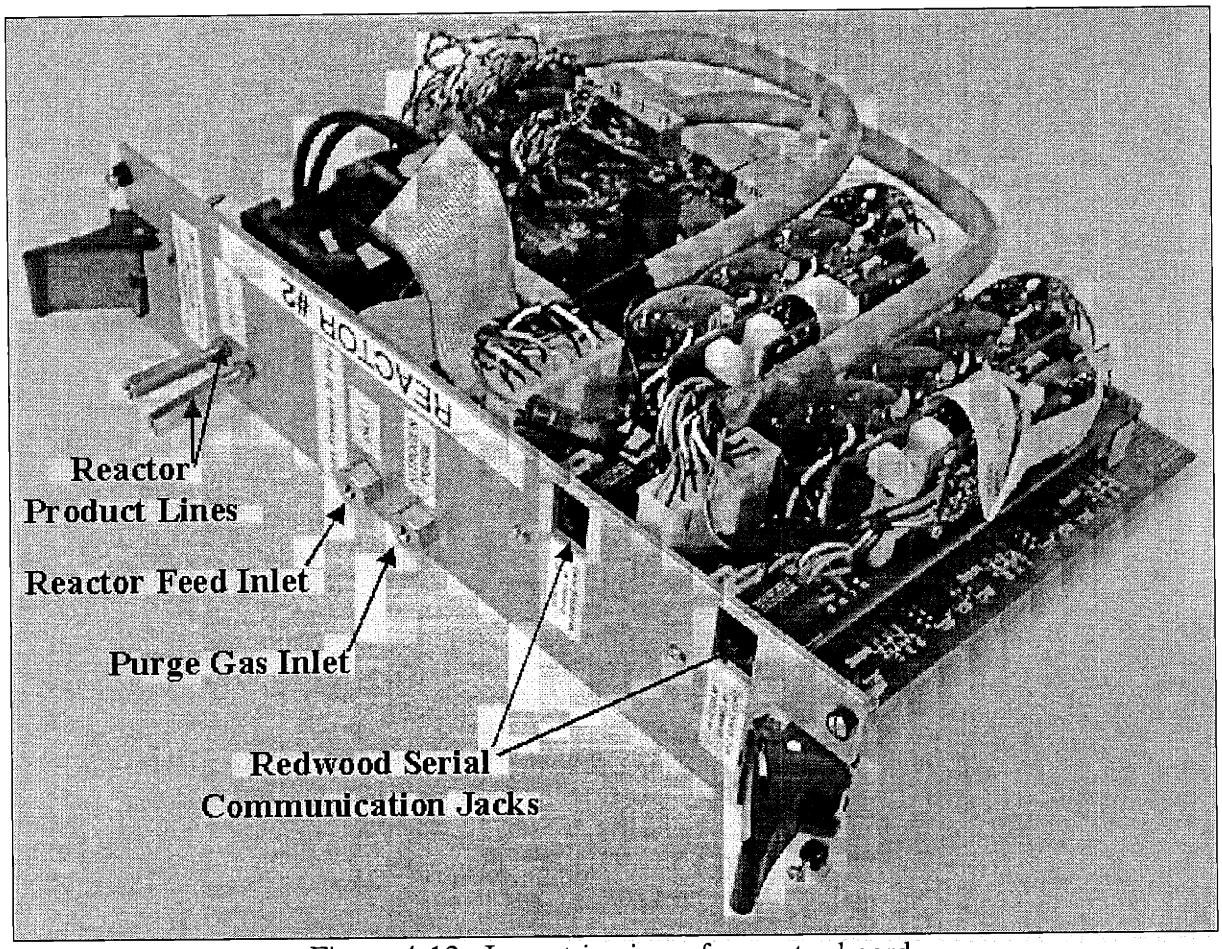

Figure 4-12. Isometric view of a reactor board.

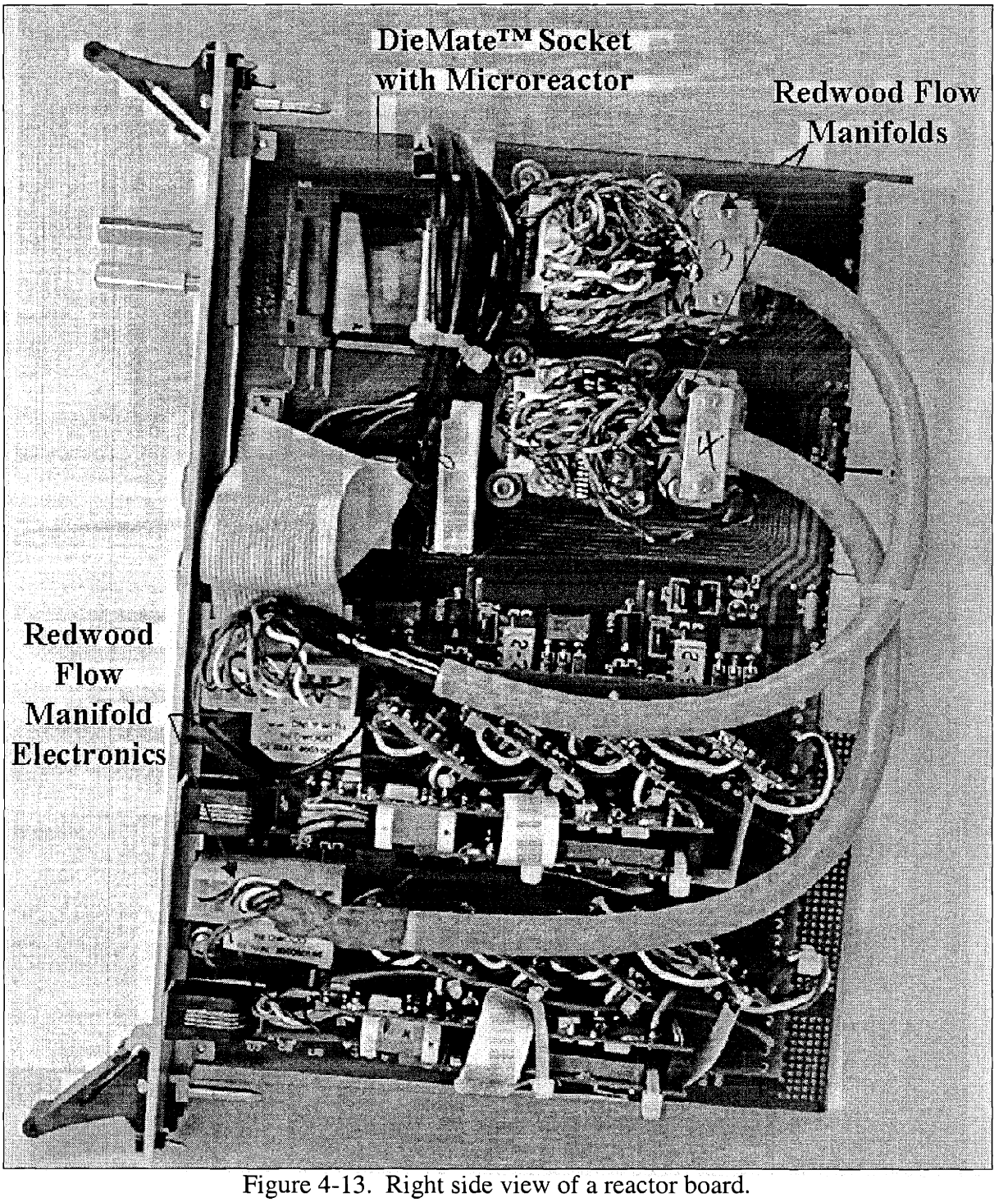

Figure 4-13. Right side view of a reactor board.

The reactor board contains the electronics for the Redwood flow manifolds as daughter and granddaughter cards, shown in Figure 4-13. Underneath these cards lies the

electronics to operate six temperature sensors on each microreactor channel. The ribbon connector, visible in Figure 4-13, is used to transfer electrical signals directly from the reactor board to the heater circuit board.

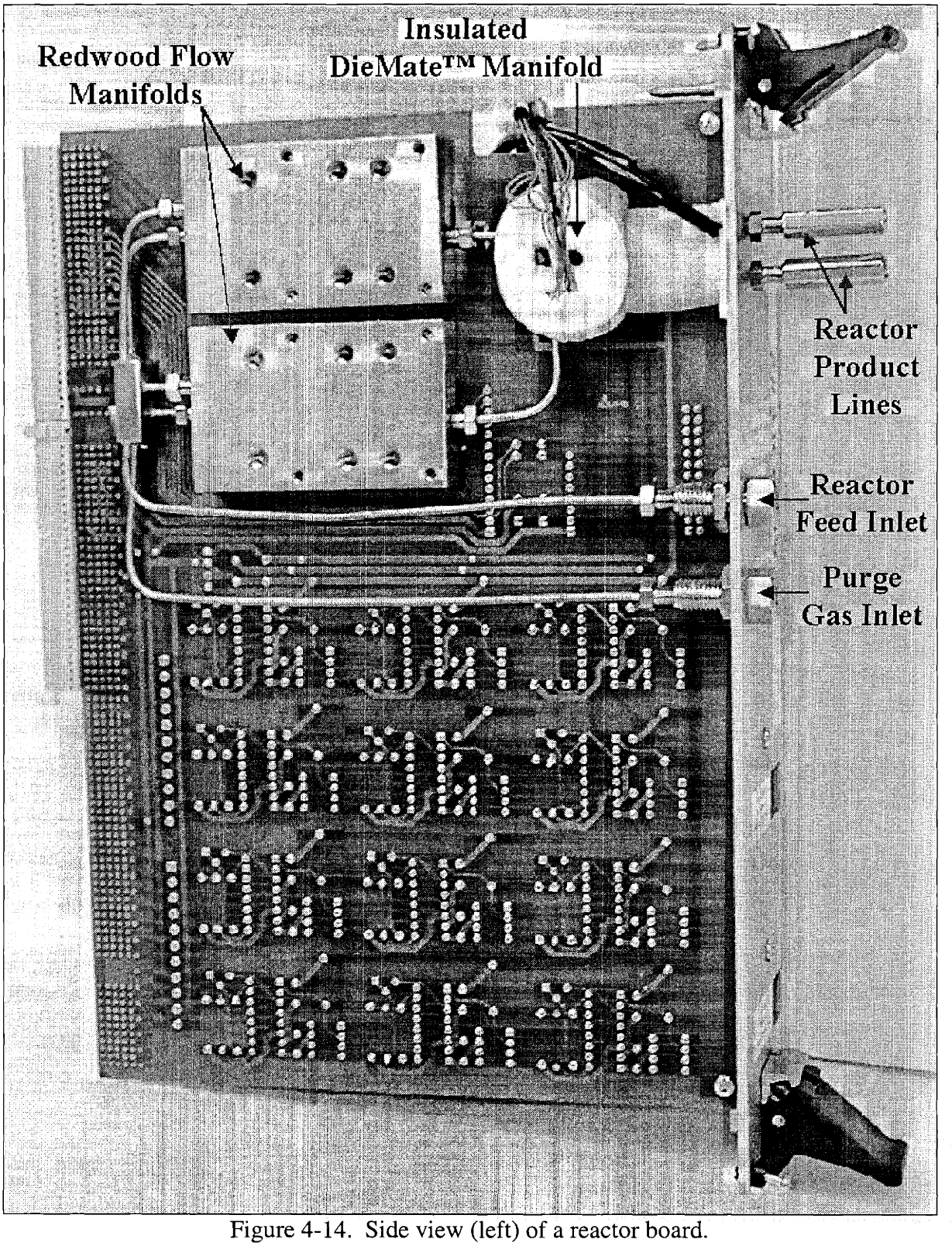

Figure 4-14. Side view (left) of a reactor board.

As described in Chapter 3, the microreactor is mounted in a DieMate™ socket with fluidic connections made through a DieMate™ manifold. Figure 4-14 shows the tubing layout for gas flow in the system as described in drawings D1489016[20] and D1489020[21]. The tubing assembly was constructed from 1/16" 316 L stainless steel tubing and fittings provided by Valco. The junction visible in Figure 4-14 was machined from 316 L stainless steel, and its construction is described in drawing D1489018[22]. The tubing was attached to the junction and the DieMate™ manifold using silver solder. The most pressure sensitive component of the tubing assembly is the microreactor membrane, which will fail around 7 psig[23].

The product transfer lines from the microreactor are heated through the heating cartridges in the DieMate™ manifold, described in Chapter 3, and a clam shell heater that encases the tubing to the front of the card. Figure 4-15 shows a picture of the clamshell heater, and its design is detailed in drawing D1489019[24]. A flexible Kapton heater that is wrapped around the clamshell provides heating power through a 24 Vdc input. The heaters were obtained from Technical Industrial Products (catalog number KHLV-101/5). The temperature of the clamshell is monitored using two 100 Ω platinum Resistive Temperature Devices (RTD) manufactured by Technical Industrial Products. One of the RTD's in the clamshell had a two-wire configuration, part number RTD15-100L-SS116-1-PVC24-12-2, which was connected to the CAL controller. The other RTD had a four-wire configuration, part number RTD15-100L-SS116-1-PVC28-12-4, and it was connected to the process control computer. Both types were 1/16" O.D. and 1" in length.

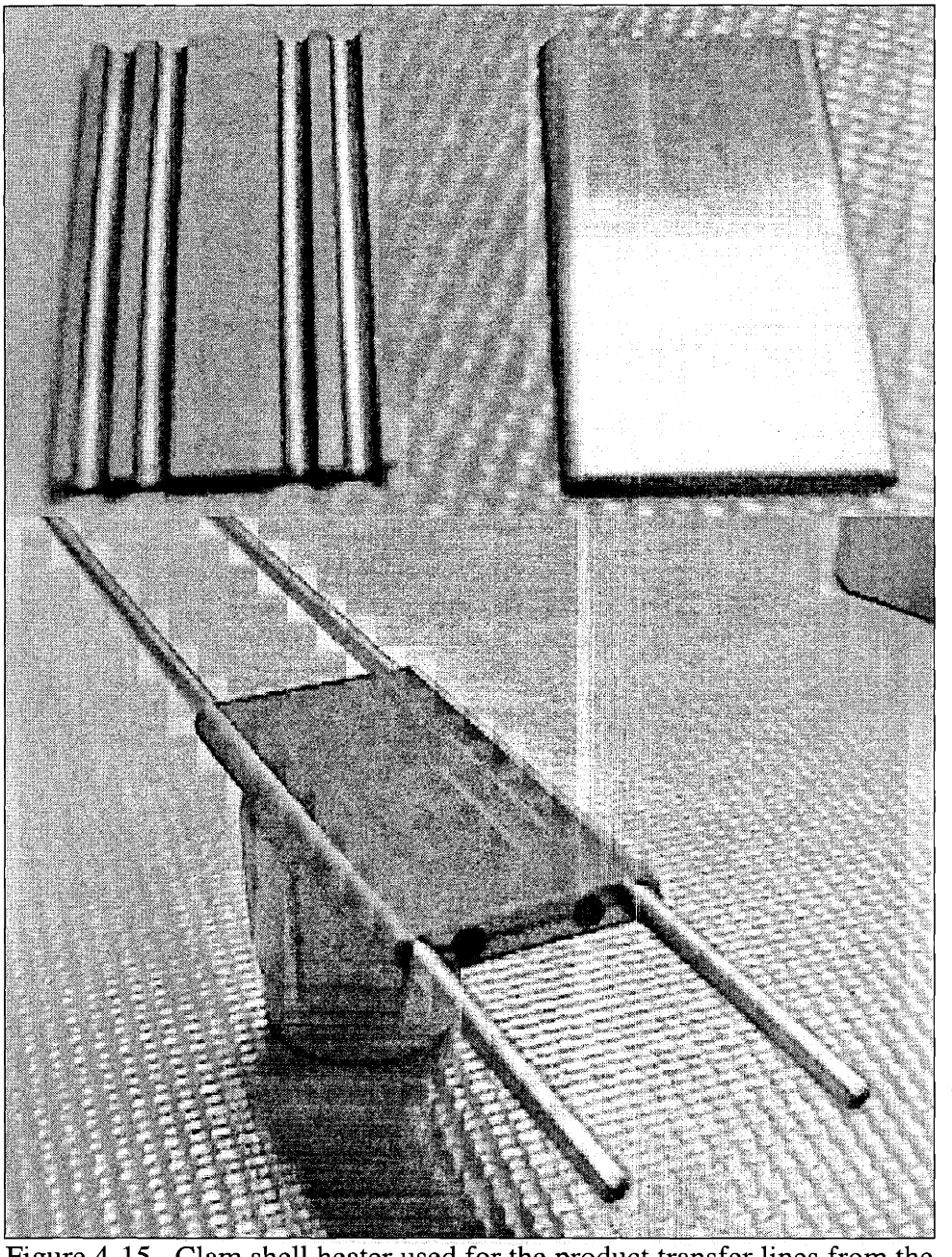

Figure 4-15. Clam shell heater used for the product transfer lines from the DieMate™ manifold to the front of the board.

The DieMate™ manifold and the clamshell heater is insulated using ceramic fiber strip obtained from McMaster-Carr. This insulation is visible in Figure 4-14. The fiber strip is 1" in width, 1/8" in thickness, and its catalog number is 87575K87. Its specified thermal conductivity is 0.38 (BTU.in)/(hr.ft^2.8F), and its maximum temperature rating is 2300°F.

Two reactor cards are used in the AIMS. Both cards are identical and interchangeable in the system chassis. For identification purposes, the reactor card left most in the chassis (as viewed from the front) is Reactor Card 1. Reactor Card 1 uses Redwood flow manifolds 001001056 for microreactor channel A and 001001065 for microreactor channel B. Reactor Card 2 uses Redwood flow manifolds 001001060 for microreactor channel A and 001001061 for microreactor channel B. Construction of the reactor boards is described in drawings D1489743[25], W1489744[26], W1489745[27], and D1489746[28]

Heater Driver Circuit Boards

There are two heater driver circuit boards in the AIMS, one for each reactor board. One of these cards, shown in Figure 4-16, contains the circuitry necessary to power twelve microheaters on a microreactor die. Both of the cards used in the system are identical and interchangeable. Again the left most board is referred to as Heater Driver Circuit Board 1. The mechanical design of the heater driver circuit boards is described in drawings W1489747[29], D1489748[30], and W1489749[31].

The heater circuits are voltage controlled so that they reduce the power input to the microreactor heaters as their temperature rises. This occurs because increasing temperature increases the resistance of the microheaters, so the current supplied to the microheaters is reduced to maintain a constant voltage. This is an important feature as the temperature increase due to ignition can be more than 100°C and occurs over a period of milliseconds.

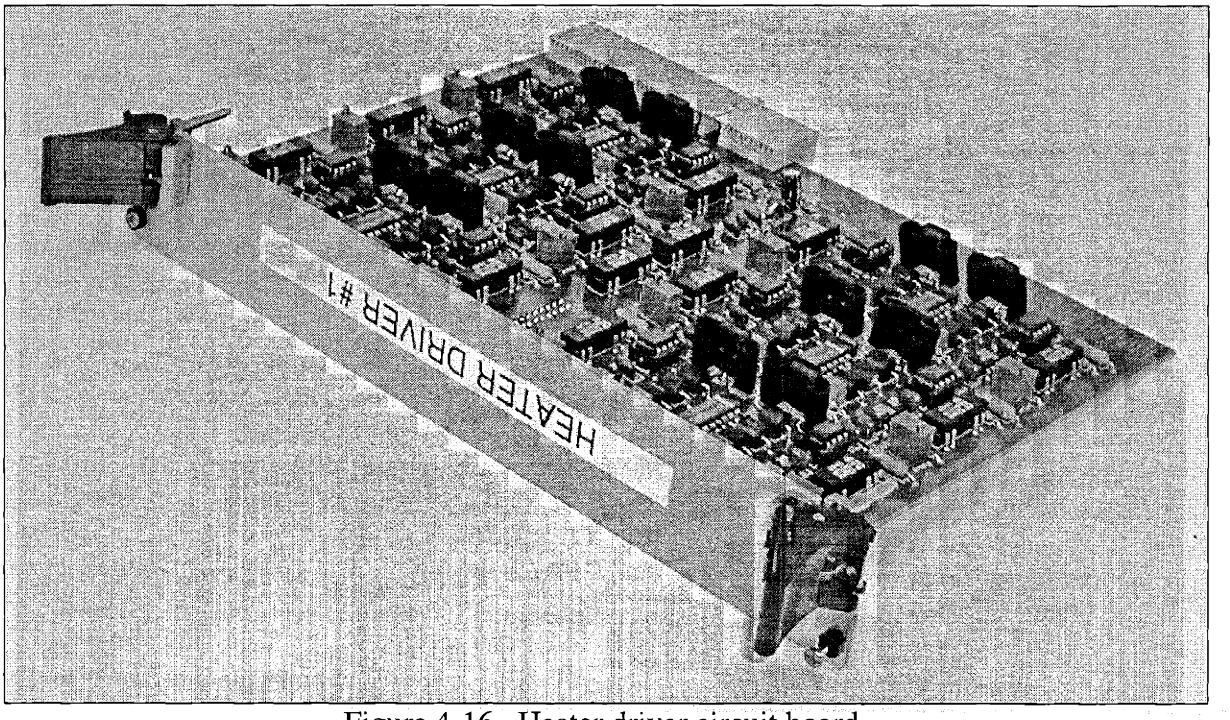

Figure 4-16. Heater driver circuit board.

System Chassis

The AIMS is housed in a standard CompactPCI chassis manufactured by Kaparel[6]. This chassis is the model 9U x 84 HP PS6090 integrated subrack, which measures 19" × 15¾" × 11¾". The AIMS chassis with mounted boards, is shown in Figure 4-17 and Figure 4-18. It holds up to fourteen 6U, 64 or 32-bit CompactPCI cards and up to two double-wide (8HP) 6U power supplies. The chassis includes two SK 3344012 RiCool 12Vdc blowers, which are located in the top compartment of the chassis as shown in Figure 4-17. These fans are capable of moving 440 cfm of air and are manufactured by Rittal Corporation[7]. They are used to cool the system components and prevent the accumulation of process gases inside the chassis.

[6] Kaparel Corporation, 97 Randall Dr., Waterloo, Ontario, N2V 1C5, Canada, (519) 725-0101.
[7] Rittal Corporation, 1 Rittal Place, Springfield, OH 45504, (800) 477-4000.

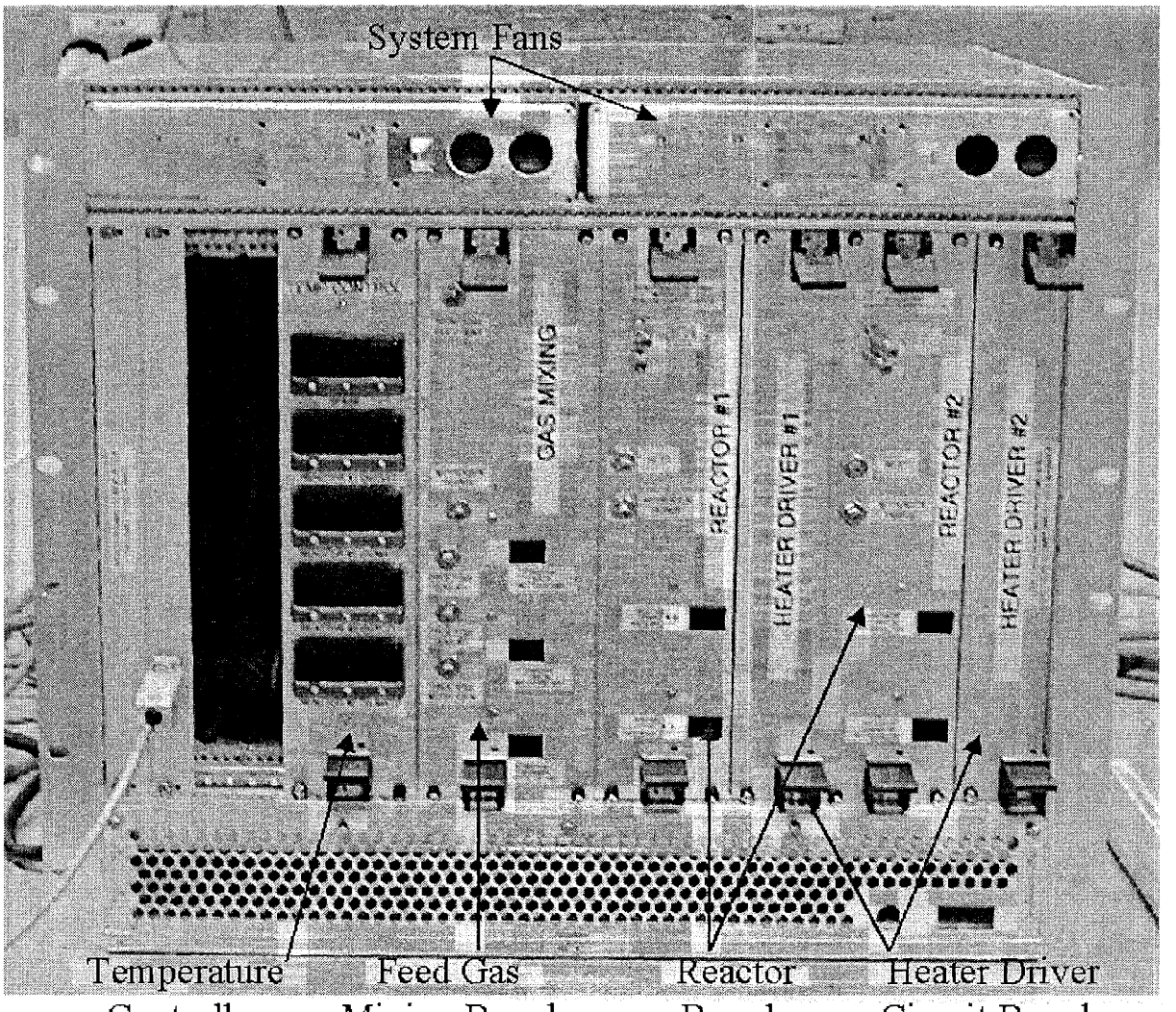

Figure 4-17. Front view of the AIMS without external fluidic connections.

Electrical interconnections between the boards are made using a backplane and ribbon cables between rear I/O cards. In addition, there are ribbon cables on the front side of the chassis that go from the reactor boards to the heater driver circuit boards. The rear I/O cards with the ribbon cable connections are visible in Figure 4-19, which shows a rear view of the AIMS without the back cover panels. The rear I/O cards are custom-built PC boards that are used to transfer signals from cables connected to the control computer to the system

boards on the front. The connectors for the cables leading to the control computer are visible in Figure 4-18. Ribbon cables are used to transfer connections between the rear I/O cards because there were not enough lines available in the backplane to make all of the connections needed.

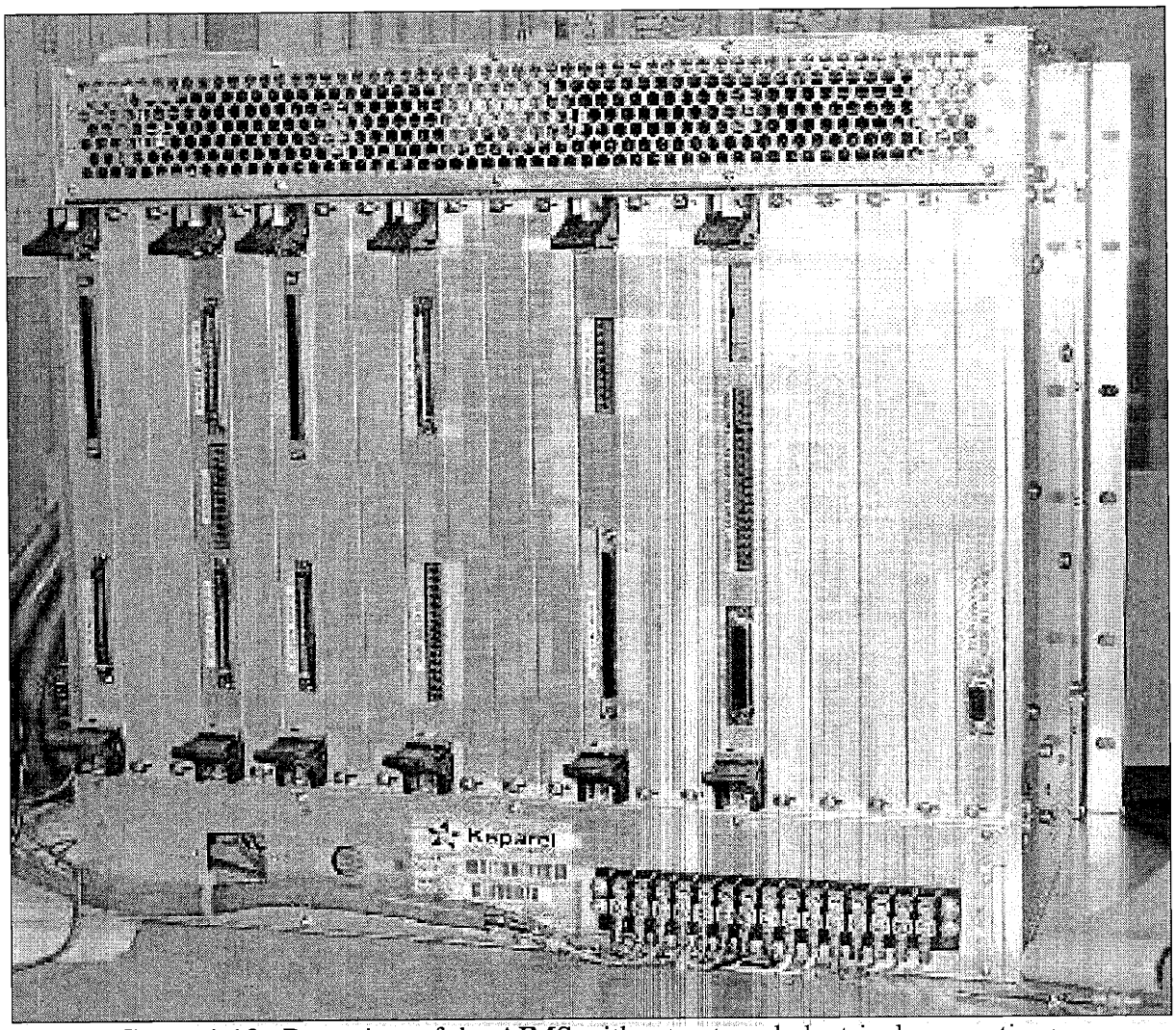

Figure 4-18. Rear view of the AIMS without external electrical connections.

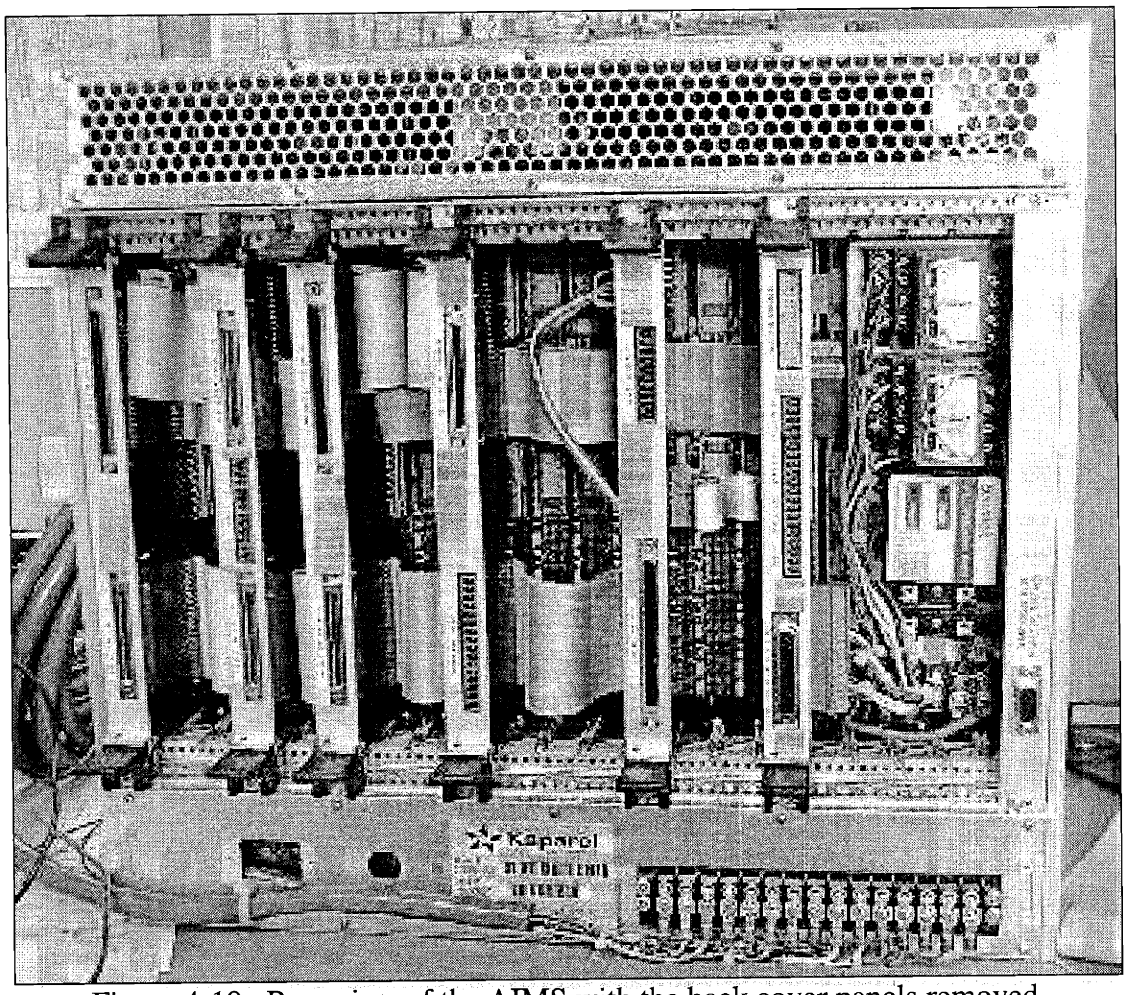

Figure 4-19. Rear view of the AIMS with the back cover panels removed.

The backplane used, shown in Figure 4-20, is a H.110 CompactPCI telephony backplane obtained from Kaparel. Two PS4400 backplane boards were used along with one PS1150 board. The backplane PCB's were slightly modified by removing selected chip capacitors that were not compatible with the amount of current being carried on the backplane. Only analog signals were transmitted by the backplane, so the digital communications capability of the backplane bus was not utilized.

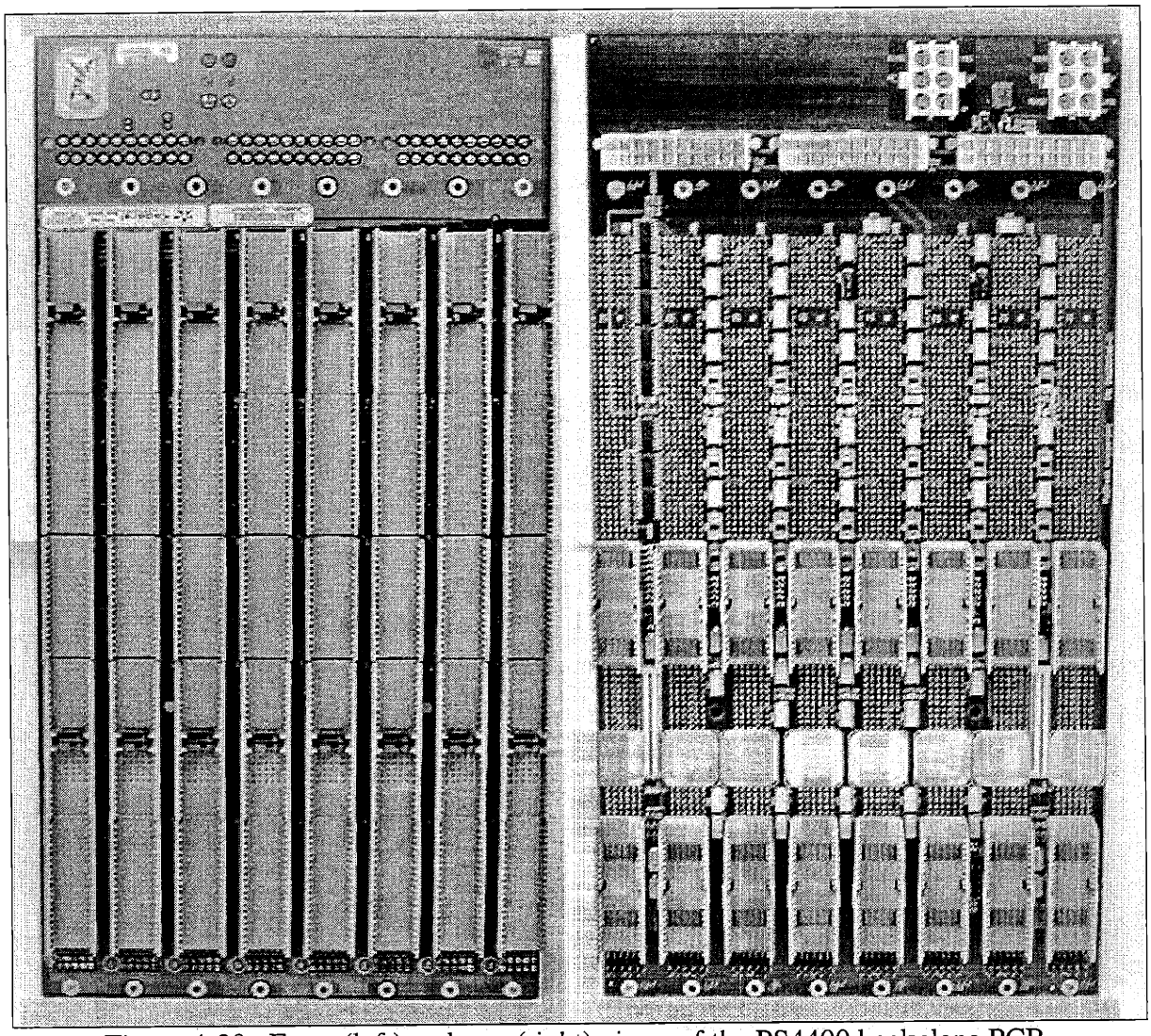

Figure 4-20. Front (left) and rear (right) views of the PS4400 backplane PCB.

The details of all of the electrical connections go beyond what can be incorporated in this dissertation. Detailed I/O net lists were made of the connections that were needed between the boards and the location of each end of the connection. In addition, these lists cover all of the connections to the system control computer and any external electrical signals such as those needed for the external normally open shut-off valve.

Testing Procedures

The components of the AIMS were tested as they were assembled to ensure that the electrical connections were correct and the fluidics functioned properly. The first testing performed on the system was to verify that the power connections inside the chassis were correct to avoid damaging any of the boards or other system electronics when power was initially applied to the chassis. This was done by probing the power locations in the rear I/O cards, power distribution wiring, and the system boards to ensure they were connected properly.

The individual system boards were also closely examined to ensure that the manufacturer had followed the specified board net lists. These lists tell the PC board manufacturer how the components on the board must be connected. The manufacturer than devises the board artwork necessary to make these connections. This verification was done on the bare boards before they were populated with components.

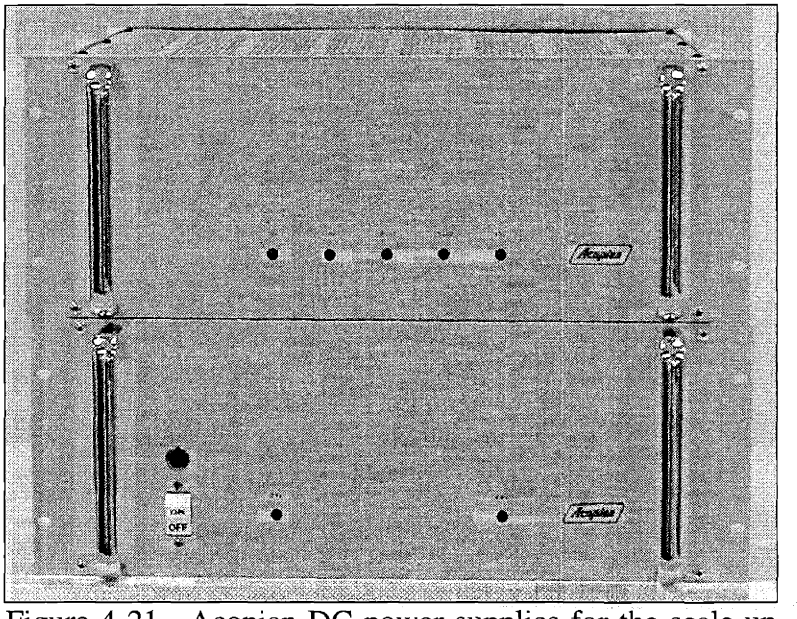

Figure 4-21. Acopian DC power supplies for the scale-up microreactor system.

After the power connections were checked, the AIMS was connected to its external Acopian[8] power supplies that supplied 5, 15, 24, 32, and 48 Vdc power to the AIMS. Because of the number of voltages needed, the Acopian supplies were in two separate rack-mountable units, the S11381 and the S11382. Figure 4-21 shows the two power supply units that each measure 19" × 7" × 16¼".

The remaining electrical connections were verified by inserting the front system boards and testing their functionality. This involved connecting the system to the control computer and creating simple test Virtual Instruments (VI's) that could exercise the relays, analog outputs, and discrete outputs of the control system. In addition, the test VI's also monitored the analog inputs and discrete inputs. Functionality was verified by either observing the operation of a component (for example, the clicking of a relay) or probing voltages in the system or coming from the control computer (for example, measuring the voltage across a resistor on one of the system boards). To test the signals from the control computer a National Instruments SCB-68 breakout board was used for the 68 pin connectors and a National Instruments SCB-100 breakout board was used for the 100 pin connectors. The measured inputs on the control system were also examined using the breakout boards and placing known voltages at points in the system and checking the reading in the LabVIEW test VI. This type of testing was necessary because the backplane pins were virtually inaccessible due to their small size, and the cost of a breakout board was prohibitive. In addition, it was difficult to probe locations on the system boards unless they were near the front of the board. In this case, an extender card would have been extremely

[8] Acopian Technical Company, P.O. Box 638, Easton, PA 18044, (610) 258-5441.

useful, but it also was costly. A picture of the AIMS setup at this point is shown in Figure 4-22.

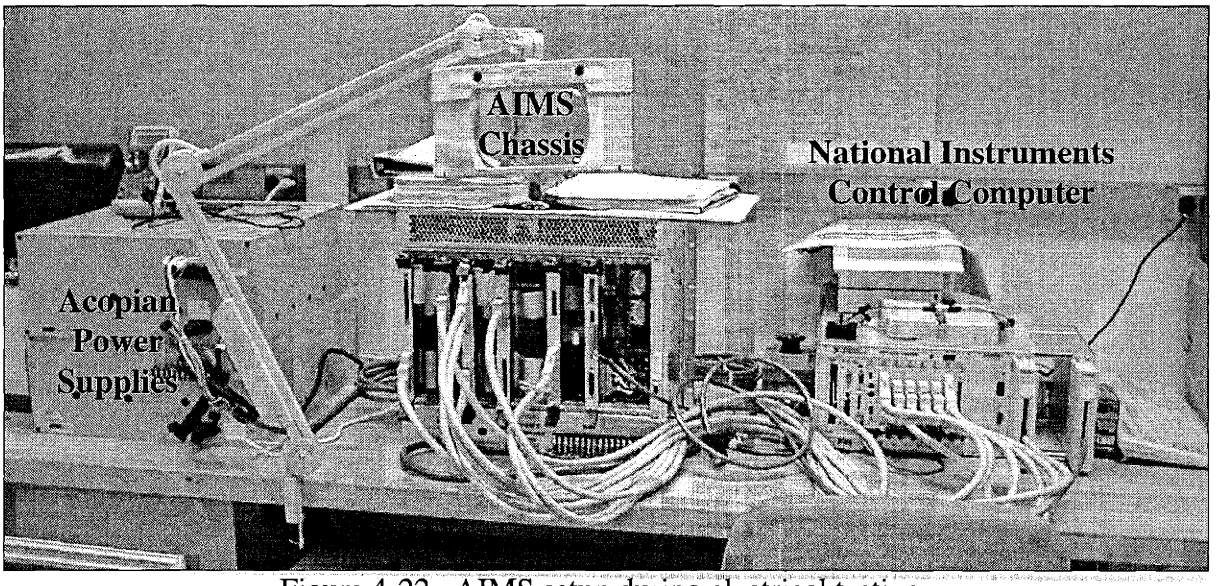

Figure 4-22. AIMS setup during electrical testing.

A more involved LabVIEW test VI was created so that the microreactor circuit outputs could be monitored and input voltages sent to the heater circuits. This VI was also capable of controlling the Redwood flow manifolds in the system. Microreactors were inserted into the reactor boards and a helium supply was connected to the fluidic inputs. The functionality of the microreactor control and monitoring components along with the Redwood flow manifolds was then checked through the LabVIEW interface. In addition, the piping on the system boards was leak-checked using the Gow-Mac gas leak detector described in Chapter 3. With this testing completed the final control and monitoring programs were written and testing under reaction conditions began.

Testing Results

Fortunately, no major problems were discovered during the initial electrical testing. Instead, only some minor setbacks were encountered, such as a lead needing to be tied to

ground and a capacitor that was inserted incorrectly. Overall, the results were very encouraging since no problems were discovered that required a redesign of one of the printed circuit boards or any other major changes.

In one case, a board malfunctioned because a tantalum capacitor was installed in reverse. One of the DieMate™ manifolds also caused a short-to-ground when one of its mounting washers rubbed through the insulating coating of a lead on a reactor printed circuit board. This was easily corrected by replacing the metal washer with a nylon washer. Also on the rear feed gas mixing board I/O card, a lead on one of the 100 pin connectors had to be jumpered to ground. In all of these cases, the most time consuming part was finding the cause of the problem rather than actually correcting it.

Testing of the system boards then began and immediately problems were found with the Redwood flow manifolds. Most of the SOV's upstream of the Redwood MFC's did not open properly. Fortunately, this problem was easily fixed by adjusting a potentiometer on the Redwood flow manifolds granddaughter cards. However, further testing revealed that some of the SOV's had completely failed. A wiring error that was present on some of the Redwood devices caused these failures. Since this error physically destroyed the valves, they were replaced by Redwood. When the other problems were corrected, flow testing with helium showed that the Redwood flow manifolds appeared to function properly. There were some cases were a zero gas flow rate still gave a flow reading from the MFC, but this was corrected by reprogramming the affected MFC's using their serial communications link with the assistance of Redwood.

The functionality of the heater driver and temperature sensor circuits was also tested. Everything worked properly on initial testing. However, the microreactor dies were slightly

too big for the socket, so there was difficulty in their insertion in the socket. This problem was corrected by sanding the edges of the dies and changing the diesaw blade thickness in future wafer-dicing steps (from 6 mils to 8 mils). One of the DieMate™ sockets was damaged during this testing such that its pins were bent out of position. This board and socket was replaced with a spare reactor board that was available. The potentiometers in the temperature sensor circuits were also successfully tuned at this point.

Conclusions

The construction of the AIMS chassis and boards went quite smoothly. The problems encountered upon receiving the parts from vendors were more time consuming to locate than to fix. Unfortunately, the problem encountered with the Redwood valves was not so easily corrected, and the time required for their repair caused a significant delay in the project. This problem was particularly frustrating since Redwood knew about the error in the wiring and actually corrected it on later units that were shipped to DuPont. However, they did not report this problem to DuPont until the SOV's were already damaged (the wiring change only required the installation of a capacitor and could have been easily done at DuPont). This early problem foreshadowed what turned out to be the weakest link in the AIMS—the MEMS valves used to control gas flow in the system. Auspiciously, the rest of the system components performed quite well, and the valves were the largest uncertainty going into testing the system under reaction conditions.

References

1. Sianni, Ralph (2001) "ESL 262 DARPA System 1 P & I Diagram", E.I. du Pont de Nemours & Co., Inc., Wilmington, DE, May 7, 2001, Drawing number W1495427.
2. ENSER Corporation (2000) "Valve Manifold", E.I. du Pont de Nemours & Co., Inc., Wilmington, DE, Feb. 17, 2000, Drawing number D1488666.

3. ENSER Corporation (2000) "Redwood, PWB", E.I. du Pont de Nemours & Co., Inc., Wilmington, DE, Apr. 14, 2000, Drawing number W1492264.

4. ENSER Corporation (2000) "Redwood, PWA", E.I. du Pont de Nemours & Co., Inc., Wilmington, DE, Apr. 14, 2000, Drawing number W1492265.

5. ENSER Corporation (2000) "Redwood Card Assembly", E.I. du Pont de Nemours & Co., Inc., Wilmington, DE, Apr. 14, 2000, Drawing number W1492266.

6. Henningsen, C.G. and Gause, S.A. (1996) "Base materials", In Coombs, C.F., (Ed.), *Printed Circuits Handbook*, 4th ed., McGraw-Hill, New York, p.1088.

7. ENSER Corporation (2000) "Temp Control, PWA", E.I. du Pont de Nemours & Co., Inc., Wilmington, DE, Mar. 22, 2000, Drawing number W1489754.

8. ENSER Corporation (2000) "Temp Control Assembly", E.I. du Pont de Nemours & Co., Inc., Wilmington, DE, Mar. 22, 2000, Drawing number W1489755.

9. ENSER Corporation (2000) "Temp Control, PWB", E.I. du Pont de Nemours & Co., Inc., Wilmington, DE, Mar. 22, 2000, Drawing number D1489756.

10. ENSER Corporation (2000) "Panel Temp Control Card", E.I. du Pont de Nemours & Co., Inc., Wilmington, DE, Mar. 22, 2000, Drawing number D1489757.

11. ENSER Corporation (2000) "Junction Block Mixing Card", E.I. du Pont de Nemours & Co., Inc., Wilmington, DE, Mar. 14, 2000, Drawing number D1489022.

12. ENSER Corporation (2000) "Feed Tubing Weldment", E.I. du Pont de Nemours & Co., Inc., Wilmington, DE, Mar. 24, 2000, Drawing number D1489021.

13. ENSER Corporation (2000) "Process Tubing Mixing Card", E.I. du Pont de Nemours & Co., Inc., Wilmington, DE, Mar. 17, 2000, Drawing number D1489023.

14. ENSER Corporation (2000) "Junction Block Weldment", E.I. du Pont de Nemours & Co., Inc., Wilmington, DE, Mar. 14, 2000, Drawing number D1489024.

15. ENSER Corporation (2000) "Purge Tubing Weldment", E.I. du Pont de Nemours & Co., Inc., Wilmington, DE, Mar. 24, 2000, Drawing number D1489025.

16. ENSER Corporation (2000) "Mixing, PWB", E.I. du Pont de Nemours & Co., Inc., Wilmington, DE, Mar. 22, 2000, Drawing number D1489750.

17. ENSER Corporation (2000) "Panel Mixing Card", E.I. du Pont de Nemours & Co., Inc., Wilmington, DE, Mar. 22, 2000, Drawing number D1489751.

18. ENSER Corporation (2000) "Mixing, PWA", E.I. du Pont de Nemours & Co., Inc., Wilmington, DE, Mar. 22, 2000, Drawing number D1489752.

19. ENSER Corporation (2000) "Mixing Card Assembly", E.I. du Pont de Nemours & Co., Inc., Wilmington, DE, Mar. 22, 2000, Drawing number D1489753.

20. ENSER Corporation (2000) "DieMate Manifold Weldment", E.I. du Pont de Nemours & Co., Inc., Wilmington, DE, Mar. 13, 2000, Drawing number D1489016.

21. ENSER Corporation (2000) "Junction Block Weldment", E.I. du Pont de Nemours & Co., Inc., Wilmington, DE, Mar. 13, 2000, Drawing number D1489020.

22. ENSER Corporation (2000) "Junction Block Reactor Card", E.I. du Pont de Nemours & Co., Inc., Wilmington, DE, Mar. 13, 2000, Drawing number D1489018.

23. Firebaugh, S. (1998) "Improving reactor yield", Feb. 9,1998.

24. ENSER Corporation (2000) "Clam Shell", E.I. du Pont de Nemours & Co., Inc., Wilmington, DE, Mar. 14, 2000, Drawing number D1489019.

25. ENSER Corporation (2000) "Reactor, PWB", E.I. du Pont de Nemours & Co., Inc., Wilmington, DE, Mar. 22, 2000, Drawing number D1489743.

26. ENSER Corporation (2000) "Reactor, PWA", E.I. du Pont de Nemours & Co., Inc., Wilmington, DE, Mar. 22, 2000, Drawing number W1489744.

27. ENSER Corporation (2000) "Reactor Card Assembly", E.I. du Pont de Nemours & Co., Inc., Wilmington, DE, Mar. 22, 2000, Drawing number W1489745.

28. ENSER Corporation (2000) "Panel Reactor Card", E.I. du Pont de Nemours & Co., Inc., Wilmington, DE, Mar. 22, 2000, Drawing number D1489746.

29. ENSER Corporation (2000) "Heater Driver, PWB", E.I. du Pont de Nemours & Co., Inc., Wilmington, DE, Mar. 22, 2000, Drawing number W1489747.

30. ENSER Corporation (2000) "Panel Heater Driver Card", E.I. du Pont de Nemours & Co., Inc., Wilmington, DE, Mar. 22, 2000, Drawing number D1489748.

31. ENSER Corporation (2000) "Heater Driver, PWA", E.I. du Pont de Nemours & Co., Inc., Wilmington, DE, Mar. 22, 2000, Drawing number W1489749.

CHAPTER 5
SYSTEM CONTROL AND MONITORING

Although construction of the AIMS boards and the assembly of the chassis was a substantial task, this represented only half of the effort of the project. The control hardware and software presented a challenge that went beyond the limits of traditional laboratory systems and involved the use of components in beta form or just released commercially. The difficulty in this task was the number of signals that were to be monitored for the high control loop rate desired. In addition, the control computer was responsible for safety monitoring and to engage interlocks as needed. As in most industrial reactor systems, the control computer only executed the process control loop, and another system provided the operator interface.

There are two major components to the AIMS control and monitoring system: one is the embedded controller, and the other is the Human-Machine Interface (HMI). Figure 5-1 is a block diagram of the AIMS control system architecture showing the connections between the AIMS chassis, the process controller, and the HMI. Process controllers usually take the form of industrially hardened computers that operate under deterministic real-time Operating Systems (OS). Determinism means that the controller will guarantee the execution of a process control loop in a specified time period. If the loop cannot be completely executed, a flag is raised, and the controller can take appropriate action. Real-Time operating systems are especially robust and not prone to failure as often seen in personal computers running in the Microsoft Windows™ environment. Because the controller is responsible for process

safety aspects, reliability is the most important factor. This eliminates any desktop machine operating in the Windows™ or Mac OS environment.

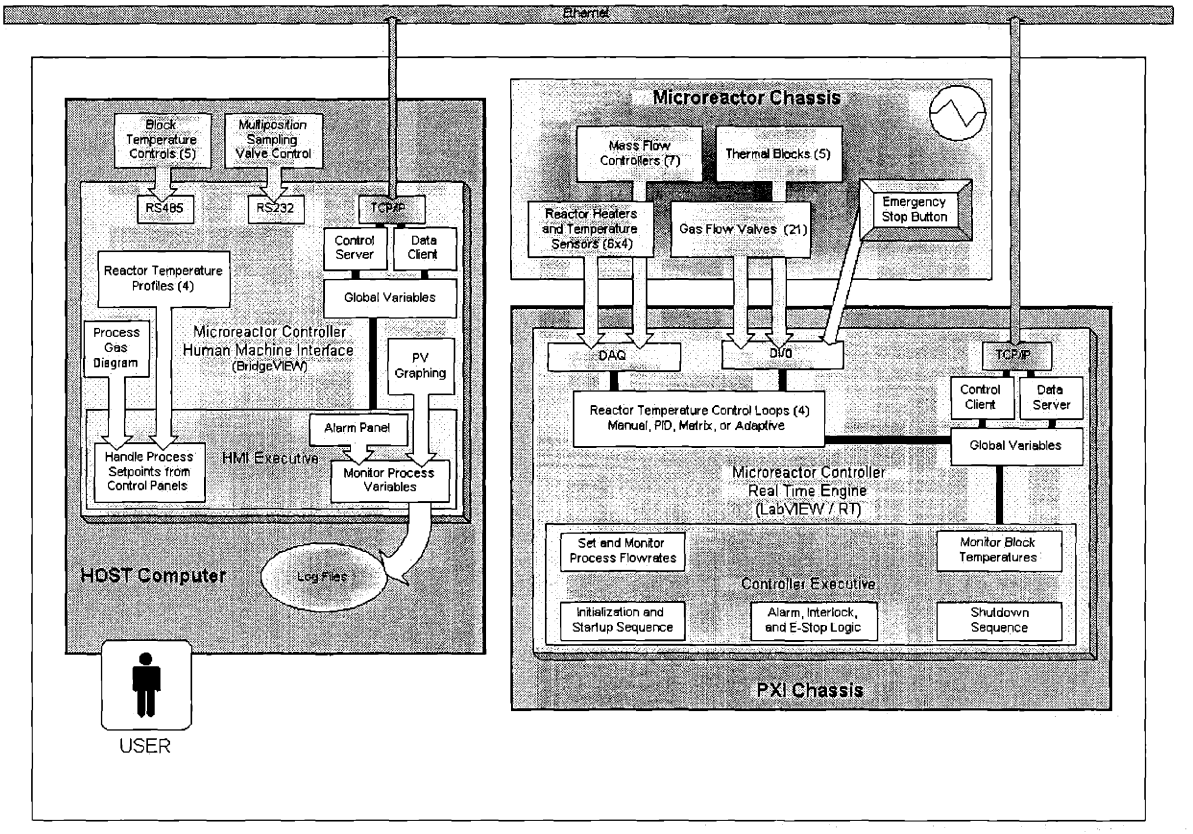

Figure 5-1. Block diagram of the AIMS control system architecture.

The controller used for the AIMS is a National Instruments (NI) PXI-1010 chassis with an embedded controller. PXI is the NI version of the CompactPCI standard. The controller can be booted with Windows™ or the Pharlap real-time operating system licensed by NI. The real-time OS is used for process control of the AIMS. This computer is responsible for monitoring all of the discrete and analog inputs from the AIMS as well as providing the discrete and analog outputs for process control.

The AIMS control system is actually composed of two NI PXI chassis, a PXI-1010 and a PXI-1000B, due to the number of boards that were required for operation. Figure 5-2

shows the two chassis with the boards used for running the AIMS. An MXI-3 bus extender cable connects these chassis by extending the bus of the system beyond the backplane of the PXI-1010 chassis. This is done by using two NI PXI-8330 boards, one in each chassis.

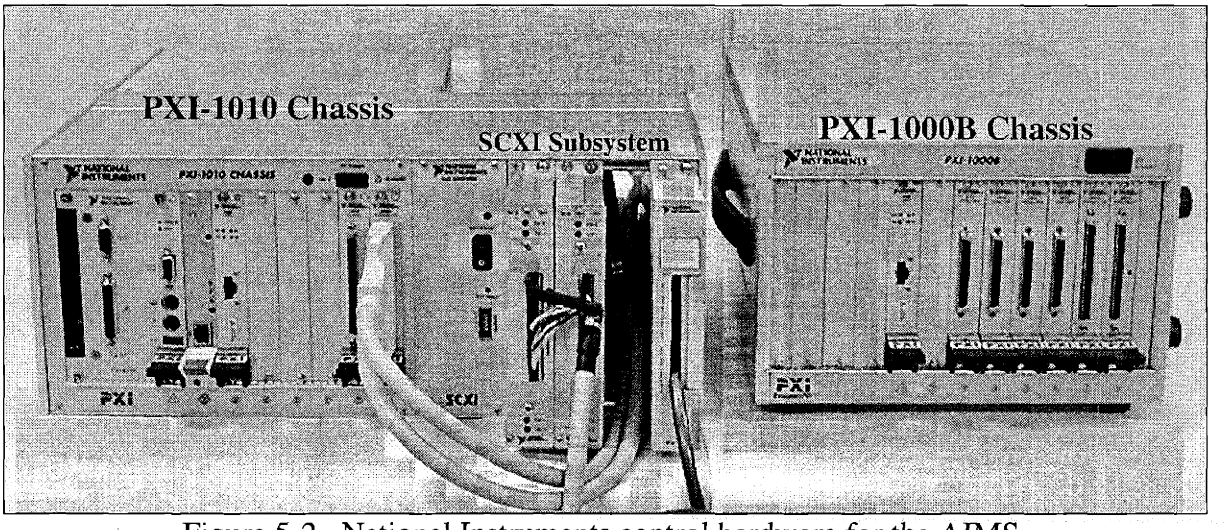

Figure 5-2. National Instruments control hardware for the AIMS.

The PXI-1010 chassis contains the embedded PXI controller board, a NI PXI-8170, which uses a 700 MHz Pentium™ III processor as the CPU. This processor runs independently of the computer running the HMI. This particular CPU was not available with an Ethernet connection port, so a Nexcom[1] MAXI 100L Ethernet card was installed. In addition, the 1010 chassis has one PXI-6527 digital I/O board, which provides the 16 needed digital output signals and the 20 needed digital input channels. This board has 24 optically isolated digital input channels and 24 solid-state relay output channels. All of the digital outputs were 0 Vdc in the low state and 24 Vdc in the high state. The Acopian power supplies provided the external power needed for these channels. The digital input channels were 0 Vdc in the low state and either 5 or 24 Vdc in the high state. A 100 pin NI SH100-100-F cable connects this board to the AIMS chassis.

The PXI-1010 chassis also contains a four slot SCXI subsystem for three signal conditioning boards that were not available in the PXI form. The SCXI subsystem contains two SCXI-1121 boards that are used to measure the temperatures of five RTD's in the AIMS. These are the RTD signals coming from the DieMate™ manifold and the product heater line. Each board is capable of measuring temperatures from four RTD's and has an accuracy of ±1°C. The RTD's are wired in a four-wire configuration. A NI SCXI-1321 high voltage terminal block is used to connect the RTD signals to the SCXI-1121 module. A NI PXI-6025E multifunction I/O board is used to read the voltage signals from the SCXI-1121 boards with the multiplexing done on channel 0 of the 6025E. A 100 pin NI SH100-100 cable connects the 6025E to the SCXI subsystem[2]. A NI SCXI-1160 general-purpose relay module is used to provide the six needed power relays for the AIMS. This board consists of 16 isolated Single-Pole Double-Throw (SPDT) latching relays. A NI SCXI-1324 high voltage terminal block is used to connect the power signals to the SCXI-1160 module. Table 5-1 summarizes the boards used in the PXI-1010 chassis for operating the AIMS.

The PXI-1000B chassis contains four PXI-6713 analog output boards that provide the 31 needed analog output signals from the PLC to the AIMS. Each PXI-6713 board has eight analog output channels with 12-bit resolution. A 68 pin shielded NI SH68-68-EP cable connects each of these boards to the AIMS chassis. The PXI-1000B chassis also contains two PXI-6071E multifunction I/O boards that provide the 55 needed analog input channels. Each board is capable of reading 32 differential analog inputs with 12-bit resolution in a

---

[1] NEX Computers, Inc., 46560 Fremont Blvd. #401, Fremont, CA 94538, (510) 656-2248.
[2] Normally, the signals from these boards would be read directly through the bus link from the SCXI subsystem to the PXI chassis; however, a bug in the software prevented this while the system was operating in real time mode.

variety of signal gain configurations. Each 6071E module is connected to the AIMS with a 100 pin SH100-100 cable. Table 5-2 summarizes the boards in the PXI-1000B chassis.

Table 5-1. Boards in the PXI-1010 Chassis.

Slot No.[3]	Module[4]	Description	No. of Channels Used	Cable[5]
1	8170	Pentium™ III 700 MHz embedded computer	N/A	N/A
2	MAXI 100L[6]	LAN Ethernet connectivity module	N/A	Ethernet
3	8330	MXI-3 bus extender module	N/A	MXI-3
7	6527	Digital I/O module	20 I/16 O	SH100-100-F
8	6025E	Multifunction I/O module for reading the system RTD's	1	SH100-100
SCXI-1	1121/1321	RTD measurement	4	Custom
SCXI-2	1121/1321	RTD measurement	1	Custom
SCXI-4	1160/1324	General purpose relay module	6	Custom

Table 5-2. Boards in the PXI-1000B Chassis.

Slot No.[3]	Module[7]	Description	No. of Channels Used	Cable[8]
1	8330	MXI-3 bus extender module	N/A	MXI-3
3	6713	Analog output module	8	SH68-68-EP
4	6713	Analog output module	8	SH68-68-EP
5	6713	Analog output module	7	SH68-68-EP
6	6713	Analog output module	8	SH68-68-EP
7	6071E	Analog input module	29	SH100-100
8	6071E	Analog input module	26	SH100-100

The software for the controller was written in G using LabVIEW version 6.0.3 RT. G is National Instruments' proprietary graphical programming language, which is used in

[3] Skipped slot numbers indicate empty slots in the chassis.
[4] Unless otherwise noted, the boards in the PXI-1010 chassis are manufactured by National Instruments.
[5] All cables are manufactured by National Instruments except the Ethernet and custom cables.
[6] Manufactured by Nexcom.
[7] All of the boards in the PXI-1000B chassis are manufactured by National Instruments.
[8] All of the cables are manufactured by National Instruments.

LabVIEW. Programs written in G can be run in a number of operating environments including Windows™ , Mac, or in the Pharlap real-time operating environment of the embedded controller. Development work was done on a separate computer that downloads the control software to the embedded controller. Monitoring of the control loop can be accomplished through the development computer, but it does not have to be operating for the controller to function.

The software executing on the controller is responsible for 1) monitoring process variables and transmitting them to the HMI; 2) examining the process variables for abnormal conditions; 3) executing interlocks based on the status of the process variables; 4) performing closed-loop control of the microreactor heaters (24 heaters in total); and 5) receiving and implementing operator input from the HMI. All of these actions are considered part of the control loop and must be executed within a specified time period for the controller to be operating in real time. Thus, the speed of the backplane, processor, and communications are all factors in determining the maximum loop execution rate.

The control software is invoked by applying power to the NI chassis or by starting LabVIEW/RT on any machine in the local subnet[9] with the NI controller selected as the development target. The latter causes the control software running on the embedded controller to synchronize with the development computer. The main control panel, shown in Figure 5-3, is then displayed on the developer's machine. Execution is started and monitored through this control panel. The execution of the control loop can be observed in this mode, but this is usually done for debugging purposes. Under normal operating conditions, the

[9] Operation can be done outside of the local subnet, but certain LabVIEW features do not function and problems can develop with the TCP/IP communications inside the control loop.

system is monitored through a separate LabVIEW program that operates as the human-machine interface (HMI) for the AIMS.

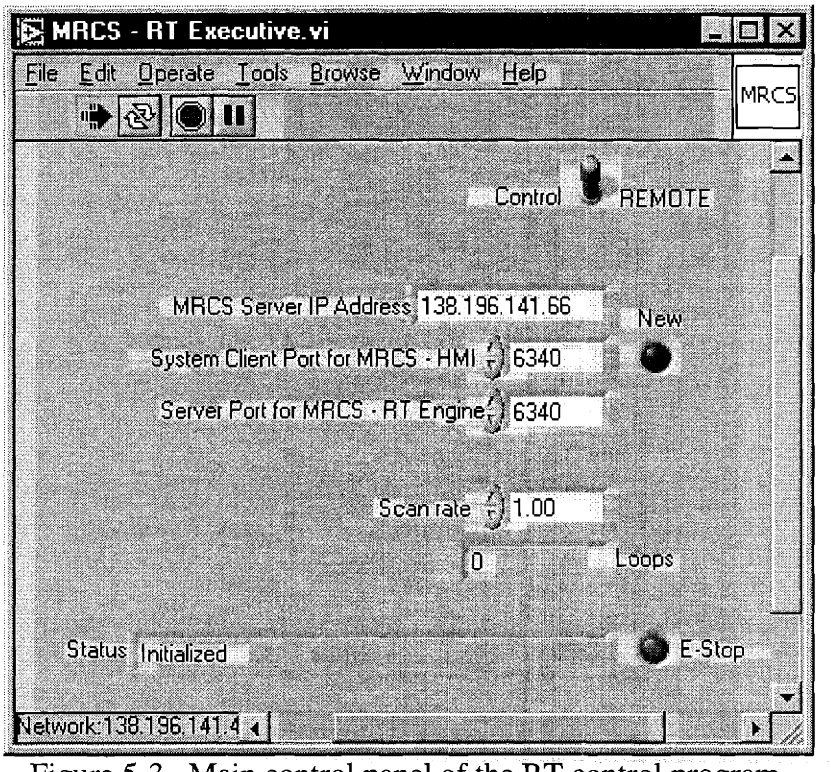

Figure 5-3. Main control panel of the RT control program.

The HMI provides the connection between the AIMS control hardware and the operator. The HMI is actually the interface program that runs on a computer connected to the embedded controller. For the AIMS, the HMI software was developed in G using LabVIEW 6.0.2 with the Datalogging and Supervisory Control (DSC) module installed. The DSC module is intended for developing HMI/SCADA applications. During testing of the AIMS, the HMI was run on a Dell OptiPlex GX110 with a Pentium™ III processor and 256 megabytes of RAM operating under Windows™ NT 4.0 service pack 5. This computer was located near the AIMS setup and is shown in Figure 5-4. LabVIEW is available for a number of operating environments including Linux, so these machine specifications are not

restrictive[10]. A 10 megabit/s Ethernet connection was established between the HMI computer and the NI embedded controller. Both machines were capable of 100 megabit/s transmission speeds, but the routers in the subnet limited operation to only 10 megabit/s. Optionally, the two machines could be connected directly using an Ethernet crossover cable. In either case, the data transmission rate was still much faster than the HMI computer could display or store, so much of the data was not seen by the operator[11]. However, this did not affect the performance of the AIMS since the real time controller executes all the necessary control functions. Instead, only the display of data and its logging was affected.

The HMI is responsible for displaying of data to the user, allowing the user to enter new process set points, and historical logging of data. Display of data is achieved through numerical displays and other visual indicators (for example, a valve colored green would be open). The designer of the HMI has to be careful in selecting the appropriate display methods and the organization of the data. With over 200 process variables in the AIMS, it would have been easy to overwhelm the operator with data. Thus, most control actions are done pictorially by clicking on a valve or another object. In this way, the data is displayed in close proximity to where the user can enter new process set points.

---

[10] Windows NT, 2000, or XP is recommended for the operating system due to its improved stability. A failure in the HMI computer will not prevent the controller from operating, but will result in the loss of data.

[11] The data was not lost. Instead, the display update rate on the HMI was set to around 10 Hz, so all of the data points were not displayed. The data logging software recorded data at a maximum rate of 4 Hz.

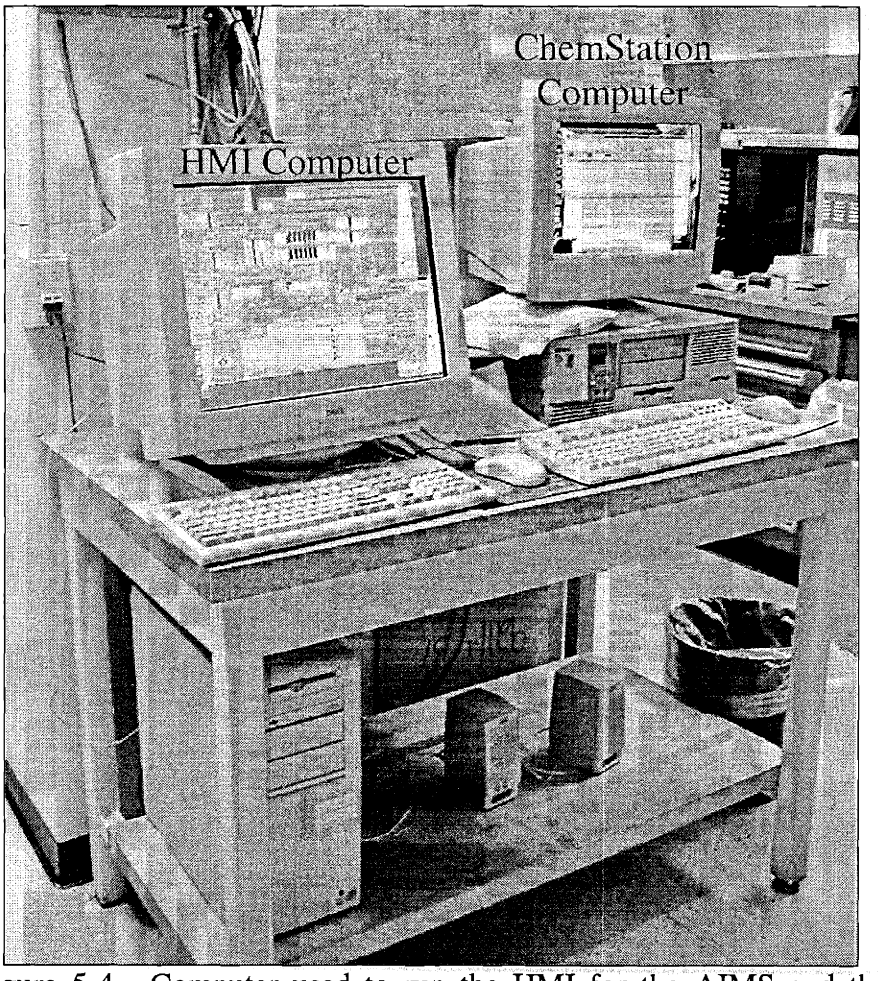

Figure 5-4. Computer used to run the HMI for the AIMS and the computer used to run ChemStation for the AIMS gas chromatograph. The AIMS experimental setup is located in the hood behind these computers.

The other task of the HMI is to log all of the process variables at a designated time interval. For this task, the LabVIEW DSC Module was installed on the HMI computer. This add-on to LabVIEW gives the developer the ability to establish automatic data logging; features for working with applications having a large I/O channel count; and alarm management and event logging capabilities. In addition, this module provides the developer with OPC connectivity tools, which were used in communicating with the CAL 3300 temperature controllers. The built-in data logging features of this package were used by

establishing tags for the process variables to be recorded. The properties of the tags could then be adjusted to the users needs (for example, the dead band for data logging can be changed to help minimize database size). Data logging began as soon as the HMI program was started, and storage was done in a National Instruments Citadel database. Data in this format can be accessed through the LabVIEW Historical Trend Viewer (HTV) or through third-party software such as Microsoft's Excel using the Citadel Open Database Connectivity (ODBC) driver. This driver allows other applications to access the data directly using Structured Query Language (SQL) queries. The LabVIEW HTV allows the user to access process variables by specifying a time window to display and the desired process variables. The data retrieval from the database is transparent in the sense that the appropriate database file is determined by LabVIEW, and the process variable values are then retrieved from the database for the given time window. Figure 5-5 shows a screen shot of the LabVIEW HTV with some sample data from the AIMS. The data displayed by the historical trend viewer can be exported to standard text file formats that can be read by spreadsheet applications.

The maximum data storage rate supported by the LabVIEW DSC module is 4 Hz, which is much slower than the time constants of the microreactor heaters. However, recording the heater temperature data during experiments that lasted hours at a rate in excess of 1000 Hz would have generated enormous files and provided only a small level of improved process information (most of the AIMS experiments were not focused on studying the very fast dynamic processes of the microreactors). Even at a data storage rate of 4 Hz and the compression techniques used by the Citadel database, a single days worth of data required about 250 megabytes of storage space due to the large number of process variables

being monitored and the small dead band used for data logging during testing. Higher speed tests were achieved outside of the DSC module by using conventional file I/O procedures.

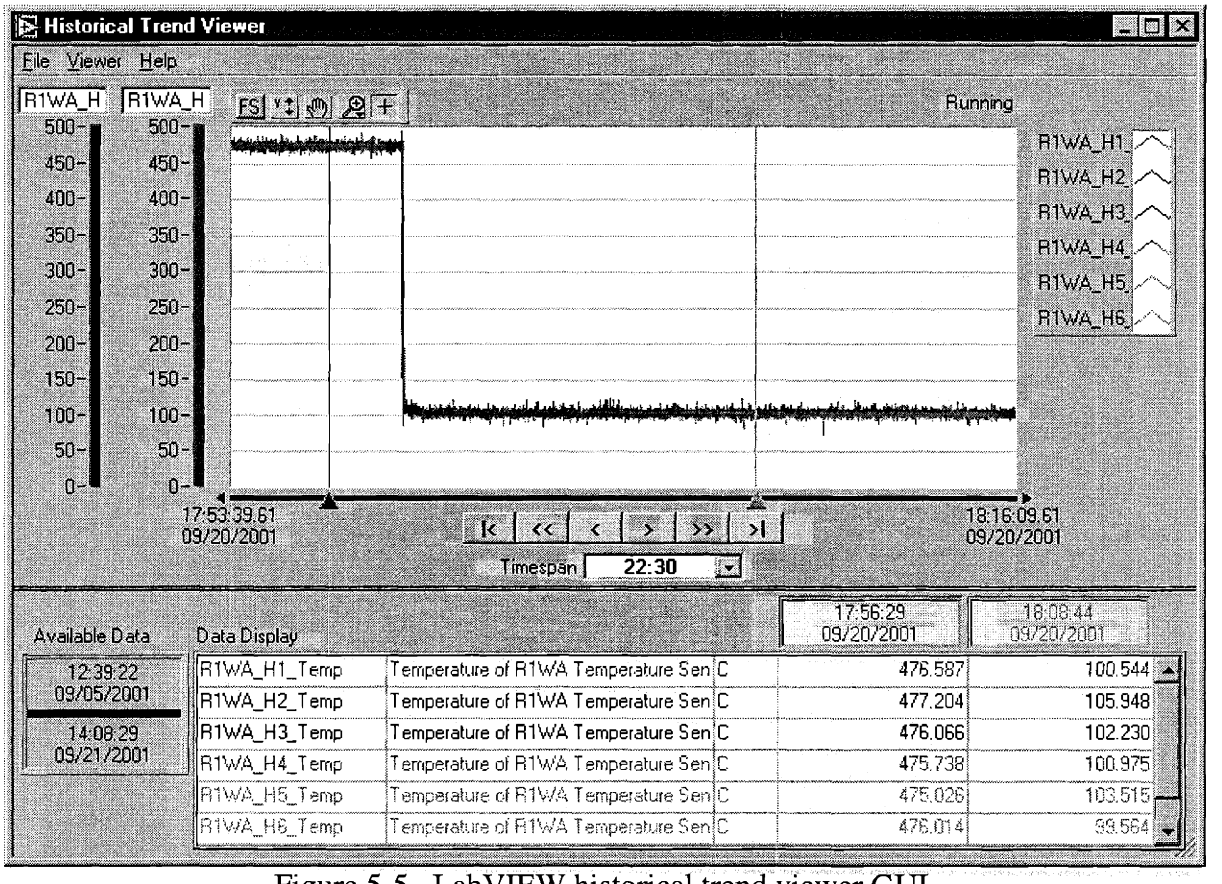

Figure 5-5. LabVIEW historical trend viewer GUI.

The AIMS HMI is organized around a central VI panel that allows the operator to quickly view many of the process variables and access more detailed panels easily. The software on the AIMS controller is started on the *RT Engine* tab of this central panel, as shown in Figure 5-6. This panel allows the operator to select the desired loop rate for the controller and to begin the operation of the control loop. It also displays the number of loops that have been completed since the last enable command was given.

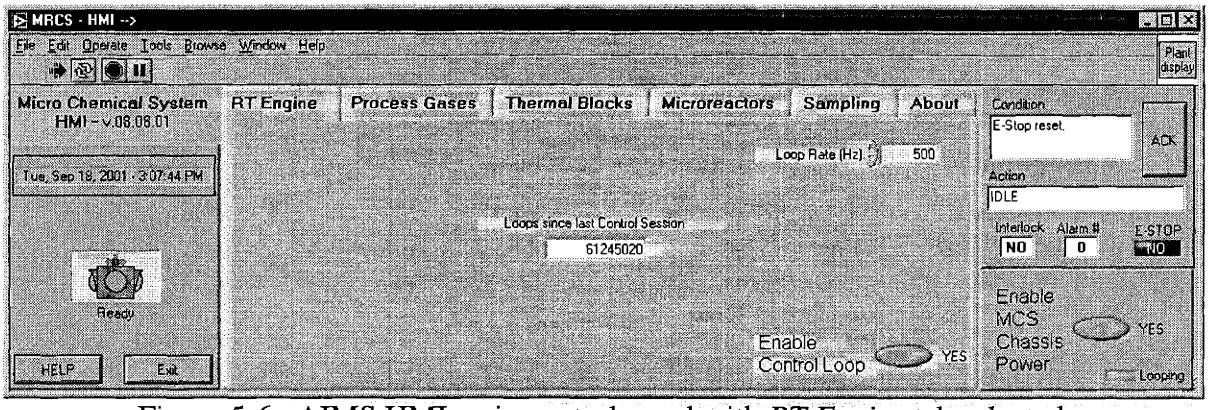

Figure 5-6. AIMS HMI main control panel with *RT Engine* tab selected.

The other tabs on this central panel allow the operator to quickly go to another area of the system and examine the process conditions. Further sub-panels can be opened from these other tabs on this central panel. The tabs are ordered from left to right according to the flow of gas in the system (except the first tab, which is used to enable the control program). Power to the AIMS chassis can be enabled or disabled to the right of the tab screens on the central panel. Disabling the power using this button is equivalent to pushing the emergency stop of the AIMS.

The second tab, *Process Gases*, displays the process variables related to the Feed Gas Mixing Board in the AIMS chassis. Figure 5-7 shows the central panel with the *Process Gases* tab selected. This panel shows the position of all of the SOV's on the board (lit indicates an open valve) and the gas flow rate through each of the process gas legs (process gas 1 is the fuel, process gas 2 is the oxygen, and process gas 3 is the diluent). The feed gas ID indicator displays the molar composition of the feed gas. The *Purge All Now* button is the immediate way to set the system to purge with nitrogen. In activating this button, a system purge is executed which has nitrogen flow throughout the AIMS for a period of five minutes to remove any residual reactive gas in the system tubing. The position of the SOV's on the

feed gas mixing board or the gas flow rates cannot be adjusted on this panel. To make these changes the *Configure Gas Mixture* button is pressed to open a sub-panel.

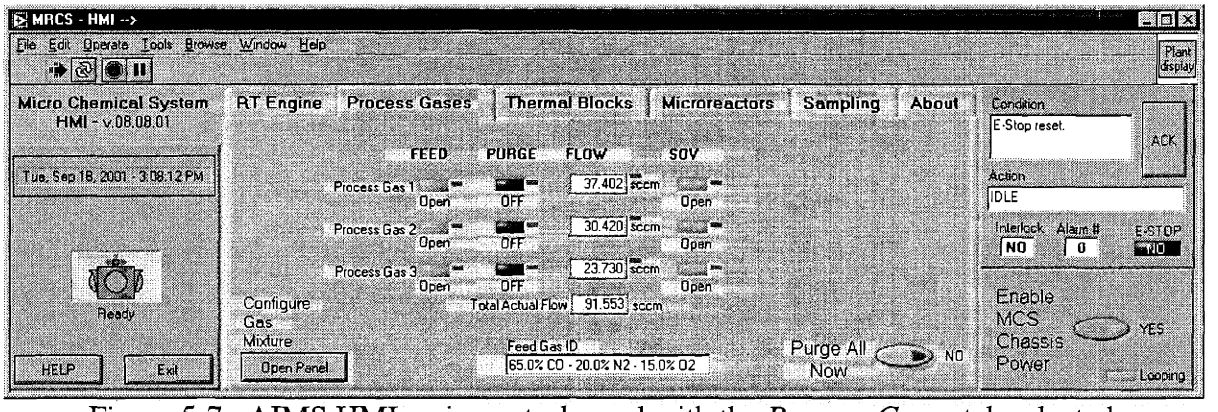

Figure 5-7. AIMS HMI main control panel with the *Process Gases* tab selected.

The *Process Gas Control* panel, shown in Figure 5-8, gives the operator a more detailed view of the Feed Gas Mixing Board and allows the operator to make changes to the process variables. The process inputs on this panel are the SOV positions and the MFC flow rate set points. The process outputs on this panel are the measured gas flow rates. The controls for the SOV's do not necessarily reflect actual positions. Instead, they only indicate the set points since Redwood Microsystems did not incorporate any means for querying the actual valve position. Instead, the functioning of the valves must be determined indirectly by monitoring the measured gas flow rates through the Redwood MFC's. This is similar to the other laboratory reactor systems at DuPont. In addition, other information can be transmitted to the controller from this panel, such as explosive limit information to prevent the user from producing a combustible feed gas mixture.

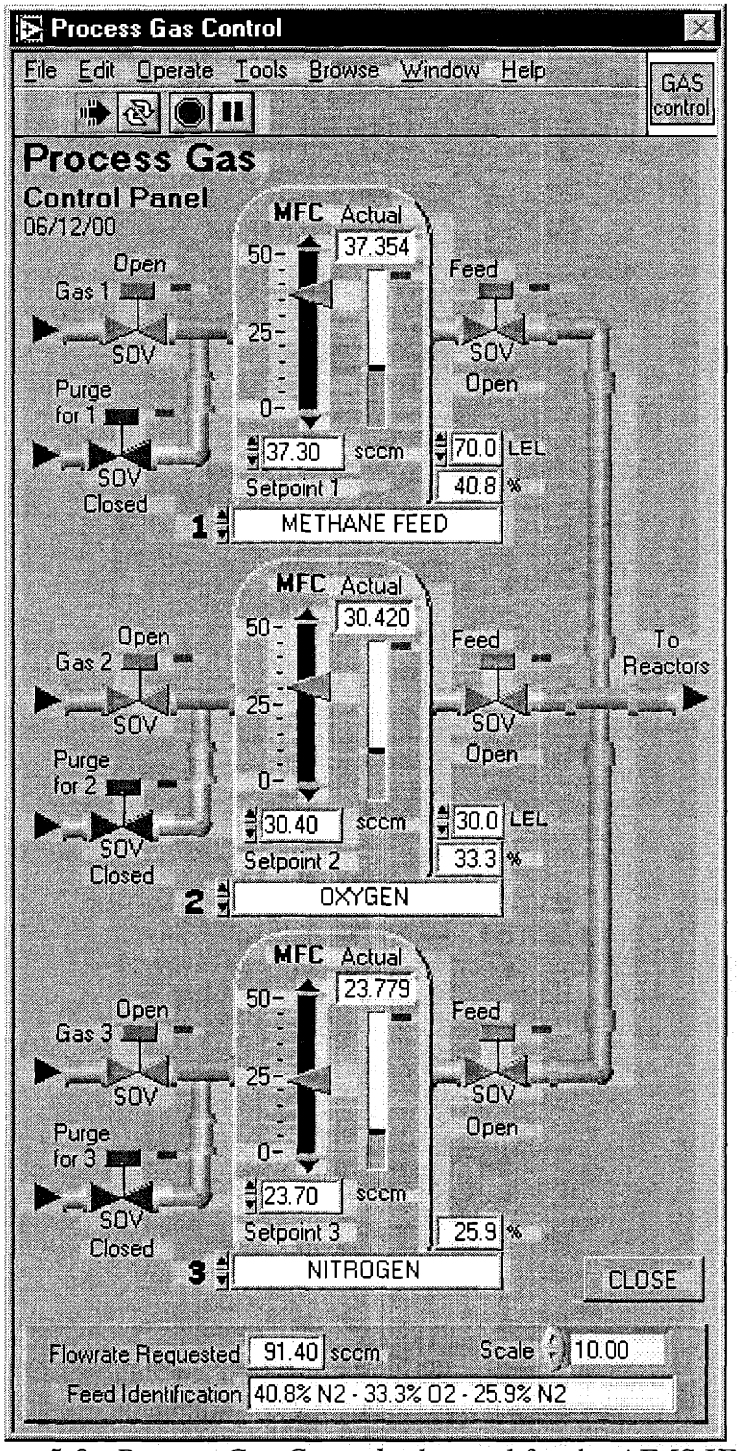

Figure 5-8. *Process Gas Control* sub-panel for the AIMS HMI.

After the Feed Gas Mixing Board, the feed gas flows into the two Reactor Boards, which are monitored through two tabs in the main control panel—the *Thermal Blocks* tab and

the *Microreactors* tab. The *Thermal Blocks* tab, shown in Figure 5-9, displays the measured RTD temperatures of the heated elements on the Reactor Boards excluding the microheaters in the reactor channels. This includes the DieMate™ manifolds, the clamshell heater blocks for the product transfer lines, and the GC sampling valve oven (although not on the Reactor Board, it is displayed on this panel since it is the only other measured RTD value in the system). The displayed temperatures are taken from the temperatures read by the SCXI-1121 boards in the PXI controller. The *Read Now* button on this panel is used to signal the controller to query these temperatures, which is not normally done during a control loop. This is due to the amount of time added to the control loop to measure these temperatures through multiplexing on channel 0 of the PXI-6025E board. The set points for these heated elements can be adjusted by pressing the *Configure Manifold Temperatures* button to open a sub-panel.

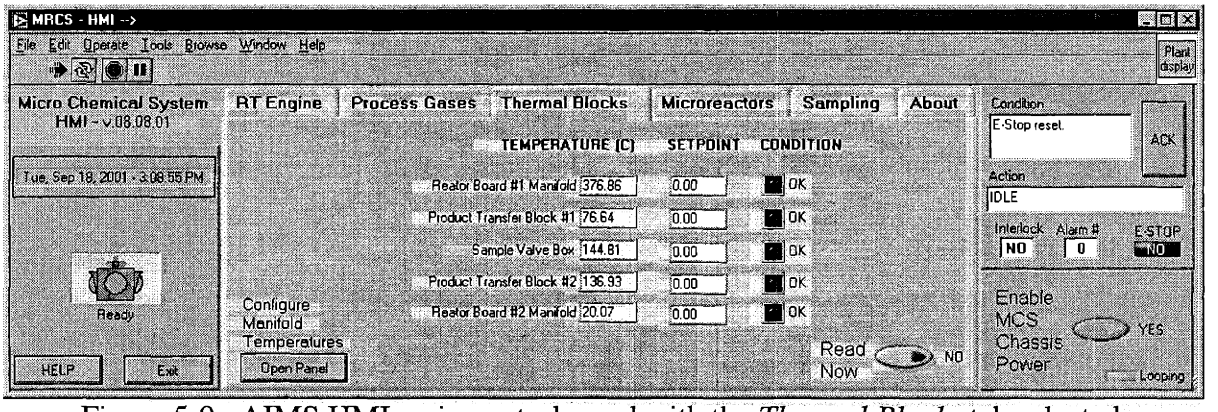

Figure 5-9. AIMS HMI main control panel with the *Thermal Blocks* tab selected.

The *Manifold Temperature Control* panel, shown in Figure 5-10, allows the operator to read the measured temperatures on the CAL 3300 temperature controllers and modify their set points. Unlike the temperatures displayed on the main control panel, these temperatures are obtained by querying the CAL 3300 controllers. Communication between the HMI

computer and the CAL controllers is done using an RS232 serial interface. However, for their operation in the AIMS it was necessary to use the RS485 communications protocol of the controllers so that they could be daisy-chained together. A Burr-Brown[12] RS232/485 converter was placed in the AIMS chassis, so the HMI computer could communicate with the CAL controllers without the need for a RS485 interface card. To allow LabVIEW to easily communicate with the CAL controllers, the CAL OPC Server version 1.1 was installed on the HMI computer. Using the OPC connectivity features of the LabVIEW DSC module, the need to develop serial communications tools for the CAL controllers was avoided.

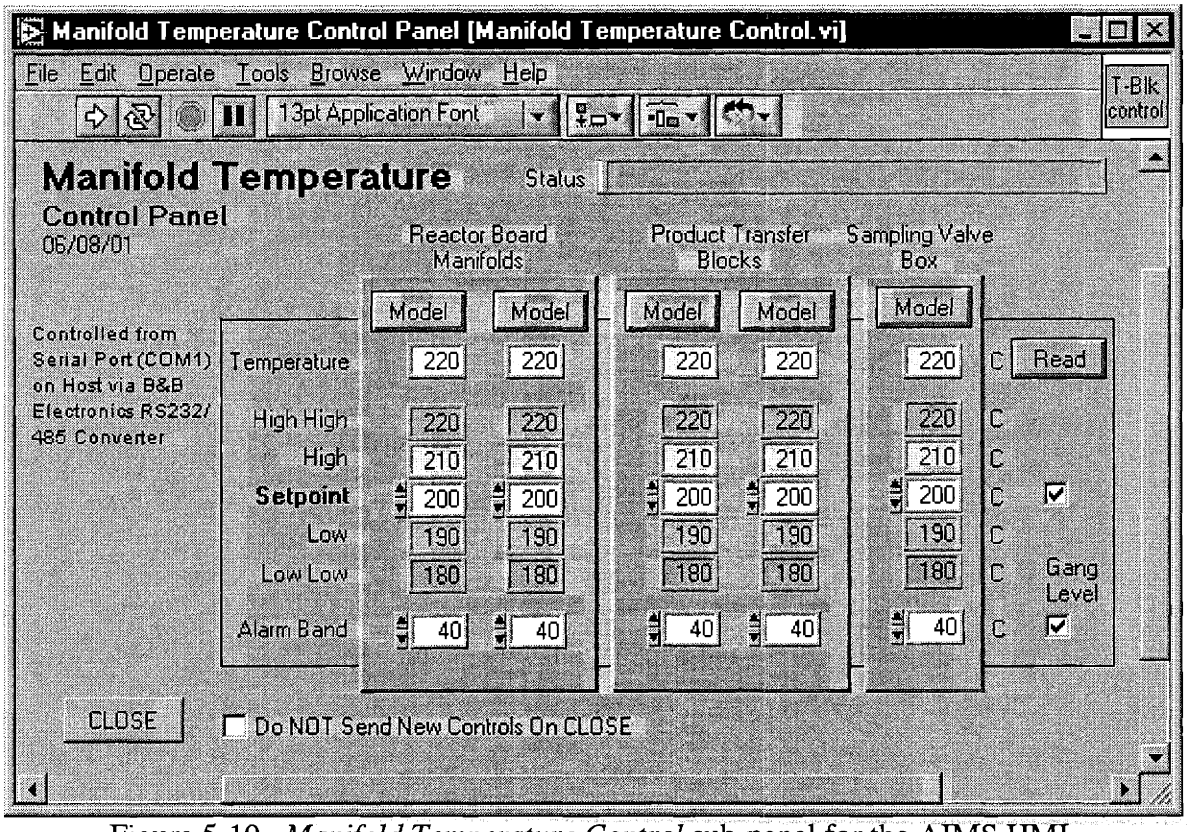

Figure 5-10. *Manifold Temperature Control* sub-panel for the AIMS HMI.

[12] Burr-Brown is now part of Texas Instruments' Analog and Mixed Signal Products division.

The operation of the microreactors is monitored through the *Microreactors* tab on the main control panel, as shown in Figure 5-11. This panel displays the position of the SOV's, the feed gas flow rate to each microreactor channel, and whether the microreactor heaters are enabled. Additional information on the operation of each of the microreactor channels can be obtained by clicking on the *Open Panel* button next to the reactor name (for example, R1WA refers to Reactor Board 1, Channel A on this panel). In addition, pressing the *Configure Reactor Control* button opens a sub-panel where the operator can configure the temperature control mode of each of the microreactor channels (either manual or automatic PID control).

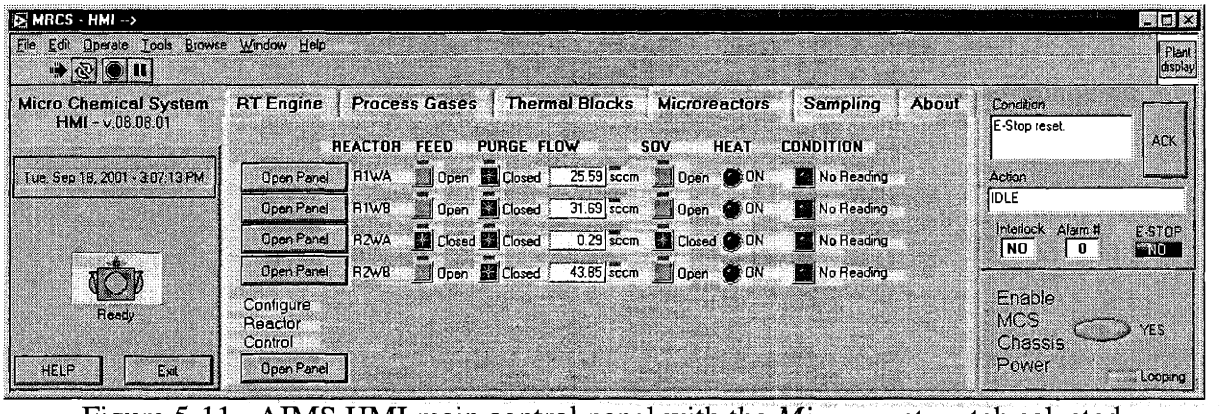

Figure 5-11. AIMS HMI main control panel with the *Microreactors* tab selected.

The *Reactor Control* panels allow the operator to see much more detailed information on the operation of an individual microreactor channel. It also allows the operator to make changes to the process set points. Figure 5-12 shows the *Reactor Control* panel for channel A of the microreactor on Reactor Board 1. Here the operator can choose the gas stream flowing to the microreactor (either feed gas or purge gas), the gas flow rate, and the set points of the microreactor heaters. The *Temperature Reading* indicators at the top of the channel block in the middle of the panel show the measured temperatures of the first six

microreactor heaters[13] in the channel using the microreactor RTD's. These temperatures are also indicated graphically with the color bars below each of the displayed values. The panel shown in Figure 5-12 is in the automatic control mode, so the temperature set point numerical and graphical controls are also displayed below the temperature indicators. Here the operator can enter new values for the temperature set points and observe the current set points. Located below these controls are the temperature sensor resistance indicators, which display the raw resistance data before it is converted to a temperature. The measured temperatures are calculated using the resistance at the triple point of water, R_{tpw}, of each of the microreactor RTD's and the platinum layer temperature coefficient of resistivity, α (alpha in the display). Both of these controls are located below the displayed sensor resistances. The operator must enter values into these fields for the temperature reading to be calculated for the microreactor RTD's. Information on the heater performance is below these controls, with indicators that display the voltage and current being applied to each of the microheaters in the reactor channel. In manual control mode, the operator enters the voltage to be applied across the microreactor heaters directly. In automatic control mode, this value is calculated by the PID control loop to maintain the set point temperature. The toggle switch located at the left of the microheater indicators allows the user to enable or disable the microreactor heaters. When the heaters are disabled, a relay on the Heater Circuit Board directs the heater power to a fixed resistor on the circuit board (designed to simulate the load of a microreactor heater). This relay was added as a safety measure to enable the system to quickly remove power from the microreactor heaters and to aid in testing by preventing unwanted power surges during startup from destroying the microreactor membranes. The lighted *Reactor*

[13] As stated previously, only the first six, of the seven microreactor heaters are utilized in the

Enabled indicator on the right of this block simply displays whether the microreactor heater is actually enabled (the position of the relay on the Heater Circuit Board is sensed by the control electronics). In the section at the bottom of this block, the operator has the ability to gang the microreactor heaters together (this allows the user to change the set points of multiple heaters by entering a single value). Indicators also tell the operator whether the control loop is keeping real-time and the current loop rate. This information is for diagnostic purposes of the control loop.

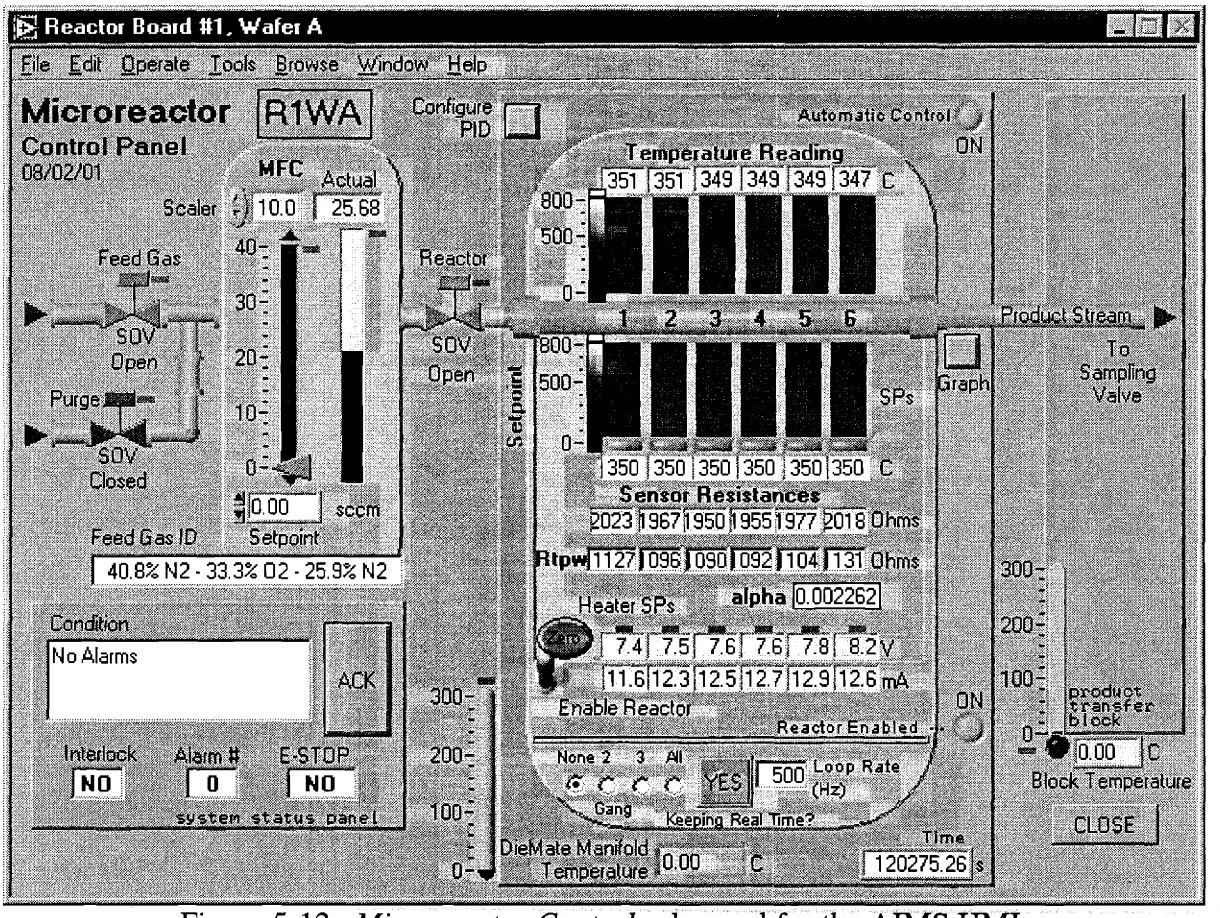

Figure 5-12. *Microreactor Control* sub-panel for the AIMS HMI.

scale-up system.

The microreactor heater control mode is displayed at the top right hand corner of this middle block in Figure 5-12. The operator can view and change the automatic PID control parameters by pressing the *Configure PID* button in the upper left hand corner of this block. This opens the *PID Parameters* sub-panel, shown in Figure 5-13. In this panel, the operator can enter unique PID parameters for each of the microreactor heaters in one of the microreactor channels (the panel shown is for Reactor Board 2, Channel B). The units of the proportional gain, K_c, are dimensionless, but correspond to the unscaled voltage input from the microreactor temperature sensors and the analog output voltage to the heater driver circuits. The integral time, T_i, and derivative time, T_d, parameters have units of minutes. There are also two controls on this panel to limit the range of the voltage applied to the microreactor heaters. These limits are the unscaled voltages that the analog output board sends to the Heater Circuit Boards in the AIMS chassis. A gain of three is applied to this voltage on the Heater Circuit Board, so the actual voltage range applied to the microreactor heaters is this range multiplied by three.

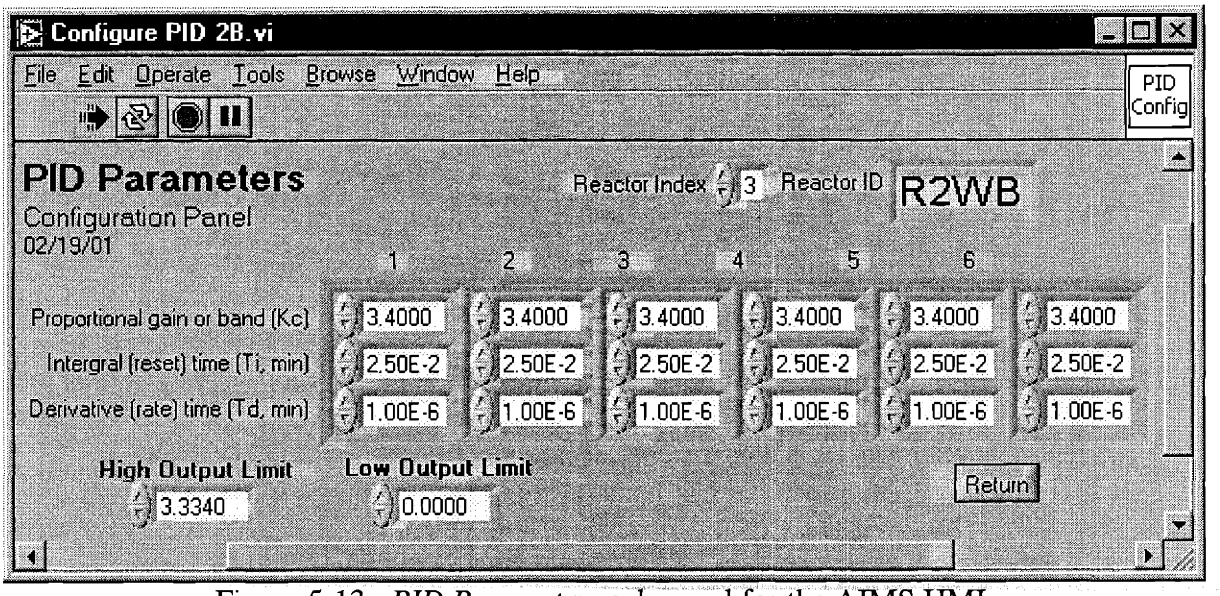

Figure 5-13. *PID Parameters* sub-panel for the AIMS HMI.

The product gas from the Reactor Boards then goes to a Valco 16 position multiposition sampling valve. The position of this valve can be monitored through the *Sampling* tab on the main control panel, shown in Figure 5-14. This panel only displays the current position of the multiposition sampling valve. To change the position the *Configure Sample Valve* button is pressed to open a sub-panel.

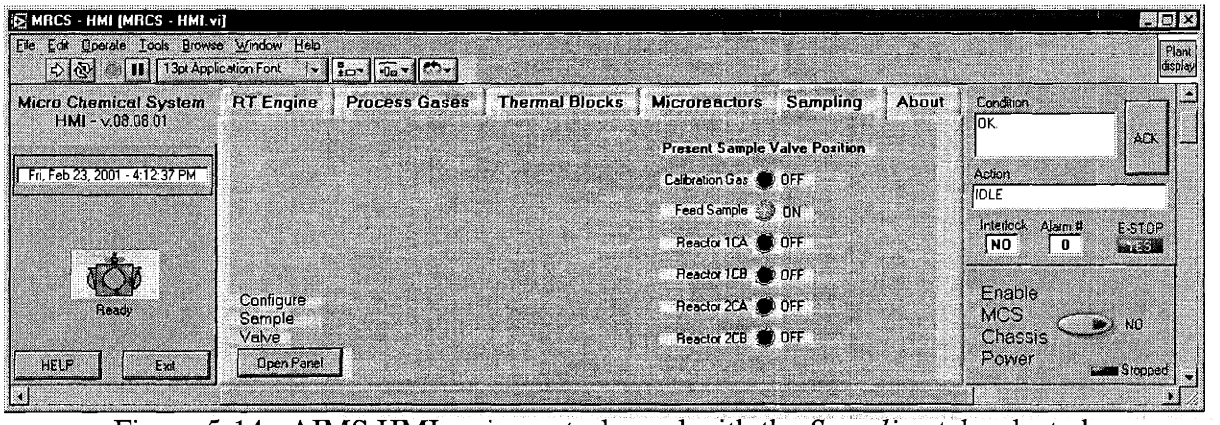

Figure 5-14. AIMS HMI main control panel with the *Sampling* tab selected.

The *Product Sampling Control* panel, shown in Figure 5-15, allows the operator to select between the four microreactor product streams, the feed sample stream, or a calibration gas stream[14]. Communications with the Valco multiposition valve was achieved through an RS232 connection between the HMI computer (COM port 2) and the valve controller. Fortunately, an ActiveX interface to this type of valve had been previously developed at DuPont, so there was no need to develop the serial communications link for the HMI. Instead, the ActiveX control was placed directly in the HMI G program, leaving only the user-interface features to develop.

[14] The calibration gas stream does not come from the AIMS. Instead, it is supplied directly to the sampling valve system from a separate gas flow manifold.

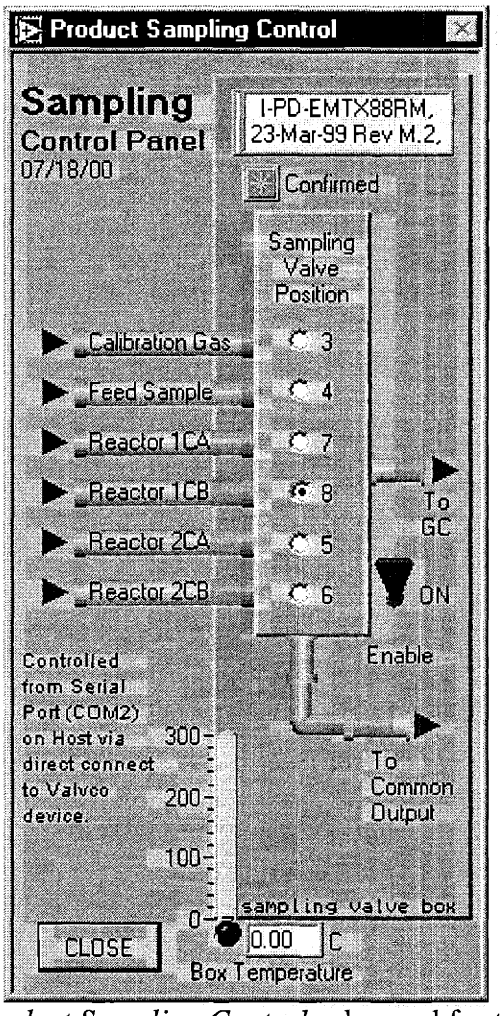

Figure 5-15. *Product Sampling Control* sub-panel for the AIMS HMI.

Testing Procedures

The control system hardware of the AIMS was tested with the AIMS hardware described in Chapter 4. The AIMS control program and HMI was developed during this testing period and was tested when the assembly of the AIMS and its control hardware was completed. Debugging and testing was an ongoing process that was performed simultaneously with the creation of the controller program and the HMI. The final software validation was done when actually running the AIMS with inert gases flowing through the system and later with reacting gases. Because of the complexity of these two programs,

debugging really occurred throughout the entire testing phase of the scale-up system. Modifications to the software were often made to add functionality and improve ease-of-use for the control program and HMI.

The performance of the HMI and controller program was carefully evaluated before testing began under reaction conditions. This meant examining all the components of both programs to verify that the system was behaving as expected. However, a rigorous mathematical analysis of the control program was not performed due to its complexity. In most cases, the problems found with the two programs usually involved the communication procedures between the HMI and the NI controller. For example, a common bug was the HMI failing to update the control program with new set points. The reasons for these types of errors were varied, but the communication procedures between the HMI and controller were performed at a lower level than is common with most industrial HMI software such as Wonderware[15] or WinCC[16].

The communications procedures were created so that their thread was isolated from the execution of the PID loops. The communications thread was set at a lower execution priority, so it would not disrupt the determinism of the main control loop. It was therefore possible to entirely choke the communications thread, if the main loop rate setting was too high. Rigorous performance tests revealed settings and code changes by which to balance between the required loop rate and the HMI's effectiveness in communicating with the controller. In fact, some of the code optimizations required to meet the project's design goals became suggestions for improving certain low-level functions of the vendor's software and

[15] Wonderware Corporation, 100 Technology Dr., Irvine, CA 92618, (949) 727-3200.
[16] Siemens Energy & Automation, Inc., 3333 Old Milton Parkway, Alpharetta, GA 30005, (800) 964-4114.

were actually implemented in their subsequent release. These challenges significantly increased the development time for the controller code and the HMI.

By the time testing under reaction conditions was begun, the performance of the two programs was well understood and all previously identified bugs were corrected. The only changes made after this point dealt with making the HMI more usable to aid in the testing of the system. However, the original version of the HMI was quite close to the final version, and this is a testament to the forethought that went into its development.

Testing Results

The majority of the HMI and PLC control program components worked as expected. However, a few items remained problematic throughout the testing. In some cases, the problem was probably due to electronics and not the software, but these are mentioned briefly as well. Difficulties with operating the Redwood SOV's and MFC's are not discussed here since this was done previously in Chapter 4.

The temperatures measured through the various RTD's in the system were almost always questionable. Although the values appeared accurate at certain times, they were definitely not accurate at other times. This was apparent since temperature readings in excess of 100°C were sometimes displayed even when no power was being applied to the corresponding heating cartridges. In general the temperature values measured by the RTD's read through the SCXI-1121 boards were almost always inaccurate. These values are displayed in the *Thermal Blocks* tab of the main control panel. Even in Figure 5-9, it is clear that at least two of the values cannot possibly be correct. The reason for the difficulty in getting accurate RTD readings is probably due to poor electrical connections inside the AIMS chassis. In particular, the connectors on the front system boards to the backplane are

likely a large part of the problem. It was noted during testing that removing a board and reinserting could dramatically improve or worsen one of the RTD values. The backplane connectors themselves are not completely at fault since the frequency of board removal and replacement in the AIMS was much higher than anticipated by the project team. In fact, most of the system boards were probably removed and replaced many hundreds of times throughout the project lifetime. This was always a tricky procedure and a good deal of care was needed to simply avoid damaging the pins on the backplane connecters. It is not difficult to believe that some of these connections were bad enough to have visible effects on system performance such as inaccuracy in RTD measurements.

It should be noted, that the RTD temperatures measured by the CAL controllers in the AIMS chassis were much better. Occasionally, a temperature measurement would be clearly inaccurate, but during most of the testing these values appeared accurate[17]. These controllers may have functioned better since there were not as many connections needed going from the Temperature Controller Board to the Reactor Boards. Thermocouples were not used for temperature measurements since the various metals used in the backplane and PCB would not have been compatible with their use. In this case, it would have been necessary to place a voltage amplifier on the thermal couple signals so that their signals could have been measured as an analog input. This would be a good way to avoid this problem in future systems. It would also be beneficial to use more robust connectors from the boards to the backplane since poor connections probably contributed to this problem. Both of these solutions required too much reworking to be implemented in this project—especially

[17] Although difficult to verify by probing directly, other indicators such as the power output by the controllers to maintain a set point temperature could be monitored to infer actual temperature.

considering that the only real benefit would have been improved temperature readings on the HMI (the CAL controllers usually worked properly during testing).

The CAL controllers did have some other operational problems. In particular, the OPC connection to the HMI was not very good. It was often difficult to initiate communication with the CAL controllers and errors were sometimes transmitted to them (set points would be changed to incorrect values or other controller parameters would be unintentionally altered). A substantial amount of time was spent trying to debug these communications problems by adjusting parameters on the controllers and the RS232/485 converter. Unfortunately, it was not possible to resolve all the problems completely. The difficulty probably was due to the converter used, but poor connections in the serial links could have also been to blame. Electrical noise should not have been a problem since RS485 communications usually works well in these types of environments. Because of these problems, it was preferred to make changes to the CAL controllers directly without using the HMI.

During testing, various values for the control loop rate were used to evaluate the ability of the system to maintain real-time while performing PID temperature control on the microreactor heaters. It was found that the control loop could successfully operate at 500 Hz with all 24 microreactor heaters being under closed loop PID control. At faster rates, the processor did not have time to complete the TCP/IP communications with the HMI, resulting in data loss. The PID algorithm did appear to be adequate in maintaining microreactor temperature control. Somewhat conservative parameters were used because of the noise in the temperature measurement signal, but the temperature was maintained stably at its set point under a wide variety of conditions (including reaction). The dynamics of the closed

loop control algorithm were not explored since the rate of data logging, 4 Hz, was not fast enough to do these types of evaluations. This would be possible with program modifications, but this was not the emphasis of this project.

Conclusions

Development of the AIMS control program and HMI presented unexpected challenges, with the result being a very sophisticated system that went well beyond the project teams experience in industrial automation systems. The high-speed loop rate required, the number of process variables being monitored, the management of safety interlocks, and usability requirements all contributed to increasing the systems complexity. Moreover, some design goals for the system tested the advertised capabilities of the control tools used. Unfortunately, this resulted in a corresponding increase in development time.

Nonetheless, the team was successful in assembling the control hardware and providing the necessary programming to operate the AIMS. Similarly, the HMI developed allowed the AIMS to be operated easily and intuitively. Obstacles that would have prevented the safe operation of the system were overcome. The few problems that were not solved really had minimal effect on the ability to use the system and did not detract at all from its safety. Perhaps, most impressive was the ability of the controller to perform closed loop PID control on 24 microreactor heaters at a rate of 500 Hz. Although this type of loop rate is achievable in specialized control systems, this rate of control for hardware costing less than $20,000 total is remarkable.

CHAPTER 6
PROCESS SAFETY

The construction and testing of the scale-up microreactor system followed the Process Safety Management (PSM) guidelines of DuPont for their Wilmington, Delaware facilities[1]. These guidelines are extensively detailed in the Wilmington Area SHE (Safety, Health, and the Environment) Manuals. These manuals have been issued to maintain safety standards throughout all DuPont facilities. Besides procedures used for auditing safety and environmental aspects of new processes, these manuals also contain detailed guidelines on common laboratory practices (for example, safe transportation of compressed gas cylinders). In general the AIMS was designed and tested to minimize the possibility of any safety incidents. This included the release of unacceptable levels of toxic gases, explosions, and deflagrations. Electrical hazards were also considered in system design due to the extensive power network in the AIMS.

To determine the level of safety audit needed for the AIMS, the DuPont Hazards Analysis Roadmap was consulted. Because the system was not to be left unattended during operation, a Research Safety Review (RSR) was deemed adequate by the research managers involved with the project. The RSR required the documentation of all process safety hazards using the RSR Checklist as a guideline. A separate document, a Process Hazards Analysis (PHA), was prepared to address in detail items requiring documentation in the RSR Checklist. The PHA for the AIMS can be found in the Appendix. In addition, an Equipment Safety Audit (ESA) was also completed as required by DuPont PSM guidelines.

The committee members for the RSR were given the process safety documentation one week prior to the RSR meeting. This meeting was scheduled well before construction of the AIMS was completed to allow for changes that may have been required by the committee. During the meeting, safety items relating to the construction and operation of the AIMS were reviewed in detail. Any items that required further action after the meeting were addressed before the system was placed in operation. A copy of all the PSM documents for the AIMS was submitted to the DuPont CR&D Safety Office. A final safety audit was performed before system testing started, and the Personal Protective Equipment (PPE) certification was approved by the research manager responsible for the project.

Process Hazards

The major hazards associated with the AIMS were feed and product flammability, chemical exposure, and high temperature. The risk of fire in the system was reduced by the use of diluted feed streams that did not allow the formation of flammable mixtures in the system. In addition, system interlocks prevented the uncontrolled release of process gases in the event of an incident. These interlocks also minimized the risk of exposure of the system operators to process gases. In addition, the process was entirely contained in a fume hood, so following the system Standard Operating Procedures (SOP's) helped prevent such exposure. The risk of injury due to high temperatures in and around the system was also be minimized by closely following the system SOP's during operation and system maintenance. A detailed description of all the process hazards is presented in the Appendix, which also contains the AIMS SOP's. These hazards are discussed briefly in the remainder of this section.

---

[1] These guidelines are specifically addressed in DuPont Corporate SHE Standard: S21A.

Process Gas Flammability

The potential for fire or explosion was present in the AIMS due to the use of flammable feed gases and oxygen in the system. To avoid fires caused by the reaction of oxygen inside the system, special care was taken to ensure all the lines used were oxygen clean. That is machined parts, tubing, and other components were solvent cleaned to remove residual oil by personnel at DuPont, ENSER Corporation, or the OEM. The flammable gases used for microreactor testing were ammonia and methane. Table 6-1 lists the flammability and physical characteristics for the reactants and principle reaction products.

Table 6-1. Physical and Flammability Properties of AIMS Process Gases.

Component	Lower Flammability Limit in Air (Volume %)	Upper Flammability Limit in Air (Volume %)	Autoignition Temperature (°C)	Flash Point (°C)	Melting Point (°C)	Boiling Point (°C)
O_2	-	-	-	-	-218	-183
N_2	-	-	-	-	-210.0	-195.9
H_2O	-	-	-	-	0.0	100.0
CO	12.5	74.0	609	-191	-205.1	-191.5
CO_2	-	-	-	-	-	-79[2]
NH_3	16	28	651	11	-77.7	-33.3
NO	-	-	-	-	-164	-151.7
N_2O	-	-	-	-	-90.9	-88.6
CH_4	5	15	537	-187.7	-182.5	-161.5
H_2	4.0	75	500	?[3]	-259.2	-252.8

During normal operation, there should never have been an explosive mixture of fuel and oxygen in any of the process lines or components. The NI control system was programmed to monitor the flow rates of fuel and oxygen used to form the feed mixture. Furthermore, an interlock was in place if the feed mixture comes to within 1.0% of the flammability limit. This interlock caused a shutdown of the process and the purging of all process lines with inert gas.

[2] Sublimation point.

For the case of methane, flammability data for methane, oxygen, and nitrogen mixtures indicates that flammable compositions of methane do not occur with less than 12.8% oxygen in a variety of geometric configurations. However, flammable compositions can be formed with as little as 5.3% methane[1]. Thus, it is better to keep the oxygen concentration below 12.8% and vary the methane concentration to achieve the appropriate ratio of methane to oxygen.

Less information is available about the flammability of ammonia than for methane. The literature indicates that the lower flammability limit for ammonia and air mixtures is 16% ammonia. The lower limit for a mixture of ammonia with pure oxygen is 14.8%[1]. The compositions used for testing purposes generally contained considerable amounts of inerts, but the 14.8% flammability limit was used to add an additional margin for safety.

In the event, that an explosive composition was reached during operation, the small volumes associated with the reactors, valves, and transfer lines, minimized the potential for injury to personnel or environmental impact. The entire system gas volume inside the chassis was 3.4 cm^3. As a worst case scenario during operation, assume that a stoichiometric composition of methane and oxygen was present in all of the gas lines. Further, assume that the system was pressurized to 150 psig (well above the point at which the pressure relief devices will activate). If this entire volume of gas undergoes complete combustion, it would have released the equivalent energy of 0.00023 lbs of TNT[4]. Thus, the only explosion hazard presented by this system was the accumulation of flammable mixtures outside the system tubing.

---

[3] This information could not be found, but is assumed to be much less than –100°C.
[4] This calculation also assumes the gas is at 20°C and uses a value of 490 kcal/lb of TNT.

This accumulation was unlikely since the chassis's two fans move approximately 180 cfm of air through the system. This corresponded to over 95 complete air changes every minute[2]. The most likely area of gas escape was above the microreactor after a membrane failure. In this case, the control system should have interlocked and shutoff the flow of combustible gas to that reaction channel. The flammable gas that does escape would have been immediately diluted by air flowing over the microreactor at an estimated rate of 120 ft/min[2].

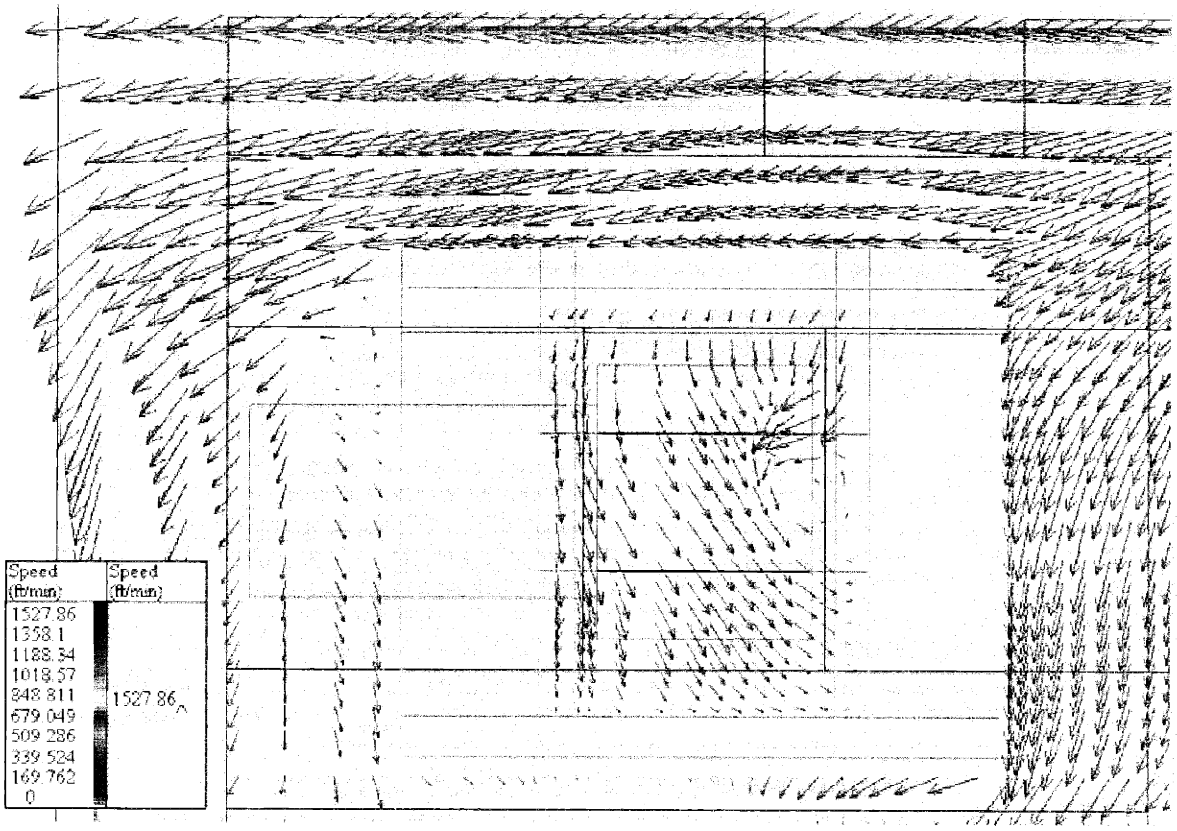

Figure 6-1. Flow profile above and around a DieMate™ socket in the AIMS[2].

The flow profile of air over the microreactor is shown in Figure 6-1. The area in white in the figure is the walls of the DieMate® socket. This simulation also shows that there

is a recirculation zone above the reactor with an airflow rate as low as 20 ft/min[2]. Nonetheless, this should have been sufficient to dilute any escaping gas.

Process Gas Toxicity

All of the process gases were handled in ventilated enclosures and cylinder storage was done in ventilated cylinder closets. Ammonia was the most toxic gas routinely used in testing, but its odor is easy to detect before it presents a significant hazard. Pressure relief valves and gas regulators were inspected regularly according to DuPont safety standards. The SOP's in the Appendix describe the procedures used to prevent the exposure of the operator to gases.

High Process Temperatures

Certain areas inside and around the AIMS were heated during testing, so there was the possibility of burn injuries. This risk was minimized by wrapping heated items outside of the chassis with fiberglass insulating tape to reduce the surface temperature to acceptable levels. This prevented unintentional contact with heated surfaces from harming operators. To prevent burns from occurring during system maintenance detailed procedures were developed for performing these tasks. The SOP's in the Appendix give the procedures used during system testing.

Permitting

Because of the small scale of the AIMS, extensive permitting with the state of Delaware was not needed for its operation. However, a hood emissions permit was applied for under Delaware Air Emission Regulation II, Sec. 3.1-i, governing hood emissions less than 0.2 lbs./day. The permit, APC-92/0436-O, was issued on March 6, 2000.

AIMS Safety Features

The AIMS was designed to fail to a safe state. System faults were normally handled by the National Instruments controller. Note that LabVIEW for this controller was running under Pharlap, a deterministic operating system. Thus, the reliability problems of LabVIEW running under Windows NT or Windows 95 were not present in this system. In addition, a Brentek[5] model P8-WDT24/PLC watchdog timer was in place to detect any failure in the NI control system. The watchdog timer requires a signal from the controller every second or a relay breaks the power to the system chassis.

Under normal operating conditions, the NI controller monitors for process faults and takes corrective action upon identification. The system will override operator commands issued at the HMI during a safety interlock. The unsafe conditions that cause interlocks are

- The feed gas composition entering the explosive regime
- Failure of a microreactor.
- An over-temperature of a heated part or the sampling valve oven.
- An under-temperature of a heated part or the sampling valve oven.
- Fume hood exhaust failure.
- Failure of one of the two CompactPCI chassis exhaust fans.
- Power failure.
- Controller timeout detected by the watchdog timer.

Most of the system interlocks are handled by the embedded NI controller. This is similar to other laboratory systems operating at DuPont except the Siemens 545 PLC's have been replaced with the National Instruments system. The NI controller monitors the status of the AIMS process variables and takes appropriate action if any interlock conditions are found. In addition to these interlocks, the external heater controllers that are used for the

[5] Brentek International, Inc., Ridgewood Rd., York, PA 17402, (717) 755-8000.

system heating tapes and sampling valve box have hardwired over temperature interlocks built-in to these controllers. However, these interlocks only shutoff power to the affected heating device, so the NI controller must still take action to shutdown the rest of the process.

Power failure is considered a system interlock, but the NI controller cannot take any active measures to return to a safe state. Instead the system was designed, so that in the case of a power failure, the system shuts down by relieving any pressure in the process lines. However, the process lines are not purged with an inert gas when this occurs. Thus, any time system maintenance was performed (such as replacing a microreactor), it was necessary to purge all the process lines with an inert gas. Ideally a combination of normally open and normally closed valves would have made it possible to have the system automatically purge with an inert gas during power failure. Unfortunately, the Redwood MicroSystems SOV's were not available in a normally open configuration, so this was not possible. However, an external normally open valve was placed on the reactor feed line to vent excess pressure in the system during a power failure.

Similarly, the hood status was monitored by a discrete contact closure that was tied into the power circuits of the hood. Thus a failure of the hood exhaust effectively caused a system interlock by removing power to the AIMS (The NI controller was not plugged into one of the affected circuits, so it remained operational. Nonetheless, without power in the AIMS it could not take further action with the system.)

Conclusions

The safety features and hazards of the AIMS were briefly discussed in this chapter. More detail can be found in the Appendix, which contains the PHA and SOP's developed for the AIMS. In addition to the PHA, an ESA and the RSR Checklist was completed for the

AIMS. They have not been included as appendices due to their proprietary nature. In any case, these documents reiterate the items discussed in the PHA. Further information on the safety precautions used for common laboratory procedures can be found in the DuPont Corporate SHE Standards.

References

1. Coward, H.F. and Jones, G.W. (1952) *Limits of Flammability of Gases and Vapors*, United States Government Printing Office, Washington, D.C.

2. Heck, M. and Manning, A. (2000) "Flotherm analysis and modeling of airflow patterns and temperature distributation in the Kaperel card cage", Flomerics, Inc., Marlborough, MA, Report #USE0400-11.

CHAPTER 7
EXPERIMENTAL METHODS

After the construction of the AIMS was completed, the system performance was evaluated using methane oxidation and ammonia oxidation as the test reactions. Since these reactions have previously been demonstrated in microreactors, the purpose of this testing was not to identify new reaction behavior. Instead, the goal was to assess the functionality of the AIMS in comparison to other laboratory reactor systems currently being used at DuPont. For example, both the MARS II and MARS III are reactor test stations whose design is similar to the AIMS. By showing that the AIMS produced data that compared favorably to the MARS, a first step in the miniaturization of complex reactor systems would be achieved. To accomplish this, it was necessary to demonstrate that the MEMS components could effectively control gas flow and other reaction variables in the system as well as provide the same level of safety management designed into conventional equipment. The ability of the microreactor to operate according to the standards of conventional laboratory tube reactors was not examined since the membrane microreactor design did not resemble a plug flow reactor in its operation. However, the membrane microreactor did have unique features not available in traditional tube reactors, such as the ability to control the catalyst temperature in the reaction zone over a length scale on the order of 1 mm or less.

Comparison to conventional reactor system operation is discussed here by describing the procedure followed during a normal run of the AIMS. This discussion is less detailed than the system Standard Operating Procedures (SOP's), but focuses more on experimental

protocol. After this, a description of the GC analysis methods used is given. Finally, the methods used to extract information from the raw GC data are discussed.

Experimental Protocol

Record keeping for the AIMS testing was done with the Electronic Laboratory Notebook (ELN) system in place at DuPont during this period. ELN was accessed using Lotus[1] Notes v. 4.5.2b. ELN is a proprietary Notes database developed by DuPont for electronic record keeping of laboratory notes.

The procedure for conducting a reaction experiment with the AIMS can be broken down into the following steps: 1) replacing the microreactors in the Reactor Boards; 2) leak checking the tubing connections; 3) calibrating the AIMS' MFC's; 4) setting up the GC for testing; 5) analyzing the reactor feed gas; 6) analyzing the product gas from the unheated microreactors; 7) conducting the reaction experiment; and 8) shutting down the system by purging with inert gas. The first step in preparing the AIMS for a run was the installation of new microreactors into the two Reactor Boards. This was done by first purging the system lines with an inert gas to eliminate the possibility of an explosion or toxic gas exposure. External piping to the system was disconnected by first removing the heat tracing and then breaking the Valco fitting connections on the front of the Reactor Boards. These boards were then removed from the system with the Heater Circuit Boards since the ribbon cable connecting the two boards made it impossible to remove the boards individually. The microreactors that were in the Reactor Boards from the previous experiment were carefully removed by loosening the socket head cap screws on the DieMate™ manifold and then pressing on the top of the DieMate™ socket to release the contact pins of the socket. The

Kalrez™ o-rings on the DieMate™ manifold were examined to ensure that they were in good condition and seated properly. A new microreactor was inserted into the DieMate™ by again pressing on the top of the socket to clear the pins for the microreactor. The socket head cap screws of the DieMate™ manifold were then carefully tightened to provide a sealing force for the Kalrez™ o-rings. This last step was the most difficult since if the screws were too loose, there would not be a good seal. If the screws were over-tightened, the microreactor would crack in half, which happened on a number of occasions. The Reactor Boards and the Heater Circuit Boards were then replaced in the system chassis by reversing the procedure described above.

As the final mechanical preparation step, the external piping to the Reactor Boards and the product sampling system was replaced along with the heat tracing. After this step, the AIMS appeared as shown in Figure 7-1. The piping leading from the Reactor Boards to the sampling valve box is clearly visible due to the heat tracing. The untraced lines leading from the Feed Gas Mixing Board to the external pressure controller and normally open two-way valve are also visible (these lines are ultimately connected with the two Reactor Boards).

The fittings that were disconnected and reassembled during the microreactor replacements were leak-checked using the Gow-Mac model 21-250 gas leak detector described previously (a local helium cylinder was used as the supply gas during this test). However, it was not possible to check the o-ring seals between the microreactors and the DieMate™ manifolds using this device because there was no way to access this area with the leak detector tip when the boards were inserted into the system (The normally closed Shut-Off Valves (SOV's) prevented the testing of the seals when the boards were not powered).

---

[1] Lotus Development Corporation, 55 Cambridge Parkway, Cambridge, MA 02142, (617)

To test these seals, power was applied to the system and the helium gas supply used in the previous step was used to introduce a controlled flow of gas through the microreactors. A Humonics[2] model ADM1000 flowmeter was used to measure the flow coming from the microreactors at the product gas exits of the Reactor Boards for different MFC set points (ranging from 3 to 11 ml/min). This method would not detect the smallest leaks (less than 1 ml/min), but previous experience with mounting the microreactors suggested that the seal either did not leak at all or it leaked substantially (greater than 5 ml/min).

The product transfer lines leading from the Reactor Boards to the sampling valve box and then to the GC were all heat-traced with Amptek[3] ½ inch wide heating tapes obtained from Technical Industrial Products. The lengths of the heating tapes varied from 2 ft to 8 ft, but they all had a watt density of 8.67 W/in^2. The heating tapes and transfer lines were wrapped with Flextex[4] fiberglass insulating tape. The purpose of this insulation was to improve thermal uniformity of the lines and to prevent accidental burns that might occur by touching them. A dual-tipped Type J thermocouple was inserted at one location for each of the heating tapes. Two CAL 3200 temperature controllers were used to monitor and control the temperature for each of the heating tapes. DuPont safety standards required using one for control and the other to monitor for an overtemperature excursion. A total of three control loops were needed for the heating tapes used in testing.

577-8500.
[2] Humonics has since been acquired by Agilent Technologies.
[3] Amptek Company, P.O. Box 1381, Stafford, TX 77497, (281) 340-9800.
[4] Flextex, 162 Keystone Dr., Montgomeryville, PA 18936, (215) 646-1318.

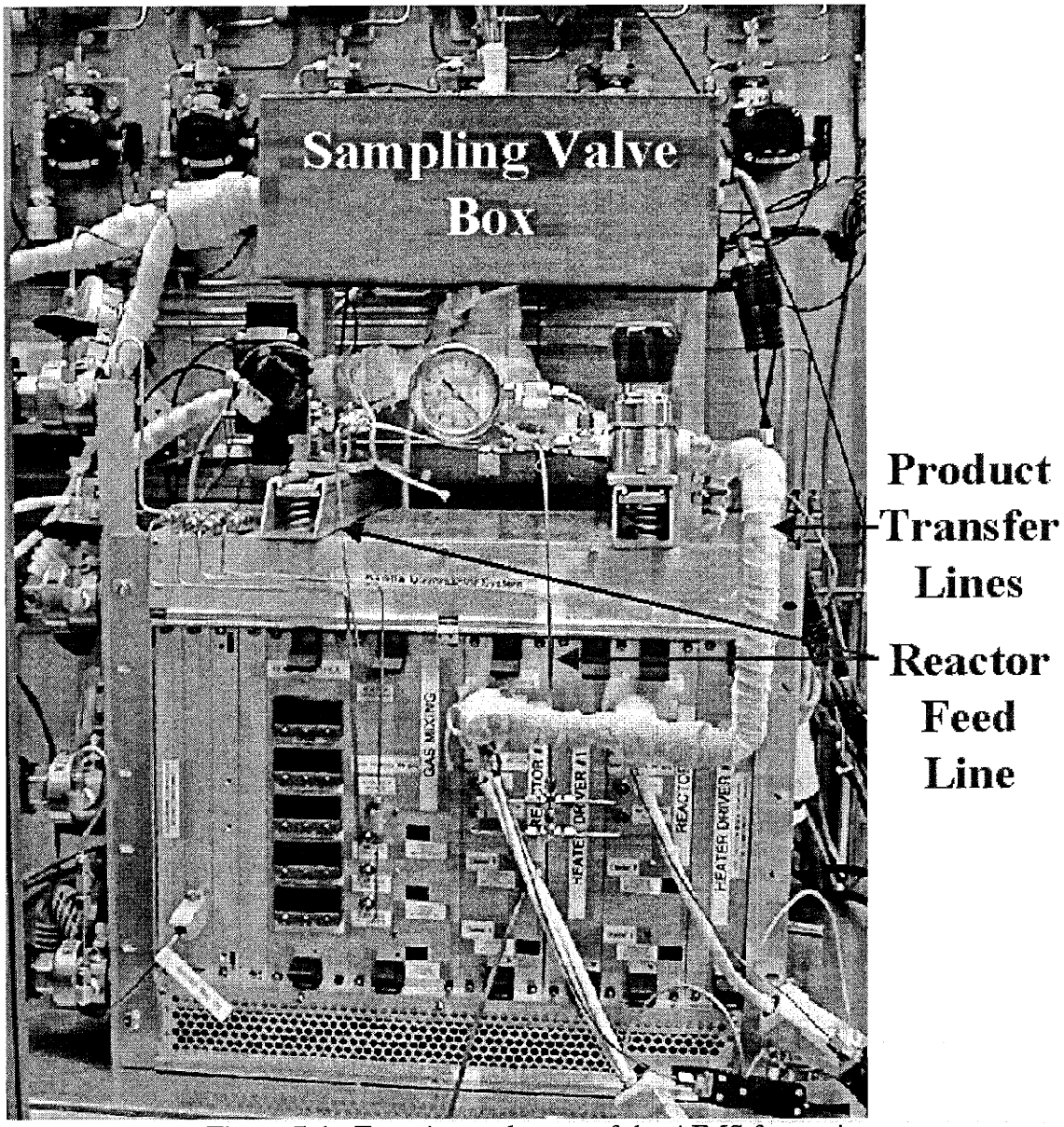

Figure 7-1. Experimental setup of the AIMS for testing.

Because of the bulky Valco union fittings on the front of the Reactor Boards, a separate heating method was developed since these components had substantially more thermal mass than the 1/16 in. transfer lines. A cylindrical aluminum block was fabricated as shown in Figure 7-2 with two holes machined for the two Valco unions (the block extended the entire length of the union fitting). In addition, two 1/8 in. holes were machined for two

1½ in. long heating cartridges. A 1/16 in. well was added for a dual-tipped Type J thermocouple. The cartridges were wired in parallel and control was provided using two CAL 3200 temperature controllers (one for control, one for overtemperature).

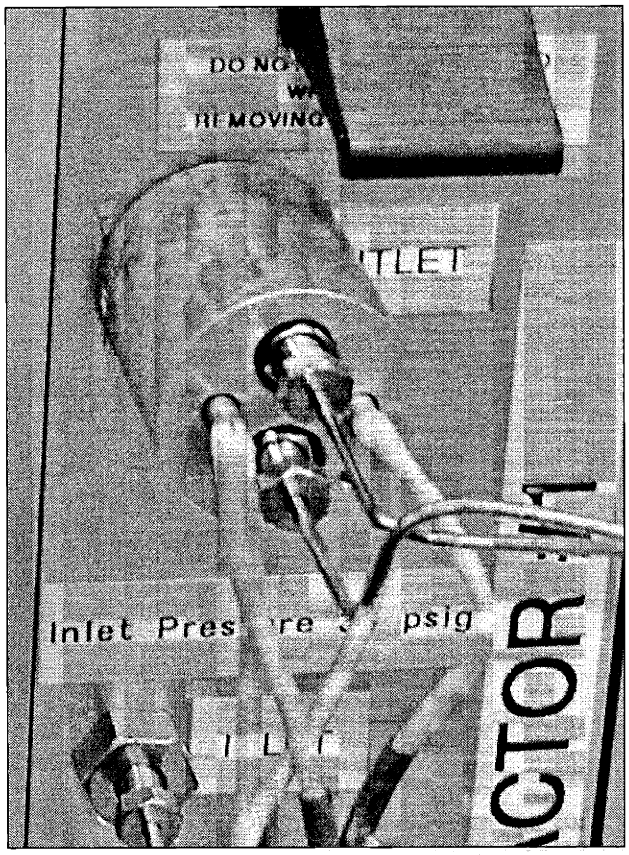

Figure 7-2. Reactor Board product line heater.

The replacement of microreactors in the AIMS was comparable to the amount of effort required to replace a reactor in one of the MARS. For the MARS units, a significant amount of time was spent disconnecting the reactors from the system, disposing of spent catalyst, cleaning the reactors, filling the reactors with fresh catalyst, and reconnecting the disassembled piping in the system. Some heat tracing also had to be removed and replaced during this process. In some cases, it took a technician an entire workday to complete this process. The installation of the reactor tube into the reactor oven was the most critical part of

the task since leaks would often develop at these fittings because of the thermal cycling they went through. The best practice was to leak check the seals around the reactors before they were replaced into the system piping.

Before the DieMate™ manifold heaters were activated, a temperature vs. power curve was measured for each of the microreactor heaters on the four microreactor channels. This was done to determine the reference temperature resistance of each of the temperature sensors (from the unpowered measurement) and to test the functionality of the microreactor heaters and temperature sensors. The temperature vs. power curve was well-characterized by the large number of microreactors studied. By examining this curve, it was possible to discover flaws in the heaters or temperature sensors, which included temperature measurement inaccuracy caused by previous runs of the microreactor at temperatures greater than 500°C. This step is not comparable to any procedure done in conventional reactors since the reactor oven is not usually integrated so completely into the reactor.

After the microreactors were replaced and the system piping reconnected, the Redwood MFC's used during the next run were recalibrated. Although conventional laboratory MFC's are somewhat stable in their performance from day-to-day, the Redwood MFC's were unproven. For this reason, MFC calibrations were performed before every experiment. In any case, for both micro and macro systems, the reactor line MFC's had to be recalibrated for each run since the gas composition affected the MFC calibration.

The first step in the MFC calibration procedure was to isolate the desired MFC from the rest of the system. For example, to calibrate the fuel gas MFC on the Feed Gas Mixing Board, the SOV's on the other Redwood Flow Manifolds on that board (oxygen and diluent) would all be closed to isolate them. The flowmeter was then attached to the appropriate gas

vent coming from the sampling valve box with the multiposition valve set to sample the feed gas. Between eight and twelve data points were typically taken for a MFC calibration, depending on the behavior of the MFC and the flow range being used during the next experiment. At each data point, a set point was given to the MFC as an unscaled voltage signal using the HMI. The actual gas flow rate was recorded using the Humonics flowmeter described previously. The measured MFC flow rate displayed on the HMI as an unscaled voltage was also recorded. The ambient temperature was recorded during this calibration since the Redwood MFC's were known from prior experience to have thermal drift. The calibration curve was produced by plotting actual volumetric gas flow rate versus the MFC output voltage.

MFC calibration on conventional reactor systems is very similar. For example, one HMI required the operator to enter ten data points to generate the MFC calibration curve. Calibration was also done frequently to improve experimental accuracy, but conventional MFC's generally did not require as much care to generate these curves. These MFC's also operated somewhat differently in that a forward pressure regulator was placed upstream of the MFC and a back pressure regulator was placed downstream so a constant pressure drop could be maintained across the MFC. This helped to improve the stability of the MFC. Similar pressure adjustments are made in the AIMS with the external forward and back pressure regulators. However, the Redwood MFC's were designed to operate at only specified inlet and outlet pressures. Specifically, the internal tuning parameters in these MFC's were adjusted for given gases and the operating upstream and downstream pressures. Deviating from these design specifications could and did cause the flow control to degrade substantially. For example, the flow rate could oscillate over a large range of flow rates.

After the flow controllers on the Feed Gas Mixing Board were calibrated, these MFC's were set to produce the desired reactor feed gas composition using the HMI. After the feed gas composition had stabilized, the Reactor Board MFC's were calibrated. The calibration procedure for these MFC's was the same as the one followed for the Feed Gas Mixing Board MFC's. The desired flow rates for each of the microreactors was then set at this point, but this could be changed as desired during the experiment. This calibration step was also needed in conventional laboratory reactor systems since the feed gas composition generally changed from run to run.

Before the microreactor heaters were enabled on the HMI, multiple GC shots of the reactor feed gas were taken to determine the actual composition of the feed gas. The feed gas injections were taken by selecting the feed gas vent coming from the external back pressure regulator on the Valco multiposition valve. This analysis period was also used to make any adjustments to the GC method that were needed. Specifically, the column compensation data was set during this period and its quality was examined through the feed shots and by taking blank shots. The column compensation feature was used to improve the signal baseline during oven temperature programs. More detail on the GC method used can be found in the following section.

After determining the feed gas composition, injections of the microreactor product gas were taken with the heaters still disabled. The catalyst was not heated with the microheaters and was only heated by the heating cartridges in the DieMate™ manifold. The catalyst temperature at this point was approximately 100°C[5] as measured by the microreactor temperature sensors. This was done to measure any reaction that was occurring at this

[5] The DieMate manifold temperature was set around 175°C

temperature and to ensure that the feed gas going to the reactors had the same composition as previously measured. This was an effective way of checking for leaks in the system since changes in composition usually indicated leaks.

Reaction testing was initiated by enabling the microreactor heaters and setting the heaters either in manual or automatic control mode. In the manual control mode, the operator set the microreactor heater voltages. While in the automatic control mode, the operator set the desired microreactor heater temperature. GC product shots of the four reactor channels were taken to determine product gas composition. Since the reactors could be operated independently, sometimes all four were running and at other times only one was running.

The GC analysis time was the limiting step in the data collection process. The microreactor heaters reached equilibrium extremely quickly (on the order of 10 milliseconds), so transient product data was not be observed by the GC. Further limiting the maximum testing speed of the system was the tubing volume between the microreactor exit and the multiposition valve. This took less than one minute to thoroughly sweep at the feed flow rates used in testing. In most experiments, the flow rates going to the microreactors were unchanged, but the temperature of the microreactor heaters were varied. Since the GC analysis required about 15 mins/cycle, only five to ten different temperature settings were explored in a single run. During the longer runs, additional reactor feed gas injections were taken to determine if variation in the feed gas composition had occurred.

At the end of a run, the microreactor channels were purged with nitrogen or helium (depending on the purge gas connected to the system at the time) and additional GC injections of feed gas were taken. During a few runs, a microreactor failed through

membrane rupture or the heaters becoming inactive. At this point, the microreactor channel was purged for one minute and that line was isolated from the rest of the system by closing its SOV's. After the additional feed gas injections were completed, the system was shut-down by purging all the lines with inert and removing power from the chassis. The heated components outside of the AIMS chassis were also turned off except for the sampling valve box to avoid thermal cycling of these valves, which could create leaks between the valve rotor and seal.

The experimental procedures followed in the operation of the AIMS after startup were taken directly from procedures previously in place to operate the MARS units at DuPont. The analysis of feed and product gas composition was essentially the same with the GC analysis techniques also borrowed from the MARS. The MARS units did allow unattended automated testing, so they could be used effectively to perform long-term catalyst life studies as well. The automation to do this was in place with the AIMS, but the uncertainties in using this system did not allow for unattended operation. Future work could consider the development of a methodology for long-term (greater than 500 hours) of unattended operation.

GC Method

The GC techniques used for analyzing the AIMS product and feed gas were taken directly from methods developed at DuPont for use with the MARS units[1-4]. Although the temperature program and columns used for methane and ammonia oxidation were chosen for the products of these reactions, the physical setup of the sampling system was the same. The gas chromatograph used was an Agilent[6] HP 5890 Series II Plus. Data collection was done

[6] Agilent Technologies, 395 Page Mill Rd., Palo Alto, CA 94303, (650) 752-5000.

with Agilents' GC ChemStation software revision A.06.03. Although ChemStation is in-use at DuPont, the MARS units typically used more traditional Laboratory Information Management Systems (LIMS) for GC data management.

Gas sampling of the product and feed gas streams was performed using three Valco gas sampling valves located in a heated valve box, which are shown in Figure 7-3. The following figure, Figure 7-4, shows a schematic of the flow path through the sampling system. All of the AIMS transfer lines first enter at the 16-position Valco multiposition valve (located in the center of the box). This valve was actuated using a Valco microelectric actuator. As discussed previously, the stream was selected through the HMI. A 16-position valve was used since these had the fastest switch times available of the Valco multiposition valves (this was to avoid dead-heading the reactor streams during valve switching and possibly causing the membrane to rupture).

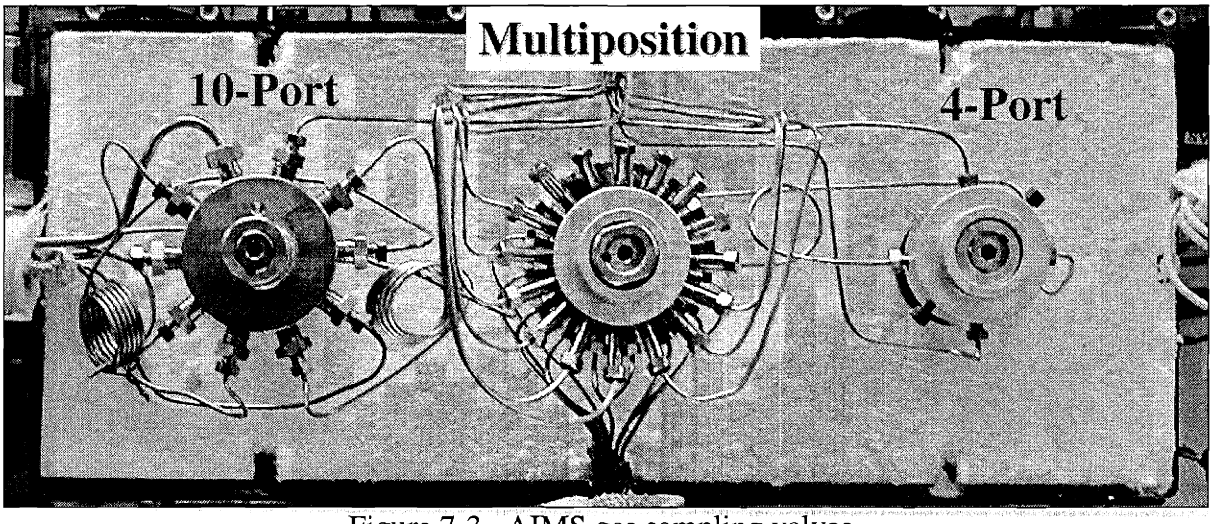

Figure 7-3. AIMS gas sampling valves.

The gas stream that is selected by the multiposition valve flows to the 4-port valve, which is shown at the right in Figure 7-4. The unselected gas streams each have individual

outlets that are vented just above the sampling valve box (these lines are not shown in Figure 7-4). The 4-port valve is used to allow the gas sampling loops to equilibrate to atmospheric pressure after the loops are filled. This acts to stabilize the molar volume of gas injected. When the valve is in the position shown in Figure 7-4, the gas stream from the multiposition valve flows through to the 10-port valve. When the valve is switched, the gas stream from the multiposition valve goes to vent. The line connecting the 4-port to the 10-port is also connected to vent, allowing the sampling loops to equilibrate in pressure (if the 10-port is in the position shown in Figure 7-4).

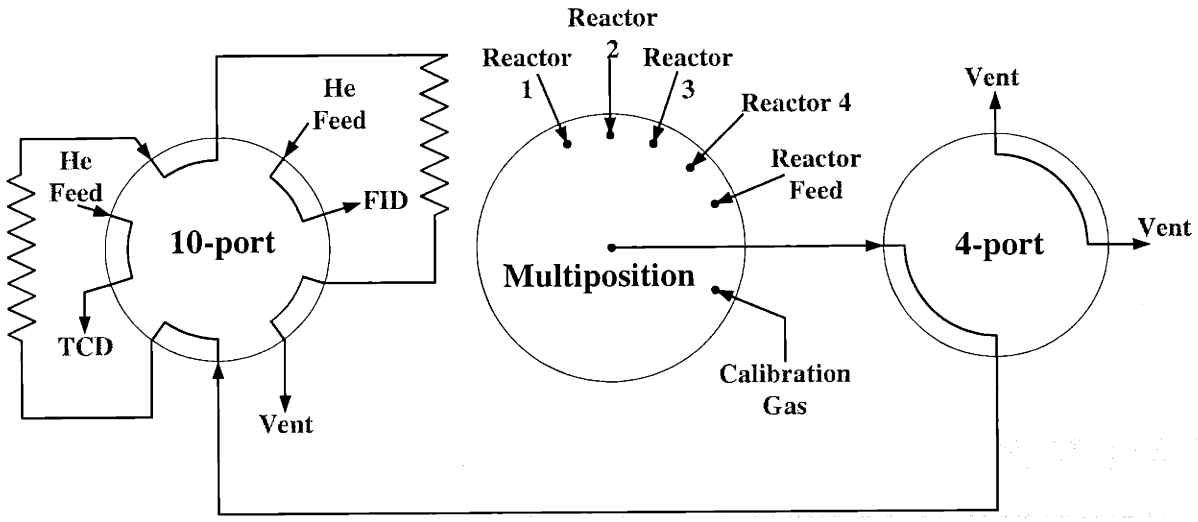

Figure 7-4. Schematic of the gas sampling valve flow configuration.

The 10-port valve (located at the left) was used to fill and inject sample to the two GC injection ports. Two sampling loops obtained from Valco, each having a volume of 250 μL, were used to control the amount of sample injected. When the 10-port was in the position shown in Figure 7-4, both of the sampling loops were being filled with the gas selected from the multiposition valve, or the sampling loops were being equalized in pressure (depending on the position of the 4-port). When the 10-port valve was switched, the helium supply that

was normally going to the GC injection ports was diverted to sweep the sampling loops and inject their contents into their respective columns. During this time, the gas line coming from the 4-port valve was connected to vent.

The GC line with the Flame Ionization Detector (FID) was a capillary column with a split/splitless injector. The column used was a Restek[7] Rtx-1701 with a film thickness of 3 μm, which was 30 m long and 0.53 mm ID. The injector temperature was kept at 230°C, and the detector temperature was kept at 250°C. The column flow rate was set to 10 ml/min of helium (oven temperature compensation was used to maintain constant volumetric flow). Because FID's do not respond to any of the inorganic products of the ammonia oxidation or methane oxidation reactions, this column was mainly used to help identify impurities present in the feed gases.

The GC line with the Thermal Conductivity Detector (TCD) was used for a packed column analysis with a purged packed injector. There were actually two columns used in series for this detector—a polar phase column and a molecular sieve column. Because the molecular sieve column retained or irreversibly adsorbed extremely polar or large molecules, it was necessary to bypass this column for the species retained on the polar phase packed column. Figure 7-5 shows a schematic of the arrangement used during testing.

In the setup used, the entire injection was first introduced into a polar liquid phase column. For the methane oxidation studies, a 316 SS Supelco[8] column, 8 ft × 1/8 in OD, packed with 80/100 mesh Hayesep R was used. For the ammonia oxidation studies, a 316 SS Restek column, 6 ft × 1/8 in, packed with 80/100 mesh Hayesep C was used for the first experiments, and a custom packed 316 SS Hayesep T column, 4 ft × 1/8 in, was used for the

[7] Restek Corporation, 110 Benner Circle, Bellefonte, PA 16823-8812, (800) 356-1688.

later experiments. The mesh size for the Hayesep T packing was 60/80. This packing was pretreated with a 5% KOH solution to reduced the adsorption of ammonia and improve the peak shape. This column was provided by Constantin Milionis of DuPont CR&D. For all the experiments, a volumetric flow-rate of 30 ml/min of carrier gas was set to flow through the columns at ambient temperature[9].

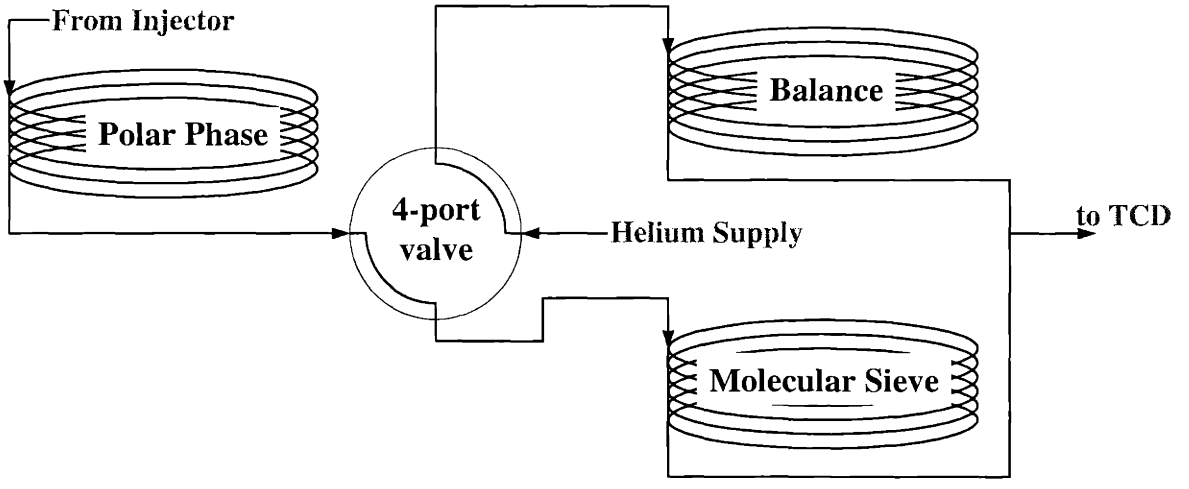

Figure 7-5. Schematic of the column flow configuration for the TCD.

After the sample eluted from the polar liquid phase column, it went to a Valco 4-port valve where the stream was sent to either a balance column or a molecular sieve column. The balance column was simply a coil of glass-lined stainless tubing that was not packed with any material. The small inner diameter, 0.1 mm, and the length of the tubing (approximately 3 ft.) created a pressure drop that was equivalent to the pressure drop of the molecular sieve column. The molecular sieve column was a 316 SS Supelco column, 10 ft × 1/8 in, with a 1-3830 5A 60/80 mesh packing.

---

[8] Supelco, Supelco Park, Bellefonte, PA 16823-0048, (814) 359-3441.
[9] This volumetric flow rate does change as the temperature of the GC oven is adjusted during an analysis. To compensate for this effect, the column compensation feature on the HP 5890 GC was utilized.

Since the pressure drops of the molecular sieve and balance columns were approximately the same, the helium flow rate through both columns was also approximately the same. When the Valco 4-port valve was switched, the gas flow rate going to the TCD did not change so the signal baseline was stable. In general, only a small change in the baseline occurred during a valve switch and this did not usually impact the analysis of the chromatogram. Of course, it was critical to time the valve switch so that any species that would be retained on the molecular sieve would flow through the balance column. This was not difficult since all the sampling valve switching that occurred during an injection was automated using ChemStation and the electronics on board the GC.

Temperature programming of the GC oven was used during the injections to speed the analysis time and improve peak shapes. Because two separate gas streams were flowing to the TCD, it was very important to determine the retention time of each of the components of the reaction being studied. The temperature program was also used to ensure that multiple components did not elute from the molecular sieve and the balance column at the same time. Because temperature programming was used, the baseline of the TCD signal was not constant even for a blank injection. To compensate for this effect, the column compensation feature of the HP 5890 Series II Plus GC was used. This feature simply subtracts the baseline from a blank injection from a gas sample injection. This helps to produce a steady baseline in the composite chromatogram.

GC Data Analysis Methods

Product and feed gas composition were determined by analyzing the component peak areas on the gas chromatograms. In general, the data from the flame ionization detector was not used because it could only detect ions generated from methane and ammonia. All the

components were analyzed using the thermal conductivity detector. Previous researchers have shown that the absolute response of a TCD in terms of peak area percentages does not correlate to either molar or weight percentages[5-7]. Thus, it was necessary to use a response factor to correlate the TCD data with component molar or weight percentages. The Relative Molar Response (RMR) factor method was used in this work for data analysis due to the wide array of literature available on it. The RMR factor of a compound is defined by the following equation[8]:

$$RMR_i = (A_i / A_r) \times (M_r / M_i) \times 100 \tag{7.1}$$

where A_i is the peak area for compound i, A_r is the peak area for the reference compound, M_r is the molar percent of the reference compound, and M_i is the molar percent of compound i.

RMR Factor Determination Method

To determine the compositions of the product and feed gas from the TCD data, it was necessary to determine the RMR values of all the components in the methane and ammonia oxidation experiments. Many researchers have used RMR values published in the literature when available, or they have used RMR correlations based on component and carrier gas thermodynamic properties. However, the relative molar response factor of a compound does depend on the geometry of the thermal conductivity detector used[9]. Moreover, a wide variation of response factors have been reported for RMR's of the same compound determined using different TCD designs. However, the component relative molar response factors are portable between detectors of the same design[8].

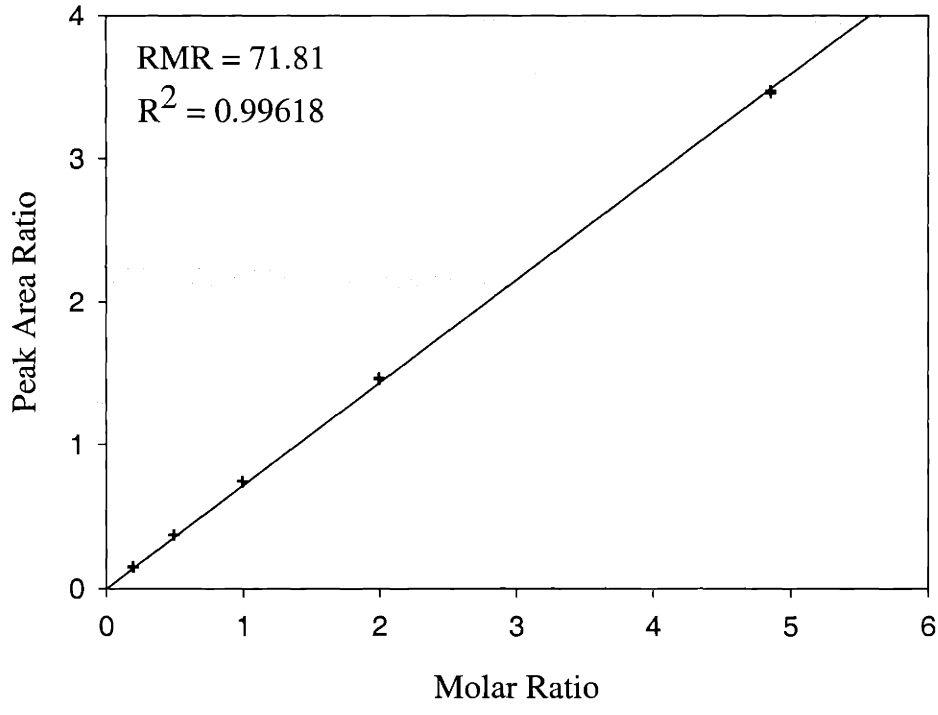

Figure 7-6. Plot used to calculate the relative molar response factor of nitrogen to krypton.

The RMR factors were found by introducing known sample concentrations to the GC and analyzing the peak area ratio of the desired component to the reference component. For the methane oxidation experiments, nitrogen was used as the reference component. However, krypton was used as the reference component for the ammonia oxidation experiments since nitrogen is a product of that reaction. The sample concentrations were created by using three gas flow manifolds to control the amount of the component to be measured, the amount of reference component, and the diluent[10] concentration (to prevent saturation of the thermal conductivity detector). The term gas flow manifold in this case refers to a conventional mass flow controller with a forward pressure regulator located immediately upstream and a back pressure regulator located immediately downstream. The

[10] The diluent used was always helium since this was the gas chromatograph carrier gas used.

three gases were taken from pure gas cylinders, so their composition was known[11]. The mass flow controllers used during the experiments were all calibrated immediately before these calibration injections were made. By varying the concentration of the three components over the range expected in the feed and product gas samples, a correlation could be developed between the peak area ratios and the molar ratios. Generally, five concentration levels were studied during each calibration with at least five injections performed at each concentration level. Linear regression analysis was used to determine the actual RMR values and determine the error in the measurement as illustrated in Figure 7-6 (quantified using the 95% confidence interval).

Determining Sample Composition from the GC Data

Determination of the sample composition from the peak area data was done by dividing each of the component peak areas by their appropriate RMR factor to give the true response. These true response values were then normalized to give the sample composition[10]. As a means to check the accuracy of this calculation, a reference gas was used in all the AIMS experiments. Again, the reference used for the methane oxidation experiments was nitrogen, and the reference used for the ammonia oxidation experiments was krypton (nitrogen could not be used for the ammonia oxidation experiments since it is a product of this reaction). Nitrogen was introduced as part of the methane feed in the methane oxidation experiments by using a pre-mixed cylinder of methane, nitrogen, and helium for the fuel gas. The composition of this cylinder was determined using the methods described here (to verify the composition given by the vendor). Krypton was introduced as a secondary stream in the ammonia oxidation experiments. By comparing the weight percentage of the

[11] Samples were analyzed of each of the pure component cylinders used in the experiments to verify their purity. In general, the gases had impurities less than 0.1% or the impurities were

reference component determined using the RMR factor method to the weight percentage calculated from the gas flow rates, a simple check for accuracy in the analysis (or flow controller performance) was provided[12].

Calculation of Reaction Parameters

The performance of the microreactors was assessed by using reactant conversions, selectivities, and yields. The conversion of a component (either the fuel or oxygen) refers to the change in the amount of a component divided by the original component amount[13]. This is represented as

$$X_i = \frac{F_i - P_i}{F_i} \times 100\% \tag{7.2}$$

where X_i is the conversion of component i, F_i is the amount of component i in the feed, and P_i is the amount of component i in the product. Selectivities are calculated on atom basis such that the selectivity to a reaction product i with respect to element a is defined as

$$S_i^a = \frac{\text{moles of } a \text{ converted to product } i}{\text{moles of } a \text{ converted from reactants to all products}} \times 100\% \tag{7.3}$$

The yield of product i with respect to element a is defined as

$$Y_i = \frac{X_i}{100\%} \times \frac{S_i^a}{100\%} \times 100\% \tag{7.4}$$

These later two definitions are not used by all researchers, so care must be used when comparing values presented in this work to those in the literature. In particular, many define the selectivity as the rate of formation of desired products divided by the rate of formation of undesired products. However, the definition used here allows the yield to be directly defined

---

simply too low to be measured by the analysis method.

[12] Weight percentages must be used here not molar percentages, since mass not moles is conserved under reaction conditions.

from the conversion and selectivity. In addition, graphical presentation of the data is aided since all the values range from 0 to 100%.

The errors in these parameters were calculated by closing the mass balance on the reaction. Specifically, by comparing the feed gas composition to the product gas composition, an estimate of the error in the composition measurements could be obtained. Large errors in the mass balance were indicative of physical problems with the system, usually leaks. The small errors were caused by the uncertainties in the RMR values and the fluctuations in flow rates of the MFC's on the Feed Gas Mixing Board.

Conclusions

The experimental procedure used in testing the AIMS was similar to the procedures used for operating conventional catalyst test systems, such as the MARS units at DuPont. In particular, the experiment setup time for the AIMS is the same or less than the MARS units. This is due to the microreactors having their catalyst predeposited. Normally, the loading of catalyst requires careful attention to details to provide consistent results between runs. The other steps involved are the same or require similar amounts of effort.

A multi-dimensional GC method was implemented for analyzing the feed and product compositions during AIMS testing. Although the flame ionization detector could not detect the reaction products for the chemistries studied, the GC method developed allowed all reaction products to be quantified on a single thermal conductivity detector. With the addition of the appropriate GC data analysis methods, it was possible to quantitatively analyze the feed and product streams for all components. Data from this testing is presented in the following chapter.

---

[13] Amount can be expressed in molar, mass, or volumetric flow rates for this calculation.

References

1. Guise, W.E. and Mills, P.L. (1994) "A multidimensional gas chromatographic method for on-line process analysis of isobutane or isobutylene partial oxidation reaction products", Presented at 33rd Eastern Analytical Symposium and Exposition, Somerset, NJ, November 15, 1994, Session on Gas Chromatography.

2. Mills, P.L. and Guise, W.E. (1996) "A multidimensional gas chromatography method for analysis of n-butane oxidation reaction products", *Journal of Chromatographic Science,* **34**(10), pp. 431-459.

3. Delaney, T.M. and Mills, P.L. (1999) "Multidimensional process gas chromatography based on a single GC with dual ovens", Presented at 38th Annual Eastern Analytical Symposium, Somerset, NJ, 15, 1999, Gas Chromatography Poster Session, Poster 71.

4. Nicole, J.F., Mills, P.L., and Delaney, T.M. (2000) "Multidimensional on-line process gas chromatography based on a single GC with two independently controlled ovens", Presented at AIChE 2000 Annual Meeting, Los Angeles, November 14, 2000, Session on Lab and Pilot Scale Instrumentation, Paper 276d.

5. Rosie, D.M. and Barry, E.F. (1973) "Quantitation of thermal conductivity detectors", *Journal of Chromatographic Science,* **11**, pp. 237-250.

6. Browning, L.C. and Watts, J.O. (1957) "Interpretation of areas used for quantitative analysis in gas-liquid partition chromatography", *Analytical Chemistry,* **29**, pp. 24-27.

7. Craats, F. (1958) *Gas Chromatography*, Academic Press, New York.

8. Gislason, J. and Wharry, S.M. (2000) "Relative molar response factors for thermal conductivity detectors", *Journal of Chromatographic Science,* **38**(3), pp. 129-132.

9. Guiochon, G. and Guillemin, C.L. (1988) *Quantitative Gas Chromatography for Laboratory Analysis and On-Line Process Control*, Elsevier, New York.

10. Dietz, W.A. (1967) "Response factors for gas chromatographic analyses", *Journal of Gas Chromatography,* **5**, pp. 68-71.

CHAPTER 8
AIMS TESTING RESULTS

Operating the AIMS under reaction conditions was similar to operating the other catalyst test systems at DuPont that utilize reactors operating in parallel. Considerable care was needed to setup the system for operation to obtain quality, reproducible results. However, after this step, operation was straightforward. This was mainly due to the advanced automation used to operate the AIMS and the MARS units at DuPont. Specifically, the operator could quickly scan all of the relevant process variables using the HMI, and automatic system interlocks ensured that they were maintained within safe bounds during a run. Automated GC sampling methods, taken directly from experience with the MARS, required minimal operator intervention to acquire reaction data. The most involved part of obtaining this data was analyzing the GC results. This could also be automated as had been done to a certain extent with the various MARS units.

The following sections summarize the testing results of the AIMS. The first section gives an overview of the operation of the AIMS and makes comparisons between the AIMS with the MARS units. Additional information is given concerning the operation of the AIMS as is related to its evaluation. The subsequent section discusses in detail the operation of the Redwood Microsystems components used in the AIMS. Because of the number of problems associated with these devices, they were generally considered the major obstacle in operation of the AIMS. The third section focuses on the GC methods used to analyze the reaction products since all subsequent data analysis is based upon the GC-derived data. Examples are given of some of the chromatograms taken during reaction experiments. In addition, the

values obtained for the Relative Molar Response (RMR) factors of each of the reaction components are given. The following section then presents some of the reaction results obtained from operating the AIMS with the ammonia and methane oxidation reactions. Finally, a summary of the key findings from the system testing is given.

Overview of AIMS Operation

The main difference between the AIMS and the MARS units was the size of the components. Although miniaturization of reaction systems was an objective of this project, this also led to some unexpected problems. Specifically, debugging and fixing hardware problems in the AIMS was usually more difficult than with the MARS units. In particular, the closed system chassis prevented direct monitoring of the individual components during operation (i.e., for probing with a gas leak detector or multimeter). Since debugging is easiest to do under energized conditions, this aspect did present a problem. However, being a prototype unit, the difficulty of maintenance should not be viewed as an overriding disadvantage. In particular, future versions are expected to contain more robust components, and could incorporate features allowing easier diagnosis, such as placing electrical test points near the front of the system boards to monitor important voltages.

On the other hand, miniaturization did have some advantages in that the entire system could be easily moved to another location for maintenance. For example, Figure 8-1 shows a picture of the AIMS with the flow manifold for a MARS in the background (the MARS reactor oven was removed from the hood). The front area of the AIMS is about one tenth of the area of the flow manifold in the background. Obviously, the AIMS does have a significant advantage in reducing cost by reducing the requirement for space in a fume hood.

In addition, an operator can easily reach all of the parts of the AIMS without needing a footstool or stepping inside of the hood.

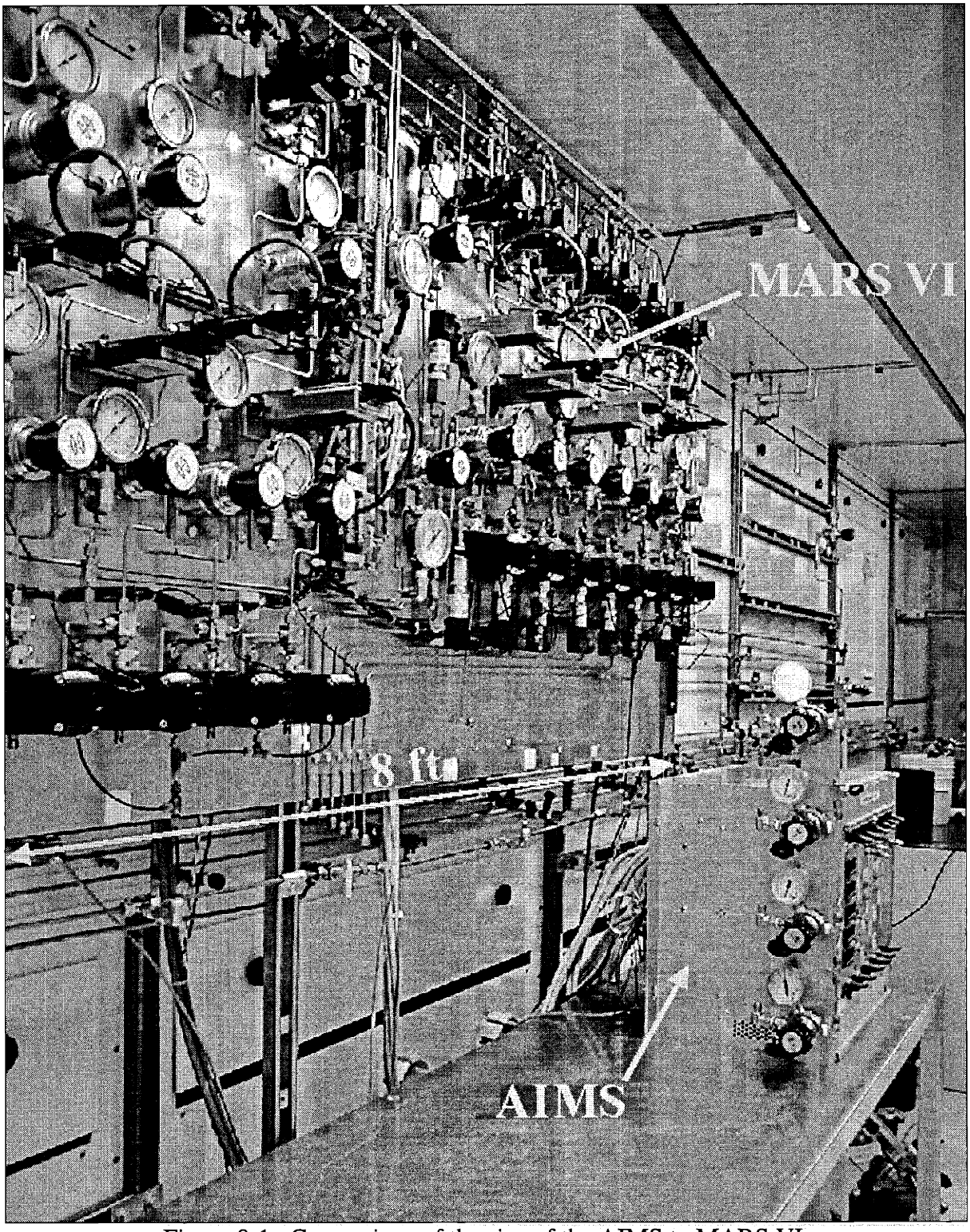

Figure 8-1. Comparison of the size of the AIMS to MARS VI.

Although the size of the flow manifold and reactor components have been substantially reduced in the AIMS, no such reduction has occurred in the control system since both the MARS and AIMS rely on components that have already been miniaturized. Figure 8-2 shows both the Siemens S7-300 controller for the MARS VI and the National Instruments controller for the AIMS. Their size is essentially the same, with both having a similar number of inputs and outputs. The Siemens controller used for the MARS VI could have been used for operating the AIMS, but it was not capable of PID control loop rates faster than 20 Hz.

One great advantage of the AIMS was the simplicity of setting up the wiring. Because all of the components in the AIMS chassis were wired internally to connectors on the rear of the chassis, there was no need to connect individual wires from the components to the controllers. This is necessary for the MARS units, and adds a significant cost to their construction. For example, wiring the MARS VI took about two workdays for an instrumentation technician. The wiring for the AIMS was done through cables connecting the AIMS chassis to the NI PXI chassis. This took only about ½ hour to complete when the AIMS was moved into the fume hood for testing. Future versions of miniaturized reactor systems could improve on this even further by converting the analog signals into a digital format so communications could be done through a standard digital communications protocol such as TCP/IP. This would require customized electronics in the reactor system chassis, but it would reduce the complexity of the external controller substantially by eliminating many of the boards. In addition, the proximity of the controller to the reactor system would not be as important since analog signals would no longer need routing.

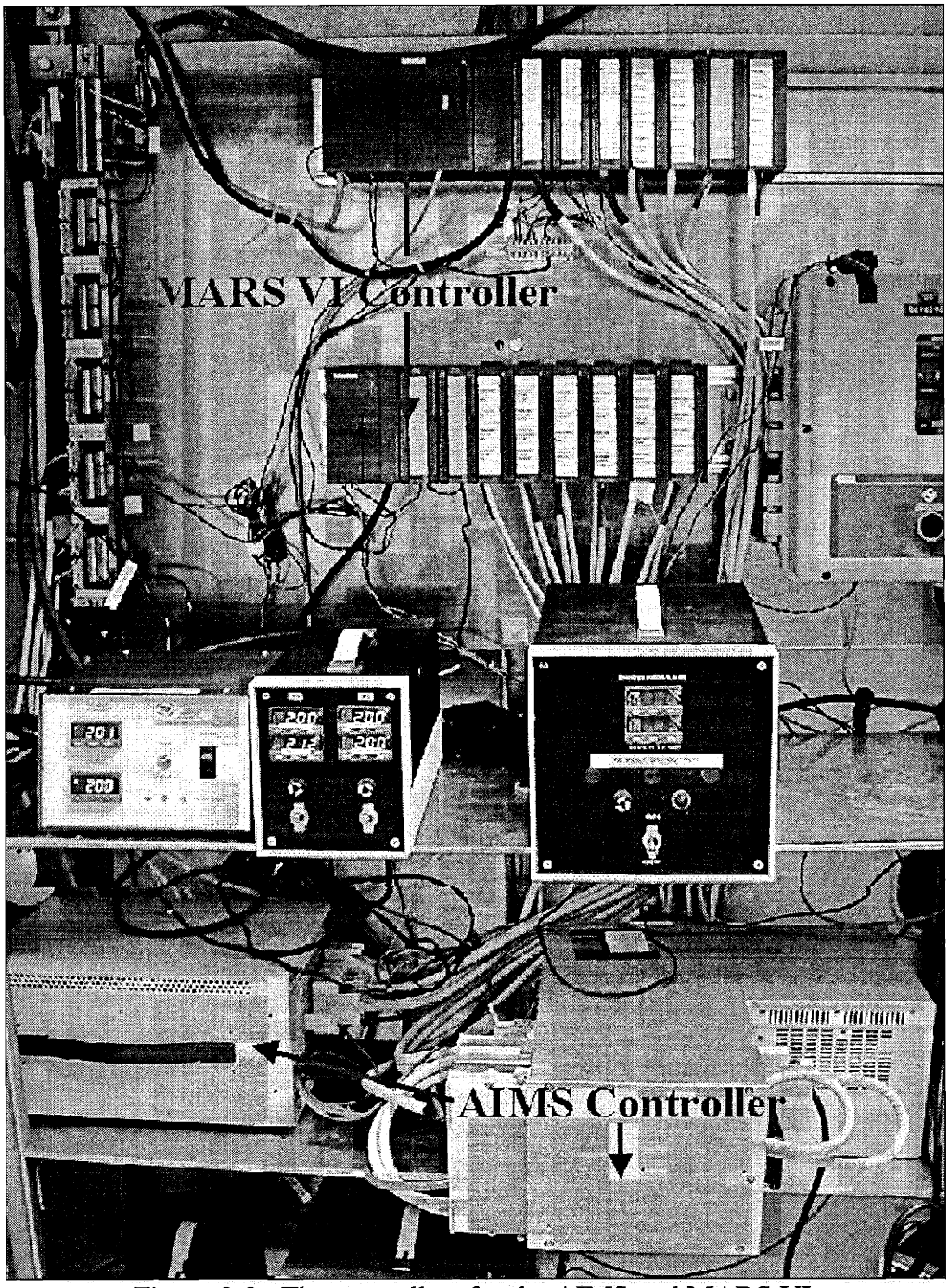

Figure 8-2. The controllers for the AIMS and MARS VI.

The routine operation of the AIMS offered no surprises except for the Redwood components. The microreactors almost always functioned properly in the experiments. During one experiment, it was found that there was a substantial leak at the o-ring seal

between the DieMate™ manifold and one of the reaction channels. This line was manually isolated from the system before the feed gas was introduced to the reactors, so no danger was posed. The cause for this was improper adjustment of the socket head cap screws on the DieMate™ manifold. This was avoided in subsequent runs by taking greater care in adjusting the torque on these screws. In addition, the microreactors did fail when the heaters produced an excessive temperature. In many cases, the heaters simply stopped functioning, but the membrane remained intact (morphological changes in the platinum layer broke the continuity of the heater lines). However, the membrane did break on many of the reactors, but this had been observed previously for this type of reactor[1,2]. When this happened, the reactor line was automatically purged with inert gas and then isolated from the remaining active reactor lines.

Evaluation of Redwood Microsystems Components

The Achilles heel of the system was the Redwood microvalves. By the end of the testing, it was expected to have at least one problem related to these valves occur in setting up for every new experiment. Fortunately, the failures generally happened when the system was first powered, which may indicate that power transients were the cause of many of the problems. In fact, the unusual power draw characteristics of these valves did cause problems in themselves. Specifically, these valves were thermally actuated, so opening one of the SOV's produced a large transient current draw of about one amp, but for less than ½ second. Nonetheless, this could cause a significant problem if five of these valves actuate simultaneously. The three amp fuses that had been placed on the boards to prevent damage to the backplane were often blown in the initial testing of the system. Adjustments were made in the LabVIEW control program to prevent the simultaneous actuation of multiple

valves. In particular, the valves could not be allowed to actuate when power was first applied to the chassis.

In addition, the SOV's had another problem that made testing the AIMS difficult. Sometimes, these normally-closed valves would fail to open when actuated. Normally, the valves had about a five-minute warm-up period, but occasionally the valves would never open. There were some potentiometers on the Redwood daughter cards that were mounted on the system boards that could be adjusted to solve the problem. These potentiometers controlled the amount of power that was applied to the heaters in the valve. This usually corrected the problem, but for some reason these potentiometers need continuous adjustment. On some occasions, even adjusting the potentiometers seemed to have no effect. At this point, it was necessary to simply replace the Redwood flow manifold with another manifold. Fortunately, some spare manifolds had been ordered that could be used while the components were repaired by Redwood.

On two occasions, the SOV's just failed completely to the open state (they are normally closed valves), which indicated a mechanical failure in the valve or in the seals around the valve. In addition, one MFC stopped responding to analog and digital inputs completely. On other occasions, these problems were not in the valve itself, but in the electronics located on the daughter cards. To be fair in their evaluation, the valves and the electronics were exposed in the system, so some of these problems may have been caused by handling (wires were resoldered on more than one occasion). In addition, Redwood did not have very much experience in designing valves for operation at above atmospheric pressure. However, the other components inside the AIMS chassis functioned without any failure

during the tests. The only item that needed replacing was a DieMate™ socket whose pins had been damaged by improper handling.

Finally, the Redwood MFC's were able to control mass flow, but with some limitations. In particular, great care had to be used when calibrating the MFC's since the calibration curve sometimes had a discontinuity in it. Figure 8-3 shows an example of this where there appear to be two lines that should be fit to the data, one for the low flow range and one for the high flow range. A few of the MFC's did have linear calibration curves, but many exhibited this non-linearity to varying extents. The reason for this was probably the flow measurement and control techniques of these MFC's, which operated by controlling the pressure drop across an orifice. Discussions with Redwood staff indicated that adjusting the internal flow control and measurement parameters for these controllers required a considerable amount of work.

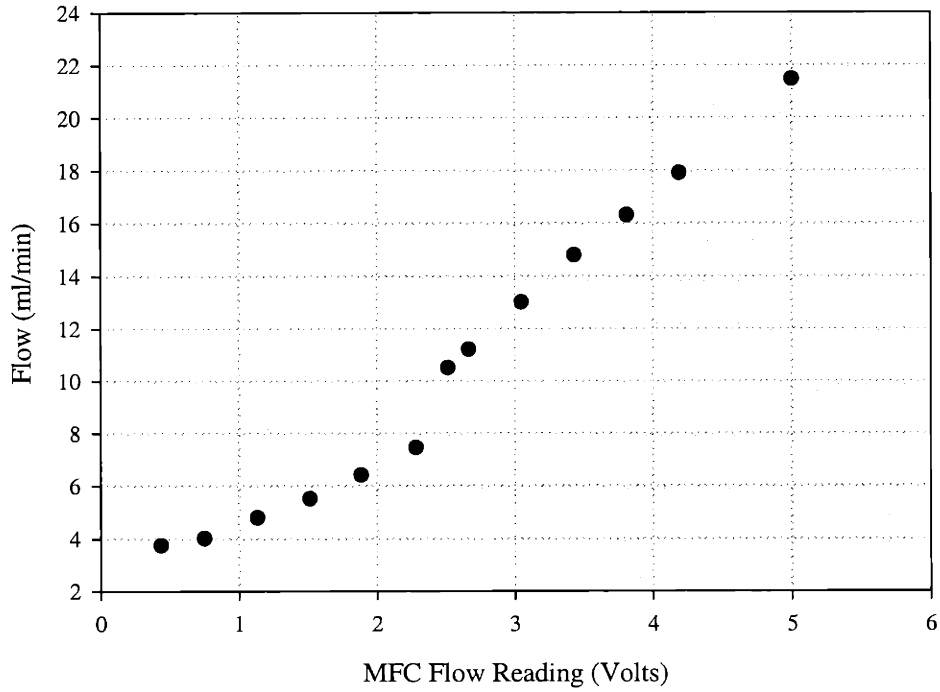

Figure 8-3. Calibration curve for the oxygen feed MFC in the AIMS.

In addition, two of the upstream feed flow controllers gave a positive flow reading when there was a downstream pressure. This occurred even if there was no gas flow through the valve. An example of this is shown in Figure 8-4. Obviously, conventional MFC's are not affected by downstream pressures that are within their design specifications. This problem was overcome by using the calibration curve and realizing there may be no flow even if the MFC was returning over a one volt signal on a five volt scale.

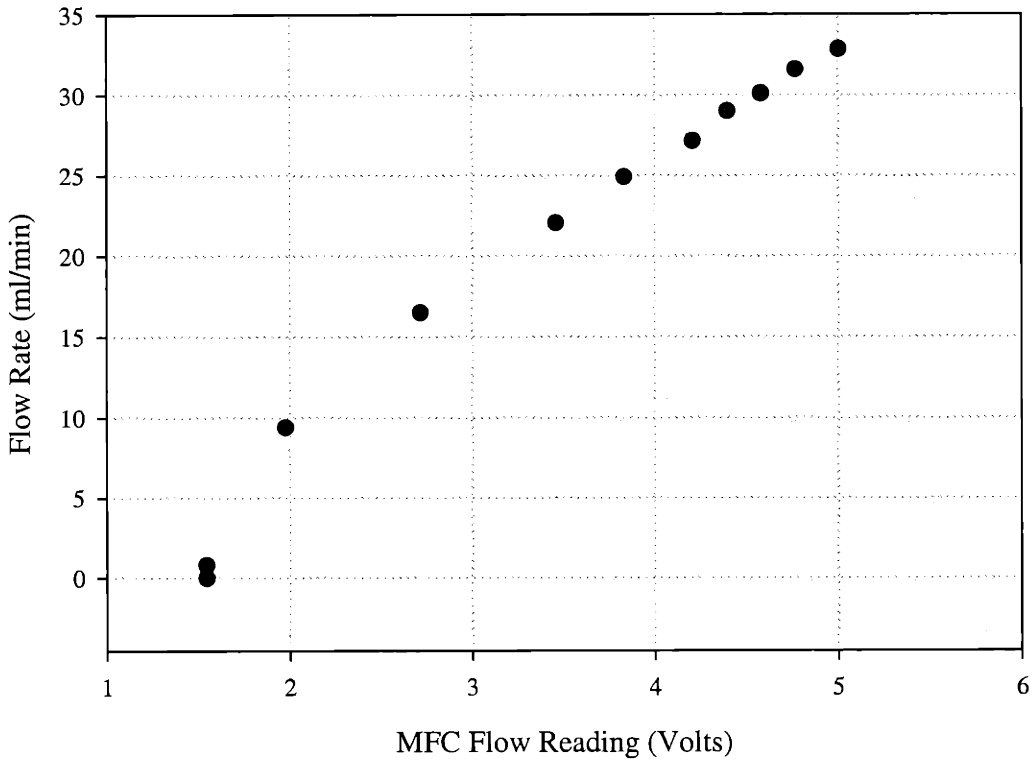

Figure 8-4. Calibration curve for the ammonia feed in the AIMS.

Overall, many of the problems presented by the Redwood valves simply had to be worked around during testing of the AIMS. For example, the non-linearity of the flow controllers prevented the use of certain flow ranges. For the calibration curve shown in Figure 8-3, a flow set point between 8 and 10 ml/min would not have been possible.

Unfortunately, many of the problems with the physical action of the valves required interrupting a planned test to correct the problem.

Relative Molar Response Factors and GC Results

Experiments were conducted for determining most of the RMR factors for the components found in the methane oxidation and ammonia oxidation reactions. The factors used for the methane oxidation experiments are listed in Table 8-1, and the factors for the ammonia oxidation experiments are listed in Table 8-2. The molecular weights of the components are also listed in these two tables since there is a weak correlation between the RMR factor and the component molecular weight[1]. For the methane oxidation experiments, nitrogen was used as the reference component. It was assigned a RMR of 100 as commonly reported in the literature for a reference component. For the ammonia oxidation experiments, krypton was used as the reference component.

Table 8-1. RMR Values for Methane Oxidation Reaction Components

Component	RMR Value[2]	RMR Error[3]	Molecular Weight
Carbon Dioxide	116.3	0.5	44
Carbon Monoxide	99.5	0.3	28
Hydrogen[4]	1.014	0.011	2
Methane	76.9	0.4	16
Nitrogen	100	N/A	28
Oxygen	93.6	0.5	32
Water[5]	63.4	Unknown	18

[1] The correlation is actually much more complicated with most literature correlations depending on the cross-sectional collision area of the component with the carrier gas.
[2] Nitrogen was used as the reference component and its value was set to 100.
[3] The error was calculated as the 95% confidence interval of the regressed parameter.
[4] Because hydrogen has a thermal conductivity less than helium, it gives a negative peak as its TCD response. This peak was integrated accordingly.
[5] See discussion in the text for how the RMR value of water was determined.

Unfortunately, it was not possible to directly measure the RMR factor for water because of the difficulties associated with introducing precisely known quantities of water with the reference gas. In fact, introducing small but controlled concentrations of steam into laboratory reactors has undergone extensive investigation at DuPont. As a substitute for the actual measurement, the RMR value of ammonia was used as the RMR value of water. This seemed reasonable since they have very similar molecular weights and are similar in size. It was believed that this would introduce the same or less error than using a value that was derived from a correlation. Similarly, the RMR value for nitric oxide was not measured because of the extremely corrosive action of this compound. The RMR determination experiments required the use of pure nitric oxide, which presented too many safety and compatibility problems with the equipment. Instead, the RMR values of oxygen and carbon monoxide were averaged to obtain the RMR of nitric oxide. This was done since oxygen and carbon monoxide are both two atom species and the molecular weight of nitric oxide is approximately the average of the molecular weight of oxygen and carbon monoxide.

Table 8-2. RMR Values for Ammonia Oxidation Reaction Components

Component	RMR Value[6]	RMR Error	Molecular Weight
Ammonia	45.6	1.0	17
Argon	77.0	0.6	40
Krypton	100	N/A	83.8
Nitric Oxide[7]	69.4	Unknown	30
Nitrogen	71.8	0.4	28
Nitrous Oxide	88.4	1.3	44
Oxygen	67.2	0.4	32
Water[5]	45.6	Unknown	18

[6] Krypton was used as the reference component and its value was set to 100.
[7] See discussion in the text for how the RMR value of nitric oxide was determined.

The quality of the chromatograms obtained from the TCD were usually good since they had a steady baseline and the peaks were baseline resolved. As mentioned in the previous chapter, the column compensation feature of the HP-5890 GC was used to improve the baseline since the GC oven was temperature programmed. The main challenge with the method was the difficulty in resolving all of the peaks due to the combining of the outlets of the polar liquid phase column and the molecular sieve column. Another complicating factor was that the same temperature program had to be applied to both columns. A much more efficient analysis could have been achieved if a dual oven method had been used as in the work by Mills et al.[3,4] The GC method for analysis of the methane oxidation reaction products, required about nine minutes. Figure 8-5 shows a chromatogram obtained during a run of the AIMS with methane oxidation. Carbon dioxide and water were separated on the Hayesep R column while the other components were separated on the molecular sieve column.

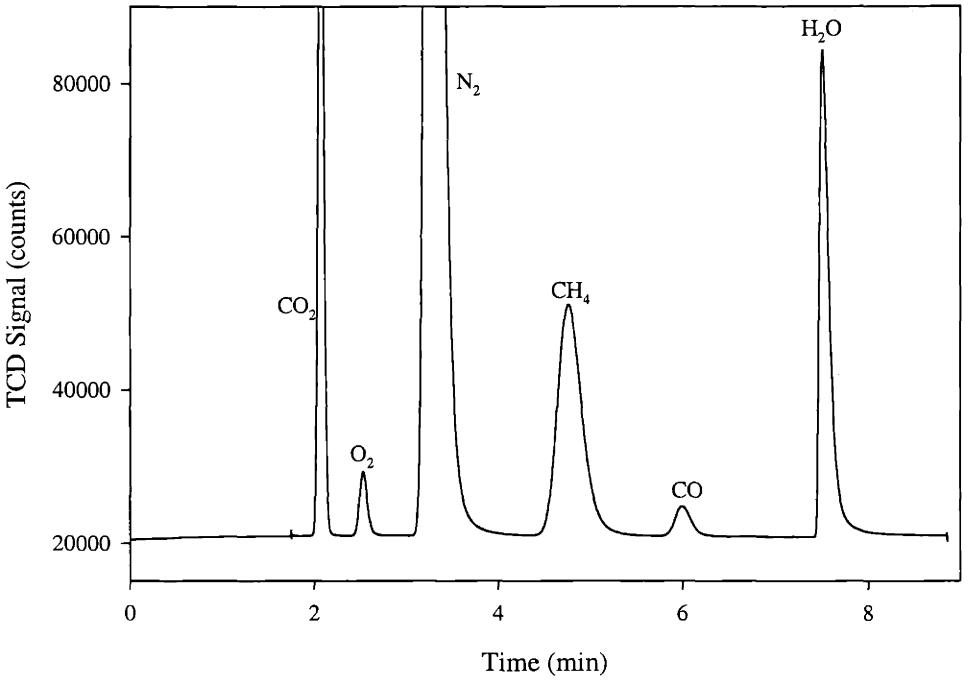

Figure 8-5. Sample chromatogram of the products of methane oxidation.

Analysis of the ammonia oxidation reaction products was considerably more difficult since it is hard to find a column that gives a good peak shape for ammonia and elutes water in a reasonable amount of time. This problem had undergone some prior investigation at DuPont, and the best column found for studying this reaction was a custom-packed Hayesep T, that had been treated with a 5% KOH solution to deactivate some of the adsorption sites. Nonetheless, the complete analysis still required fifteen minutes, which severely limited the quantity of reaction data that could be obtained for ammonia oxidation. Unfortunately, this was really the better reaction to study since nearly complete conversion is achievable at less than 300°C. Figure 8-6 shows a chromatogram obtained during a run of the AIMS with ammonia oxidation. Nitric oxide, ammonia, and water were separated on the Hayesep T column while the other components were separated on the molecular sieve column. Note that argon and oxygen were not baseline resolved since separation of these components requires cryogenic column temperatures.

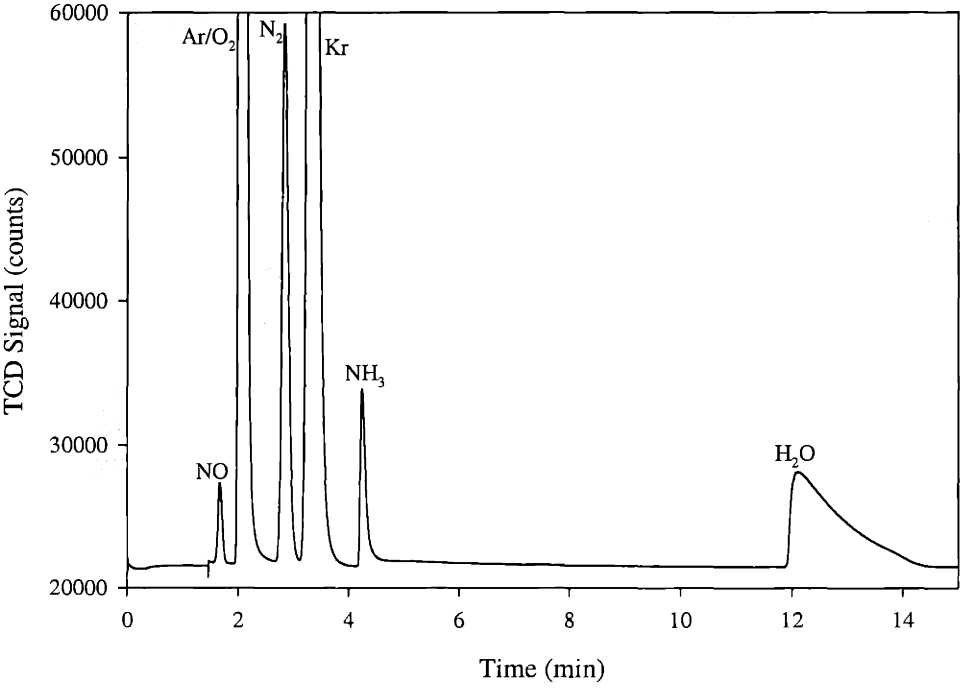

Figure 8-6. Sample chromatogram of the products of ammonia oxidation.

Reaction Testing Results

Methane oxidation was the first reaction studied with the AIMS. The desired goal was to produce a significant amount of the partial oxidation products, carbon monoxide and hydrogen, in a millisecond contact time type of reaction[5,6]. Unfortunately, the temperature required (greater than 700°C) for the partial oxidation reaction was barely achievable, and the reactors generally failed when the temperature became high enough to produce significant amounts of carbon monoxide. Only on occasion was any hydrogen detected in the product stream. Because of this, the ammonia oxidation reaction was also studied since nearly complete conversion of ammonia can be obtained at less than 300°C. Unfortunately, as mentioned in the previous section, the GC analysis of the ammonia oxidation products was considerably more difficult. Open-loop temperature control was used for the initial testing, but for later testing, closed loop temperature control was added. The following sections summarize the reaction results and also discuss the PID temperature control results of the microreactor heaters.

Methane Oxidation

Methane oxidation was difficult to run in the scale-up microreactor design due to the high temperatures required for the reaction. Generally, differential level conversions (less than 10%) of methane were observed. The main problem was due to the degradation of the platinum microreactor heaters. The heater lines usually lost continuity when operated at temperatures greater than 600°C. To a lesser extent, membrane failure also prevented the microreactors from reaching these high temperatures. Because high temperatures could not be sustained for a long period of time (greater than 10 minutes), very limited reaction data was available at these temperature points since a GC analysis took about ten minutes to complete. Very low selectivities, less than 10%, to CO were observed, and none or

extremely small amounts of hydrogen (less than 0.5%) were observed because of this temperature limit.

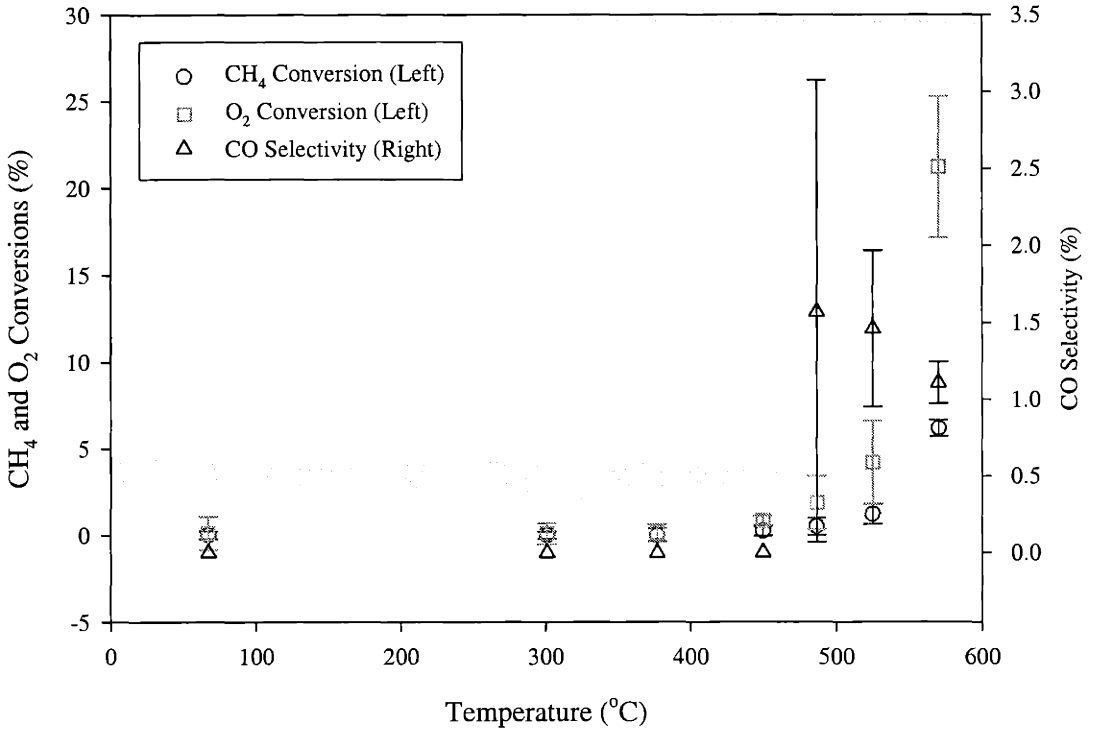

Figure 8-7. Methane oxidation reaction data for microreactor ACT-G2-4 channel B with a feed gas flow rate of 10.1 ml/min. The feed composition was 14.9% methane, 10.3% oxygen, 39.8% nitrogen, and balance helium. This microreactor was placed in Reactor Board 2. Error bars represent the 95% confidence interval of each value.

Despite these difficulties, methane oxidation was the first reaction run in the AIMS, and it was successful in proving that the AIMS could operate with multiple microreactors operating under reaction conditions simultaneously. Figure 8-7 shows an example of the type of data obtained from the AIMS for the methane oxidation reaction. In this case, the

extremely small amounts of hydrogen (less than 0.5%) were observed because of this temperature limit.

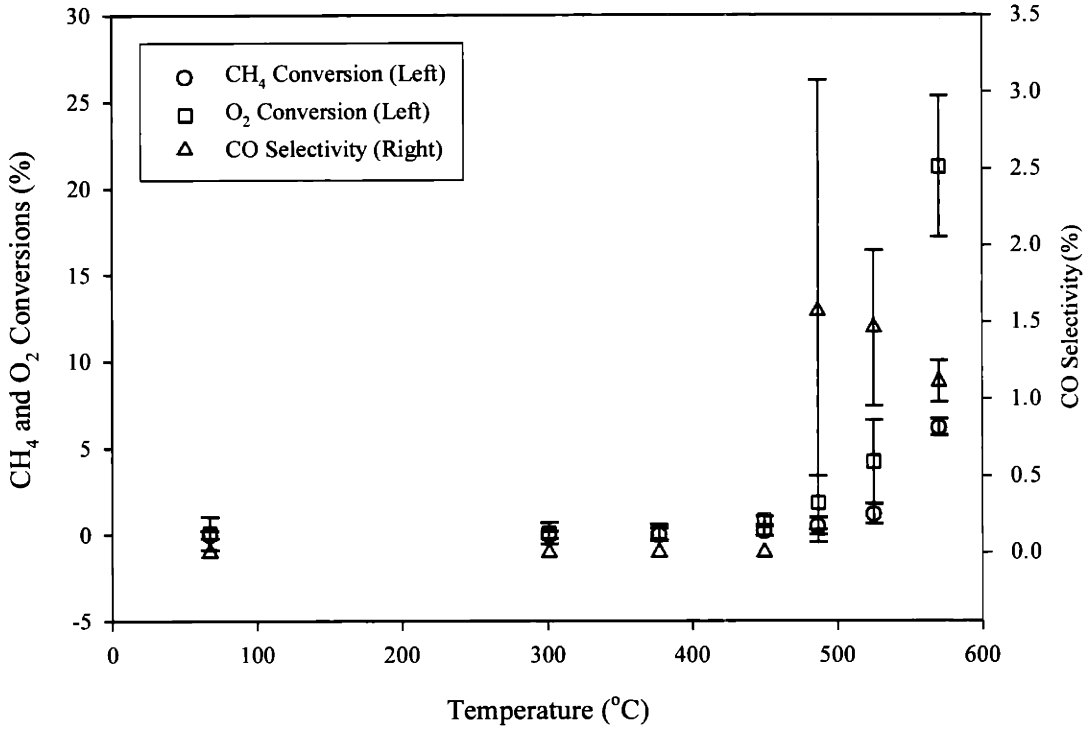

Figure 8-7. Methane oxidation reaction data for microreactor ACT-G2-4 channel B with a feed gas flow rate of 10.1 ml/min. The feed composition was 14.9% methane, 10.3% oxygen, 39.8% nitrogen, and balance helium. This microreactor was placed in Reactor Board 2. Error bars represent the 95% confidence interval of each value.

Despite these difficulties, methane oxidation was the first reaction run in the AIMS, and it was successful in proving that the AIMS could operate with multiple microreactors operating under reaction conditions simultaneously. Figure 8-7 shows an example of the type of data obtained from the AIMS for the methane oxidation reaction. In this case, the

microreactor successfully operated to an upper temperature limit of about 575°C[8]. The large error bars for the selectivity to carbon monoxide values are due to the low conversion of methane. This requires extremely precise measurement of small quantities of CO beyond the capabilities of the GC method used. In addition, the error bars on the oxygen conversion are large because the mass balance with the feed gas samples was used to compute this error. The problem is that the RMR value for water was not precisely measured, so the RMR value of ammonia was used as an estimate. The error introduced by this estimate is reflected in the errors on the calculated oxygen conversion.

For the methane oxidation reaction, a comparison was made between microreactors operating under the same reaction conditions. This was done not only to examine possible problems with the AIMS, but also to indicate the magnitude of differences between microreactor channels. Figure 8-8 shows the methane conversion for three different reaction channels operating with the same feed gas composition and feed gas flow rate. The values for the low temperature conversions, less than 550°C are quite close and lie well within the calculated error bounds of the values. The large error bars seen for the high temperature values arise from the changing structure of the platinum catalyst and temperature sensors. Change of the platinum catalyst structure was indicated by large fluctuations in the product gas composition during the analysis[9]. In addition, the further annealing of platinum lines of the temperature sensors made the temperature measurements much less accurate. It was observed during testing that high temperatures caused the resistance of the temperature

[8] Temperatures measured above 500°C by the microreactor RTD's are questionable since the platinum layer morphology starts changing rapidly at high temperatures. This subsequently changes the behavior of the platinum temperatures sensors.
[9] The microreactors usually did not last long enough under these conditions to find a steady-state condition.

sensor to irreversibly change to a lower value. This results in the transformation of temperatures above 600°C to a value closer to 600°C than the true temperature. That is temperatures much higher than 600°C still give a resistance reading corresponding close to 600°C because of the change of the platinum structure.

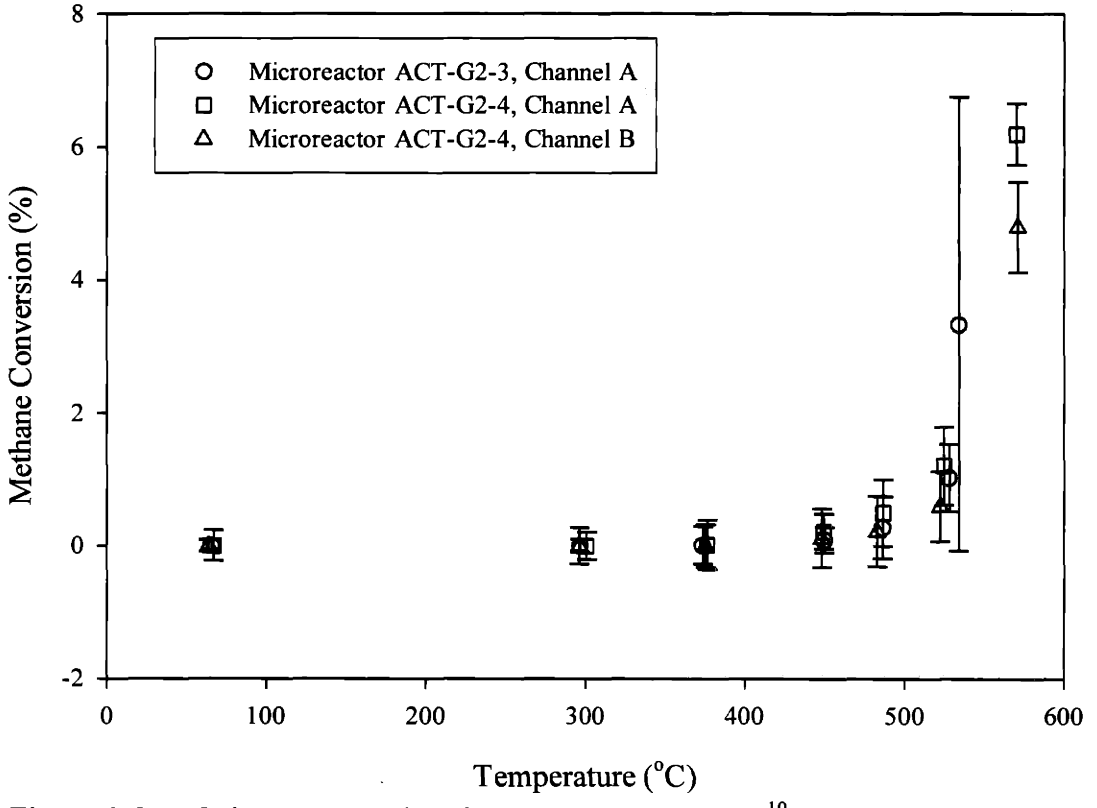

Figure 8-8. Methane conversion data versus temperature[10] for the methane oxidation reaction for three microreactor channels. These results come from one AIMS experiment with three microreactors running simultaneously[11]. The feed gas composition was 14.9% methane, 10.3% oxygen, 39.8% nitrogen, and balance helium. Feed gas flow rate to each microreactor channel was 10 ml/min. Error bars represent the 95% confidence interval of each value.

[10] Open-loop temperature control was used in this experiment with each heater set to the same heater voltage. The temperature used for the plot is the average of the measured RTD temperatures.

[11] There was a gas leak in Reactor Board 1 for microreactor channel B, so this channel was not utilized.

Similarly, Figure 8-9 and Figure 8-10 show the oxygen conversion and carbon monoxide data, respectively, for the same experiment. The carbon monoxide selectivity data appears somewhat random, but the large amount of error in the measurement makes it impossible to precisely determine selectivities for these low conversions. Because of the difficulty in obtaining high conversion for the methane oxidation reaction, the ammonia oxidation reaction was subsequently studied.

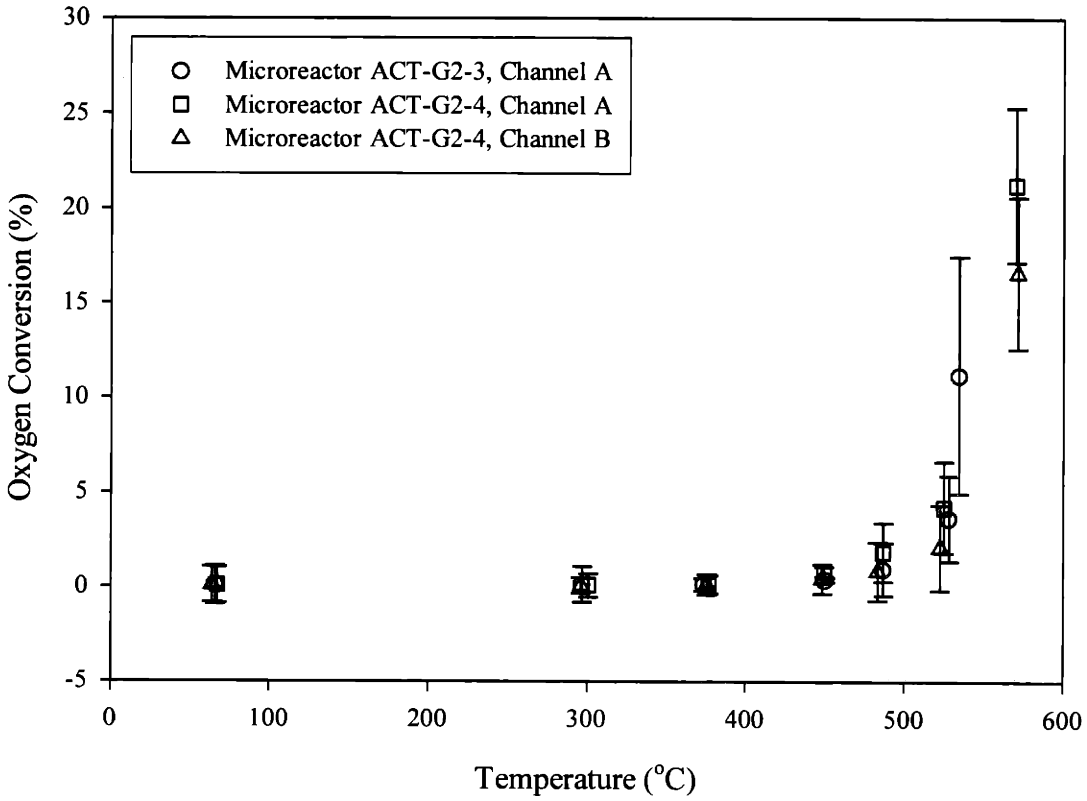

Figure 8-9. Oxygen conversion data versus temperature[10] for the methane oxidation reaction for three microreactor channels. These results come from one AIMS experiment with three microreactors running simultaneously. The feed gas composition was 14.9% methane, 10.3% oxygen, 39.8% nitrogen, and balance helium. Feed gas flow rate to each microreactor channel was 10 ml/min. Error bars represent the 95% confidence interval of each value.

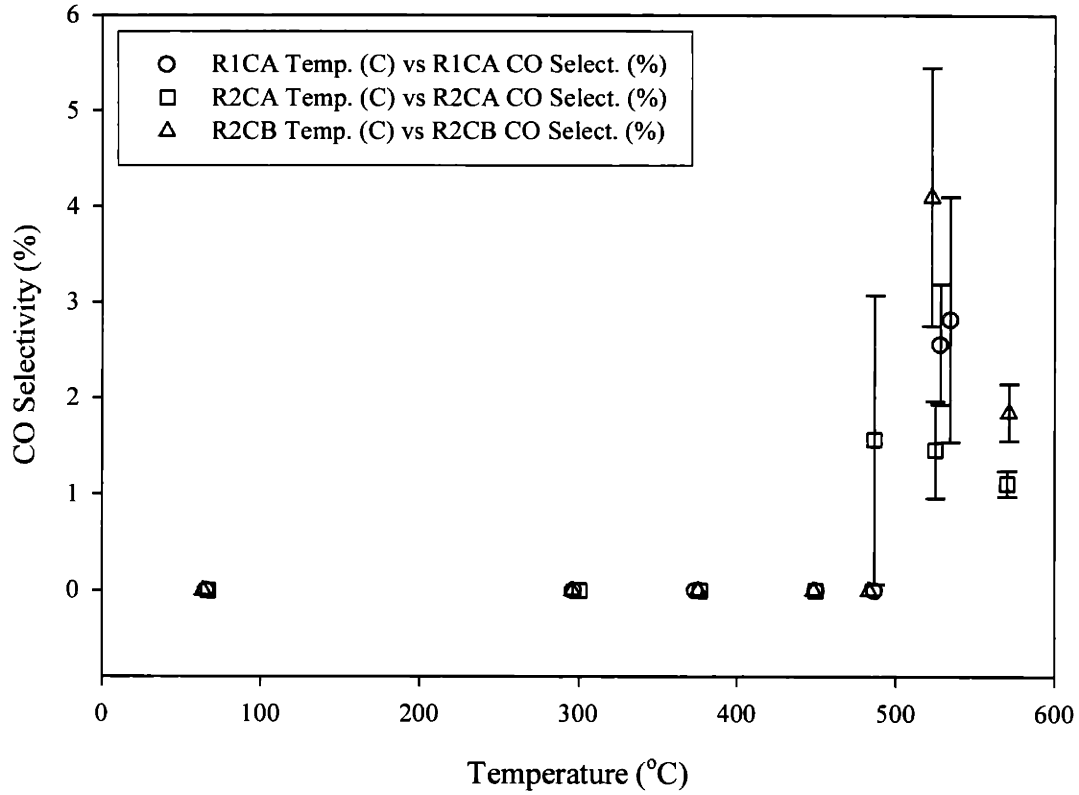

Figure 8-10. Carbon monoxide selectivity data versus temperature[10] for the methane oxidation reaction for three microreactor channels. These results come from one AIMS experiment with three microreactors running simultaneously. The feed gas composition was 14.9% methane, 10.3% oxygen, 39.8% nitrogen, and balance helium. Feed gas flow rate to each microreactor channel was 10 ml/min. Error bars represent the 95% confidence interval of each value.

Ammonia Oxidation

The ammonia oxidation reaction was easier to study in the sense that complete conversion was obtainable with the heater temperatures set to 300°C. For safety reasons, ammonia was kept as the limiting reagent. Figure 8-11 shows an example of the reaction results for testing the AIMS with ammonia oxidation. Conversion below 200°C was not measurable, whereas conversion above 300°C was complete. In between these two values, the product gas composition exiting from the microreactor was not stable. This resulted in the large error bounds for the ammonia and oxygen conversion values in this region.

Unfortunately, the GC analysis method was not fast enough to investigate this phenomenon, but it is believed to be related to the large amount of heat released by the reaction. For example, Figure 8-12 shows the heater power applied to the microreactor heaters for 200°C, 250°C, and 300°C. For 200°C there is very little heat contribution from the reaction so the power profile is almost flat. However, there is significant heat generated by the reaction for 300°C, so each heater steadily needs more power as there is less reaction occurring to provide the heat as the gas travels down the length of the heated segment. The 250°C set point is almost in between these two examples with the profile rising linearly at the beginning and then steadying out for the later heaters.

The selectivity data shown in Figure 8-11 indicates that significant amounts of nitric oxide are produced by the microreactor during ammonia oxidation. The data indicates that selectivity improves dramatically from almost none at 250°C to approximately 30% at 500°C. Similarly, small amounts of nitrous oxide began to be measured at approximately 400°C, and this product was observed during most of the ammonia oxidation trials. Srinivasan[1,2] probably did not report the presence of nitrous oxide, since its molecular weight is the same as carbon dioxide, which could have been a contaminant present in the analysis system during this reaction.

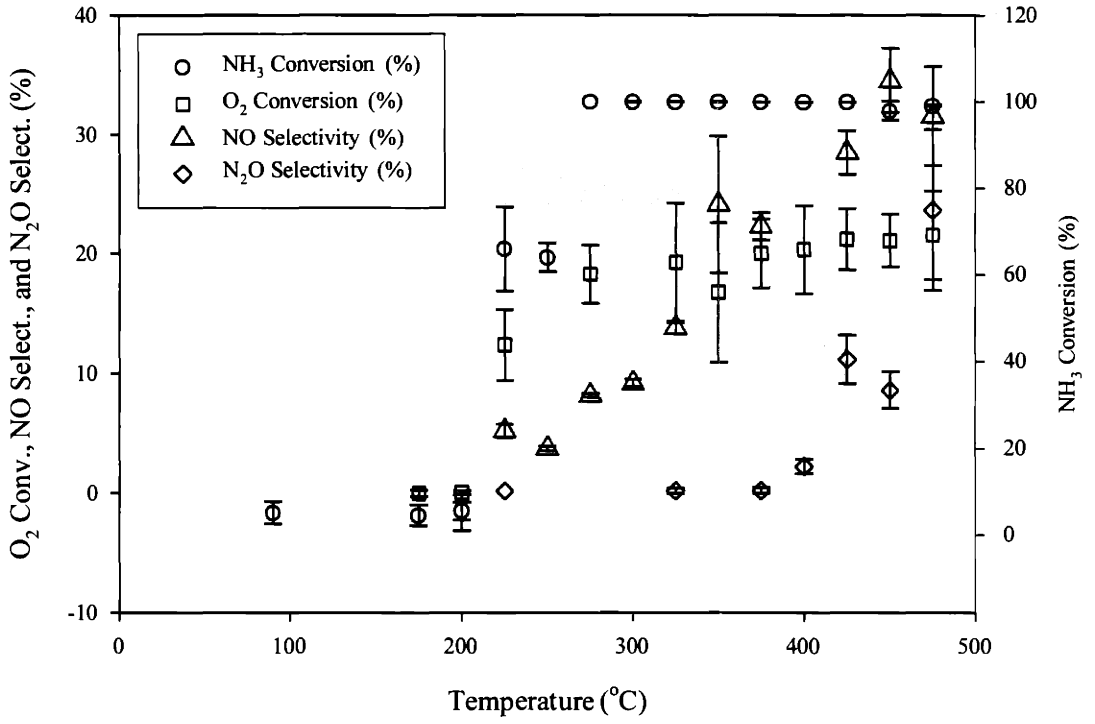

Figure 8-11. Ammonia oxidation reaction data versus temperature[12] for microreactor ACT-G3-7 channel A with a feed gas flow rate of 4.0 ml/min. The feed composition was 8.8% ammonia, 25.6% oxygen, 6.9% argon, 14.3% krypton, and the balance helium. This microreactor was placed in Reactor Board 1. Error bars represent the 95% confidence interval of each value.

[12] Closed-loop temperature control was used for this experiment, and each heater was given the same set point temperature.

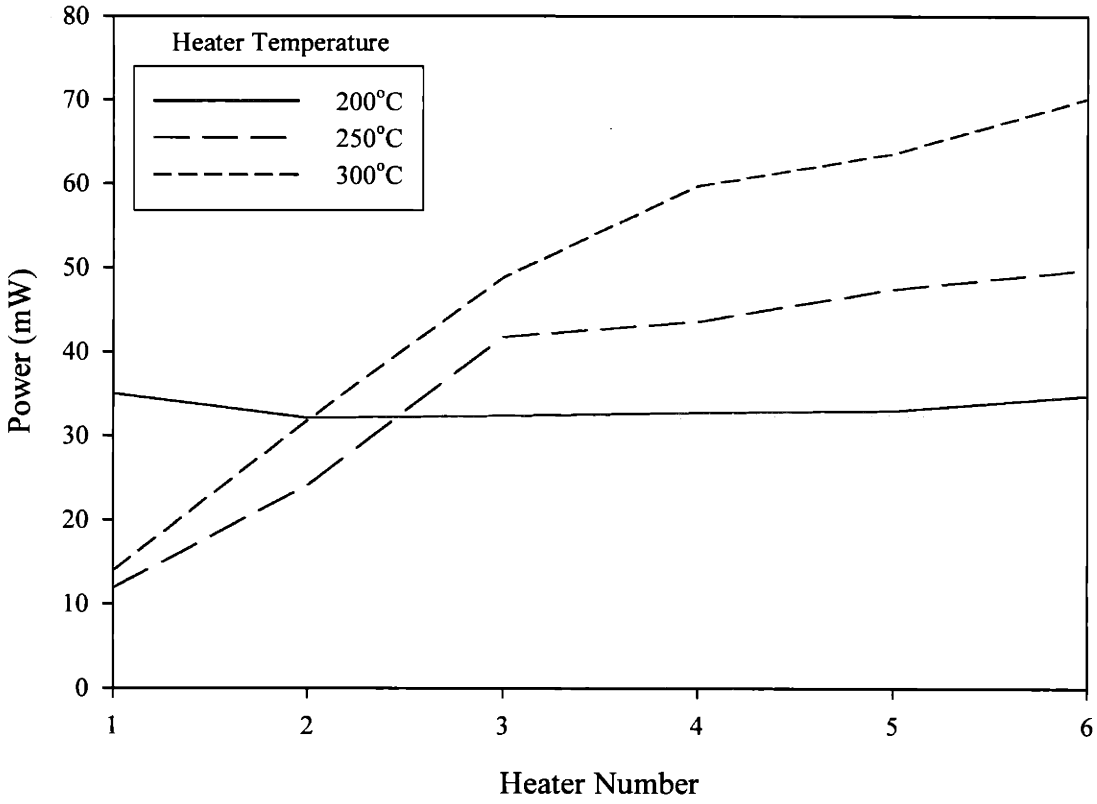

Figure 8-12. Power profile of the microreactor heaters for 200°C, 250°C, and 300°C.

Conclusions

The testing of the AIMS revealed some minor problems in the mechanical layout of the components. This made diagnosing and repairing problems difficult since direct access to most components was limited. However, the biggest difficulty in its operation was the Redwood Microsystems MEMS valves. These valves were not very robust and required component replacement on many occasions. In addition, the MFC's, when they were functioning, did not behave similar to conventional MFC's. This increased the difficulty of setting up the system for testing. Despite these obstacles, the system automation did make the AIMS safe, and easy to use. It was tested with the methane oxidation and ammonia oxidation reactions. Because of temperature limitations of the microreactors used in this

scale-up system, methane conversion was generally less than 10% for the methane oxidation reaction. Subsequently, ammonia oxidation was studied because of prior success in working with this reaction. This allowed exploration of the AIMS over a wide variety of conversions of ammonia. Closed-loop PID temperature control was successfully tested on this reaction system. Overall, the AIMS functioned comparably to the conventional catalyst test stations used at DuPont. Individual reactors could be started or shut-down independently of the other reactors in the system. In addition, the safety systems responded appropriately during testing and prevented the occurrence of any safety incidents during this project.

References

1. Srinivasan, R., Hsing, I.-M., Berger, P.E., Jensen, K.F., Firebaugh, S.L., Schmidt, M.A., Harold, M.P., Lerou, J.J., and Ryley, J.F. (1997) "Micromachined reactors for catalytic partial oxidation reactions", *AIChE Journal,* **43**(11), pp. 3059-3069.

2. Srinivasan, R. (1998) *Microfabricated Reactors for Partial Oxidation Reactions*, Ph.D. Dissertation at the Massachusetts Institute of Technology, Cambridge, MA.

3. Delaney, T.M. and Mills, P.L. (1999) "Multidimensional process gas chromatography based on a single GC with dual ovens", Presented at 38th Annual Eastern Analytical Symposium, Somerset, NJ, 15, 1999, Gas Chromatography Poster Session, Poster 71.

4. Nicole, J.F., Mills, P.L., and Delaney, T.M. (2000) "Multidimensional on-line process gas chromatography based on a single GC with two independently controlled ovens", Presented at AIChE 2000 Annual Meeting, Los Angeles, November 14, 2000, Session on Lab and Pilot Scale Instrumentation, Paper 276d.

5. Browning, L.C. and Watts, J.O. (1957) "Interpretation of areas used for quantitative analysis in gas-liquid partition chromatography", *Analytical Chemistry,* **29**, pp. 24-27.

6. Craats, F. (1958) *Gas Chromatography*, Academic Press, New York.

CHAPTER 9
CONCLUSIONS

Construction of the first demonstration scale-up microreactor system was successfully completed. Previous systems integration work in the area of microreaction technology has only focused on building components that can be easily incorporated into systems. No prior work had demonstrated the construction of a microreactor system with integrated fluidic components and control system. The Automated, Integrated Microreactor System (AIMS) had four microreactor channels that could be independently controlled along the dimensions of catalyst temperature and reactor feed flow rate. The fluidic control components, the microreactors, and their associated electronics were housed in a standard CompactPCI chassis measuring 19" × 15¾" × 11¾". The gas analysis and sampling systems were located outside of this chassis and were not miniaturized in this project. Control of the AIMS was accomplished through two National Instruments (NI) PXI chassis, one with an embedded controller operating under a real-time Operating System (OS). A separate component, the Human-Machine Interface (HMI) allowed the operator to quickly monitor and change the systems Process Variables (PV's). In addition, the HMI functioned as the system data logger.

The components of the AIMS were mounted on custom-made Printed Circuit Boards (PCB's) that were inserted into the CompactPCI chassis. The AIMS PCB's consisted of a 1) Temperature Controller Board, 2) a Feed Gas Mixing Board, 3) two Reactor Boards, and 4) two microreactor Heater Circuit Boards. The Temperature Controller Board had five

conventional CAL temperature controllers that were used to maintain the temperature of the heated transfer lines inside the system chassis. The Feed Gas Mixing board controlled the composition of the feed gas for all four microreactor channels. This board directed the flow of three gas streams to make-up the reactor feed gas. These streams were oxygen, a fuel, and a diluent.

Redwood Microsystems MEMS valves were used to control the gas flow in the AIMS chassis. These microvalves were packaged in a Redwood Flow Manifold that consisted of a Mass Flow Controller (MFC) with two Shut-Off Valves (SOV's) located upstream of the MFC and one SOV located downstream of the MFC. The SOV's upstream of the MFC were used to direct either process gas or purge gas to the valve. The SOV downstream of the MFC was used to isolate the Flow Manifold from other downstream components as needed. There were three Redwood Flow Manifolds on the Feed Gas Mixing Board.

The Reactor Boards consisted of two Redwood Flow Manifolds, which were used to control the feed gas flow rate to the two microreactor channels. Because the Redwood Flow Manifolds could direct purge gas to the microreactor channel and isolate it from the rest of the system, a channel could be easily shutdown or started up without disturbing the operation of the other microreactor channels (one on this board, and two on the other Reactor Board). The Reactor Board contained one microreactor die with two independent reaction channels. Fluidic and electrical connections to this die were made with a Texas Instruments DieMate™ socket, which was slightly modified to allow the fluidic connections. In addition, the Reactor Board also housed the electronic circuits needed to measure the resistances of the microreactor Resistive Temperature Devices (RTD's). The electronics needed to provide power to the microreactor heaters were housed on a separate board, the Heater Circuit Board.

Electrical connections between the system boards in the AIMS chassis were accomplished through a standard telephony backplane, rear I/O cards (mounted in the backside of the chassis), and ribbon cables. The analog and discrete I/O signals were connected to the system through shielded cables connected to the rear of the AIMS chassis. Where possible, standard NI cables were used for signal transmission. These signals ultimately led to the NI PXI controller system.

Control of the AIMS was done through two NI CompactPXI chassis with the appropriate PXI cards installed. One chassis contained an embedded controller, which was a 700 MHz Pentium™ III processor. This control system could operate under Windows™ or Pharlap, a deterministic real-time OS. The Pharlap OS was used for controlling the AIMS since guaranteed execution of the system control loop in a specified time period was needed for safety reasons. The control program, which ran on the embedded controller, was custom developed for the AIMS using LabVIEW 6.0.3 RT. The control program monitored and implemented the I/O signals associated with the AIMS chassis. As part of this monitoring, it examined the PV's to ensure they were within safe bounds. If a PV was outside of this range, an interlock would be engaged to return the system to a safe state. In addition, the controller allowed automatic PID control of the microreactor heater temperatures (24 PID loops in total). The fastest execution rate of the control loop was found to be 500 Hz. Rates above this level resulted in the loss of data communications with the HMI.

A HMI was developed to allow the system operators to view and change the PV's in the AIMS chassis. The HMI ran independently of the embedded control program with TCP/IP communications used to transfer data between these components. The HMI allowed easy access to the system data and convenient entry of system control parameters. In

addition, the HMI was responsible for logging the system data in an ODBC compliant database. The HMI was written in LabVIEW 6.0.2 with the Datalogging and Supervisory Control (DSC) module installed.

The AIMS was tested with methane oxidation and ammonia oxidation. Because of temperature limitations of the microreactor used in the AIMS, conversion of methane was less than 10% for all of the experimental conditions obtainable for methane oxidation. Under these conditions only small concentrations of carbon monoxide were detected in the reaction products with selectivities limited to less than 10% on a carbon basis. Ammonia oxidation was subsequently studied since complete conversion of ammonia was achievable with the microreactor used in the AIMS. At 200°C almost no ammonia was consumed by reaction, but complete consumption was found at 300°C. Nitric oxide production varied from less than 5% selectivity at 250°C to about 30% selectivity at 500°C on a nitrogen basis. Nitrous oxide production was observed starting at about 400°C and reached as high as 20% selectivity at 500°C on a nitrogen basis. These results corresponded well with previous experiments with the T microreactor at MIT and experiments with conventional ammonia oxidation reactors reported in the literature.

The AIMS is the first scale-up microreactor system comprised of multiple reactors operating in parallel, integrated into a system that uses MEMS valves to control fluid flow in the system. It is similar in design and function to industrial catalyst testing systems with multiple reactors running in parallel. Although the number of reactor channels in this system was limited to four for demonstration purposes, the methodology developed here can be applied to make larger parallel systems. More importantly, the integration concepts implemented in this work show the potential for miniaturization of laboratory reactor

systems. It also validates the idea of operating multiple microreactors in parallel to produce chemicals. The insights gained during this project should further push this concept to becoming a commercial reality.

Recommendations for Future Work

One of the main lessons illustrated in this project is the necessity for the area of microreactor research to be expanded to include the study of other miniaturized or MEMS components for use in conjunction with microreactors. For example, the on/off and proportional microvalves used in this project were a point of constant difficulty. Although MEMS microvalves have been around for more than a decade, very few designs appear appropriate to microreactor applications. This is illustrated by the fact that only one company produces commercial MEMS valves for use in industrial fluid control components (Redwood Microsystems). Microreactor researchers clearly need to focus on producing robust on/off and proportional microvalves that can operate under a variety of process conditions, such as high pressure, with minimal power requirements.

In addition to the area of microvalves, miniaturized product analysis systems are key to advancing the field of microreactor systems. This area has received more attention since it also applies to the field of micro-Total Analysis Systems (μTAS). The near commercial release of devices suitable for use in the chemical industry is extremely promising. The potential for large volume production for standard uses makes it likely that these components could one day be incorporated into microreactor systems for process monitoring and control. This would result in very compact chemical systems that would only need to be interfaced with external control equipment for operation.

The most underestimated challenge of building the AIMS was control system development. The large number of I/O signals that needed to be transferred between the AIMS chassis and the NI PXI control chassis increased the complexity of the system design. In addition, this correspondingly increased the number of data acquisition boards needed for the PXI controller. This raised the price of the controller, but not above levels of controllers for similar conventional reactor systems. Similarly, the control software developed for the embedded controller required more than 40 hours of debugging due to its complexity. Nonetheless, additional features would still need to be added to make the software robust enough for commercial release.

The solution to these problems may lie in distributing the signal processing and control throughout the AIMS chassis. In particular, the use of a digital communications protocol in the backplane of the chassis to transfer data would make the system easier to expand and reduce the amount of wiring between the AIMS chassis and the NI chassis. Ultimately, it would be ideal for all of the analog signals exiting the PC boards of the AIMS to be converted into a digital format. This would increase the flexibility of the system tremendously, and wiring limitations would not interfere with plans to increase the number of components. A further step would be to implement local control algorithms that would operate independently of the master controller. These slave controllers could be responsible for tasks such as temperature regulation of the microheaters. The master controller would then be responsible for monitoring the slave controllers and aggregate this information to obtain total system performance.

Although these ideas would be difficult to implement for a single prototype system, they are not beyond the capabilities of existing technology. The problem is in identifying

applications that could immediately benefit from this technology, and whose demand is significant enough to reduce the cost per system to an acceptable level. Ideally, the solutions currently available for this application would be lacking enough that changing to an untried technology is economically attractive. By moving into niche application areas, the volume of microreactor systems could be steadily increased, resulting in reduced cost, and more importantly, customer acceptance of the technology[1,2]. The question now remains in identifying and pursuing such opportunities.

References

1. Moore, G.A. (1991) *Crossing the Chasm: Marketing and Selling High Tech Products to Mainstream Customers*, Harper Business, New York.

2. Moore, G.A. (1995) *Inside the Tornado: Marketing Strategies From Silicon Valley's Cutting Edge*, 1st ed, Harper Business, New York.

APPENDIX
AIMS PROCESS HAZARDS ANALYSIS

Document History

This document was created for evaluation of the safety aspects of the DARPA Microreactor System. The process hazards review of the Multi-Stage p-Xylene Oxidation Unit and the process hazards review of the vinyl acetate monomer oxidation unit were used as a guideline for content and layout.

Origination Date: July 12, 2000
Author: David J. Quiram

Modifications:
July 19, 2000 Modification of SOP 9, Line Break Procedure. DJQ

August 21, 2000 Modifications made according to recommendations from review by Kathy A. Saturday. DJQ

May 1, 2001 Modifications made to address additional items with the constructed system. SOPs modified and detail added to address operation of the HMI and to clarify operating instructions.

Objective

The purpose of this system is to demonstrate the operation of multiple microfabricated reactors running in parallel for a heterogeneously catalyzed gas phase reaction. Furthermore, the completed system is automated for minimal operator intervention and is designed to be safe. The construction of this system demonstrates the packaging of microfabricated chemical reactors in a scalable fashion, the fluidic and electrical interconnections of reactor networks, and the operation of the microreactor sensing and

control schemes. This work is sponsored by the DARPA MicroFlumes Program[1] under a joint contract between MIT and DuPont.

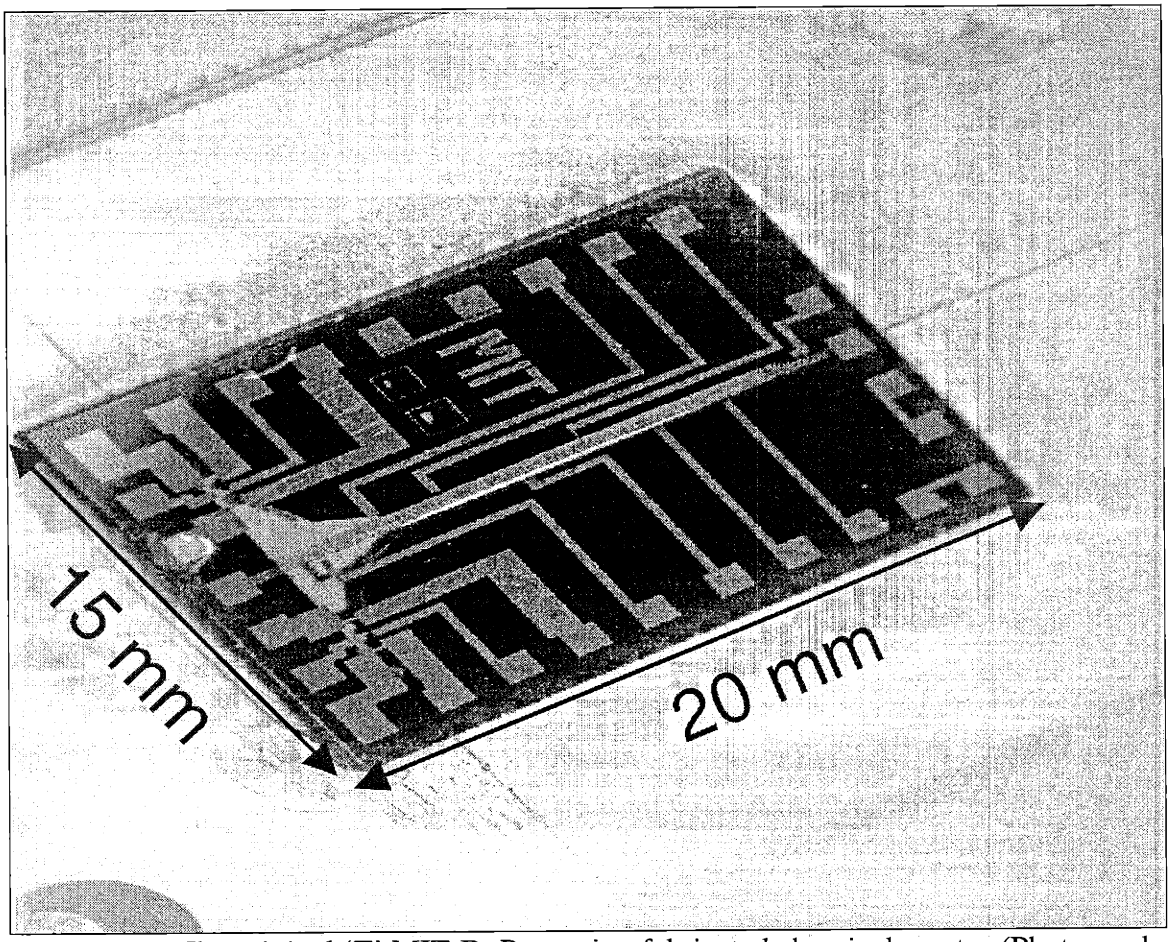

Figure A-1. The original 'T' MIT-DuPont microfabricated chemical reactor (Photograph by Felice Frankel).

Process Description

The core of this system is a silicon microfabricated reactor that replaces the conventional ¼" tube reactors of the MARS units. This microfabricated reactor design is based on a thin-film device originally developed at MIT by funding through a DuPont grant

[1] Defense Advanced Research Projects Agency (DARPA), Microsystems Technology Office, MicroFluidic Molecular Systems (MicroFlumes), Abraham Lee (Program Manager), contract

[1]. This device is shown in Figure A-1. Although the design of microreactors[2] is not an objective of this program, considerable detail is given on the MIT-DuPont microreactor and its known operating characteristics. This information is used to analyze the hazards in the DARPA Microreactor System.

The DARPA Microreactor System (DARPA MS) described in this PHA is designed to be functionally equivalent to a conventional heterogeneous gas phase catalyst testing system, such as MARS II or MARS III. These systems are comprised of 1) a bank of Mass Flow Controllers (MFC's) to mix the feed gas for the reactors; 2) a bank of reactors and MFC's for individual reactor control; and 3) a feed and product gas analysis system. A block diagram of this structure is shown in Figure A-2. The difference in the DARPA MS is the use of MicroElectrical Mechanical Systems (MEMS) components such as microvalves and micro-MFC's to replace the conventional components of the MARS units. Because the MEMS components do not always have the same flexibility or operating characteristics as their conventional counterparts, changes have been made where necessary to the MARS layout. In addition, the MIT-Dupont microreactors are highly integrated in that they include sensing and actuating capabilities through micro-heaters and micro-temperature sensors. These devices require electronic circuitry, and this results in the final unit resembling an electronics chassis with tubing for gas handling. The best practices of the MARS units developed over the past decade of their operation are used in this system where appropriate.

---

number F30602-97-2-0100.

[2] The use of the term 'microreactor' in this PHA refers to microfabricated chemical reactors and not to the small, but conventionally fabricated tubular reactors currently used in the MARS units.

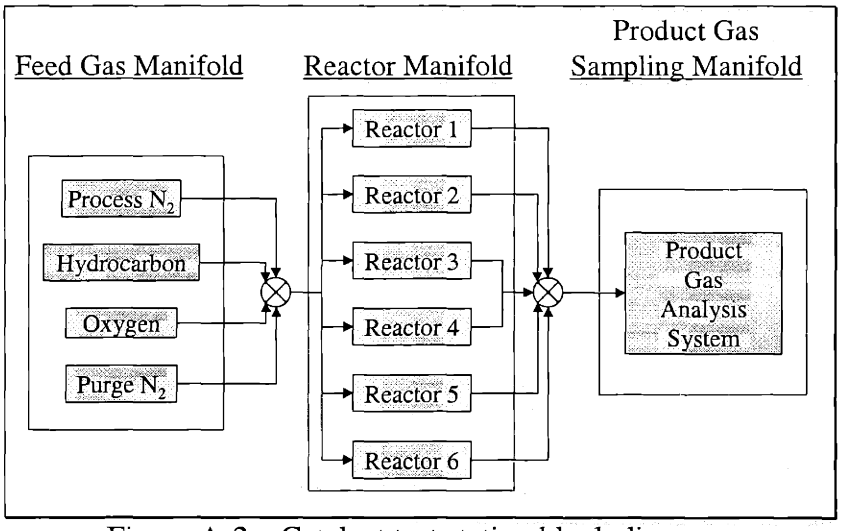

Figure A-2. Catalyst test station block diagram.

Microreactor Design

The DARPA Microreactor System utilizes a heterogeneous, gas-phase microreactor design developed at MIT. This device has a single channel with integrated heating and temperature sensing. Figure A-3 shows the top and cross-sectional views of the reactor, which has a reactant inlet and product outlet on opposite ends of the channel. The cross-section shown in Figure A-3 illustrates the use of a silicon nitride membrane to separate the heaters and temperature sensors from the reaction channel. The 1 μm thick membrane is impermeable to gas flow but provides an intimate thermal contact between the catalyst on one side of the membrane and the heaters on the opposite side. The bottom of the channel is sealed by a Pyrex® 7740 layer that is anodically bonded to the silicon die. The Pyrex layer has drilled holes for the gas inlet and outlets. The fabrication method for this device is similar to the T microreactor described previously[1].

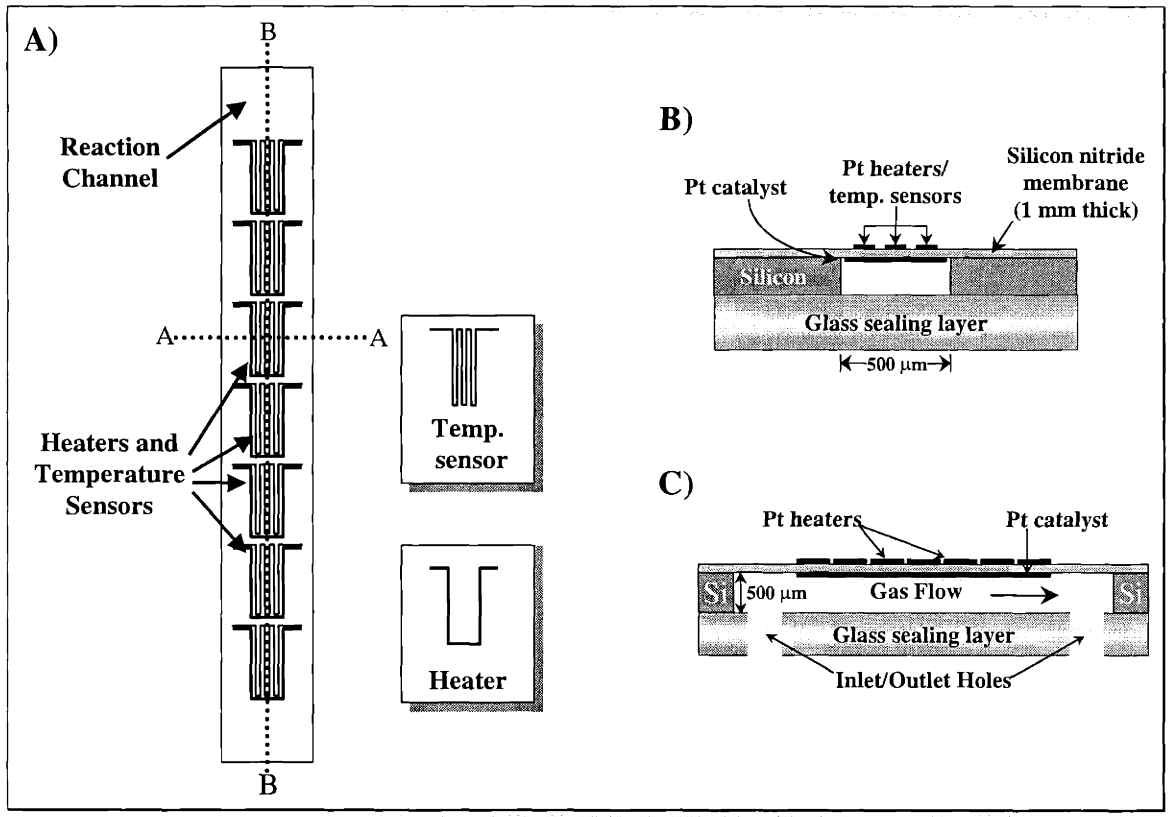

Figure A-3. MIT-DuPont scale-up slot microreactor. A) Top-view B) Cross-sectional view AA C) Cross-sectional view BB.

This reactor differs from the original T microreactor in that reactant mixing takes place off-chip in the gas feed manifold. This was done to 1) improve membrane stability; 2) allow direct sampling of the reactant mixture into the product analysis system; and 3) to reduce the overall reactor size. The reaction channel is 0.5 mm wide, 0.5 mm deep, and 11 mm long. It has seven distinct zones for heating and temperature sensing. Each heater is 0.94 mm in length and the temperature sensors are 0.77 mm long. The size and number of heater and temperature sensor elements was chosen to give more resolution in the reactor temperature profile and allow greater control over this profile. Smaller structures were not used because there is a space constraint on the die for the metal lines connecting the

structures to the bond pads. An enlargement of the heater and temperature sensor configuration is shown in Figure A-4.

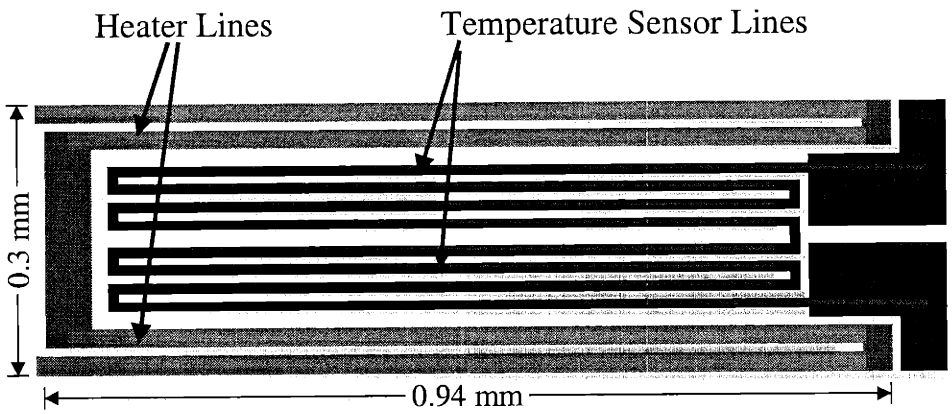

Figure A-4. Enlargement of the heater and temperature sensor configuration.

Microreactor Operation

The operation of the T microreactor has been described in several previous publications, and these results are summarized here[1-6]. The reactions that have been demonstrated in this unit are 1) carbon monoxide oxidation, 2) ammonia oxidation, 3) ethane oxidation, and 4) hydrogen oxidation. Platinum was typically used as the catalyst in the microreactor, but efforts have been made to deposit other materials.

The catalyst deposition technique most commonly used was electron beam evaporation. Because platinum adheres poorly to silicon and silicon nitride surfaces, a 10 nm layer of titanium was first deposited on the silicon nitride membrane. 100 nm of Pt was then placed on the titanium layer[1]. Wet deposition techniques using drying and electrolysis have also been used to deposit platinum. These techniques are better for catalyst deposition since the Pt surface is rough with more area for reactions. However, only electron beam evaporation was used to deposit Pt for the microreactors used in the DARPA Microreactor

System. This was done because of the difficulty of achieving reproducible Pt layers using the wet deposition methods.

Results with the oxidation reactions listed above showed that the reactor could be operated safely within the entire composition range of these highly exothermic reactions. This was due to the small reactor volume and the high rate of heat removal from the reaction zone, which prevented the reaction from thermal runaway. Bifurcation behavior was observed in the microreactor, but these reactions did not run autothermally. Thus, operation in the upper-steady state was well controlled since the power to the heaters, the feed gas composition, and the feed gas flow rate were used to control the reaction.

During these characterization tests, some reactors failed due to high membrane temperature. This occurred if stoichiometric mixtures of reactants were used. In this case, the energy released during reaction, raised the membrane above its failure temperature, which is approximately 650°C[1]. For the ammonia oxidation reaction, the membrane also failed during the initial light-off stage when the catalyst was fresh. During the first light-off, the catalyst surface was restructured by chemical etching/deposition and temperature. This produced a much rougher surface that was significantly more active for ammonia oxidation. Thus, during light-off the high power used to initiate the reaction on the fresh catalyst surface would give the reactor too much energy after the catalyst restructured, which occured almost instantaneously. This required the operator to immediately reduce the heater power after ignition to prevent the membrane from rupturing.

Although the membrane rupture destroys the microreactor, this failure is safe in that it does not release enough energy to cause injury or equipment damage (other than the microreactor itself). During operation at MIT, no serious or potentially serious explosions or

deflagrations occurred. In addition, when the membrane ruptures, the heater power lines are simultaneously broken. Thus, power is immediately removed from the reaction device. In tests with the original T reactor, some membrane failures occurred locally so that only part of the membrane was broken. Heaters and temperatures sensors outside of the broken region were still able to function. However, the partial failure of the membrane was easy to detect from the break in at least one of the heater lines and temperature sensors. Furthermore, the rupture generally progressed through the entire membrane in a few minutes. The system controller will monitor for complete or partial membrane failure by testing for an open circuit in any of the heater or temperature sensors. A system interlock will occur that removes power and turns off reactive gas flow if a break is detected.

The most significant risk from a microreactor failure is from the gas release that occurs after the membrane rupture. However, safety measures can be taken to ensure that the flow of reactants is immediately turned off in the case of a reactor failure. Furthermore, the system will be operated in a ventilated enclosure to ensure the reactant mixture is immediately diluted to a safe level after release from a membrane rupture. The system chassis is ventilated by two fans that provide an estimated flow rate of 176 cfm of air, and the chassis will be placed inside a hood. All gas containing equipment will be inside the enclosure except for gas supply cylinders, which will be stored in ventilated cylinder closets adjacent to the hood or in the building cylinder bay.

To minimize the risk of accidents, the DARPA Microreactor System is NOT intended to run with explosive mixtures of reactants. Although the microreactors may operate safely with explosive mixtures, there is always the possibility of these mixtures accumulating in an area in or outside the system.

As an additional safety measure, the microreactor heater control circuit has been modified to help prevent reactor failure during light off. The original circuit used for the experiments at MIT was current controlled. During ignition, the temperature of the Pt heater lines increased resulting in an increase in their resistance. Since current was held constant by the circuit, this resulted in an increase in power going to the heater. By controlling the voltage going to the Pt heaters, this problem is avoided. In this case, increasing the heater resistance requires a decrease in the heater current to maintain constant voltage. Thus, the power going to the heaters decreases as the heater temperature increases.

Process Chemistry

Because of the small reactor volume and channel length, only reactions with high rates can be studied effectively. For that reason, past work has focused on complete and partial oxidation reactions as discussed in Section II B. The reactions of interest to verify the operation of the DARPA Microreactor System are

1) Carbon monoxide oxidation
2) Ammonia oxidation
3) Methane oxidation

The above reactions will be catalyzed by a platinum, thin-film deposited on the silicon nitride membrane as described in Section II B. These three reactions have been well characterized on platinum and the following subsections describe the chemistry in greater detail. All chemistries will be run at atmospheric pressure since the microreactor membrane cannot survive pressurization.

Carbon Monoxide Oxidation

This reaction proceeds readily on platinum with both carbon monoxide and oxygen adsorbing onto the platinum surface. The overall reaction chemistry is

$$CO + \frac{1}{2}O_2 \rightarrow CO_2 \qquad (H_{rxn}^{\circ} = -67.6 \text{ kcal/mol CO})$$

Engl and Ertl[7] have reviewed this reaction and have listed the following relevant reaction steps:

$$CO \underset{k_2}{\overset{k_1}{\Leftrightarrow}} CO_{ad} \qquad (1)$$

$$O_2 \xrightarrow{k_3} 2O_{ad} \qquad (2)$$

$$O_{ad} + CO_{ad} \xrightarrow{k_4} CO_2 \qquad (3)$$

$$O_{ad} + CO \xrightarrow{k_5} CO_2 \qquad (4)$$

$$O_2 + 2CO_{ad} \xrightarrow{k_6} 2CO_2 \qquad (5)$$

No byproducts are expected from this chemistry.

Ammonia Oxidation

The production of nitric oxide from ammonia using a platinum catalyst, known as the Ostwald process, has been used since 1906 for nitric acid manufacture[8]. In this scheme, ammonia oxidation gives nitric oxide as the desired product with nitrogen and nitrous oxide as undesired by products. The overall chemistry for this reaction is

$$4NH_3 + 5O_2 \rightarrow 4NO + 6H_2O \qquad (H_{rxn}^{\circ} = -69.9 \text{ kcal/mol } NH_3)$$

$$2NH_3 + O_2 \rightarrow N_2O + 3H_2O \qquad (H_{rxn}^{\circ} = -81.7 \text{ kcal/mol } NH_3)$$

$$4NH_3 + 3O_2 \rightarrow 2N_2 + 6H_2O \qquad (H_{rxn}^{\circ} = -91.5 \text{ kcal/mol } NH_3)$$

This chemistry has been extensively studied in the microreactor[1,6]. Conversion of ammonia depends strongly on flow rate due to mass transfer limitations in the microreactor.

Selectivity to nitric oxide typically ranges from 85% to 35% and depends on temperature and flow rate. Nitric oxide and nitrogen are the main products of the reaction. Nitrous oxide was formed in significant quantities (~15% selectivity) at temperatures less than 350°C. It was completely absent at temperatures greater than 400°C.

Methane Oxidation

The use of short contact time reactors for the partial oxidation of methane to produce synthesis gas gained considerable attention during the last decade. In this system, the production of syngas, which is slightly exothermic, competes with the complete oxidation of methane, which is highly exothermic. The overall chemistry with the heats of reaction is given below.

$$CH_4 + 2O_2 \rightarrow CO_2 + 2H_2O \qquad (H_{rxn}^{\circ} = -212.9 \text{ kcal/mol } CH_4)$$

$$CH_4 + 1/2O_2 \rightarrow CO + 2H_2 \qquad (H_{rxn}^{\circ} = -8.6 \text{ kcal/mol } CH_4)$$

$$H_2 + \frac{1}{2}O_2 \rightarrow H_2O \qquad (H_{rxn}^{\circ} = -57.8 \text{ kcal/mol } H_2)$$

For operation in the microreactor, it is critical to adjust the flow rate and feed gas composition to prevent overheating of the reactor from the complete combustion reaction. Little experimentation has been done with this system in the microreactor. Testing is needed to examine the feasibility and to determine temperature control capabilities. Schmidt and coworkers typically run this reaction autothermally at ~1000°C with a methane/oxygen ratio between 1 and 2. However, by increasing the methane/oxygen ratio the complete combustion reaction is limited by lack of oxygen resulting in a decrease in operating temperature[9].

Material and Energy Balances

The reactions listed in the previous section are very fast over platinum, so there will be significant mass transfer limitations in the microreactors. Thus, conversion will be strongly dependent on the feed conditions. The typical feed flow to a microreactor will be 20 sccm. For the ammonia oxidation reaction, operating under mass transfer limitations with ammonia as the limiting reagent, an 80% conversion of ammonia is achieved for this flow rate[6]. Similar conversions are expected for carbon monoxide oxidation and methane oxidation since both of these reactions will run under mass transfer limitations. Estimates for selectivity are based on previous experimental data for the microreactors and data available in literature. The following subsections give the material and energy balances for each of the reactions described in Section II C.

Carbon Monoxide Oxidation

The flammability of carbon monoxide, oxygen, and nitrogen mixtures is best controlled through the carbon monoxide concentration. Coward and Jones[10] reported that mixtures with less than 12.5% carbon monoxide did not form explosive mixtures in a tube 6 feet in length and 2 inches in diameter. In the DARPA microreactor system, the tubing diameter is substantially smaller, so this should be a safe upper carbon monoxide limit.

A typical reactor feed composition would be 10% carbon monoxide, 10% oxygen, 10% nitrogen, and 70% helium. For four reactors with a feed flow rate of 20 sccm, the total daily flow rate is 59.6 g/day. Table A-1 lists the feed flow rates and composition along with the predicted product gas composition.

Compound	Feed Rate (sccm)	Feed Concentration (molar)	Product Concentration (molar)	Probable Range of Product Concentration[3] (molar)
Carbon monoxide	2	0.1	0.0208	0.0 to 0.0526
Oxygen	2	0.1	0.0625	0.0526 to 0.0781
Nitrogen	2	0.1	0.1042	0.1026 to 0.1053
Helium	14	0.7	0.7292	0.7179 to 0.7368
Carbon dioxide	0	0.0	0.0833	0.0526 to 0.1053

Table A-1. Feed composition and flow rates that will be used for CO oxidation testing along with predicted product concentration. The table gives a typical feed composition and flow rate, but other conditions may be used that are in the non-flammable regime.

With carbon monoxide being the limiting reagent the worst possible case for heat generation is the complete conversion of all carbon monoxide to carbon dioxide. Assuming the feed conditions given above, this results in the generation of 421 mW of heat to the membrane. Simulations used in the design of the latest version of the microheaters showed that the power requirement to raise the heater temperature to 300°C was 132 mW. Thus, to raise the entire length of the six active microheaters in the current reactor design requires approximately 792 mW (there is little interaction between adjacent heaters). Therefore, the 421 mW of heat that could be generated by the reaction would not raise the heated region of the reactor above 300°C, so there is little chance of overheating the device. Furthermore, this amount of power is not significant enough to raise the temperature of the entire reactor die or its mounting block, so no hazard is presented apart from the possibility of membrane rupture due to overheating.

Ammonia Oxidation

Less information is available about the flammability of ammonia than for carbon monoxide and methane. The literature indicates that the lower flammability limit for

[3] Probable concentration range assumes reactor flow rate can vary from 0 to 30 sccm. This

ammonia and air mixtures is 16% ammonia[10]. The lower limit for a mixture of ammonia with pure oxygen is 14.8%[10]. The compositions used for testing purposes will generally contain less than 21% oxygen, but the 14.8% LEL value will be used to add an additional margin for safety.

A typical reactor feed composition would be 10% ammonia, 20% oxygen, 20% nitrogen, and 50% helium. For four reactors with a feed flow rate of 20 sccm, the total daily flow rate is 80.7 g/day. The data of Srinivasan indicates that at this flowrate in the microreactor there is 80% conversion of ammonia with a 60% selectivity to the formation of NO[6]. In most experiments, no nitrous oxide was produced since the catalyst temperature was too high (see previous discussion). Table A-2 lists the feed flow rates and composition along with the predicted product gas composition.

Compound	Feed Rate (sccm)	Feed Concentration (molar)	Product Concentration (molar)	Probable Range of Product Concentration[4] (molar)
Ammonia	2	0.1	0.0196	0.0 to 0.0494
Oxygen	4	0.2	0.1137	0.1137 to 0.1605
Nitrogen	4	0.2	0.2118	0.2014 to 0.2439
Helium	10	0.5	0.4902	0.4739 to 0.4938
Nitric oxide	0	0.0	0.0471	0.0 to 0.0569
Nitrous oxide	0	0.0	0.0	0.0 to 0.0071
Water	0	0.0	0.1176	0.0730 to 0.1463

Table A-2. Feed composition and flow rates that will be used for ammonia oxidation testing along with predicted product concentration. The table gives a typical feed composition and flow rate, but other conditions may be used that are in the non-flammable regime.

---

corresponds to 50% to 100% conversion based on mass transfer limitations[11].

[4] Probable concentration range assumes reactor flow rate can vary from 0 to 30 sccm. This corresponds to 50% to 100% conversion based on mass transfer limitations[11]. The case for 50% conversion assumes the same selectivities as 80% conversion. For complete ammonia conversion, the same selectivities were used along with the assumption of only complete combustion of ammonia to nitrogen. The upper limit for nitrous oxide production was calculated assuming complete conversion of ammonia with 15% selectivity to nitrous oxide and 60% selectivity to nitric oxide.

With ammonia being the limiting reagent the worst possible case for heat generation is the complete conversion of all ammonia with oxygen to form nitrogen and water. Assuming the feed conditions given above, this results in the generation of 570 mW of heat to the heater membrane. This is close to the 792 mW that are needed to raise the membrane heaters to 300°C. Thus, the heater temperature should not be close to membrane failure temperatures if the complete combustion reaction occurs. In addition, this amount of power is still not significant enough to raise the temperature of the entire reactor die or its mounting block, so no hazard is presented apart from the possibility of membrane rupture due to overheating.

Methane Oxidation

According to the work of Schmidt et al.[9], the best conditions for the partial oxidation of methane occur between a methane to oxygen ratio of 1 and 2. Flammability data for methane, oxygen, and nitrogen mixtures indicates that flammable compositions of methane do not occur with less than 12.8% oxygen in a variety of geometric configurations. However, flammable compositions can be formed with as little as 5.3% methane[10]. Thus, it is better to keep the oxygen concentration below 12.8% and vary the methane concentration to achieve the appropriate ratio.

A typical reactor feed composition would be 10% oxygen, 20% methane, 20% nitrogen, and 50% helium. For four reactors with a feed flow rate of 20 sccm, the total daily flow rate is 72.0 g/day. The data of Schmidt and coworkers gives an oxygen conversion of 100% and a methane conversion of 66% for a methane to oxygen ratio of 2:1 with a platinum catalyst[11]. Since oxygen is the limiting reagent for this composition, an 80% conversion of oxygen is assumed. This is based on the reaction being mass transfer limited in the microreactor. Their data gives a carbon atom selectivity to carbon monoxide of ~95% and a

hydrogen atom selectivity to hydrogen of ~77%[11]. Actual selectivities and conversions are expected to vary since this data is based on the complete consumption of oxygen and their conversion is not mass transfer limited. Table A-3 lists the feed flow rates and composition for this reaction along with the predicted product gas composition.

Compound	Feed Rate (sccm)	Feed Concentration (molar)	Product Concentration (molar)	Probable Range of Product Concentration[5] (molar)
Methane	4	0.2	0.0831	0.0580 to 0.15
Oxygen	2	0.1	0.0177	0.0 to 0.0462
Nitrogen	4	0.2	0.1767	0.1717 to 0.20
Helium	10	0.5	0.4417	0.4292 to 0.50
Carbon monoxide	0	0.0	0.0942	0.0 to 0.1080
Carbon dioxide	0	0.0	0.0047	0.0031 to 0.05
Hydrogen	0	0.0	0.1442	0.0 to 0.1751
Water	0	0.0	0.0431	0.0281 to 0.10

Table A-3. Feed composition and flow rates that will be used for methane oxidation testing along with predicted product concentration. The table gives a typical feed composition and flow rate, but other conditions may be used that are in the non-flammable regime.

With oxygen being the limiting reagent the worst possible case for heat generation is the complete conversion of all oxygen with methane to form carbon dioxide and water. Assuming the feed conditions given above, this results in the generation of 1326 mW of heat to the heater membrane. This is significantly higher than the 792 mW that are needed to raise the membrane heaters to 300°C. Thus, the heater temperature could be close to membrane failure temperatures if the complete combustion reaction occurs. However, this amount of power is still not significant enough to raise the temperature of the entire reactor

[5] Probable concentration range assumes reactor flow rate can vary from 0 to 30 sccm. This corresponds to 50% to 100% conversion based on mass transfer limitations[11]. The case for 50% conversion assumes the same selectivities as 80% conversion. For complete oxygen conversion, the same selectivities were used along with the assumption of only complete combustion of methane.

die or its mounting block, so no hazard is presented apart from the possibility of membrane rupture due to overheating.

P&I Diagrams

The DARPA Microreactor System is functionally equivalent to the MARS units run in laboratory E262/100. Figure A-5 shows the piping diagram of the system. The process flows from left to right in the diagram. The process gas cylinders for the system are shown at the left except for the nitrogen purge gas supply and the helium gas supply. Three reactant gases are used during a run: a fuel, an oxidizer, and a diluent. The fuel gas in the Microreactor System is carbon monoxide, ammonia, or methane. The fuel will generally be diluted with nitrogen and helium. This is done both for safety reasons and to aid in the GC analysis methods. Helium is added to the fuel to dilute the mixture to safer level. In the case of ammonia, this also raises the condensation pressure of the mixture, which simplifies handling. Nitrogen is used as calibration gas usually, but another gas may be substituted for the ammonia oxidation reaction since nitrogen is also a product in this case. The oxidizer used is oxygen. The diluent used is helium or nitrogen. Single stage forward pressure regulators located on the gas manifold next to the DARPA Microreactor System control the upstream feed gas pressure. These regulators are in turn fed from two-stage pressure regulators on each of the gas supply cylinders. These pressure regulators are adjusted manually and must be set properly before startup.

The reactant feed mixture is controlled by a bank of MFC's that adjust the flow rate of each of the process gases. These are shown in the diagram directly after the cylinders and the feed gas pressure regulators. The reactor feed mixing takes place on the feed gas mixing board in the DARPA MS chassis. This board, shown in Figure A-6, consists of three

manifolds that control the process gas flow rates using a Redwood Microsystems[6] MEMS-Flow® MFC and three Redwood Microsystems normally closed microvalves. The top of the board houses the Redwood Microsystems components along with their control electronics that are placed on the main board as daughter and granddaughter cards. The bottom of the board has the fluidics manifolds for the Redwood components along with process transfer lines.

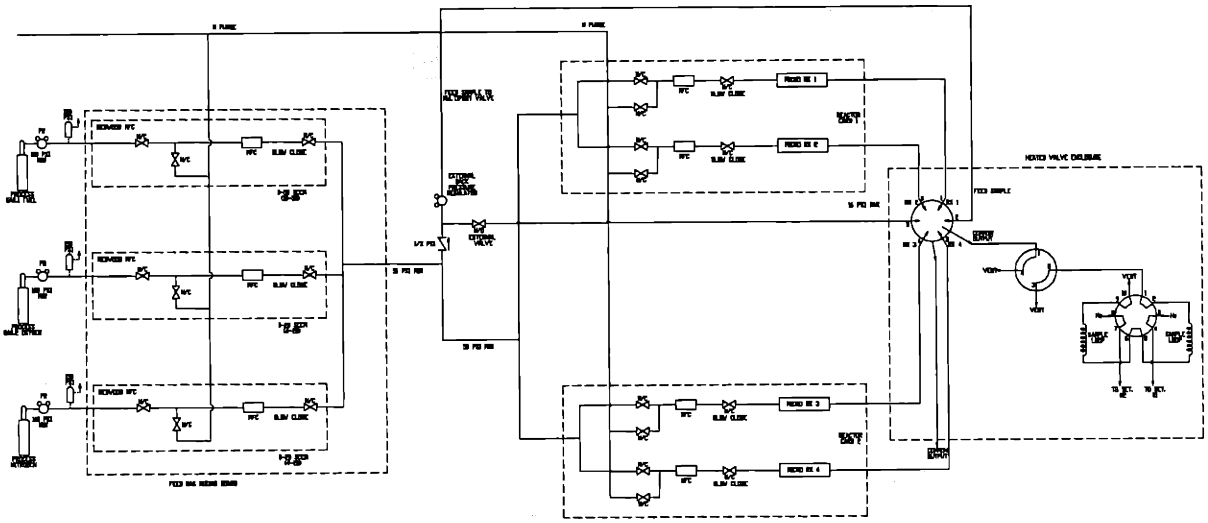

Figure A-5. Piping diagram of the DARPA Microreactor System

The MFC arrangement used on this board has two normally closed valves that are teed into the feed of a Redwood MicroSystems MEMS-Flow® MFC. One normally closed valve is for the process gas and the other is for the purge nitrogen gas. During startup and shutdown, the process gas valve is closed and the purge nitrogen gas valve is opened to remove any reactive gases from the system. There is another normally closed valve after the MFC that can be used to isolate the line from the rest of the system. Note that this

[6] Redwood MicroSystems, Inc., 959 Hamilton Ave., Menlo Park, CA, 94025, 650-617-1200.

arrangement is also used for the process nitrogen stream. This allows for the use of a second fuel stream if desired during later testing.

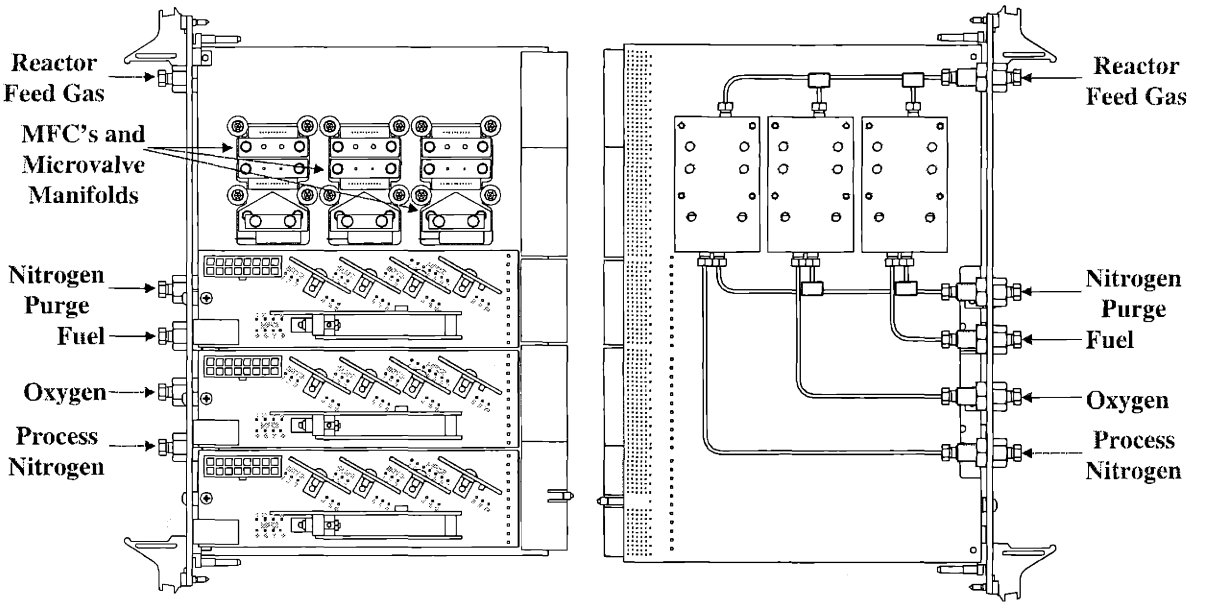

Figure A-6. Top (left) and bottom (right) views of the feed gas mixing board showing the Redwood Microsystems MFC/valve manifolds with electronics and piping scheme.

This system differs from the MARS units in that all the valves used are normally closed. Ideally, the system should purge itself with nitrogen if there is a power failure. Unfortunately, the Redwood MicroSystems microvalves are not available in a normally open configuration. To minimize the hazard during a power failure, two types of valves are used in the system: fast acting and slow acting. The fast acting valves close within one second of power loss and the slow acting valves close after two to three seconds of power loss. The normally closed valve after the MFC is slow acting while the ones upstream of the MFC are fast acting. This configuration allows the system to vent excess pressure during a power failure. The pressure downstream of the MFC is vented through the external normally open valve for the feed gas mixing board MFC's. The pressure downstream of the microreactor MFC's is vented by the sampling valve system that always has an open connection between

the microreactor and a vent leading directly to the hood exhaust. Although some process gas remains in the system the small volume of the lines and the rapid cooling of the microreactor heaters[7] helps to minimize the hazard of this situation. Another difference in the configuration of the MFC line is the absence of forward and back pressure regulators around the MFC's to control the pressure drop across the MFC. This arrangement does not work with the Redwood MicroSystems MFC's because they control flow by adjusting the pressure drop across a flow restrictor. Thus, their operation is sensitive to the inlet and exit pressures of the mass flow controller. In the Microreactor System the Redwood MFC's operate with fixed upstream and downstream pressures, but these are set by Redwood and are not normally adjusted during operation. The pressure regulators at the cylinders are used to control the upstream pressure, and the feed sample GO[8] back pressure regulator is used to control the downstream pressure.

After the feed gas mixing board, the feed gas stream is connected with the reactor boards, an external backpressure regulator, and an external normally open valve. The external components are isolated from the chassis using 1/3 psig check valves. One check valve is placed before the two-way vent valve, and the other check valve is located after the backpressure regulator. This prevents back flow of gases to the feed stream altering its composition, and reduces the possibility of oxygen from the atmosphere entering the feed and possibly forming an explosive mixture. After mixing, the reactant feed gas is split to two lines going to the two reactor boards. Figure A-7 shows the reactor board layout. Each reactor board has two MFC lines to control the flow going to each channel of the

[7] The microreactor heaters have a time constant of approximately 3 ms. They will cool down to the temperature of the DieMate manifold they are mounted on in less than 20 ms.
[8] GO Regulator, Inc., P.O. Box 3300, Corona, CA 92878, (909) 270-6304.

microreactor die (each die has two independently controlled reaction channels). The MFC lines are identical to the ones used for controlling the flow rate of the feed gases. Again, a slow acting normally closed valve is used to vent excess pressure in the event of a power failure. After the MFC and microvalve manifold, the feed gas flows to the microreactor manifold, which is heated to 160°C to prevent product condensation in the reactor and its mounting manifold. The microreactor is mounted in a Texas Instruments[9] DieMate® socket, which provides the electrical connections for the reactor die. The fluidic interconnections are made using a stainless steel manifold mounted in the DieMate socket as shown in Figure A-8. Further information on the DieMate socket and the modifications made to it can be found in section II F. The product transfer line after the reactor block is heat traced to the exit of the CompactPCI chassis.

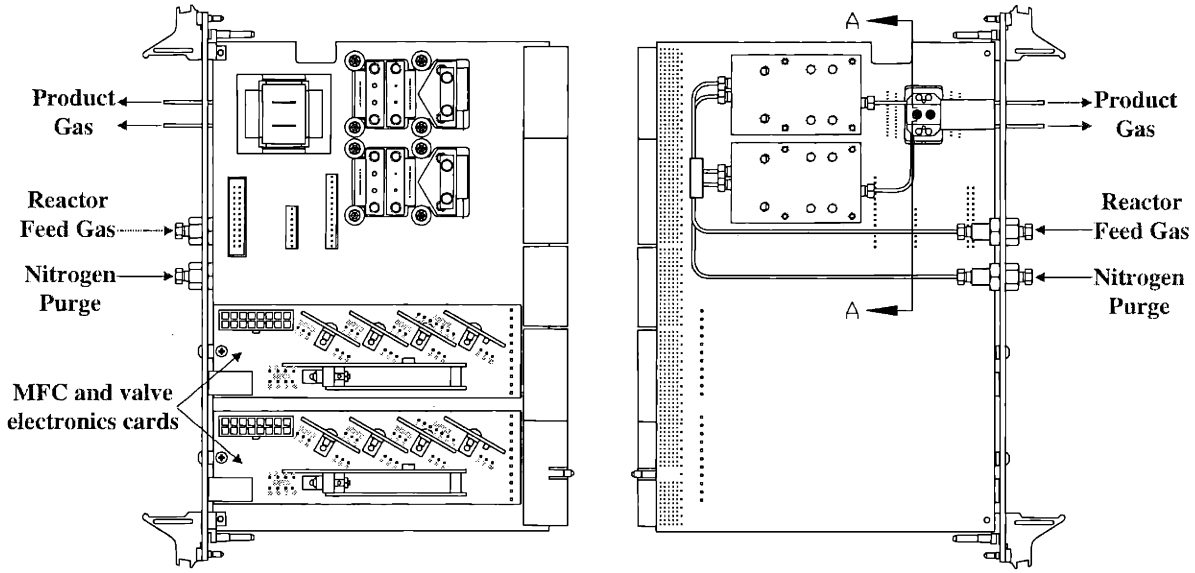

Figure A-7. Top (left) and bottom (right) views of a reactor board showing the Redwood Microsystems MFC/valve manifolds with electronics, the reactor mounted in a DieMate socket, and the piping scheme.

[9] Texas Instruments, 111 Forbes Blvd., MS 14-2, Mansfield, MA 02048, (508) 236-5216.

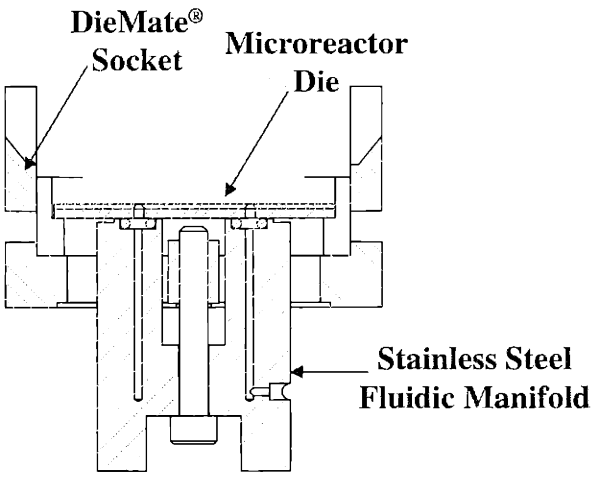

Figure A-8. Cross-section AA of the reactor board drawing in Figure A-7 showing the mounting of the reactor in the DieMate® socket and fluidic interconnection method used with the socket.

The gas sampling valve scheme is similar to the ones in the MARS units. A multiposition selector valve is used to select the reactor product stream or feed stream to be analyzed by the GC. A Valco[10] 16 port multiposition valve with microelectric actuator is used in the Microreactor System to reduce the amount of time the streams are deadheaded during the valve switch. The extra positions reduce the distance between the inlet ports, which reduces the switching time. The microelectric actuator is used because it is faster than the pneumatic actuator. It is also easier to operate and integrate with the system controller. Pneumatic actuation has been used in the past for the MARS units. The change to electric actuation should not increase any safety risk since the microelectric actuator uses a low voltage, 25 VDC, power supply. The multiposition valve selected has a separate exit stream for each line to prevent the possibility of back flow if a common exit was used. Check valves are not used after the reactors because they are extremely sensitive to pressure and can burst with as little as 7 psig of internal pressure[12]. The exit stream from the multiposition

[10] Valco Instruments Co. Inc., P.O. Box 55603, Houston, TX 77255, 800-367-8424.

valve goes to a four port valve that is used for sample loop pressure equilibration. The exit from the four port valves goes to a ten port valve that has two sampling loops, one for the FID and the other for the TCD on the GC. These valves are kept in a heated Valco enclosure operating at 200°C.

Another significant difference between the Microreactor System and the MARS units is the absence of electronic pressure transducers in the gas manifold. This limits the ability of the system to diagnose excess pressure in any of the gas streams. However, this should not be a problem since a microreactor will fail if the pressure begins to build up in a reactor line. Since clogging is most likely to occur after the reactor, this prevents the most likely area of over-pressurization. Pressure upstream of the reactors is controlled by the external back pressure regulator. If this fails, or is set improperly excess pressure could buildup in this part of the unit. However, this pressure will be limited to the pressure set at the single stage regulator on the DARPA MS gas manifold. These are set at 75 psia. These regulators will be chosen so that their maximum pressure does not exceed 150 psig. In addition, pressure relief devices will be put in place between the cylinder regulators and the gas inlet on the system chassis. These devices will activate at a pressure of 80 psig. The most pressure sensitive item besides the microreactors are the Redwood Microsystems microvalves and MFC's, which have a burst pressure of 250 psig. Thus, there will be a large safety factor to prevent over-pressurization in the feed mixing lines.

The system left of the multiposition sampling valve, excluding the feed gas cylinders, is enclosed in a Kaparel PS6090 CompactPCI size 6U chassis shown in Figure A-9. The chassis consists of a temperature controller board, a feed gas mixing board, two reactor

boards, and two heater driver circuit boards. Further information about the components of the DARPA Microreactor System can be found in the following section.

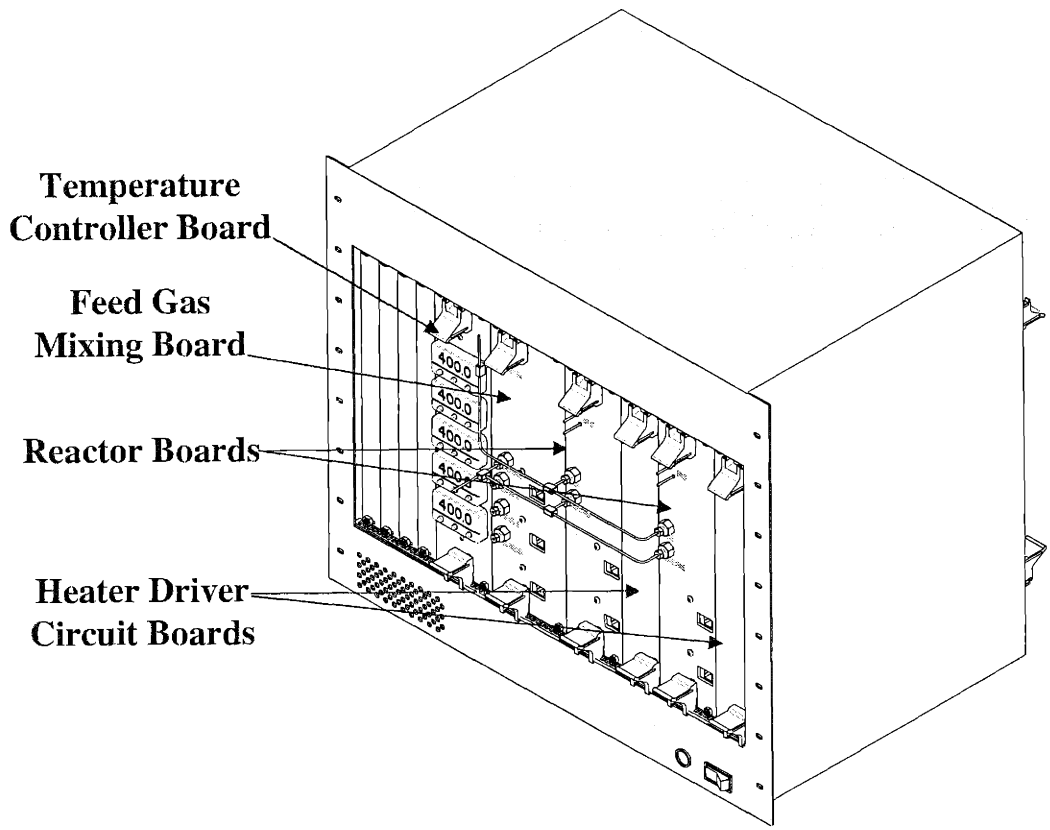

Figure A-9. DARPA Microreactor System chassis with boards.

Equipment Description

The microfabricated reactors used in the system are described above. The other MEMS components, the microvalves and micro-MFC's, are manufactured by Redwood MicroSystems. Both the MEMS-Flow® MFC's and the microvalves have a proof pressure of 150 psig and a burst pressure of 250 psig. Other than the microreactors, these devices are the most likely to fail due to overpressurization. The shut-off microvalves have a leak rate of 0.1 ml/min. The operating temperature range of these components is between 0°C and 55°C. The microvalves that are downstream of the MFC's have been modified to be slow acting

valves. That is, their control electronics have been altered to increase the time required to close the valve. This was done to allow the process lines to depressurize in case of power failure. Their shut-off time is between 2s and 3s whereas the shut-off time for the unmodified microvalves is less than 1s.

The other major components to this system are the boards that are placed in the CompactPCI chassis to form the DARPA Microreactor System. All the boards in the microreactor chassis are made out of FR-4 laminate, which is constructed of multiple plies of epoxy-resin-impregnated woven glass cloth. Its upper operating temperature limit is 130°C, and its UL flammability classification is 94V-0, which means samples self-extinguish within 10s after flame application[13]. The reactor and feed gas mixing boards have been discussed briefly in Section II E. These boards and the other boards in the system except the rear I/O cards are described in the following subsections. Drawings of the boards' circuits and wiring schematics have been omitted since they provide little help in evaluating the system safety. The CompactPCI chassis used in the system is described after the system boards.

Temperature Controller Board

The temperature controller board, shown in Figure A-10, consists of five CAL[11] 3300 temperature controllers. These controllers are used to maintain the temperature of the DieMate manifolds and the product transfer lines by controlling power to 48 VDC cartridge heaters.

[11] CAL Controls Inc., 1580 S. Milwaukee Ave., Libertyville, IL 60048, (847) 680-7080.

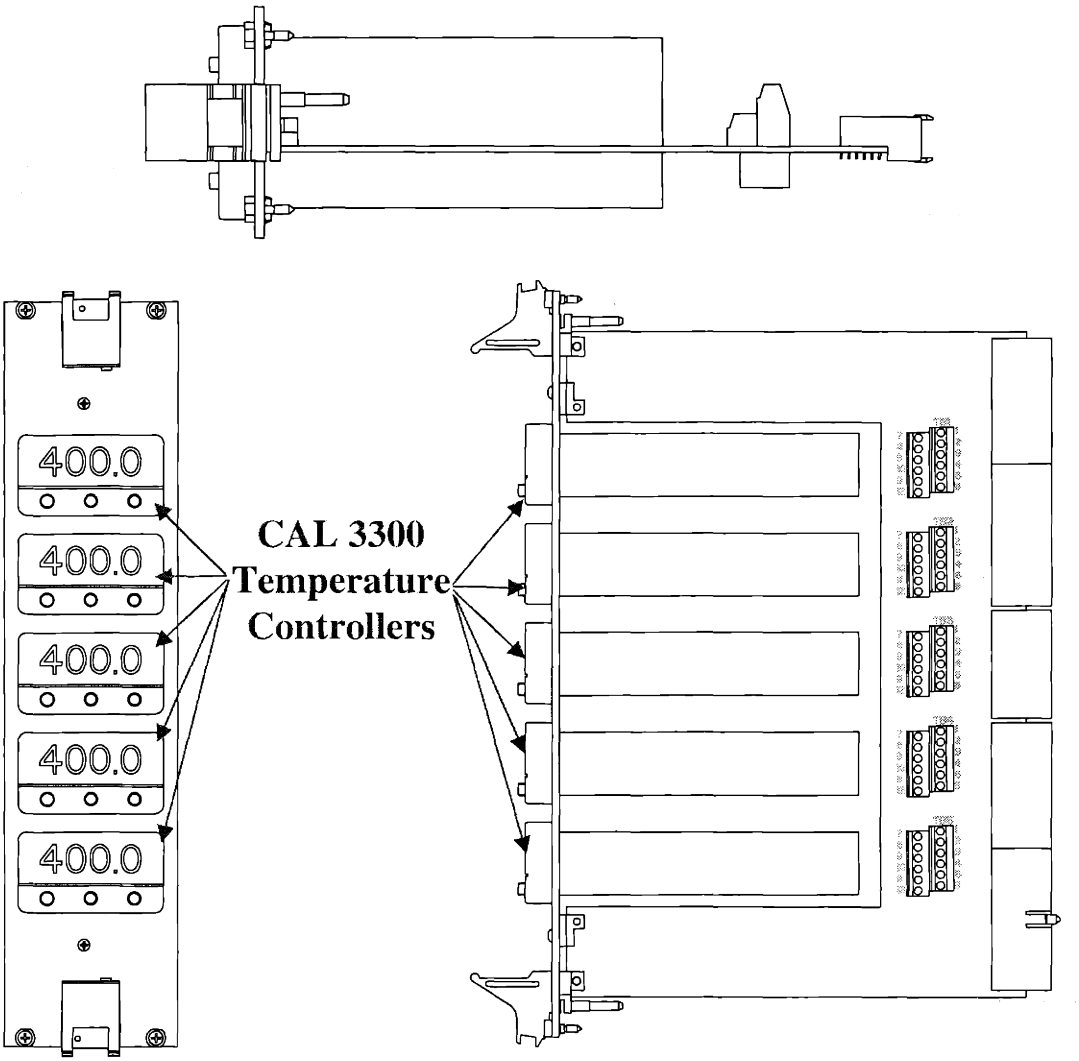

Figure A-10. Top (top), front (left), and side (right) views of the temperature controller board for the Microreactor System chassis.

Feed Gas Mixing Board

In addition to Figure A-6, Figure A-11 shows the feed gas mixing board with its three gas flow control assemblies. The Redwood Microsystems' components are mounted on a custom fabricated valve manifold[12] machined from 316 stainless steel. Final assembly of the microvalve and MFC components with the valve manifold was performed by Redwood Microsystems. Valve manifold assemblies will be leak cheaked prior to use. Burst pressure

of the complete assembly should be limited by the Redwood Microsystems' components, which is 250 psig.

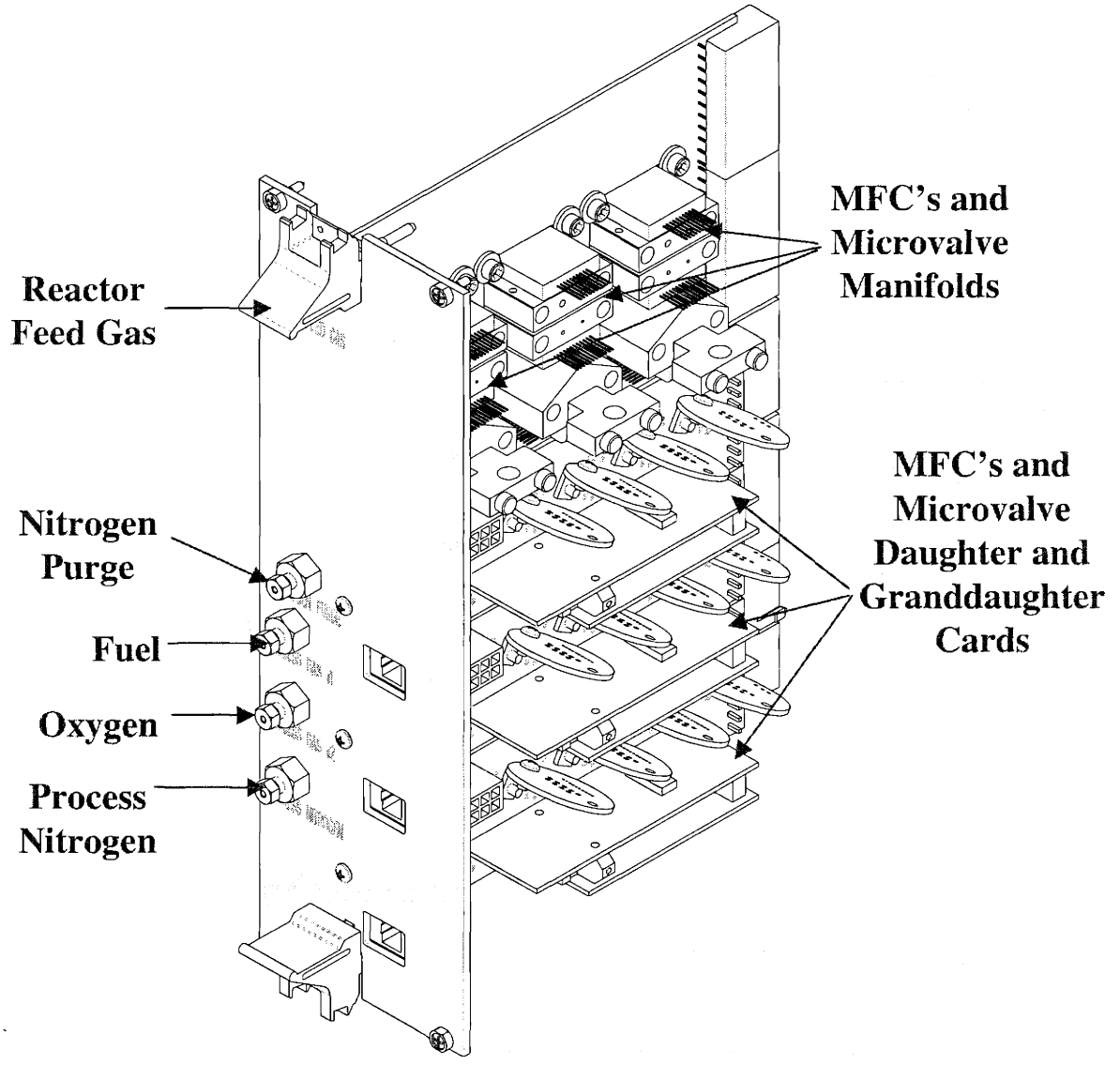

Figure A-11. Isometric view of the feed gas mixing board

Reactor Boards

Two reactor boards are used in the DARPA Microreactor System. Figure A-12 shows rendered views of the board. Engineering drawings can be seen in Figure A-7. The

[12] ENSER drawing number D1488666.

Redwood Microsystems' gas flow control assemblies are the same as those used in the feed gas mixing board discussed in the previous section. In addition, this board contains a Texas Instruments DieMate® socket to provide the fluidic interconnection to the microreactor die.

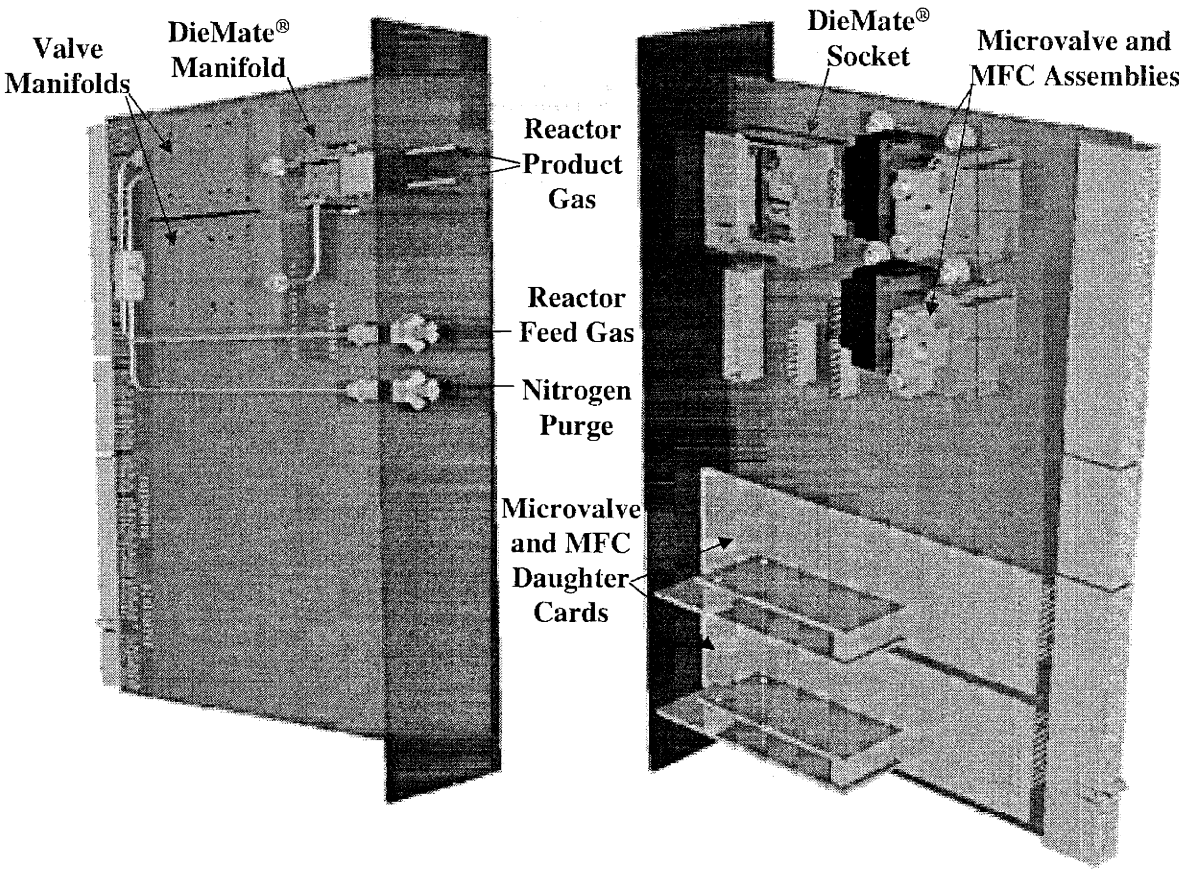

Figure A-12. Front (right) and back (left) views of the reactor board.

The 110 pin version of the DieMate® socket, shown in Figure A-13, is used for the DARPA microreactor system since it was the smallest socket available. The microreactor only uses 56 of the pins for electrical interconnections. A pin is left blank between every active pin to avoid any possibility of misalignment interfering with reactor operation. The microreactor die was specially designed to fit precisely into the socket and the bond pads on

the die are self-aligning with the DieMate pins. There has never been any problem with a microreactor die misaligning in the socket in all past tests.

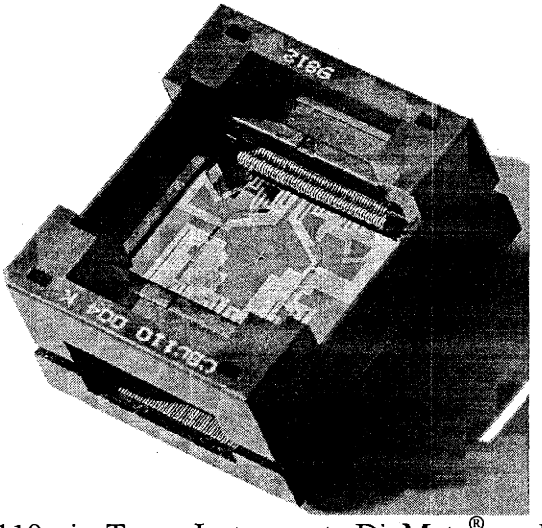

Figure A-13. 110 pin Texas Instruments DieMate® socket with a Y microreactor mounted in it.

Although the DieMate® socket provides the electrical connections, as sold it has no capability of fluidic interconnections. The microreactor die requires two reactor feed connections and two reactor product connections. These are done using a specially fabricated DieMate manifold[13] that is inserted into the bottom of the socket, under the microreactor die. The DieMate manifold is machined from 316 stainless steel. The bottom of the DieMate socket is altered[14] to allow the manifold to fit into the socket. A seal is formed between the DieMate manifold and the microreactor die using Kalrez® o-rings. Cap screws on the bottom of the DieMate manifold are used to exert the sealing force needed by the o-rings. The DieMate manifold contains holes for the placement of four 1/8", 48V heating cartridges and two 1/16" RTD's to control the microreactor die temperature to prevent

[13] ENSER drawing number D1489015.
[14] Altered according to ENSER drawing number D1489014.

product condensation inside the reactor. The 1/16" stainless steel tubing for the feed and product gas is silver soldered to the manifold. This assembly is shown in Figure A-14. The microreactor membrane is the most pressure sensitive component of the assembly and will fail at 7 psig[12]. The assembly will be leak checked prior to operation.

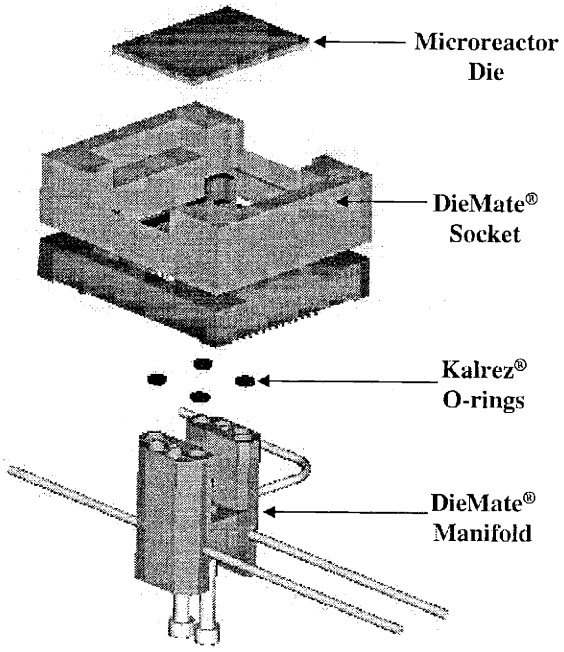

Figure A-14. Exploded view of DieMate™ assembly.

Heater Driver Circuit Boards

There are two heater driver circuit boards, one for each reactor board. These boards contain the circuitry necessary to power twelve microheaters on a microreactor chip. These boards contain no fluidics.

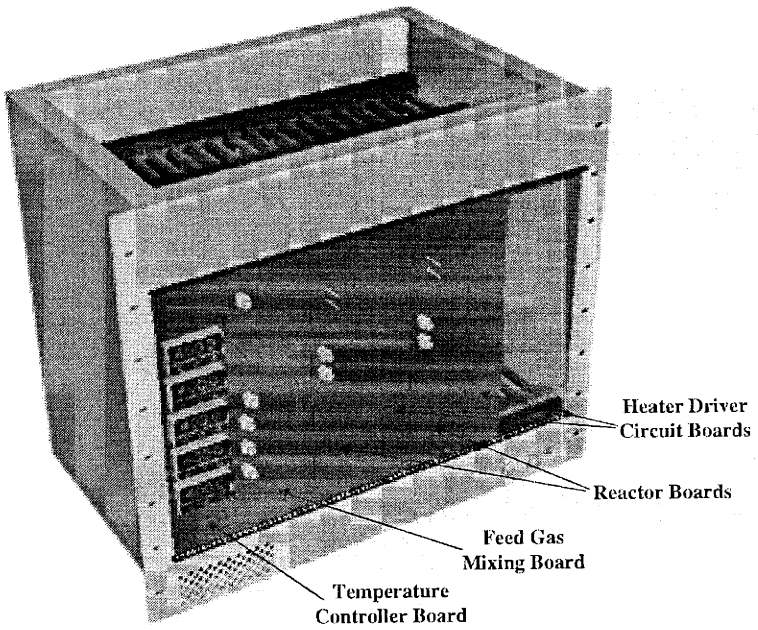

Figure A-15. Front view of the DARPA Microreactor System. Note that the fans at the top of the chassis are not shown.

CompactPCI Chassis

The DARPA Microreactor System is housed in a standard CompactPCI chassis manufactured by Kaparel[15]. This chassis is the 9U x 84 HP PS6090 integrated subrack. It holds up to fourteen 6U, 64 or 32-bit CompactPCI cards and up to two double-wide (8HP) 6U power supplies. The chassis includes two high performance 12V DC fans that are capable of moving 440 cfm of air. The chassis, with mounted boards, is shown in Figure A-9 and the figures below. Detailed computational fluid dynamic simulations of air flow and temperature profiles inside the chassis have been done by Flomerics, Inc[16]. These simulations indicated that the fans will move approximately 176 cfm of air through the populated chassis. In addition, the board temperature around the hot components (DieMate

[15] Kaparel Corporation, 564 Weber Street North, Waterloo, Ontario, N2L 5C6 Canada, 519-725-0101.
[16] Flomerics, Inc., 2 Mount Royal Avenue, Marlboro, MA 01752, (508) 460-0112.

manifold and product transfer lines) is approximately 97°C, below the upper operating limit of the FR-4 laminate. However, board temperatures are below 50°C in most areas[14].

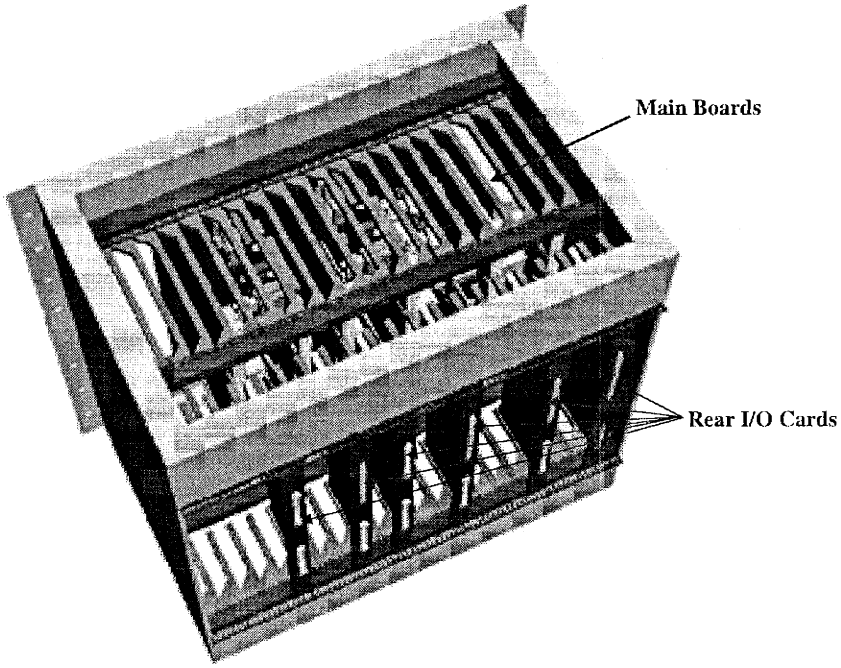

Figure A-16. Top view of the DARPA Microreactor System showing the main boards along with the rear I/O cards. Note that the chassis fans are not shown.

Electrical interconnections between the boards are made using rear I/O cards, which can be seen in Figure A-16, and an H.110 telephony backplane. In addition, to providing electrical connections between boards, the rear I/O cards interface the chassis with a National Instruments PXI-1010 chassis that contains a 233 mHz Pentium embedded controller. This controller can be operated under Windows or an RT operating system. Under the RT OS, it provides deterministic control capabilities similar to the Siemens PLC's used to control the MARS units. The PXI-1010 chassis has 8 slots for PXI modules and 4 slots for SCXI modules. Table A-4 lists the modules in the chassis.

Slot	Module	Description
PXI slot 1	PXI-8156B	Controller (233 mHz Pentium w/ethernet port)
PXI slot 2	PXI-6527	Digital I/O (64 channels)
PXI slot 3	PXI-6713	Analog out (8 channels)
PXI slot 4	PXI-6713	Analog out (8 channels)
PXI slot 5	PXI-6713	Analog out (8 channels)
PXI slot 6	PXI-6713	Analog out (8 channels)
PXI slot 7	PXI-6071E	Multifunction I/O (32 differential channels)
PXI slot 8	PXI-6071E	Multifunction I/O (32 differential channels)
SCXI slot 1	SCXI-1122	Isolated input w/SCXI-1322
SCXI slot 2	Empty	
SCXI slot 3	Empty	
SCXI slot 4	SCXI-1160	General purpose relay w/SCXI-1324

Table A-4. PXI-1010 chassis modules with descriptions.

Safety

Any run conditions outside of the scope of this Research Safety Review require a separate review.

The major hazards associated with this unit are feed and product flammability, chemical exposure, and high temperature. Fire, exposure, and explosion hazards for individual feed and product chemicals are described in detail in the Material Safety Data Sheets in Appendix A.

The DARPA Microreactor System is designed to fail to a safe state. System faults are normally handled by a Real Time (RT) National Instruments LabVIEW PXI/CompactPCI control system with an embedded processor. Note that LabVIEW for this system is running under a deterministic operating system with a dedicated microprocessor. Thus, the reliability problems of LabVIEW running under Windows NT or Windows 95 should not be present in this system. In addition, a watchdog timer is in place in case the control system fails to function properly. In case of a power failure, the system shuts down by relieving any pressure in process lines. However, the process lines are not purged with an inert gas when

this occurs. Thus, any time system maintenance is performed (such as replacing a microreactor), the operator must purge all process lines with an inert gas. Further details on the safe operation of the unit can be found in the Standard Operating Procedure (SOP) section. Further details on the interlock protocols implemented can be found in the Interlocks subsection.

Under normal operating conditions, the LabVIEW RT controller monitors for process faults and takes corrective action upon identification. The system can only be run safely using the BridgeVIEW Human-Machine Interface, which performs process actions through the LabVIEW RT controller. This system should NEVER be run in a 'manual' or 'non-auto' mode that would subvert the normal operation of the LabVIEW control system. The unsafe conditions that cause interlocks are

1) The feed gas composition entering the explosive regime
2) Failure of a microreactor.
3) An over-temperature of a heating cartridge or the sampling valve oven.
4) An under-temperature of a heating cartridge or the sampling valve oven.
5) Fume hood exhaust failure.
6) Failure of one of the two CompactPCI chassis exhaust fans.
7) Power failure.
8) Controller timeout detected by the watchdog timer.

Safety Equipment

The Kaparel PS6090 CompactPCI chassis has two cooling fans that will be used for system ventilation during operation. These cooling fans provide an estimated flow rate of 176 cfm of air through the chassis, which will act to dilute the gas from any leaks in process

lines or components to a safe level[14]. The status of these fans is monitored by the LabVIEW RT control system.

The status of the LabVIEW RT control system is monitored by a watchdog timer that will remove power to the system if the control system stops functioning.

The hood status is monitored by a discrete contact closure that is tied into the E-stop circuit of the system. This will remove power from the system, but not the LabVIEW controller.

Pressure relief valves are present on all the feed gas cylinders after the main two-stage regulator. The relief pressure is set at 80 psig. This is to minimize the risk of components bursting due to over-pressurization and to protect the Redwood Microsystems components from damage.

The locations of area safety equipment are listed below. Any operator must be familiar with the location and usage of all safety equipment in case an emergency occurs.

1) Fire extinguishers: next to the door leading to the loading bay

2) Safety showers: one located on each end of the second bay at the sinks

3) Eye wash stations: one located on each end of the second bay next to the sinks

4) Evacuation alarm: one located next to the loading bay door and one located across from the main entrance to the lab

Explosion Hazards

In any process utilizing pure oxygen there is always the potential for fire or explosion. During system construction, special care was taken to ensure all the lines used were oxygen clean. That is machined parts, tubing, and other components were solvent cleaned to remove residual oil by the personnel at DuPont, ENSER Corporation, or the OEM. The prevention of fires or explosion during system operation depends on the care of DARPA

Microreactor System operators. The SOP's provided in this document provide a guideline that should be followed for safe operation. Any system operator who observes a potential for an accident during operation under these guidelines should take appropriate measure to update the SOP's.

During normal operation, there should never be an explosive mixture of fuel and oxygen in any of the process lines or components. The LabVIEW RT control system is programmed to monitor the flow rates of fuel and oxygen to form the feed mixture. The control system is programmed to interlock if the feed mixture comes to within 1.0% of the lower flammability limit. Since this limit depends on the process gases used, it is important for the operator to ensure that the system knows what gases are being used during the process. In addition, the concentration of fuel in the fuel gas cylinder, which is diluted for analysis and handling readings, needs to be entered correctly into the BridgeVIEW HMI. Before a new fuel gas cylinder is put on-line, a GC analysis should be performed to verify its composition. Consult the SOP section for more information concerning the proper operation of the Microreactor System.

The flammable gases being used for microreactor testing are carbon monoxide, ammonia, and methane. Table A-5 lists the values for the LEL, UEL, autoignition temperature, flash point, melting point, and boiling point for the reactants and the principle reaction products. Further information about these chemicals can be found in their appropriate MSDS.

Component	Lower Flammability Limit in Air (Volume %)	Upper Flammability Limit in Air (Volume %)	Autoignition Temperature (°C)	Flash Point (°C)	Melting Point (°C)	Boiling Point (°C)
O_2	-	-	-	-	-218	-183
N_2	-	-	-	-	-210.0	-195.9
H_2O	-	-	-	-	0.0	100.0
CO	12.5	74.0	609	-191	-205.1	-191.5
CO_2	-	-	-	-	-	-79[17]
NH_3	15	28	651	11	-77.7	-33.3
NO	-	-	-	-	-164	-151.7
N_2O	-	-	-	-	-90.9	-88.6
CH_4	5	15	537	-187.7	-182.5	-161.5
H_2	4.0	75	500		-259.2	-252.8

Table A-5. Physical properties of chemicals used in or produced by the DARPA Microreactor System.

In the event, that an explosive composition is reached during operation, the small volumes associated with the reactors, valves, and transfer lines, minimize the potential for injury to personnel or environmental impact. The entire system gas volume inside the chassis is 3.4 cm^3. As a worst case scenario during operation, assume that a stoichiometric composition of methane and oxygen is present in all of the gas lines. Further, assume that the system is pressurized to 150 psig (well above the point at which the pressure relief devices will activate). If this entire volume of gas undergoes complete combustion, it will release the equivalent energy of 0.00023 lbs of TNT[18]. Thus, the only explosion hazard presented by this system is the accumulation of flammable mixtures outside the system tubing.

This accumulation is unlikely since the chassis's two fans move 176 cfm of air through the system. This corresponds to approximately 95 complete air changes every minute. The most likely area of gas escape is above the microreactor after a membrane

[17] Sublimation point.

failure. In this case, the control system should interlock and shutoff the flow of combustible gas to that reaction channel. The flammable gas that does escape will be diluted by air flowing over the microreactor at an estimated rate of 120 ft/min. The flow profile of air over the microreactor is shown in Figure A-17. The area in white in the figure is the walls of the DieMate® socket. This simulation also shows that there is a recirculation zone above the reactor with an airflow rate as low as 20 ft/min[14]. Nonetheless, this should be sufficient to dilute any escaping gas.

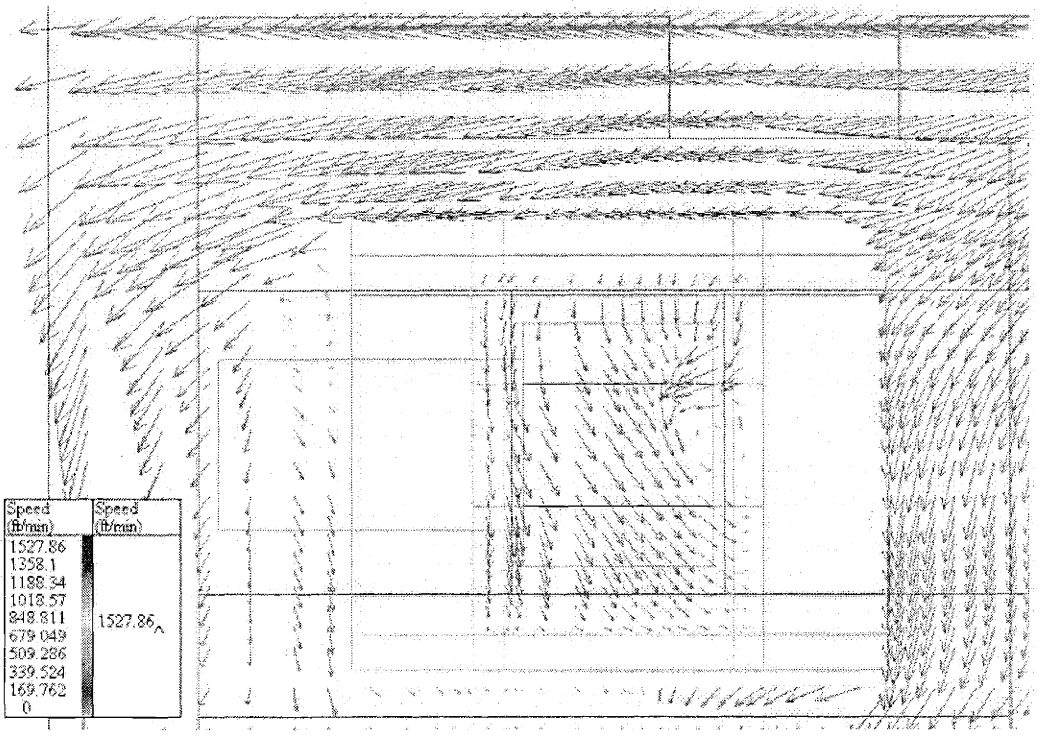

Figure A-17. Flow profile above the microreactor[14].

The other possibility for an explosion or deflagration would occur from the over-pressurization of the system. It is believed that the pressure relief points of the system will

[18] This calculation also assumes the gas is at 20°C and uses a value of 490 kcal/lb of TNT.

be the microreactors and the Redwood Microsystems components. The microreactors are isolated from the atmosphere by a 1 μm thick silicon nitride membrane. This membrane is incapable of handling a pressure differential greater than 7 psi between the reaction channel and the environment[12]. Thus, little energy is released during a membrane rupture. The Redwood Microsystems microvalves and MFC's have a burst pressure of 250 psig. Redwood Microsystems did not have any information on energy release from a burst caused by overpressurization. However, this event should be unlikely since pressure relief valves set at 80 psig are placed in the process gas lines before entering the system chassis. A back pressure regulator between the feed gas mixing board and the reactor boards also acts to limit the system pressure.

Chemical Hazards

The chemicals used in the system are all gaseous. The microreactor itself is non-hazardous, but is made out of glass so it does present a cutting hazard. Pressurized ammonia is liquid in form, so there may be the possibility of spraying when handling the cylinder. Splash goggles and a face shield should be worn when handling the cylinder. See the MSDS for more information. All gases should be handled in ventilated enclosures. The operator should not enter the enclosure when gas is flowing to the Microreactor System.

Condition	Value	Action
Reactor Failure	n/a	Alarm A.1 & Interlock A
Flammability Limit Approached Alarm	-1.5% of LEL	Alarm B.1
Flammability Limit Approached Interlock	-1.0% of LEL	Alarm B.2 & Interlock B
Purge N_2 Failure	0.25 V deviation from MFC setpoint	Alarm C.1 & Interlock C
Fuel or Oxygen Flow Failure	0.25 V deviation from MFC setpoint	Alarm B.3 & Interlock B
Hood Failure	n/a	System Power is Removed
Chassis Fan Failure	n/a	System Power is Removed
System Power Failure	n/a	Alarm[19] B.4 & Interlock B
RT System Timeout	Watchdog timer not reset	System Power is Removed
Reactor Manifold Temp. Hi	205°C (tbd)	Alarm B.5
Reactor Manifold Temp. Hi Hi	210°C (tbd)	Alarm B.6 & Interlock B
Reactor Manifold Temp. Low	180°C (tbd)	Alarm B.7
Reactor Manifold Temp. Low Low	170°C (tbd)	Alarm B.8 & Interlock B
Product Transfer Block Temp. Hi	205°C (tbd)	Alarm B.9
Product Transfer Block Temp. Hi Hi	210°C (tbd)	Alarm B.10 & Interlock B
Product Transfer Block Temp. Low	180°C (tbd)	Alarm B.11
Product Transfer Block Temp. Low Low	170°C (tbd)	Alarm B.12 & Interlock B
Sampling Valve Box Temp. Hi	205°C (tbd)	Alarm B.13
Sampling Valve Box Temp. Hi Hi	210°C (tbd)	Alarm B.14 & Interlock B
Sampling Valve Box Temp. Low	180°C (tbd)	Alarm B.15
Sampling Valve Box Temp. Low Low	170°C (tbd)	Alarm B.16 & Interlock B

Table A-6. List of alarm and interlock conditions.

System Interlocks

Most of the system interlocks are handled by the embedded LabVIEW RT controller in the data acquisition PXI chassis. This is similar to other systems such as MARS II or

[19] No alarm can be signaled without power, but the system will show an alarm as soon as power is restored.

MARS III except the Siemens 545 PLC's have been replaced with the National Instruments system. The LabVIEW controller monitors the status of the interlocks listed at the beginning of this section and takes appropriate action if any interlock conditions are found. In addition to the interlocks listed below, the external heater controllers that are used for the system heating tapes and sampling valve box have hardwired over and under temperature interlocks built-into these controllers. However, these interlocks only shutoff power to the affected heating device, so the LabVIEW controller must still take action to shutdown the rest of the process. Table A-6 lists the system alarm and interlock conditions. Table A-7 lists the alarms, and Table A-8 lists the interlocks and the actions taken by the controller during the interlock. Once an interlock is activated, the system will not return to normal operation until the interlock is acknowledged by operator. The interlock must be reset using the BridgeVIEW HMI. All interlocks will be checked prior to system startup. In addition, every interlock will be checked once per quarter to verify it is operational.

Alarm	Action
A.1	Reactor failure alarm and reactor shutdown
B.1	Flammability limit approached warning
B.2	Flammability limit approached alarm and total system shutdown
C.1	Purge N_2 failure alarm and total system shutdown
B.3	Process gas failure alarm and total system shutdown
B.4	Power failure alarm and system is purged when the power is restored.
B.5	Reactor manifold temperature high warning
B.6	Reactor manifold temperature high alarm and total system shutdown
B.7	Reactor manifold temperature low warning
B.8	Reactor manifold temperature low alarm and total system shutdown
B.9	Product transfer block high temperature warning
B.10	Product transfer block high temperature alarm and total system shutdown
B.11	Product transfer block low temperature warning
B.12	Product transfer block low temperature alarm and total system shutdown
B.13	Sampling valve box high temperature warning
B.14	Sampling valve box high temperature alarm and total system shutdown
B.15	Sampling valve box low temperature warning
B.16	Sampling valve box low temperature alarm and total system shutdown

Table A-7. List of alarms.

Interlock	Action
A	Reactor is shutdown by turning off power to heaters and temperatures sensors; switching the feed gas mixture to purge N_2; and after the line has purged for 5 min. the MFC is turned off and the on/off valve closed.
B	System is shutdown by switching the fuel and O_2 streams to purge N_2; power to the reactors and heating devices is shutoff; after 5 min. the MFC's and valves are shutoff
C	System is shutdown by turning off power to the reactors and heating devices; the process gas that is controlled to prevent flammable mixture formation is shut-off while the other gas is used to purge the system.[20]

Table A-8. List of interlocks.

In the event of a power failure, the system vents pressure, but the system is not purged with nitrogen. Only normally closed microvalves were available for constructing the system, so there was no way to purge the system lines with nitrogen during a power failure. Instead, two types of normally closed microvalves were used. The standard microvalve closes in less than one second after power is removed. The slow-acting microvalve closes in between 2 and 3 seconds after power is removed. The normal microvalves are placed upstream of the flow controllers, and the slow-acting microvalves are placed downstream. When the power fails there is between 1 and 2 seconds for the excess pressure in the system to be relieved through the slow closing valve. After power is restored, the system will purge itself with nitrogen, by opening the valves for the purge nitrogen stream. Because the system can fail with process gas still in the lines, any operator should always perform a purge sequence before beginning work on the system. Consult the SOP's for further information on system operation.

[20] The gas being shut-off must be carefully chosen since turning off the wrong gas could cause the gas mixture to pass through the flammability envelope. For example, if CO is being kept below 12.5% and there is initially 30% oxygen in the mixture, turning off the oxygen flow would cause the CO concentration to rise while the oxygen concentration is still high enough to form an explosive mixture. In this case, the CO gas flow must be turned-off

References

1. Srinivasan, R., Hsing, I.-M., Berger, P.E., Jensen, K.F., Firebaugh, S.L., Schmidt, M.A., Harold, M.P., Lerou, J.J., and Ryley, J.F. (1997) "Micromachined reactors for catalytic partial oxidation reactions", *AIChE Journal,* **43**(11), pp. 3059-3069.

2. Hsing, I.M., Srinivasan, R., Harold, M.P., Jensen, K.F., and Schmidt, M.A. (2000) "Simulation of micromachined chemical reactors for heterogeneous partial oxidation reactions", *Chemical Engineering Science,* **55**, pp. 3-13.

3. Quiram, D.J., Jensen, K.F., Schmidt, M.A., Mills, P.L., Ryley, J.F., and Wetzel, M.D. (1999) "Integrated microchemical systems: opportunities for process design", In *FOCAPD '99 Computer-Aided Design for the 21st Century*, Presented at 5th International Conference on Foundations of Computer-Aided Process Design, July 18-23, 1999, Breckenridge, CO, *AIChE Symposium Series*, **323**, pp. 147-162.

4. Quiram, D.J., Hsing, I.-M., Franz, A.J., Jensen, K.F., and Schmidt, M.A. (2000) "Design issues for membrane-based, gas phase microchemical systems", *Chemical Engineering Science,* **55**, pp. 3065-3075.

5. Hsing, I.-M. (1998) *Simulation Strategies for Microfabricated Chemical Systems*, Ph.D. Dissertation at the Massachusetts Institute of Technology, Cambridge, MA.

6. Srinivasan, R. (1998) *Microfabricated Reactors for Partial Oxidation Reactions*, Ph.D. Dissertation at the Massachusetts Institute of Technology, Cambridge, MA.

7. Engel, T. and Ertl, G. (1979) "Elementary steps in the catalytic oxidation of carbon monoxide on platinum metals", *Advances in Catalysis,* **28**, pp. 1-78.

8. Satterfield, C.N. (1980) *Heterogeneous Catalysis in Practice*, McGraw-Hill Book Company, New York.

9. Deutschmann, O. and Schmidt, L.D. (1998) "Modeling the partial oxidation of methane in a short contact time reactor", *AIChE Journal,* **44** , pp. 2465-2477.

10. Coward, H.F. and Jones, G.W. (1952) *Limits of Flammability of Gases and Vapors*, United States Government Printing Office, Washington, D.C.

11. Schmidt, L.D. and Goralski, J.C.T. (1997) "Catalytic oxidation of alkanes at millisecond contact times", In Graselli, R.K., Oyama, S.T., Gaffney, A.M. and Lyons, J.E., (Eds.), *3rd World Congress on Oxidation Catalysis*, Elsevier Science B.V., Amsterdam, pp. 491-500.

12. Firebaugh, S. (1998) "Improving reactor yield", Group Report, Feb. 9,1998.

---

to prevent a flammable mixture from forming. The control system will be preprogrammed with the correct shut-down procedure depending on the reaction be studied.

13. Henningsen, C.G. and Gause, S.A. (1996) "Base materials", In Coombs, C.F., (Ed.), *Printed Circuits Handbook*, 4th ed., McGraw-Hill, New York, p.1088.

14. Heck, M. and Manning, A. (2000) "Flotherm analysis and modeling of airflow patterns and temperature distributation in the Kaperel card cage", Flomerics, Inc., Marlborough, MA, Report #USE0400-11.

Standard Operating Procedures

Standard operating procedures for the following laboratory activities are included in the following pages:

1) Startup
2) Normal operation
3) Normal shutdown
4) Emergency shutdown
5) Microreactor replacement
6) Cylinder replacement
7) Waste disposal
8) Spills
9) Line breaks
10) Lock out

Modifications to the SOP's can be made by performing a mini hazard review. For simple changes refer to the Hazard Analysis Roadmap.

Procedure No. 1: Startup

E. I. DuPont de Nemours & Company
Central Research & Development Department
Experimental Station

Issue Date: July 12, 2000
Revised Date: May 1, 2001

Approved by: Lewis C. Goodrich	**Date:**
Reviewed by: James F. Ryley	**Date:**
Prepared by: David J. Quiram	**Date:**

Job Steps	**Safety Key Points**
	General Procedure Notes: Safety glasses must be worn at all times. Additional PPE may be required for certain procedures. Place appropriate warning signs in front of system during operation. This system is NOT to be left unattended during operation.
1.1 Repair or replace any faulty components that were discovered during the last run or in preparation for the current run.	**1.1** Replacement of components should be done with identical parts. New components should be leak checked before startup as appropriate.
1.2 Start the LabVIEW HMI on the MARS 5 computer. Load the LabVIEW HMI, and press the run button on the LabVIEW window.	
1.3 Check that the gas cylinder supply pressures are high enough to last through the anticipated run duration. This includes the process nitrogen, hydrocarbon feed, oxygen, calibration gas cylinder and all GC gases (i.e. He and H_2).	**1.3** Consult the SOP on cylinder replacement if a cylinder change is required.

1.4 Place any new microreactors into the system as needed according to the SOP for microreactor replacement.	**1.4** Microreactors should only be handled with tweezers because of sharp edges. Protective gloves are not recommended because of loss of dexterity.
1.5 Verify that the sampling valve box and transfer lines are at their operating temperature of 200°C. If any are below temperature, bring them up to temperature. After these lines are at temperature, be sure the alarm and interlock temperatures are set to the values located in Table II.1 at the end of this SOP.	**1.5** Interlocks in the LabVIEW RT control program will prevent operation of the system if these temperatures fall above or below the high-high or low-low temperatures, respectively.
1.6 Verify that the GC is working properly and communicating with the ChemStation computer.	**1.6**
1.7 Turn on the purge gas supply and set the regulator on the DARPA system gas manifold to 60 psig.	**1.7** Pressure relief devices on the cylinder regulators prevent pressurization above 80 psig.
1.8 Start the DARPA MS by clicking on the *RT Engine* tab and *Enable Control Loop*. Then *Enable MCS Chassis Power*.	**1.8** System power can be removed from the HMI at any time by clicking off the *Enable MCS Chassis Power* button.
1.9 Pop the E-stop 'mushroom' to allow power to flow throughout the system chassis.	**1.9** The E-stop 'mushroom' can be pressed at any time to remove power to most of the system. **WARNING**: This does not completely remove all power from the system. The power supplies need to be disconnected to remove power at the power input connector. In addition, the chassis fan will always be supplied power regardless of the E-stop state.
1.10 The first step of the run sequence is a system purge. During this step, the backpressure regulator external to the system should be set to 35 psig. After completing this, proceed to the next step.	**1.10** If an MFC does not reach its desired set point during this step, the system will alarm and interlock. This indicates an MFC failure or a loss of upstream pressure in the purge gas cylinder.
1.11 Adjust the two DieMate manifold heater set points to 200°C. Adjust the reactor product clam shell heater set points to 200°C. After these lines are at temperature, be sure the alarm and interlock temperatures are set to the values located in Table II.1 at the end of this SOP.	**1.11** Interlocks in the LabVIEW RT control program will prevent operation of the system if these temperatures fall above or below the high-high or low-low temperatures, respectively.

1.12 Begin preparation for the run by setting the desired gas flow rates with purge gas flowing through the system. The process gas SOV's on the Feed Gas Mixing board should be closed during this step. If necessary, calibrate any MFCs that only flow nitrogen using the HMI.	**1.12**
1.13 Verify and set, if necessary, the alarm values on the HMI according to the values located in Table II.1.	**1.13** All the process variables should be at their set point with purge gas flowing through the system. Do NOT proceed to the next step until the system is operating properly.
1.14 Turn on the process gas (O2, CO, NH3, or CH4) supply and set their regulators on the DARPA manifold to 60 psig.	**1.14** Do not enter the hood while these gases are turned on. Pressure relief devices on the cylinder regulators prevent pressurization above 80 psig.
1.15 Calibrate the feed gas MFCs as needed by closing the purge gas SOV and turning on the feed gas SOV. The other feed gas lines should be turned off at this time along with the reactor feed lines. This will force all the gas to flow out the backpressure regulator vent location. Use a flow meter at this location to perform the calibration. MFC calibration is done through the LabVIEW HMI. Record using the ELN the calibration data, date of calibration, temperature, and atmospheric pressure.	**1.15** Be careful to vent all process gas to the hood during MFC calibration. All feed gas MFCs must be calibrated weekly or whenever a process gas cylinder is changed. Correct calibration is important to prevent the formation of explosive feed mixtures.
1.16 Verify that the desired feed gas composition is not in the flammable regime using the data in the DARPA System PHA. Determine if the mixture is fuel lean or oxygen lean.	**1.16** Do NOT proceed to the next step without verifying that the feed gas composition will not be in the explosive regime.
1.17 Close the process gas SOVs leading to the microreactors on the microreactor boards. Open the purge gas SOVs leading to the microreactors on the microreactor boards.	**1.17**
1.18 If the mixture is fuel lean, turn on the flow of oxygen and process nitrogen on the feed gas mixing board. After these flows have stabilized, begin flowing fuel gas in the feed gas mixing board. If the mixture is oxygen lean, turn on the flow of fuel gas and process nitrogen on the feed gas mixing board. After these flows have stabilized, begin flowing oxygen in the feed gas mixing board.	**1.18** The reactor board SOVs should be set so that purge gas is flowing through the microreactors.

1.19 Perform GC injections of the reactor feed gas to verify its composition and to determine when the composition has stabilized.	**1.19** Verify that the feed gas composition is not in the explosive regime.
1.20 Calibrate the reactor feed MFCs of the reactors being used in this run. Use the multiposition valve to select the correct reactor and begin flowing feed gas through this reactor. The flow meter will be placed on the vent coming from the ten-port valve out of the sampling valve box. MFC calibration is done through the LabVIEW HMI. Record using the ELN the calibration data, date of calibration, temperature, and atmospheric pressure.	**1.20** Be careful to vent all process gas to the hood during MFC calibration. All reactor feed gas MFCs must be calibrated before every run since calibration depends on gas composition. The reactions being used have not been observed to take place at temperatures less than 200°C.
1.21 After the operator has verified the GC results, begin the run by powering the microreactor heaters and flowing feed gas to the microreactors. Consult the normal operation SOP for further instructions.	**1.21** The purge nitrogen flowing to the reactors is replaced with the feed gas mixture. The enclosure doors must be closed at this point and must not be opened while feed gas is flowing to the reactors.

Authorized Operators:

Name: David J. Quiram	Signature:	Date:
Name: J. Scott McCracken	Signature:	Date:
Name: James F. Ryley	Signature:	Date:

Process Variable	Alarm Type	Value
Sampling Valve Oven Temperature	High Alarm	210 °C
Sampling Valve Oven Temperature	High High Interlock	215 °C
Sampling Valve Oven Temperature	Low Alarm	185 °C
Sampling Valve Oven Temperature	Low Low Interlock	175 °C
DieMate Manifold Temperature	High Alarm	205 °C
DieMate Manifold Temperature	High High Interlock	210 °C
DieMate Manifold Temperature	Low Alarm	185 °C
DieMate Manifold Temperature	Low Low Interlock	175 °C
DieMate Product Heater	High Alarm	205 °C
DieMate Product Heater	High High Interlock	210 °C
DieMate Product Heater	Low Alarm	185 °C
DieMate Product Heater	Low Low Interlock	175 °C

Table A-9. Temperature alarm values for the DARPA Microreactor System.

Procedure No. 2: Normal Operation

E. I. DuPont de Nemours & Company
Central Research & Development Department
Experimental Station

Issue Date: July 12, 2000
Revised Date: May 1, 2001

Approved by: Lewis C. Goodrich	**Date:**
Reviewed by: James F. Ryley	**Date:**
Prepared by: David J. Quiram	**Date:**

Job Steps	**Safety Key Points**
	General Procedure Notes: Safety glasses must be worn at all times. Additional PPE may be required for certain procedures. Place appropriate warning signs in front of system during operation. This system is NOT to be left unattended during operation.
2.1 The LabVIEW HMI is used to change all system parameters. These include gas flow rates, position of SOVs, multiposition valve position, DieMate manifold temperature, and DieMate product heater temperature.	**2.1** The LabVIEW RT controller will alarm and interlock in the event of an unsafe condition. Operator intervention is required for the system to return to normal operation. The operator is not to leave the system unattended while it is running.
2.2 Changes in the feed gas mixture should be made only after verifying the new feed gas composition is not flammable. Make a note in the ELN entry when feed gas composition is changed.	**2.2** The LabVIEW RT controller will monitor the feed gas composition through the flow rates on the feed gas mixing board. The system will interlock if the composition is in or close to the flammability regime. This should NOT be relied on to ensure safe feed gas mixtures are being used.
2.4 Process conditions should be noted in the ELN entry for each GC injection.	**2.4**

Authorized Operators:

Name: David J. Quiram	Signature:	Date:
Name: J. Scott McCracken	Signature:	Date:
Name: James F. Ryley	Signature:	Date:

Procedure No. 3: Normal Shutdown

E. I. DuPont de Nemours & Company
Central Research & Development Department
Experimental Station

Issue Date: July 12, 2000
Revised Date: May 1, 2001

Approved by: Lewis C. Goodrich	**Date:**
Reviewed by: James F. Ryley	**Date:**
Prepared by: David J. Quiram	**Date:**

Job Steps	**Safety Key Points**
	General Procedure Notes: Safety glasses must be worn at all times. Additional PPE may be required for certain procedures. Place appropriate warning signs in front of system during operation. This system is NOT to be left unattended during operation.
3.1 At the end of the run, turn off power to the microreactor heaters using the LabVIEW HMI. Click on the system purge button on the HMI to clear the system of any reactive gases.	**3.1** Do not open the system chassis while the system is powered. Use care when working with product transfer lines or the DieMate® manifold after a run. Always wear thermally insulating gloves when working on or around hot equipment.
3.2 Close the valves on the process gas cylinders except for the nitrogen cylinder.	**3.2**
3.3 Check the status of the ChemStation software.	**3.3**
3.4 Turn-off the GC gas flows and temperature settings as necessary. If another run will be started in the next three days, the GC should be left on to keep the detectors and columns stable.	**3.4**

3.5 Turn-off the power to the system heaters or reduce their set point to 0°C as necessary for system maintenance or if another run will not begin until the next day. The tapes and the sampling valve oven should remain on to prevent thermal cycling and to keep the lines dry.	**3.5** Do not handle the heating tapes or open the sampling valve oven until its temperature has cooled below 50°C. Always wear thermally insulating gloves when working on or around hot equipment.
3.6 After the microreactors have cooled from the heaters in the DieMate manifold, close the valve on the purge nitrogen cylinder. Remove the microreactors as needed according to the line break procedure SOP and microreactor replacement SOP. Store the microreactor for a later run or dispose of it in a sharps container.	**3.6** Microreactors should only be handled with tweezers because of sharp edges. Protective gloves are not recommended because of loss of dexterity.
3.7 Perform system maintenance as needed. Use the lockout and line break SOP's to render the system safe for maintenance.	**3.7**

Authorized Operators:

Name: David J. Quiram	Signature:	Date:
Name: J. Scott McCracken	Signature:	Date:
Name: James F. Ryley	Signature:	Date:

Procedure No. 4: Emergency Shutdown

E. I. DuPont de Nemours & Company
Central Research & Development Department
Experimental Station

Issue Date: July 12, 2000
Revised Date: May 1, 2001

Approved by: Lewis C. Goodrich	**Date:**
Reviewed by: James F. Ryley	**Date:**
Prepared by: David J. Quiram	**Date:**

Job Steps	**Safety Key Points**
	General Procedure Notes: Safety glasses must be worn at all times. Additional PPE may be required for certain procedures. Place appropriate warning signs in front of system during operation.
4.1 Press the *Purge All Now* button on the HMI. This will turn off the microreactor heaters and purge the process lines with nitrogen. This will prevent changing of system parameters until the reactive gases have been cleared from the system.	**4.1** Do not enter or open the hood doors during an emergency. If the situation requires immediate action or there is an electrical hazard, use the system crash button to remove power. Note that the LabVIEW RT controller will remain energized after the system crash button is pressed. For more serious situations involving additional equipment, press the hood crash button to remove power from every device in the hood.
4.2 Turn-off the system heaters or adjust their set points to 0°C.	**4.2**
4.3 Close all the process gas cylinder valves except for nitrogen and cylinders in the ventilated enclosure.	**4.3**

4.4 After the emergency situation has ended, resume with the normal system shutdown procedure.	**4.4**

Authorized Operators:

Name: David J. Quiram	Signature:	Date:
Name: J. Scott McCracken	Signature:	Date:
Name: James F. Ryley	Signature:	Date:

Procedure No. 5: Microreactor Replacement

E. I. DuPont de Nemours & Company
Central Research & Development Department
Experimental Station

Issue Date: July 12, 2000
Revised Date: May 1, 2001

Approved by: Lewis C. Goodrich	**Date:**
Reviewed by: James F. Ryley	**Date:**
Prepared by: David J. Quiram	**Date:**

Job Steps	**Safety Key Points**
	General Procedure Notes: Safety glasses must be worn at all times. Microreactors should only be handled with tweezers because of sharp edges. Protective gloves are not recommended because of loss of dexterity.
5.1 If the system has not already been suthdown, begin the shutdown procedure according to the Normal Shutdown SOP.	**5.1** Follow all safety guidelines given in that procedure.
5.2 Disconnect the electrical power to the Microreactor System by pressing the red crash button for the unit or removing power using the HMI.	**5.2** Never open the Microreactor System chassis while the red crash button is not lit.
5.3 Disconnect the feed and product gas lines to the appropriate microreactor board.	**5.3** Be sure the heated transfer lines and manifolds are below 50°C before opening the system.
5.4 Carefully remove the microreactor board and the heater driver board at the same time. A ribbon cable connects the two boards preventing individual removal.	**5.4** Never remove a board from the Microreactor System chassis while the red crash button is not lit.

5.5 Loosen the cap screws on the DieMate manifold to relieve the sealing force used for the o-ring seal.	**5.5**
5.6 Remove the old microreactor from the DieMate socket using tweezers.	**5.6**
5.7 Place the new microreactor in the DieMate socket. Make a note in ELN with the replacement date and time and the microreactor number.	**5.7**
5.8 Gently tighten the cap screws on the DieMate manifold to form a seal between the manifold and the microreactor.	**5.8**
5.9 Replace the microreactor board and the heater driver board into the system chassis.	**5.9** Never insert a board into the Microreactor System chassis while the red crash button is not lit.
5.10 Reconnect the reactor feed and product lines to the microreactor board.	**5.10**
5.11 Test electrical connections to the microreactor using the LabVIEW HMI.	**5.11**

Authorized Operators:

Name: David J. Quiram	Signature:	Date:
Name: J. Scott McCracken	Signature:	Date:
Name: James F. Ryley	Signature:	Date:

Procedure No. 6: Cylinder Replacement

E. I. DuPont de Nemours & Company
Central Research & Development Department
Experimental Station

Issue Date: July 12, 2000
Revised Date: May 1, 2001

Approved by: Lewis C. Goodrich	**Date:**
Reviewed by: James F. Ryley	**Date:**
Prepared by: David J. Quiram	**Date:**

Job Steps	**Safety Key Points**
	General Procedure Notes: Remember the proper PPE: leather gloves, safety glasses, and toe protection. Cylinder caps must be in place during transport. Cylinders must be secured before the cap is removed.
6.1 Load a cylinder on a cylinder cart at the loading dock.	**6.1**
6.2 Bring cylinder inside laboratory area.	**6.2**
6.3 Close the needle valve on the gas cylinder regulator.	**6.3**
6.4 Close main valve of the cylinder to be replaced.	**6.4** Make sure the valve is seated properly.
6.5 Slowly open vent valve.	**6.5** For ammonia or other hazardous gases stored in the hood, the enclosure doors should be closed with only room to turn the vent valve. Do not stand inside the hood during this step.

6.6 Disconnect cylinder from regulator at the CGA fitting. Loosen the fitting slowly to be certain the cylinder valve is fully closed.	**6.6** Wear leather gloves to avoid hand injury when loosening this fitting. For ammonia or other hazardous gases stored in the hood, the enclosure doors should be closed with only the room required to loosen the fitting. Do not stand in the hood during this step.
6.7 If necessary, place a plug in the cylinder valve. Place cap on cylinder.	**6.7** Double check to make certain the cap is properly seated and on securely. Only certain gases require a cylinder plug.
6.8 Unchain cylinder, and remove from cylinder closet.	**6.8** Be careful placing cylinder in a position/spot that does not pose a risk of being bumped by somebody walking by.
6.9. Place replacement cylinder in the cylinder closet and reattach chain to cylinder.	**6.9**. Beware of pinch points.
6.10 Place spent cylinder on cylinder cart and attach chain.	**6.10**.
6.11 Remove cap from replacement cylinder and tighten CGA fitting.	**6.11**.
6.12 Close vent valve. Check that the process valve for this gas is closed. If not, close this valve.	**6.12**.
6.13 Open the cylinder valve.	**6.13** Verify that the system has ample pressure now. Do not proceed until you are sure that system is properly pressurized.
6.14 Open the needle valve after the regulator.	**6.14** Listen for gas leaks in the lines. Check the fittings around the regulator for leaks with Snoop.
6.15 Return the empty cylinder to proper space on the loading dock. Be sure the cylinder is marked empty. Does a replacement cylinder need to be ordered?	**6.15**

Authorized Operators:

Name: David J. Quiram	Signature:	Date:
Name: J. Scott McCracken	Signature:	Date:
Name: James F. Ryley	Signature:	Date:

Procedure No. 7: Waste Disposal

E. I. DuPont de Nemours & Company
Central Research & Development Department
Experimental Station

Issue Date: July 12, 2000
Revised Date: May 1, 2001

Approved by: Lewis C. Goodrich	**Date:**
Reviewed by: James F. Ryley	**Date:**
Prepared by: David J. Quiram	**Date:**

Job Steps	**Safety Key Points**
7.1 Deposit all waste in ESL approved waste containers with a partially completed waste tag attached to this primary container.	**7.1-7.2** Safety Glasses, cotton lab coat; use Neoprene gloves to handle waste containers. Waste containers must be kept and transported in secondary containers.
7.2 When waste container is at the specified "full" mark, transport the container with a properly completed waste tag, to the designated short-term storage facility.	
7.3 Microreactors should be disposed of in a sharps container.	**7.3** Microreactors should only be handled with tweezers because of sharp edges. Protective gloves are not recommended because of loss of dexterity.
7.3 Non precious metal must be disposed of in the scrap metal dumpsters	**7.4** Wear leather gloves when handling scrap metal.

Authorized Operators:

Name: David J. Quiram	Signature:	Date:
Name: J. Scott McCracken	Signature:	Date:

Name: James F. Ryley	Signature:	Date:

Procedure No. 8: Spills

E. I. DuPont de Nemours & Company
Central Research & Development Department
Experimental Station

Issue Date: July 12, 2000
Revised Date: May 1, 2001

Approved by: Lewis C. Goodrich	**Date:**
Reviewed by: James F. Ryley	**Date:**
Prepared by: David J. Quiram	**Date:**

Job Steps	**Safety Key Points**
8.1 Alert emergency personnel by calling 53131 or #311.	**8.1** Spills consist of any unexpected release of chemicals.
8.2 Secure the area using whatever means necessary to avoid others being affected by the incident.	**8.2-8.4** Appropriate PPE should be worn dictated by the level of the spill and the chemical(s) involved. At a minimum, safety Glasses, cotton lab coat; and neoprene gloves are required.
8.3 Injured personnel should only be removed by emergency personnel unless leaving them where they are would result in further harm.	
8.4 Arrange to have the MSD sheets and the names of the chemicals involved available for emergency responders.	

Authorized Operators:

Name: David J. Quiram	Signature:	Date:
Name: J. Scott McCracken	Signature:	Date:
Name: James F. Ryley	Signature:	Date:

Procedure No. 9: Line Breaks

E. I. DuPont de Nemours & Company
Central Research & Development Department
Experimental Station

Issue Date: July 12, 2000
Revised Date: May 1, 2001

Approved by: Lewis C. Goodrich	**Date:**
Reviewed by: James F. Ryley	**Date:**
Prepared by: David J. Quiram	**Date:**

Job Steps	**Safety Key Points**
	General Procedure Notes: Safety glasses must be worn. Leather gloves must be used for any mechanical work.
9.1 Be sure the system has been shutdown properly. If not, perform a shutdown according the Normal System Shutdown SOP.	**9.1** Follow safety guidelines of the Normal System Shutdown SOP.
9.2 Close all the valves on the process cylinders except for nitrogen.	
9.3 In the main menu of the HMI, go to the *Process Gases* tab and press the *Purge All Now* button. If purging the system with nitrogen is not possible, a line may be broken by slowly loosening the fittings and allowing the process gases to escape. Additional PPE may be necessary depending on the gases trapped in the system. The other steps in the procedure should still be followed.	**9.3** The system will purge with nitrogen for 5 minutes in automatic mode. The HMI will notify the operator when this is completed.
9.3 Open two-way valve to release the pressure between the feed gas mixing board and the microreactor boards using the HMI.	**9.3**

9.4 Remove electrical power from the system chassis. The system should first be shut-off by pressing the E-stop button or removing system power through the HMI. The power supplies to the system should then be shut-off if doing work beyond removal of system boards.	**9.4** Never open the Microreactor System while it has electrical power.
9.5 Proceed with caution in breaking the lines on the front of the chassis. Remove system boards as needed. If you are unsure how to proceed, consult another authorized system operator.	**9.5** If the system was not vented with nitrogen, additional PPE may be required when opening the process lines. Consult the MSD sheets for the process gases.

Authorized Operators:

Name: David J. Quiram	Signature:	Date:
Name: J. Scott McCracken	Signature:	Date:
Name: James F. Ryley	Signature:	Date:

Procedure No.10 Lock Out

E. I. DuPont de Nemours & Company
Central Research & Development Department
Experimental Station

Issue Date: July 12, 2000
Revised Date: May 1, 2001

Approved by: Lewis C. Goodrich	**Date:**
Reviewed by: James F. Ryley	**Date:**
Prepared by: David J. Quiram	**Date:**

Job Steps	**Safety Key Points**
	General Procedure Notes: Safety glasses must be worn at all times. Leather gloves must be worn for any mechanical work.
10.1 De-energize equipment to be locked out.	**10.1**
10.2 Install or fabricate appropriate locking devices. Complete and apply approved tag	**10.2** Physical separation from the process is the preferred method of locking out.
10.3 Clear all personnel from the affected area.	**10.3**
10.4 Physically attempt to energize the locked out equipment.	**10.4** All personnel working on the system shall try the system or witness the trying of the system. Be aware of the possibility of stored energy such as isolated sections of piping and uninterruptible power supplies.

Authorized Operators:

Name: David J. Quiram	Signature:	Date:
Name: J. Scott McCracken	Signature:	Date:
Name: James F. Ryley	Signature:	Date:

Review Meeting Notes

Research Safety Review meeting on July 12, 2000

Attendees:
James W. Ashmead, Lewis C. Goodrich, J. Scott McCracken, Patrick L. Mills, David J. Quiram, James F. Ryley, Kathy A. Saturday, Mark D. Wetzel

Comments:

1) The use of carbon monoxide in the system presents a danger to operators who need to enter the hood. Because of the possibility of a leak from the CO cylinder, it was suggested to place a CO detector inside the hood or use a handheld CO detector while working in the hood. A statement should be added to the SOP warning operator not to enter the hood if the CO cylinder is leaking. Instead, it should be allowed to vent down.
2) SOP 9, the line break procedure, was examined for the case that the system could not be purged. Since the normally closed valves do not purge the system with nitrogen on power loss, it is possible a line break may be necessary when the system has not been purged. It was suggested to modify this SOP for the case when purging the system was not possible.

Actions:

1) SOP 9, the line break procedure, was modified for the case when purging the system with nitrogen is not possible. 7/21/00 DJQ

Memo to Lewis Goodrich concerning use of butane oxidation in system testing

To: Lewis C Goodrich/AE/DuPont@DuPont
cc: James F Ryley/AE/DuPont@DuPont
Subject: Safety Memorandum for Operation with n-Butane

The main safety issue for the use of n-butane in studying the MIT-DuPont microreactors is the potential to form explosive mixtures. The explosive conditions for n-butane have been investigated and documented in the past at DuPont for the direct oxidation of butane to produce maleic anhydride. The lower and upper flammability limits are 1.9% and 8.8% by volume, respectively. The flammability limits as a function of butane and oxygen compositions are available from the PHR for the Riser Reactor and are available at room temperature and 200 C[1]. The minimum oxygen for combustion (MOC) for n-butane with nitrogen as the inert is 12.5% by volume[2]. This number changes to 15.1% with carbon dioxide added to the air/butane mixture as the inert. This number depends on the heat capacity of the inert used (on a molar basis)[3]. The heat capacity for helium is 21.3384 J/(mol K). The heat capacity for nitrogen is 28.8705 J/(mol K). The heat capacity for carbon dioxide is 36.8188 J/(mol K). The heat capacity for the nitrogen/carbon dioxide mixture that results in an MOC of 14.5% is 31.7479 J/(mol K). The heat capacity of the nitrogen/helium inert mixture in the butane feed gas[4] is 22.1873 J/(mol K). Since this is significantly lower than the value for only nitrogen, caution must be used in reducing the oxygen concentration. It is probably best to keep the oxygen concentration below 7.5% to prevent the accidental formation of flammable mixture. Unfortunately, data is not available for the MOC of butane with

nitrogen/helium mixtures. With the given feed gas it is impossible to go above the UFL, and the LFL is so low that little change in feed gas is possible.

The combustion of n-butane over a platinum catalyst is expected to produce mainly carbon monoxide, carbon dioxide, and water. Lower hydrocarbon oxygenates are possible, but not expected in significant quantities. The standard enthalpy of combustion for n-butane is 2874.9 kJ/mol. n-Butane is a colorless gas with a gasoline-like odor. Inhalation of the vapor will initially cause discomfort, such as nausea, headaches, weakness, or temporary nervous system depression with anesthetic effects.

The safety hazards of using n-butane are not believed to be significantly different from the hazards associated with methane. n-Butane has a slightly higher heat of combustion than methane, but the difference does not make it substantially more dangerous. The autoignition temperature of butane is 287 C while the autoignition temperature of methane is 537 C. This difference does increase the possibility of explosion due to the formation of flammable mixtures, but only the microreactor itself will be operating at temperatures in excess of 200 C. As long as care is taken during reactor feed gas mixing, performing n-butane oxidation is safe.

[1]I have a copy of this chart, but I do not have it available in electronic form.
2 H.F. Coward and G.W. Jones, *Limits of Flammability of Gases and Vapors*, Bulletin 503, Bureau of Mines, U.S. Government Printing Office, Washington D.C., 1952.
[3]Heat capacity is traditionally reported on a mass basis but we are concerned with volumes here, which depend on a molar basis according to the ideal gas law.
[4]The butane feed gas is premixed and reported to be 10.2% N_2, 9.5% butane, and the balance helium.

*Other physical and thermodynamic property data obtained from the CRC Handbook of Chemistry and Physics, 72nd edition.